DISSERTATION

INTERROGATING REACTIONS OF GOLD NANOCLUSTERS: INSIGHTS INTO CATALYSIS AND THE BRUST-SCHIFFRIN SYNTHESIS

Submitted by

Timothy Andrew Dreier

Department of Chemistry

In partial fulfillment of the requirements

For the Degree of Doctor of Philosophy

Colorado State University

Fort Collins, Colorado

Spring 2017

Doctoral Committee:

Advisor: Christopher J. Ackerson

Alan J. Kennan
Charles Henry
Christie Peebles

ABSTRACT

INTERROGATING REACTIONS OF GOLD NANOCLUSTERS: INSIGHTS INTO CATALYSIS AND THE BRUST-SCHIFFRIN SYNTHESIS

Over the past several decades, interest in the synthesis and behavior of atomically precise gold nanoclusters has gained substantial momentum. Herein, both catalytic behavior and synthetic mechanisms are explored using techniques more typically applied to organic chemistry. In the case of catalysis, $Au_{25}(SR)_{18}$ has emerged as a well-studied model system. In an effort to investigate their potential as intact, homogeneous, unsupported catalysts, we have discovered that $Au_{25}(SR)_{18}$ clusters are not stable in oxidizing conditions reported for catalytic styrene oxidation. Further investigation suggests that the active catalytic species is an Au(I) species resulting from oxidative decomposition of the starting gold cluster. Equally important to chemical behavior is an understanding of the reaction dynamics during the synthesis of atomically precise clusters. Because the Brust-Schiffrin method is the standard procedure by which gold nanoclusters are synthesized, the role of oxygen in it has been investigated for both organic and aqueous systems. In either case, it is clear obtaining the desired product depends on a radically mediated etching step. These results give new insight into how the Brust-Schiffrin method might be modified to further synthesis of uniquely interesting nanocluster systems.

ACKNOWLEDGEMENTS

They say to write the acknowledgements last, but I've never been all that great at following directions. Probably one of my biggest flaws, come to think of it. Well, that and my insatiable bloodlust. In any case, this is my opportunity to say what I like, about whom I like, in whatever way I choose so I suppose I should get right down to it.

When I decided to come to Colorado State for my Ph.D., I wasn't exactly sure it was the best choice. I had been debating between CSU and Michigan for some time, but my wonderful partner, Amanda, had a clear preference for the sunnier climes of Fort Collins. Without her love and support the following pages would not exist. I would not be a scientist; I'd probably still be a miserable banker. I cannot be effusive enough about her role in enriching my life, keeping me sane, and helping me through the past few years.

The rest of my family has also been incredibly supportive. My mother, Melissa, and my father, Greg, have taken the time to try reading my published work (despite its near incomprehensibility to them), listened when I would stress rant at them, and been surprisingly calm about their son in his mid-30s not having a real job. At least to my face, anyway, and that's all I can really ask. My Colorado family has offered many a warm meal and cold beer so thanks Mark, Christine, Jeannie and Steve.

I have been fortunate in my life to know far too many great people to thank individually, but among my friends several have been real sources of strength throughout my graduate career.

My gaming buddies: Sam, Svet, Howard, P.J. and Jen. Without getting to roll dice while pretending to have magical powers life would be bleaker, and my free time spent entirely wallowing on the sofa watching mediocre television. Thanks for all the distractions and support.

Also, I must thank Rocktoberfest and all who attend it. The annual harkening back to a time when I had fewer responsibilities and a much higher tolerance for alcohol is something I look forward to every year. I couldn't do without it, and it's great to be able to tie one on every year with people I deeply cherish. Moreover, the first rule of Rocktoberfest – no not believing in yourself – has gotten me through a lot of hard times. And, should I ever have children, I will certainly not homeschool them: in accordance with Rocktoberfest's second and final rule. Special thanks are due to Zac Bond and Matt Chorpenning, whose tireless efforts to make Rocktoberfest bigger & better every year are a thing of wonder. Plus, Matt lets me crash at his place when I go.

Strap in, the transitions are going to be a bit rough. When I first came to graduate school, I was convinced that I wanted to be an organic chemist. I'd done organometallic chemistry during my undergraduate time at the University of Texas – San Antonio, and quite liked it. My undergraduate advisor, Dr. Doug Frantz, was as encouraging a mentor as a marginally competent undergraduate could have wanted. Doug has been a huge advocate for me over the years, got me pointed in the right direction early on in my research training, and helped me navigate coming to graduate school in the first place. The graduate students I worked with in Doug's lab were also incredible, and I owe a great debt to each of them.

In any case, as a result of that experience, I started out at CSU as an organic chemist. I joined the lab of Dr. Eric Ferreira, where I soon failed at developing new C–H activation chemistry in every conceivable way. It was rough sledding throughout my time in the Ferreira group, but my fellow students were mostly kind, supportive, and willing to help. I learned a lot of chemistry from Eric "Little Mike" Newcomb, Curtis Seizert, and Paul Allegretti. Little Mike & Paul were especially generous with their time and knowledge; I am a much better chemist for having worked

with them. Curtis and Brian Knight get a special shout out for helping me deal with a difficult advising situation.

When Ferreira was denied tenure by CSU, I was in my third year, and having a fairly difficult time of things with my project. Worse, I had no desire to move to Georgia where the weather is terrible and many of the inhabitants seem to have learned precisely the wrong lesson from the Civil War. Not that I have anything other than its entire history against the American South, mind. At the midpoint of my 3rd year, I was left in a bit of a pinch – no desire to follow my advisor to his new institution, not keen on taking an M. Sc., and uncertain as to my future in science.

I approached Chris Ackerson about moving into his lab, and probably despite his better judgement he said yes. I've been extremely lucky in my life generally speaking, but this was likely the best turn of fortune in my scientific career to this point. There is no level of hyperbolic praise that will sufficiently describe how great working in the Ackerson lab has been. The work that follows, all 200 and some pages of it, would not have been possible without Ack's guidance. To say that my experience in the Ackerson lab has been good is, while true, not nearly comprehensive enough. At this point, I would call myself a nanochemist who has a surprisingly strong grasp of organic chemistry, and I couldn't be happier about it. My research interests have gone in a direction I never would have expected, and I've worked on some fascinating (so fascinating) problems in nanocluster chemistry. None of that would've been possible if Chris hadn't taken a flier on bringing another weird arrow-pusher into his group. I've gotten to push our fundamental understanding of some synthetic processes forward just a bit, and I hope Chris can find the right students to keep doing that in the future.

My time in the Ack lab also introduced me to coworkers I'd never have gotten to know otherwise. To all of the Ack lab – thanks for being supportive, weird, hilarious, uncouth jackholes with little, if any, sense of decorum. Y'all are fantastic. So long, and thanks for all the fish.

Dr. Andrea Wong – sure, she grabbed my nipple like the very first time we met, but Andrea started some of the projects I ended up working on and was a fantastic coworker for the brief period we overlapped in the lab.

Dr. Thomas Ni – Thomas did pretty much everything in the group. All the mundane operational tasks nobody likes, all the dealing with prospective students and first years when Ack wasn't around, solving crystal structures, getting electron microscopy images, figuring out how to get various pieces of equipment to work…all Thomas. His elbows may be creepy as hell, but he's a great guy and fabulous lab mate.

Dr. Marcus Tofanelli – Marcus is a genius. I've met maybe half a dozen geniuses in my life, Marcus is one of them. A brilliant synthetic chemist with a strong grasp of theory and an extremely broad interest in electronic & geometric properties of nanoparticles. Marcus was one of the best people to bounce ideas off of and to discuss *how* properties emerge in nanoclusters with. There are few topics in chemistry that don't at least pique his interest, and I'm better for getting to work with him. He's a good enough scientist that I almost don't mind that he will metastasize to any unoccupied bench space, steal your squirt bottles, and randomly leave stuff in your hood.

Dr. Scott Compel – I wouldn't try to teach Scott a complicated board game again, but it's hard to think of a more meticulously thorough coworker. Scott was great at helping me think of details I hadn't considered and experiments that had not occurred to me. Scott is also fantastic at putting me in my place when I have it coming.

So, in conclusion, I have probably missed any number of people who deserve a thorough accounting here, but I have only so much patience for trying to think of them. If you feel you should be acknowledged by name, but have not been, please feel free to make up some mild praise for yourself and proceed as if it appeared above. I would like to take a moment to specifically deny any such praise to Creepy Jeff, who sucked and we all hated.

Blood for the blood god, skulls for the skull throne!

AUTOBIOGRAPHY

I was born in Houston, TX and grew up mostly in the Portland, OR suburb of Lake Oswego. My parents are good people who did a good job raising us. I have had few difficulties in life that were not, in some way, self-inflicted. In 2000 I graduated from Lake Oswego High School. Later that same year I enrolled at the University of Oregon, which I attended from 2000 to 2004, obtaining a Bachelor of Science degree in Economics. This is widely viewed as a youthful mistake. In the fall of 2004, having little money and no job, I moved in with my parents in San Antonio, TX where I soon took a job as a bank analyst. This was also a mistake – the bank analyst thing, living with my folks was fine. By 2007 I was bored of my job and looking for an escape. I enrolled part time at the University of Texas – San Antonio to explore other educational options. In 2009 I quit my job at the bank and pursued a Bachelor of Science in Chemistry, graduating in 2011. I was fortunate during my time at UTSA to do some research in the laboratory of Dr. Douglas Frantz. In fall of 2011 I began my graduate career at Colorado State University, starting off as an organic chemist and finishing as a nanoparticle chemist who knows a surprising amount of organic chemistry. My next adventure involves polymers, quantum dots, and light/matter interactions. In my spare time, I plan to awaken at least one Elder God. *Ph'nglui mglw'nafh Cthulhu R'lyeh wgah'nagl fhtagn.*

DEDICATION

For the people who believed in me, and a few of the ones who didn't.

TABLE OF CONTENTS

CHAPTER 1: AN INTRODUCTION TO GOLD NANOPARTICLES AND CLUSTERS

1.1 Synopsis

Since the introduction of the Brust-Schiffrin synthesis in 1994,[1-2] and the later fully solved crystal structures,[3-6] gold nanoclusters have been an active area of inquiry in nanoscience. Nanoclusters are distinct from nanoparticles in several important ways, and have been reported as catalysts for organic reactions. The mechanism of the Brust-Schiffrin synthesis, however, remains somewhat mysterious. Herein these important factors are discussed in detail to provide context for the work that follows.

1.2 Gold Nanoparticles vs. Gold Nanoclusters

Metal-containing species can best be thought of as existing on a continuum with small, monometallic complexes at one end and bulk metals at the other. Between these two extremes a variety of species are known: multimetallic cage complexes, nanoclusters, nanoparticles, mesoscale nanomaterials, etc. The body of this work concerns the synthesis and behavior of thiolated gold nanoclusters, which are distinct from larger nanoparticles in several ways.

Generally speaking, nanoparticles are defined by their size and dispersity (e.g. 5 nm ± 1 nm), with the explicit chemical formula of any particle being unknown. In contrast, gold nanoclusters (AuNCs) are molecules with known formulae (e.g. $Au_{25}(SR)_{18}$, $Au_{38}(SR)_{24}$, $Au_{102}(SR)_{44}$, $Au_{144}(SR)_{60}$).[6-10] Additionally, unlike larger gold nanoparticles, nanoclusters have molecular electronic transitions rather than surface plasmons.[11] Due to these unique structural and electronic properties, gold nanoclusters have been widely investigated for a variety of applications.[12-16]

1.3 Background for AuNC Catalysis

The work in the following chapters first investigates the catalytic performance of $Au_{25}(SR)_{18}$ nanoclusters for the oxidation of styrene, as shown in Figure 1.1.

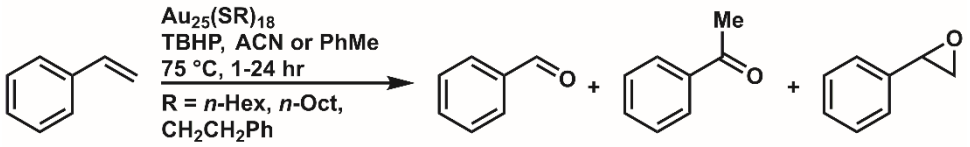

Figure 1.1. Styrene oxidation by Au/TBHP

With a wealth of Au_{25}-catalyzed organic reactions in the literature, further understanding of their performance & mechanistic details seemed worthwhile.[17-24] The styrene oxidation reaction was chosen owing to the ease of identifying the products & evaluating reaction outcomes. We were initially surprised by the poor performance of the literature conditions, and the finding that the decomposition products are the active catalysts. However, given the heavily oxidizing reaction conditions and lack of other control experiments in the literature, perhaps we should have anticipated these results.

In relation to catalytic performance, the oxidative stability of $Au_{25}(SR)_{18}$ clusters ligated by organo-soluble thiolates is often based on experiments using aqueous H_2O_2 and a solution of clusters in toluene.[25-26] Given the poor solubility of aqueous H_2O_2 in toluene, these experiments do not give conditions analogous to those in catalytic reactions. The use of a soluble oxidant such as *tert*-butyl hydroperoxide (TBHP) is necessary to give reliable results in oxidative decomposition experiments. As such, work relying solely on H_2O_2/toluene experiments to claim oxidative stability for AuNCs should be discounted.

A further discussion of the merits of pursuing catalysis with AuNCs is warranted here, considering the implications for the field. AuNCs, with or without adsorption on a supporting substrate, have been reported as efficacious catalysts for a number of reactions including reduction

of nitro groups,[27-28] the above styrene oxidation,[29] and several others that have been recently reviewed.[16] In each case, however, the synthetic chemist has any number of more attractive options.[30]

Figure 1.2 summarizes the severity of this issue, showing the reaction conditions for AuNC-based reactions above the reaction arrow, and the alternative means below each product. Every reaction listed in Figure 1.2 is performed regularly by practicing synthetic chemists, on a wide variety of substrates, and most have been for some time. The alternative methods shown are more selective than the AuNC conditions, cheaper, better yielding, and do not involve the synthesis of AuNCs to access the pre-catalyst. It seems that many of the researchers insistent upon using AuNCs in catalytic reactions are, perhaps, unaware of the well-established organic literature.

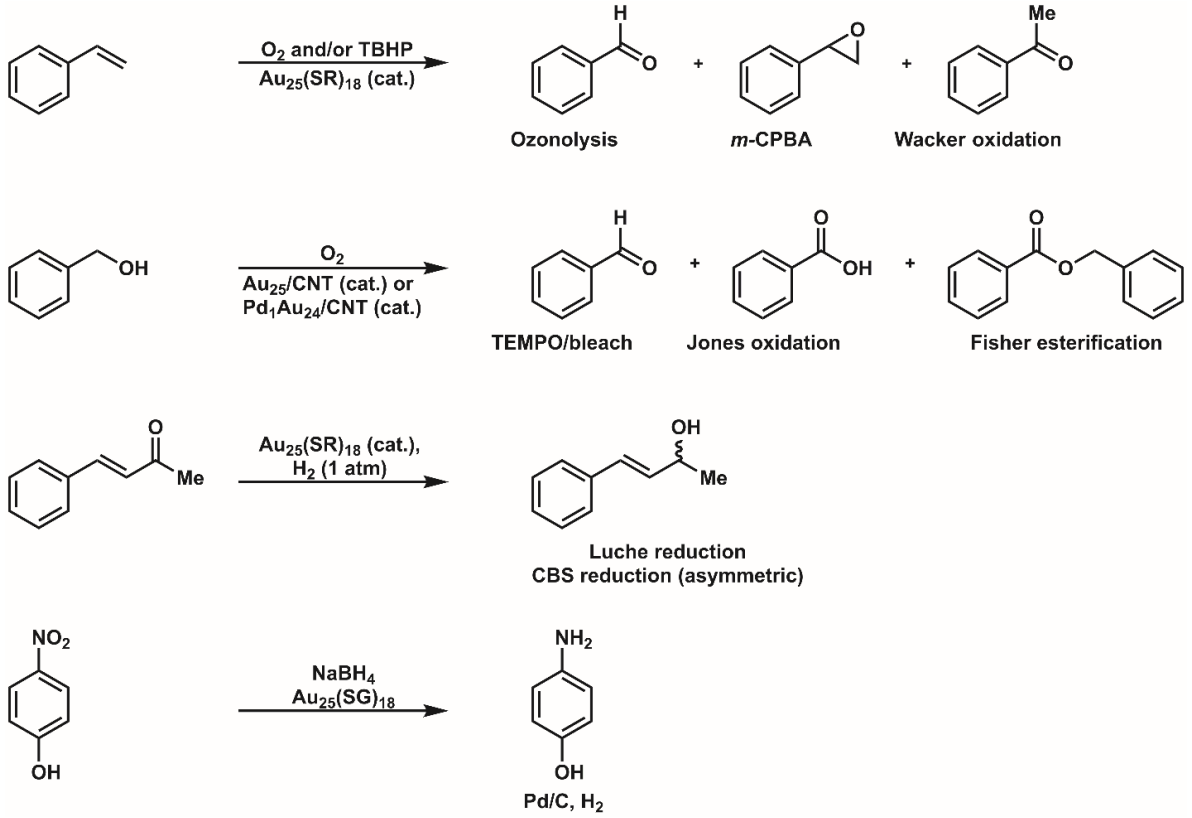

Figure 1.2. AuNC catalysis with alternative methods

While some examples of AuNCs proving useful in catalytic reactions exist,[31] most provide little, if any, synthetic utility. Furthermore, experimental investigations are lacking, with several authors claiming DFT calculations "prove" the catalytic importance of the intact cluster.[20, 22, 26, 32-34] One hopes that as the field matures the quality of these investigations improves, or they are left behind entirely for more productive areas of inquiry.

1.4 The Brust-Schiffrin Synthesis

Despite lack of catalytic utility, AuNCs still hold promise across many applications.[12-13, 35-43] A predictable, understood synthesis is therefore important to accessing clusters of desired size.

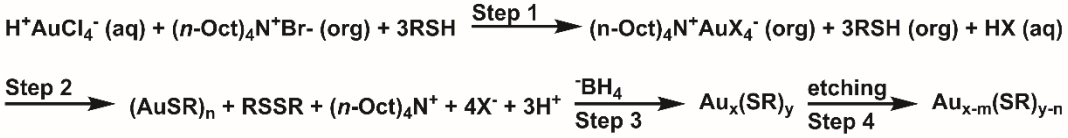

Figure 1.3. Brust-Schiffrin reaction scheme

The various known sizes of thiolated gold nanoclusters are most often synthesized by variations on a method first reported by Brust in 1994.[1]

This synthesis is comprised of four distinct steps, as shown in Figure 1.3. First, a gold salt, most often $HAuCl_4 \bullet 3H_2O$, is dissolved in water, then phase-transferred to an organic solvent (toluene in the initial report) by tetraoctylammonium bromide (TOAB). The aqueous layer is then removed, and the desired thiol is then added, forming an Au(I)-thiolate species with the excess thiol serving to reduce Au(III) to Au(I), giving a disulfide as the byproduct. After Au(III) has been completely reduced to Au(I), a cold aqueous solution of $NaBH_4$ is added, giving a fast reduction to a polydisperse mixture of Au particles & clusters. The reaction is then allowed to proceed until a thermodynamically stable cluster size is reached. A 1995 follow-up, also by Brust, omits the first step and dissolves the gold salt directly in a TOAB solution in organic solvent.[2] By adjusting reaction parameters such as solvent composition, equivalents of thiol to Au, equivalents of $NaBH_4$ to Au, and reaction time the reaction can be tuned to give a variety of cluster sizes.[44-49] The work

contained herein focuses on the synthesis of $Au_{25}(SR)_{18}$ and $Au_{102}(SR)_{44}$, the former in both organic and aqueous solvents, as well-defined systems for understanding mechanistic aspects of the Brust-Schiffrin method.

1.5 Background of Mechanistic Investigations into the Brust-Schiffrin Method

Fortunately, we are far from the first group with an interest in understanding the Brust-Schiffrin method. It is easiest to present these earlier investigations in accordance with each of the steps presented in Figure 1.3. In the case of the two-phase method, Kumar has recently investigated the way in which TOAB catalyzes transfer of the Au(III) salt into the organic phase.[50] While in the monophasic synthesis complexation of the TOAB to Au(III) is the only route for solubilizing the salt in the organic phase,[2] the two-phase synthesis could in principle proceed through either complexation or the formation of inverse micelles.[51-56] Through a variety of techniques including ^{1}H NMR, small-angle X-ray scattering (SAXS), and light scattering, Kumar convincingly demonstrates that reverse micelle formation is critical for phase transfer in the two-phase Brust-Schiffrin method.

The next critical step in the synthesis is formation of the Au(I)-thiolate precursor. Lennox and coworkers have thoroughly investigated this process.[52] By titrating in thiol and monitoring the reduction of Au(III) to Au(I) by UV/Visible spectroscopy, Lennox shows that the reduction is complete after addition of two equivalents of thiol to Au are added. This result demonstrates that in the two-phase Brust-Schiffrin synthesis the previously assumed M(I)-thiolate polymer is not an intermediate species. However, this result holds only for synthesis in non-polar solvents such as toluene. In single-phase synthesis performed in more polar solvents such as THF, or in protic solvents like water, methanol, or ethanol, it is possible that polymeric species do serve as precursors to cluster & particle formation. Lennox notes this, as it is consistent with results previously reported.[57-61]

The last procedural step in the Brust-Schiffrin synthesis, whether in a one or two-phase process is addition of the $NaBH_4$ reductant. Although procedurally a single step, it is best viewed as two distinct mechanistic steps: 1) an initial reduction to polydisperse AuNPs and 2) an etching step that converts the polydisperse precursors to the desired nanocluster. The initial reduction step has been evaluated from a theoretical perspective by Aikens.[62]

By examining the addition of 1-4 electrons to various 1:1 complexes of formula $Au_n(SCH_3)_m$ (n = 3-7, m = 3-7),[63] Aikens investigated the dissociation of $^-SCH_3$ from Au and electron-driven Au–Au bond formation. Addition of a single electron to each of the complexes investigated led to slight structural changes, but no dissociation of thiolate anions. Additionally, in the gas phase simulations initially employed, three electrons are required to cause dissociation of the gold-thiolate complexes. However, rather than the Au(0) required for particle formation, Au^- and anionic gold-thiolate complexes are formed. This holds for both cyclic and acyclic gold-thiolate precursors examined. Models using explicit solvent, in this case water and toluene, indicate that dissociation can occur with addition of two or three electrons depending on the exact nature of the precursor species examined. The dissociation products remain Au^- and anionic gold-thiolate complexes, and as such single electron processes seem unlikely to be involved in the mechanism as Au would have to be oxidized somehow under the highly reductive reaction conditions to give Au(0) and form particles.

By contrast, modeling the addition of hydride from $NaBH_4$ – its common mode of reduction being a hydride donor – will cause release of $HSCH_3$ and the formation of an Au–Au bond, depending on the angle of approach. Once the first Au–Au bond has formed, the resulting cyclic complexes can dimerize to give larger Au clusters. This gives a reasonable picture for initial particle growth.

An overall mechanism involving continuous nucleation and growth was recently proposed by Kumar.[64] While this work does present compelling evidence for continuous nucleation and growth in the formation of Au colloids during the Brust-Schiffrin synthesis, the authors specifically exclude any investigation into magic-number clusters from their work. Because of this, a comprehensive understanding of AuNC formation under Brust-Schiffrin conditions is lacking.

The observation that the Brust-Schiffrin synthesis fails under anaerobic atmosphere was unexplained prior to our work as reported in chapters 3 and 4. Murray forwarded a hypothesis invoking decomposition of the THF solvent, but offered no experimental evidence.[65] With this in mind we undertook a series of experiments to isolate and understand the oxygen-dependent step in the Brust-Schiffrin synthesis. Chapters 3 and 4 explain our results in detail, but we were able to develop a fairly comprehensive picture of oxygen's role in the synthesis.

REFERENCES

1. Brust, M.; Walker, M.; Bethell, D.; Schiffrin, D. J.; Whyman, R. Synthesis of thiol-derivatised gold nanoparticles in a two-phase liquid-liquid system. *J. Chem. Soc., Chem. Commun.* **1994**, 801-802.

2. Brust, M.; Fink, J.; Bethell, D.; Schiffrin, D. J.; Kiely, C. Synthesis and reactions of functionalized gold nanoparticles. *J. Chem. Soc., Chem. Commun.* **1995**, 1655-6.

3. Heaven, M. W.; Dass, A.; White, P. S.; Holt, K. M.; Murray, R. W. Crystal Structure of the Gold Nanoparticle [N(C8H17)4][Au25(SCH2CH2Ph)18]. *J. Am. Chem. Soc.* **2008**, *130*, 3754-3755.

4. Crasto, D.; Barcaro, G.; Stener, M.; Sementa, L.; Fortunelli, A.; Dass, A. Au24(SAdm)16 nanomolecules: X-ray crystal Structure, theoretical analysis, adaptability of adamantane ligands to form Au23(SAdm)16 and Au25(SAdm)16, and its relation to Au25(SR)18. *J. Am. Chem. Soc.* **2014**, *136*, 14933-14940.

5. Das, A.; Li, T.; Li, G.; Nobusada, K.; Zeng, C.; Rosi, N. L.; Jin, R. Crystal structure and electronic properties of a thiolate-protected Au24 nanocluster. *Nanoscale* **2014**, *6*, 6458-6462.

6. Jadzinsky, P. D.; Calero, G.; Ackerson, C. J.; Bushnell, D. A.; Kornberg, R. D. Structure of a thiol monolayer-protected gold ganoparticle at 1.1 Å resolution. *Science* **2007**, *318*, 430-433.

7. Parker, J. F.; Fields-Zinna, C. A.; Murray, R. W. The Story of a Monodisperse Gold Nanoparticle: Au25L18. *Acc. Chem. Res.* **2010**, *43*, 1289-1296.

8. Donkers, R. L.; Lee, D.; Murray, R. W. Synthesis and isolation of the molecule-like cluster Au38(PhCH2CH2S)24. *Langmuir* **2004**, *20*, 1945-1952.

9. Lopez-Acevedo, O.; Akola, J.; Whetten, R. L.; Gronbeck, H.; Hakkinen, H. Structure and Bonding in the Ubiquitous Icosahedral Metallic Gold Cluster Au144(SR)60. *J. Phys. Chem. C* **2009**, *113*, 5035-5038.

10. Qian, H.; Jin, R. Ambient synthesis of Au144(SR)60 nanoclusters in methanol. *Chem. Mater.* **2011**, *23*, 2209-2217.

11. Walter, M.; Akola, J.; Lopez-Acevedo, O.; Jadzinsky, P. D.; Calero, G.; Ackerson, C. J.; Whetten, R. L.; Gronbeck, H.; Hakkinen, H. A unified view of ligand-protected gold clusters as superatom complexes. *Proc. Natl. Acad. Sci. U. S. A.* **2008**, *105*, 9157-9162.

12. Bowman, M.-C.; Ballard, T. E.; Ackerson, C. J.; Feldheim, D. L.; Margolis, D. M.; Melander, C. Inhibition of HIV fusion with multivalent gold nanoparticles. *J. Am. Chem. Soc.* **2008**, *130*, 6896-6897.

13. Wong, O. A.; Hansen, R. J.; Ni, T. W.; Heinecke, C. L.; Compel, W. S.; Gustafson, D. L.; Ackerson, C. J. Structure-activity relationships for biodistribution, pharmacokinetics, and excretion of atomically precise nanoclusters in a murine model. *Nanoscale* **2013**, *5*, 10525-10533.

14. Heinecke, C. L.; Ackerson, C. J. Preparation of gold nanocluster bioconjugates for electron microscopy. *Methods. Mol. Biol.* **2013**, *950*, 293-311.

15. Salorinne, K.; Malola, S.; Wong, O. A.; Rithner, C. D.; Chen, X.; Ackerson, C. J.; Hakkinen, H. Conformation and dynamics of the ligand shell of a water-soluble Au102 nanoparticle. *Nat. Commun.* **2016**, *7*, 10401.

16. Li, G.; Jin, R. Atomically Precise Gold Nanoclusters as New Model Catalysts. *Acc. Chem. Res.* **2013**, *46*, 1749-1758.

17. Landman, U.; Yoon, B.; Zhang, C.; Heiz, U.; Arenz, M. Factors in gold nanocatalysis: oxidation of CO in the non-scalable size regime. *Top. Catal.* **2007**, *44*, 145-158.

18. Zhu, Y.; Qian, H.; Jin, R. An Atomic-Level Strategy for Unraveling Gold Nanocatalysis from the Perspective of Aun(SR)m Nanoclusters. *Chem. Eur. J.* **2010**, *16*, 11455-11462.

19. Andreiadis, E. S.; Vitale, M. R.; Mezailles, N.; Le Goff, X.; Le Floch, P.; Toullec, P. Y.; Michelet, V. Chiral undecagold clusters: synthesis, characterization and investigation in catalysis. *Dalton Trans.* **2010**, *39*, 10608-10616.

20. Liu, J.; Krishna, K. S.; Losovyj, Y. B.; Chattopadhyay, S.; Lozova, N.; Miller, J. T.; Spivey, J. J.; Kumar, C. S. S. R. Ligand-Stabilized and Atomically Precise Gold Nanocluster Catalysis: A Case Study for Correlating Fundamental Electronic Properties with Catalysis. *Chem. Eur. J.* **2013**, *19*, 10201-10208.

21. Yang, H.; Wang, Y.; Lei, J.; Shi, L.; Wu, X.; Makinen, V.; Lin, S.; Tang, Z.; He, J.; Hakkinen, H., et al. Ligand-Stabilized Au13Cux (x = 2, 4, 8) Bimetallic Nanoclusters: Ligand Engineering to Control the Exposure of Metal Sites. *J. Am. Chem. Soc.* **2013**, *135*, 9568-9571.

22. Li, G.; Jiang, D.-e.; Kumar, S.; Chen, Y.; Jin, R. Size Dependence of Atomically Precise Gold Nanoclusters in Chemoselective Hydrogenation and Active Site Structure. *ACS Catal.* **2014**, 2463-2469.

23. Yamazoe, S.; Koyasu, K.; Tsukuda, T. Nonscalable Oxidation Catalysis of Gold Clusters. *Acc. Chem. Res.* **2014**, *47*, 816-824.

24. Lavenn, C.; Demessence, A.; Tuel, A. Atomically well-defined Au25(SR)17/18 nanoclusters deposited on silica supports for the aerobic epoxidation of trans-stilbene. *Catal. Today* **2014**, *235*, 72-78.

25. Jung, J.; Kang, S.; Han, Y.-K. Ligand effects on the stability of thiol-stabilized gold nanoclusters: Au25(SR)18-, Au38(SR)24, and Au102(SR)44. *Nanoscale* **2012**, *4*, 4206-4210.

26. Jin, R. Atomically precise metal nanoclusters: stable sizes and optical properties. *Nanoscale* **2015**, *7*, 1549-1565.

27. Shivhare, A.; Ambrose, S. J.; Zhang, H.; Purves, R. W.; Scott, R. W. J. Stable and recyclable Au25 clusters for the reduction of 4-nitrophenol. *Chem. Commun.* **2013**, *49*, 276-278.

28. Li, G.; Zeng, C.; Jin, R. Thermally Robust Au99(SPh)42 Nanoclusters for Chemoselective Hydrogenation of Nitrobenzaldehyde Derivatives in Water. *J. Am. Chem. Soc.* **2014**, *136*, 3673-3679.

29. Lin, S.; Pei, Y. Mechanistic Insight into the Styrene-Selective Oxidation on Subnanometer Gold Clusters (Au16-Au20, Au27, Au28, Au30, and Au32-Au35): A Density Functional Theory Study. *J. Phys. Chem. C* **2014**, *118*, 20346-20356.

30. Kurti, L.; Czako, B. *Strategic Applications of Named Reactions in Organic Synthesis*. Elsevier Academic Press: Boston, 2005; p 864.

31. Chakraborty, S.; Babanova, S.; Rocha, R. C.; Desireddy, A.; Artyushkova, K.; Boncella, A. E.; Atanassov, P.; Martinez, J. S. A Hybrid DNA-Templated Gold Nanocluster For Enhanced Enzymatic Reduction of Oxygen. *J. Am. Chem. Soc.* **2015**, *137*, 11678-11687.

32. Zhu, Y.; Qian, H.; Drake, B. A.; Jin, R. Atomically Precise Au25(SR)18 Nanoparticles as Catalysts for the Selective Hydrogenation of α,β-Unsaturated Ketones and Aldehydes. *Angew. Chem. Int. Ed.* **2010**, *49*, 1295-1298.

33. Xu, Q.; Kumar, S.; Jin, S.; Qian, H.; Zhu, M.; Jin, R. Chiral 38-gold-atom nanoclusters. Synthesis and chiroptical properties. *Small* **2014**, *10*, 1008-1014.

34. Deng, H.; Wang, S.; Jin, S.; Yang, S.; Xu, Y.; Liu, L.; Xiang, J.; Hu, D.; Zhu, M. Active metal (cadmium) doping enhanced the stability of inert metal (gold) nanocluster under O2

atmosphere and the catalysis activity of benzyl alcohol oxidation. *Gold Bull. (Berlin, Ger.)* **2015**, *48*, 161-167.

35. Bresee, J.; Maier, K. E.; Melander, C.; Feldheim, D. L. Identification of antibiotics using small molecule variable ligand display on gold nanoparticles. *Chem. Commun.* **2010**, *46*, 7516-7518.

36. Bresee, J.; Maier, K. E.; Boncella, A. E.; Melander, C.; Feldheim, D. L. Growth inhibition of Staphylococcus aureus by mixed monolayer gold nanoparticles. *Small* **2011**, *7*, 2027-2031.

37. Gifford, J. C.; Bresee, J.; Carter, C. J.; Wang, G.; Melander, R. J.; Melander, C.; Feldheim, D. L. Thiol-modified gold nanoparticles for the inhibition of Mycobacterium smegmatis. *Chem. Commun.* **2014**, *50*, 15860-15863.

38. Bresee, J.; Bond, C. M.; Worthington, R. J.; Smith, C. A.; Gifford, J. C.; Simpson, C. A.; Carter, C. J.; Wang, G.; Hartman, J.; Osbaugh, N. A., et al. Nanoscale structure-activity relationships, mode of action, and biocompatibility of gold nanoparticle antibiotics. *J. Am. Chem. Soc.* **2014**, *136*, 5295-5300.

39. Huang, C.-C.; Chiang, C.-K.; Lin, Z.-H.; Lee, K.-H.; Chang, H.-T. Bioconjugated Gold Nanodots and Nanoparticles for Protein Assays Based on Photoluminescence Quenching. *Anal. Chem.* **2008**, *80*, 1497-1504.

40. Bassu, M.; Strambini, M. L.; Barillaro, G.; Fuso, F. Light emission from silicon/gold nanoparticle systems. *Appl. Phys. Lett.* **2010**, *97*, 143113/1-143113/3.

41. Wu, Z.; Jin, R. On the Ligand's Role in the Fluorescence of Gold Nanoclusters. *Nano Lett.* **2010**, *10*, 2568-2573.

42. Arachchige, I. U.; Szymanski, P. L.; Ivanov, S. A. *Electrochemical routes to luminescent gold nanoclusters*, Presented at the National Meeting of the American Chemical Society, 2010; INOR-985.

43. Zheng, J.; Zhou, C.; Yu, M.; Liu, J. Different sized luminescent gold nanoparticles. *Nanoscale* **2012**, *4*, 4073-4083.

44. Hutchings, G. J.; Brust, M.; Schmidbaur, H. Gold-an introductory perspective. *Chem. Soc. Rev.* **2008**, *37*, 1759-1765.

45. Dass, A.; Holt, K.; Parker, J. F.; Feldberg, S. W.; Murray, R. W. Mass Spectrometrically Detected Statistical Aspects of Ligand Populations in Mixed Monolayer Au25L18 Nanoparticles. *J. Phys. Chem. C* **2008**, *112*, 20276-20283.

46. Toikkanen, O.; Ruiz, V.; Ronnholm, G.; Kalkkinen, N.; Liljeroth, P.; Quinn, B. M. Synthesis and Stability of Monolayer-Protected Au38 Clusters. *J. Am. Chem. Soc.* **2008**, *130*, 11049-11055.

47. Lennox, R. B.; Goulet, P. J.; Milette, J.; Kassam, A.; Laferriere, M.; Fuller, E.; Reven, L. G. *Perspectives on gold nanoparticle synthesis and stabilization*, Presented at the 2010; MATNANO-5.

48. Zhao, P.; Li, N.; Astruc, D. State of the art in gold nanoparticle synthesis. *Coord. Chem. Rev.* **2013**, *257*, 638-665.

49. Wang, T.; Jiao, Y.; Chai, Q.; Yu, X. Gold Nanoparticles: Synthesis and Biological Applications. *Nano LIFE* **2015**, *5*, 1542007.

50. Perala, S. R. K.; Kumar, S. On the Mechanism of Phase Transfer Catalysis in Brust-Schiffrin Synthesis of Metal Nanoparticles. *Langmuir* **2013**, *29*, 14756-14762.

51. Hostetler, M. J.; Wingate, J. E.; Zhong, C.-J.; Harris, J. E.; Vachet, R. W.; Clark, M. R.; Londono, J. D.; Green, S. J.; Stokes, J. J.; Wignall, G. D., et al. Alkanethiolate Gold Cluster Molecules with Core Diameters from 1.4 to 5.2 Nanometers: Core and Monolayer Properties as a Function of Core Size. *Langmuir* **1998**, *14*, 17-30.

52. Goulet, P. J. G.; Lennox, R. B. New insights into Brust−Schiffrin metal manoparticle synthesis. *J. Am. Chem. Soc.* **2010**, *132*, 9582-9584.

53. Li, Y.; Zaluzhna, O.; Tong, Y. Y. J. Critical role of water and the structure of inverse micelles in the Brust-Schiffrin synthesis of metal nanoparticles. *Langmuir* **2011**, *27*, 7366-7370.

54. Li, Y.; Zaluzhna, O.; Xu, B.; Gao, Y.; Modest, J. M.; Tong, Y. Y. J. Mechanistic insights into the Brust-Schiffrin two-phase synthesis of organo-chalcogenate-protected metal nanoparticles. *J. Am. Chem. Soc.* **2011**, *133*, 2092-2095.

55. Li, Y.; Zaluzhna, O.; Xu, B.; Gao, Y.; Modest, J. M.; Tong, Y. Y. J. Mechanistic Insights into the Brust-Schiffrin Two-Phase Synthesis of Organo-chalcogenate-Protected Metal Nanoparticles [Erratum to document cited in CA154:269681]. *J. Am. Chem. Soc.* **2012**, *134*, 6498.

56. Li, Y.; Zaluzhna, O.; Zangmeister, C. D.; Allison, T. C.; Tong, Y. J. Different Mechanisms Govern the Two-Phase Brust-Schiffrin Dialkylditelluride Syntheses of Ag and Au Nanoparticles. *J. Am. Chem. Soc.* **2012**, *134*, 1990-1992.

57. Wu, Z.; Suhan, J.; Jin, R. *J. Mater. Chem.* **2009**, *19*, 622.

58. Al-Sa'ady, A. K. H.; McAuliffe, C. A.; Parish, R. V.; Sandbank, J. A. *Inorg. Synth.* **1985**, *23*, 191.

59. Schaaff, T. G.; Knight, G.; Shafigullin, M. N.; Borkman, R. F.; Whetten, R. L. *J. Phys. Chem. B* **1998**, *102*, 10643.

60. Susha, A. S.; Ringler, M.; Ohlinger, A.; Paderi, M.; LiPira, N.; Carotenuto, G.; Rogach, A. L.; Feldmann, J. *Chem. Mater.* **2008**, *20*, 6169.

61. Reilly, S. M.; Krick, T.; Dass, A. *J. Phys. Chem. C* **2010**, *114*, 741.

62. Barngrover, B. M.; Aikens, C. M. Electron and Hydride Addition to Gold(I) Thiolate Oligomers: Implications for Gold-Thiolate Nanoparticle Growth Mechanisms. *J. Phys. Chem. Lett.* **2011**, *2*, 990-994.

63. These calculations were done at the BP86/TZP level of theory.

64. Perala, S. R. K.; Kumar, S. On the Mechanism of Metal Nanoparticle Synthesis in the Brust-Schiffrin Method. *Langmuir* **2013**, *29*, 9863-9873.

65. Parker, J. F.; Weaver, J. E. F.; McCallum, F.; Fields-Zinna, C. A.; Murray, R. W. Synthesis of monodisperse [Oct4N+][Au25(SR)18-] nanoparticles, with some mechanistic observations. *Langmuir* **2010**, *26*, 13650-13654.

CHAPTER 2: DECOMPOSITION OF $Au_{25}(SR)_{18}$ CLUSTERS IN A CATALYTIC CONTEXT*

2.1 Synopsis

Gold nanoparticle catalysis of chemical transformations has emerged as a subject of intense interest over the past decade. In particular, $Au_{25}(SR)_{18}$ has emerged as a model catalyst. In an effort to investigate their potential as intact, homogeneous, unsupported catalysts, we have discovered that $Au_{25}(SR)_{18}$ clusters are not stable in oxidizing conditions reported for catalytic styrene oxidation. Further investigation suggests that the active catalytic species is an Au(I) species resulting from oxidative decomposition of the starting gold cluster. This conclusion appears independent of R-group on thiolate-ligated $Au_{25}(SR)_{18}$ clusters.

2.2 Introduction

Due in part to the noble nature of bulk gold, the advent of gold based catalytic transformations is recent.[1-2] The work of Hutchings and Haruta established selective oxidation of hydrocarbons and low-temperature CO oxidation by supported gold clusters and nanoparticles.[3-4] A variety of other reactions catalysed by ligated gold nanoclusters are also recently investigated, with both phosphine and thiolate protected clusters proposed as catalytic species.[5] In supported catalysis, the ligands are often removed by calcination.[6]

Of all ligated clusters, the $Au_{25}(SR)_{18}$ nanocluster stands out as a widely studied model system for catalysis.[6] Since its initial discovery,[7] the $Au_{25}(SR)_{18}$ cluster has been synthesized with an array of R groups, including saturated alkanes, aromatic species (e.g. 4-mercaptobenzoic acid, 4-bromothiophenol), phenylethane (R = CH_2CH_2Ph), and small polypeptides like glutathione, with

* The work presented herein is published in *Chemical Communications*. Timothy A. Dreier's contributions include experimental design, data gathering & interpretation, and preparation of the manuscript. *Chem. Commun.* **2015**, *51*, 1240-1243.

syntheses reproduced in many labs.[8-15] $Au_{25}(SR)_{18}$ clusters are isolable and stable in 3 different charge states: -1, 0, and +1 with crystal structures for each represented in the literature.[10, 14-20]

$Au_{25}(SR)_{18}$ clusters calcinated on support are reported for the 1,2-reduction of α,β-unsaturated ketones, reduction of aryl nitro groups, and oxidation of alkenes.[6, 21-22] $Au_{25}(SR)_{18}$ clusters adsorbed on support without calcination are reported as effective catalysts for styrene oxidation.[23] In addition, there are scattered reports of homogeneous catalysis using intact $Au_{25}(SR)_{18}$ clusters.[24-25]

We report here an initial reinvestigation of homogeneous catalysis with $Au_{25}(SR)_{18}$ clusters, stemming from our longstanding interest in the properties of small gold clusters.[26-31] Homogeneous catalysis often offers a distinct benefit with respect to product selectivity, and affords the opportunity to take advantage the unique properties of $Au_{25}(SR)_{18}$ clusters without the practical and conceptual complexity introduced by support and calcination.

2.3 Results and Discussion

We began our investigation by examining oxidative cleavage of styrene (Figure 2.1). This model reaction was selected for several reasons: it has been reported by multiple research groups, the starting materials are inexpensive, and the product mixtures are well-suited for quantitative analysis by gas chromatography.[6, 23, 32]

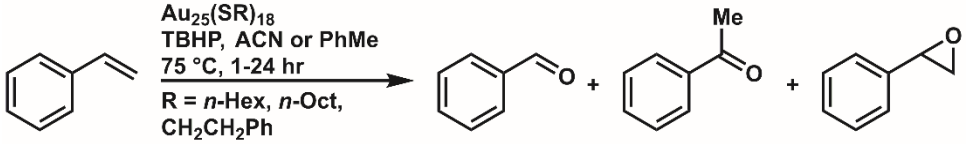

Figure 2.1. Styrene Oxidation

We found that while we could reproduce the catalytic products previously reported, $Au_{25}(SR)_{18}$ clusters are not stable to oxidizing reaction conditions similar to those reported by Jin.[21] Further investigation suggests that the active catalytic species is an Au(I) species that results from oxidative decomposition of $Au_{25}(SR)_{18}$. This conclusion is supported by comparison of catalytic

activity of $Au_{25}(SR)_{18}$, the Au–thiol polymer precursor, and $Au_{25}(SR)_{18}$ decomposition products. Kinetic catalyst poisoning experiments also suggest a mononuclear gold species as the active catalyst, and X-ray photoelectron spectroscopy (XPS) data also point toward a mononuclear Au(I) species.

We began our investigation into the catalytic behaviour of homogeneous $Au_{25}(SR)_{18}$ clusters by replicating results previously reported.[6, 23] Figure 2.2 shows the GC trace from this initial experiment, with the expected product peaks indicated. After 24 h at 75 °C in $CHCl_3$, we observed product distributions similar to those previously reported, although at lower conversion. During the course of these early experiments, we observed little or no difference in conversion between 6 and 24 hours reaction time, and also no differences between reactions run under ambient visible light or in the darkness.

To establish cluster lifetime under the oxidative reaction conditions – typically employing 167 equivalents of t-butylhydrogenperoxide (TBHP) to Au25(SR)18 cluster – we exposed the clusters to TBHP (167 equiv. to Au25) at 37 °C and monitored the resulting mixture by ultraviolet/visible spectroscopy.

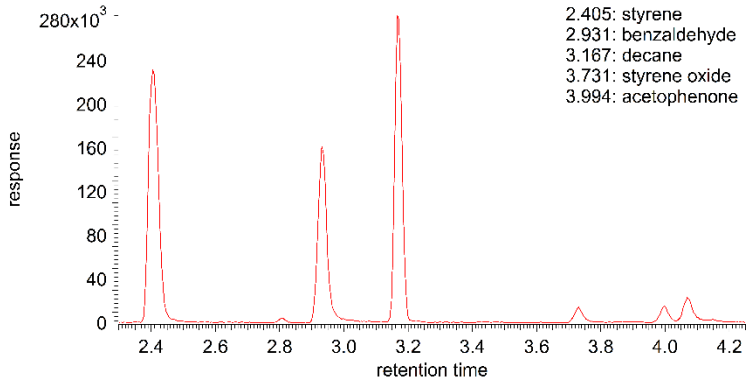

Figure 2.2. Styrene Oxidation by $Au_{25}(Sn\text{-}Oct)_{18}$. Decane peak results from TBHP being used as a 5.5 M solution in decane.

Figure 2.2 shows decomposition of $Au_{25}(SR)_{18}$ as judged by the disappearance of the characteristic absorbance peaks of the cluster. An absorbance peak at 400 nm is one characteristic of $[Au_{25}(SR)_{18}]^0$ spectra; this and all other distinctive features disappear within 5 minutes even at the reduced temperature. Decomposition occurs before significant conversion to product is seen, even at elevated temperature (Appendix A, Figure A.79). This result led us to consider the possibility that the active catalytic species in styrene oxidation was not the cluster itself, but rather oxidative decomposition products of $Au_{25}(SR)_{18}$. Oxidative decomposition of Au clusters by H_2O_2 and iodine have been reported previously,[33-34] and as such decomposition by a similarly strong oxidant, TBHP, is unsurprising.

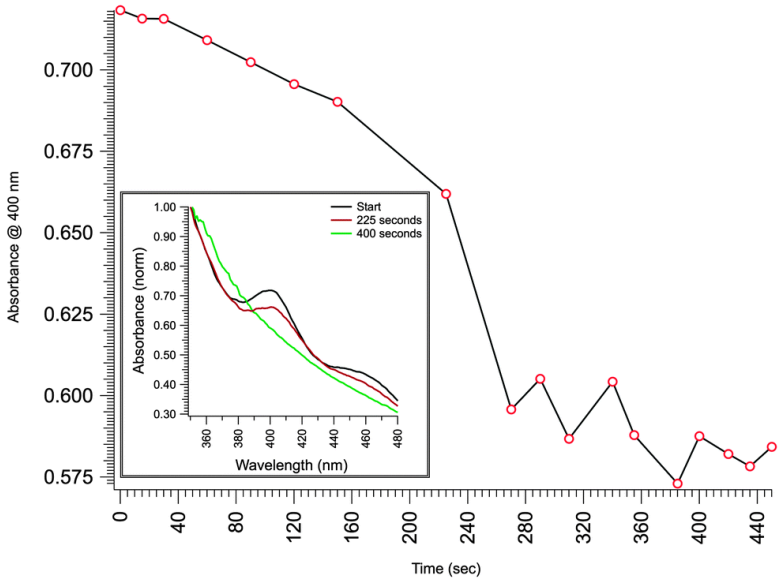

Figure 2.3. Oxidative decomposition of $[Au_{25}(SCH_2CH_2Ph)_{18}]^0$

To interrogate the active Au species in this catalytic styrene oxidation, independent of their origin, we compared catalysis by initially intact $Au_{25}(SR)_{18}$, $Au_{25}(SR)_{18}$ oxidatively decomposed prior to use as a catalyst, and the Au(I)–SR oligomers or polymers that are a precursor to $Au_{25}(SR)_{18}$ during its synthesis. To decompose the $Au_{25}(SR)_{18}$ before the catalytic reaction we

added TBHP to a solution of $Au_{25}(SR)_{18}$, heated for 10 minutes at 75 °C, allowed the reaction to cool to room temperature, added styrene, and reheated to 75 °C.

As can be seen in Table 2.1 (entries 3 and 6), oxidatively decomposing the $Au_{25}(PET)_{18}$ cluster before beginning the catalytic reaction results in a more active catalyst. We observed a three-fold increase in conversion to benzaldehyde at 1 h with $Au_{25}(PET)_{18}$.[33] Further studies using n-hexanethiol and n-octanethiol ligated clusters gave similar results (Table 2.1, entries 7–16).

Table 2.1. Cluster, polymer and decomposition products

Entry	Starting gold species	Solvent	%Conversion to PhCHO (1 hr)
1	$[Au_{25}(PET)_{18}]^0$	PhMe	2.30 (0.14)
2[a]	Au-(PET) polymer	PhMe	10.5 (3.72)
3[b]	decomposed $[Au_{25}(PET)_{18}]^0$	PhMe	6.79 (1.18)
4	$[Au_{25}(PET)_{18}]^0$	ACN	0.33 (0.15)
5[a]	Au-(PET) polymer	ACN	1.51 (0.37)
6[b]	decomposed $[Au_{25}(PET)_{18}]^0$	ACN	1.34 (0.03)
7[a]	Au-(S*n*-Hex) polymer	PhMe	10.5 (2.55)
8[b]	decomposed $[Au_{25}(Sn\text{-Hex})_{18}]^0$	PhMe	13.0 (0.96)
9[a]	Au-(S*n*-Hex) polymer	ACN	4.19 (1.28)
10[b]	decomposed $[Au_{25}(Sn\text{-Hex})_{18}]^0$	ACN	1.28 (0.04)
11	$[Au_{25}(Sn\text{-Oct})_{18}]^0$	PhMe	10.5 (2.07)
12[a]	Au-(S*n*-Oct) polymer	PhMe	9.88 (3.42)
13[b]	decomposed $[Au_{25}(Sn\text{-Oct})_{18}]^0$	PhMe	9.79 (1.41)
14	$[Au_{25}(Sn\text{-Oct})_{18}]^{-1}$	ACN	4.72 (0.79)
15[a]	Au-(S*n*-Oct) polymer	ACN	2.22 (0.51)
16[b]	decomposed $[Au_{25}(Sn\text{-Oct})_{18}]^0$	ACN	1.27 (0.07)

Reaction Conditions: 25 mol% Au in PhMe (0.078 M), 0.157 mmol styrene and 0.275 mmol TBHP at 75 °C for 1 h. [a]Polymer synthesized as described in Appedix A. [b]Clusters were decomposed as described in the text, detailed procedure in Appendix A.

To further probe if the cluster was necessary for oxidative cleavage of styrene, we tested the $Au_{25}(SR)_{18}$ precursors in the reaction. Table 2.1 (entries 2, 5, 7, 9, 12 and 15) shows the results of these experiments. As can be seen, the Au–SR polymeric precursor gave similar results to the oxidatively decomposed $Au_{25}(SR)_{18}$ cluster. At 1 h of reaction time we observed benzaldehyde as the sole product under each set of reaction conditions tested above. Table 2.1, entry 14 used the anionic rather than neutral charge state of the starting cluster to examine if this had any effect on

overall catalytic behaviour. As can be seen, it did not. Taken together these results indicate that intact $Au_{25}(SR)_{18}$ clusters are not necessary for the oxidative cleavage of alkenes, and that mononuclear Au species are likely the active catalyst.

Further support for this conclusion comes from kinetic poisoning experiments. Kinetic poisoning is commonly used to differentiate between mononuclear metal species and small clusters as the active catalyst.[35-36] Experiments of this sort have been quite informative in other catalytic gold reactions,[37-38] and we surmised that kinetic poisoning would be equally useful here. In general, if a monometallic species is the active catalyst, it is expected that one or more equivalents of poison will be required to fully inhibit the catalytic reaction. If a polymetallic species is the active catalyst, it is expected that less than one equivalent of poison will be required. The structure of $Au_{25}(SR)_{18}$ shows 12 Au atoms on the surface with thiolate ligands. Of these, two have significant solvent exposure and four others are solvent exposed to some degree.[20] Thus we expect that any $Au_{25}(SR)_{18}$ cluster should have two highly active sites for catalysis, although up to six may be possible.[20, 24]

Therefore, if the intact clusters are the active catalytic species less than one equivalent of poison per gold atom should substantially decrease the reaction rate. However, if a mononuclear Au species is the active catalyst, at least one equivalent of poison per gold atom should be required to substantially attenuate catalysis. This follows methodology established by Finke for differentiation of nanocluster catalysis from homogeneous, mononuclear catalysis in other systems.[36, 39]

We conducted poisoning experiments using diphenylphosphinoferrocene (dppf) and triphenylphosphine (PPh_3) as poisons. These compounds were chosen as based on our observation that $Au(PPh_3)Cl$ was not a competent catalyst for styrene oxidation (Appendix A, Figures A.87

and A.88). Additionally, triphenylphosphine has been previously used to poison gold-catalyzed reactions.[40] We hypothesized that dppf, being bidentate and having a large bite angle, would sequester any Au(I) species without leaving any free coordination sites. Triphenylphosphine was used for comparison in the event that free iron from decomposition of dppf muddied the results of those experiments.

Table 2.2 shows the results of our kinetic poisoning investigation. As can be seen from entries 1 and 2, addition of small amounts of phosphine gives a result similar to that from the decomposed cluster (Table 2.1, entry 3). In order to observe meaningful reductions in rate, 10 equivalents of poison per Au atom were required, corresponding to 250 equivalents per intact $Au_{25}(SR)_{18}$ cluster. We were concerned; however, that consumption of the oxidant by oxidation of the phosphine could be a confounding factor in our results.

Table 2.2. Kinetic poisoning results

Entry	Poison	Equiv to Au	Equiv to $Au_{25}(PET)_{18}$	Conversion to PhCHO (%)
1[a]	dppf[b]	0.040	1.00	8.35 (1.70)
2[a]	dppf	2.00	50.0	7.99 (1.93)
3[a]	dppf	10.0	250.0	3.03 (0.73)
4[c]	PPh_3	0.040	1.00	7.37
5[c]	PPh_3	2.00	50.0	3.38
6[c]	PPh_3	10.0	250.0	0.22
7[c]	N/A	0.00	0.00	18.8
8[c]	NHC	0.040	1.00	17.9
9[c]	NHC	2.00	50.0	3.51
10[c]	NHC	10.0	250.0	0.00

Entries 1-6 run for 1 h in PhMe (0.078 M), with 1 mol% $[Au_{25}(PET)_{18}]^0$, and 0.157 mmol styrene at 75 °C. Entries 7-10 run for 75 min in $CHCl_3$ (0.078 M), with 1 mol% $[Au_{25}(PET)_{18}]^{-1}$, and 0.135 mmol styrene at 75 °C. NHC is not soluble in PhMe. [a]Average of 3 runs, standard error in parethesese. [b]Diphenylphosphinoferrocene. [c]Single run, shown for comparison.

Further poisoning studies were conducted with 1,3-dimethylbenzimidazolium iodide. Addition of base to this precursor gives an N-heterocyclic carbene (NHC), which binds gold with high

affinity and cannot be oxidized by the oxidant.[41] As can be seen in Table 2.2 (entries 8–10), 250 equivalents of poison to cluster were also required to halt catalysis in this case. These results, taken together, are highly indicative of a mononuclear gold species as the active catalyst.

To further probe the structure of the active catalyst, we undertook XPS of both the $Au_{25}(PET)_{18}$ precursor polymer and the oxidative decomposition products of $Au_{25}(PET)_{18}$. The precursor and oxidative decomposition products show the Au $4f_{7/2}$ peak at 84.8 eV and 85.6 eV, respectively. These are consistent with Au(I) species previously reported in the literature.[42] ^{1}H NMR of the decomposition product suffers interference from the Au nucleus and is of low quality. However, COSY spectra of the decomposition product show no signals off of the diagonal, indicating no through-space interactions. These data, when evaluated as a whole, indicate that Au(I)–thiolate species are likely the active catalyst in this reaction. Spectra are presented in Appendix A.

In addition to our data, there are similar reports of Au(I) catalysed oxidative cleavage of alkenes using mononuclear Au(I) species. In 2006, Shi and co-workers reported using AuCl and an organic ligand to cleave a number of alkenes, generally with high yields (Figure 2.4).[43]

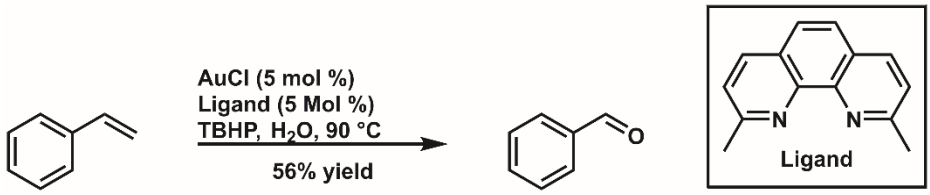

Figure 2.4 Oxidation of styrene by Au(I) - Shi 2006

Although their reaction was optimized using aqueous conditions, they report comparable results using PhMe as the solvent (reference 43, Table 1, entries 4 and 5). These results show that oxidative alkene cleavage with mononuclear gold species and TBHP is possible under a variety of reaction conditions, further implicating mononuclear gold species in those reactions previously reported for $Au_{25}(SR)_{18}$.

We also conducted some decomposition experiments with $Au_{25}(SR)_{18}$ clusters adsorbed on silica gel support without calcination. These experiments are presented in Appendix A starting on page 158. While not dispositive, results show that supported clusters decompose when exposed to TBHP and elevated temperature.

2.4 Conclusion

Interest in the chemical reactivity of thiolate-protected gold nanoclusters has grown substantially in the last several years,[2] and our findings raise an important question about the potential for such applications. While our results are silent on calcinated $Au_{25}(SR)_{18}$ catalysts, it is clear that unsupported $Au_{25}(SR)_{18}$ clusters are unstable under oxidative reaction conditions previously reported.

Despite the remarkable stability of $Au_{25}(SR)_{18}$ nanoclusters, questions remain regarding their viability as homogeneous catalysts.[14] The nature of the true catalytic species is an important consideration in reaction development, especially within the realm of atomically defined nanoclusters.[35, 44] While these species have immense potential owing to their aforementioned stability and unique electronic properties, that potential can only be fully realized by exploiting reactions wherein the clusters themselves are likely to survive.

Herein we have presented evidence that not only are $Au_{25}(SR)_{18}$ clusters unstable to oxidations with TBHP, but also that the Au–thiol cluster precursor and cluster decomposition products are equally effective in the oxidation of styrene. Even at temperatures significantly lower than that of the reaction, TBHP completely decomposes $Au_{25}(SR)_{18}$ before notable product appearance is observed. Further, kinetic poisoning experiments have shown that far more than one equivalent of poison per gold atom is required to observe any meaningful reduction in reaction rate – indicating that the active catalytic species is likely not the intact cluster. Lastly, XPS studies show that the

Au species present after decomposition and before cluster formation are Au(I), which indicates that Au(I) thiolates are likely the active catalyst in this reaction.

Furthermore, our results using acetonitrile as solvent indicate that unsupported $Au_{25}(SR)_{18}$ clusters are not stable to these reaction conditions even when used as a heterogeneous suspension. In light of our findings, recent literature reports may need to be re-evaluated.[6, 23]

Overall, our data support the conclusion that mononuclear Au(I) species are the active catalyst in the oxidative cleavage of styrene.

REFERENCES

1. Hutchings, G. J.; Brust, M.; Schmidbaur, H. Gold-an introductory perspective. *Chem. Soc. Rev.* **2008**, *37*, 1759-1765.

2. Raubenheimer, H. G.; Schmidbaur, H. The Late Start and Amazing Upswing in Gold Chemistry. *J. Chem. Educ.* **2014**, *[Online Early Access]*, DOI: 10.1021/ed400782p.

3. Haruta, M. When Gold Is Not Noble: Catalysis by Nanoparticles. *The Chemical Record* **2003**, *3*, 75-87.

4. Haruta, M.; Kobayashi, T.; Sano, H.; Yamada, N. Novel Gold Catalysts for the Oxidation of Carbon Monoxide at a Temperature far Below 0 °C. *Chem. Lett.* **1987**, *16*, 405-408.

5. Yamazoe, S.; Koyasu, K.; Tsukuda, T. Nonscalable Oxidation Catalysis of Gold Clusters. *Acc. Chem. Res.* **2014**, *47*, 816-824.

6. Li, G.; Jin, R. Atomically Precise Gold Nanoclusters as New Model Catalysts. *Acc. Chem. Res.* **2013**, *46*, 1749-1758.

7. Negishi, Y.; Nobusada, K.; Tsukuda, T. Glutathione-Protected Gold Clusters Revisited: Bridging the Gap between Gold(I)−Thiolate Complexes and Thiolate-Protected Gold Nanocrystals. *J. Am. Chem. Soc.* **2005**, *127*, 5261-5270.

8. Yuan, X.; Zhang, B.; Luo, Z.; Yao, Q.; Leong, D. T.; Yan, N.; Xie, J. Balancing the Rate of Cluster Growth and Etching for Gram-Scale Synthesis of Thiolate-Protected Au25 Nanoclusters with Atomic Precision. *Angew. Chem. Int. Ed.* **2014**, *53*, 4623-4627.

9. Das, S.; Goswami, A.; Hesari, M.; Al-Sharab, J. F.; Mikmekova, E.; Maran, F.; Asefa, T. Reductive Deprotection of Monolayer Protected Nanoclusters: An Efficient Route to Supported Ultrasmall Au Nanocatalysts for Selective Oxidation. *Small* **2014**, *10*, 1473-1478.

10. Dainese, T.; Antonello, S.; Gascón, J. A.; Pan, F.; Perera, N. V.; Ruzzi, M.; Venzo, A.; Zoleo, A.; Rissanen, K.; Maran, F. Au25(SEt)18, a nearly naked thiolate-protected Au25 cluster: structural analysis by single crystal X-ray crystallography and electron nuclear double resonance. *ACS Nano* **2014**, *8*, 3904-3912.

11. Jin, S.; Meng, X.; Jin, S.; Zhu, M. High yield synthesis of Au25 nanoclusters by controlling the reduction process. *J. Nanosci. Nanotechnol.* **2013**, *13*, 1282-1285.

12. Yu, Y.; Yao, Q.; Luo, Z.; Yuan, X.; Lee, J. Y.; Xie, J. Precursor engineering and controlled conversion for the synthesis of monodisperse thiolate-protected metal nanoclusters. *Nanoscale* **2013**, *5*, 4606-4620.

13. Kumar, S.; Jin, R. Water-soluble Au25(Capt)18 nanoclusters: synthesis, thermal stability, and optical properties. *Nanoscale* **2012**, *4*, 4222-4227.

14. Parker, J. F.; Fields-Zinna, C. A.; Murray, R. W. The Story of a Monodisperse Gold Nanoparticle: Au25L18. *Acc. Chem. Res.* **2010**, *43*, 1289-1296.

15. Parker, J. F.; Weaver, J. E. F.; McCallum, F.; Fields-Zinna, C. A.; Murray, R. W. Synthesis of monodisperse [Oct4N+][Au25(SR)18-] nanoparticles, with some mechanistic observations. *Langmuir* **2010**, *26*, 13650-13654.

16. Heaven, M. W.; Dass, A.; White, P. S.; Holt, K. M.; Murray, R. W. Crystal Structure of the Gold Nanoparticle [N(C8H17)4][Au25(SCH2CH2Ph)18]. *J. Am. Chem. Soc.* **2008**, *130*, 3754-3755.

17. Zhu, M.; Eckenhoff, W. T.; Pintauer, T.; Jin, R. Conversion of Anionic [Au25(SCH2CH2Ph)18]− Cluster to Charge Neutral Cluster via Air Oxidation. *J. Phys. Chem. C* **2008**, *112*, 14221-14224.

18. Qian, H.; Eckenhoff, W. T.; Bier, M. E.; Pintauer, T.; Jin, R. Crystal structures of Au2 complex and Au25 nanocluster and mechanistic insight into the conversion of polydisperse nanoparticles into monodisperse Au25 nanoclusters. *Inorg Chem* **2011**, *50*, 10735-9.

19. Tofanelli, M. A.; Ackerson, C. J. Superatom electron configuration predicts thermal stability of Au25(SR)18 nanoclusters. *J. Am. Chem. Soc.* **2012**, *134*, 16937-16940.

20. Ni, T. W.; Tofanelli, M. A.; Phillips, B. D.; Ackerson, C. J. Structural basis for ligand exchange on Au25(SR)18. *Inorg. Chem.* **2014**, *53*, 6500-6502.

21. Zhu, Y.; Qian, H.; Zhu, M.; Jin, R. Thiolate-Protected Aun Nanoclusters as Catalysts for Selective Oxidation and Hydrogenation Processes. *Adv. Mater.* **2010**, *22*, 1915-1920.

22. Zhu, Y.; Qian, H.; Jin, R. An Atomic-Level Strategy for Unraveling Gold Nanocatalysis from the Perspective of Aun(SR)m Nanoclusters. *Chem. Eur. J.* **2010**, *16*, 11455-11462.

23. Liu, J.; Krishna, K. S.; Losovyj, Y. B.; Chattopadhyay, S.; Lozova, N.; Miller, J. T.; Spivey, J. J.; Kumar, C. S. S. R. Ligand-Stabilized and Atomically Precise Gold Nanocluster Catalysis: A Case Study for Correlating Fundamental Electronic Properties with Catalysis. *Chem. Eur. J.* **2013**, *19*, 10201-10208.

24. Li, G.; Jiang, D.-e.; Kumar, S.; Chen, Y.; Jin, R. Size Dependence of Atomically Precise Gold Nanoclusters in Chemoselective Hydrogenation and Active Site Structure. *ACS Catal.* **2014**, 2463-2469.

25. Antonello, S.; Hesari, M.; Polo, F.; Maran, F. Electron transfer catalysis with monolayer protected Au25 clusters. *Nanoscale* **2012**, *4*, 5333-5342.

26. Knoppe, S.; Wong, O. A.; Malola, S.; Hakkinen, H.; Burgi, T.; Verbiest, T.; Ackerson, C. J. Chiral Phase Transfer and Enantioenrichment of Thiolate-Protected Au102 Clusters. *J. Am. Chem. Soc.* **2014**, *136*, 4129-4132.

27. Wong, O. A.; Hansen, R. J.; Ni, T. W.; Heinecke, C. L.; Compel, W. S.; Gustafson, D. L.; Ackerson, C. J. Structure-activity relationships for biodistribution, pharmacokinetics, and excretion of atomically precise nanoclusters in a murine model. *Nanoscale* **2013**, *5*, 10525-10533.

28. Yi, C.; Tofanelli, M. A.; Ackerson, C. J.; Knappenberger, K. L. Optical properties and electronic energy relaxation of metallic Au144(SR)60 nanoclusters. *J. Am. Chem. Soc.* **2013**, *135*, 18222-18228.

29. Heinecke, C. L.; Ackerson, C. J. Preparation of gold nanocluster bioconjugates for electron microscopy. *Methods. Mol. Biol.* **2013**, *950*, 293-311.

30. Heinecke, C. L.; Ni, T. W.; Malola, S.; Makinen, V.; Wong, O. A.; Hakkinen, H.; Ackerson, C. J. Structural and Theoretical Basis for Ligand Exchange on Thiolate Monolayer Protected Gold Nanoclusters. *J. Am. Chem. Soc.* **2012**, *134*, 13316-13322.

31. Wong, O. A.; Heinecke, C. L.; Simone, A. R.; Whetten, R. L.; Ackerson, C. J. Ligand symmetry-equivalence on thiolate protected gold nanoclusters determined by NMR spectroscopy. *Nanoscale* **2012**, *4*, 4099-4102.

32. Zhu, Y.; Qian, H.; Drake, B. A.; Jin, R. Atomically Precise Au25(SR)18 Nanoparticles as Catalysts for the Selective Hydrogenation of α,β-Unsaturated Ketones and Aldehydes. *Angew. Chem. Int. Ed.* **2010**, *49*, 1295-1298.

33. Qian, H.; Jiang, D.-e.; Li, G.; Gayathri, C.; Das, A.; Gil, R. R.; Jin, R. Monoplatinum Doping of Gold Nanoclusters and Catalytic Application. *J. Am. Chem. Soc.* **2012**, *134*, 16159-16162.

34. Langille, M. R.; Personick, M. L.; Zhang, J.; Mirkin, C. A. Defining rules for the shape evolution of gold nanoparticles. *J. Am. Chem. Soc.* **2012**, *134*, 14542-14554.

35. Widegren, J. A.; Finke, R. G. A review of the problem of distinguishing true homogeneous catalysis from soluble or other metal-particle heterogeneous catalysis under reducing conditions. *J. Mol. Catal. A: Chem.* **2003**, *198*, 317-341.

36. Bayram, E.; Linehan, J. C.; Fulton, J. L.; Roberts, J. A. S.; Szymczak, N. K.; Smurthwaite, T. D.; Özkar, S.; Balasubramanian, M.; Finke, R. G. Is It Homogeneous or Heterogeneous Catalysis Derived from [RhCp*Cl2]2? In Operando XAFS, Kinetic, and Crucial Kinetic Poisoning Evidence for Subnanometer Rh4 Cluster-Based Benzene Hydrogenation Catalysis. *J. Am. Chem. Soc.* **2011**, *133*, 18889-18902.

37. Beret, E. C.; van Wijk, M. M.; Ghiringhelli, L. M. Reaction cycles and poisoning in catalysis by gold clusters: A thermodynamics approach. *Int. J. Quantum Chem* **2014**, *114*, 57-65.

38. Kumar, M.; Hammond, G. B.; Xu, B. Cationic Gold Catalyst Poisoning and Reactivation. *Org. Lett.* **2014**, *16*, 3452-3455.

39. Stracke, J. J.; Finke, R. G. Distinguishing Homogeneous from Heterogeneous Water Oxidation Catalysis when Beginning with Polyoxometalates. *ACS Catal.* **2014**, *4*, 909-933.

40. Nigra, M. M.; Arslan, I.; Katz, A. Gold nanoparticle-catalyzed reduction in a model system: Quantitative determination of reactive heterogeneity of a supported nanoparticle surface. *J. Catal.* **2012**, *295*, 115-121.

41. Crudden, C. M.; Horton, J. H.; Ebralidze, II; Zenkina, O. V.; McLean, A. B.; Drevniok, B.; She, Z.; Kraatz, H. B.; Mosey, N. J.; Seki, T., et al. Ultra stable self-assembled monolayers of N-heterocyclic carbenes on gold. *Nat. Chem.* **2014**, *6*, 409-414.

42. Shul'ga, Y. M.; Bulatov, A. V.; Gould, R. A. T.; Konze, W. V.; Pignolet, L. H. X-ray photoelectron spectroscopy of a series of heterometallic gold-platinum phosphine cluster compounds. *Inorg. Chem.* **1992**, *31*, 4704-4706.

43. Xing, D.; Guan, B.; Cai, G.; Fang, Z.; Yang, L.; Shi, Z. Gold(I)-Catalyzed Oxidative Cleavage of a C−C Double Bond in Water. *Org. Lett.* **2006**, *8*, 693-696.

44. Hagen, C. M.; Vieille-Petit, L.; Laurenczy, G.; Süss-Fink, G.; Finke, R. G. Supramolecular Triruthenium Cluster-Based Benzene Hydrogenation Catalysis: Fact or Fiction? *Organometallics* **2005**, *24*, 1819-1831.

CHAPTER 3: RADICALS IN THE ETCHING OF GOLD SURFACES BY THIOLATES IN ORGANIC SOLVENT*

3.1 Synopsis

Etching of gold with excess thiol ligand is used in both synthesis and analysis of gold particles. Mechanistically, the process of etching gold with excess thiol is opaque. Previous studies have obliquely considered the role of oxygen in thiolate etching of gold. Herein, we show that oxygen or a radical initator is a necessary component for efficient etching of gold by thiolates. Attenuation of the etching process by radical scavengers in the presence of oxygen, and the restoration of activity by radical initiators under inert atmosphere, strongly implicate the oxygen radical. These data led us to propose an atomistic mechanism in which the oxygen radical initiates the etching process.

3.2 Introduction

Thiolate-protected gold nanoparticles, owing to their remarkable stability, are of interest for both fundamental and applied research.[1-6] Synthesis of many 'atomically precise' nanoclusters incorporates an etching step in which excess thiolate ligand converts larger particles into smaller and more thermodynamically stable ones.[7] Alternatively, larger nanoparticles may be etched using excess thiol.[8-9] Syntheses incorporating an etching step, alternatively described as size focusing or digestive ripening, are recently shown to give high yield of many clusters including $Au_{18}(SR)_{14}$,[10-12] $Au_{20}(SR)_{16}$,[13-15] $Au_{23}(SR)_{16}$,[16-18] $Au_{24}(SR)_{20}$,[14, 19-22] $Au_{25}(SR)_{18}$,[23] $Au_{28}(SR)_{20}$,[8, 24-26] $Au_{36}(SR)_{24}$,[27-30] $Au_{38}(SR)_{24}$,[31-35] $Au_{40}(SR)_{24}$,[36-37] $Au_{68}(SR)_{34}$,[38] $Au_{99}(SR)_{42}$,[39] $Au_{144}(SR)_{60}$,[40] $Au_{333}(SR)_{\sim 80}$,[41] and $Au_{\sim 500}(SR)_{\sim 120}$ through tuning of the synthetic conditions.[42] In addition,

* The work presented herein is published in *Angewandte Chemie International Edition*. Timothy A. Dreier's contributions include all experimental design, data gathering & analysis, proposal of the radical etching mechanism, and preparation of the manuscript. *Angew. Chemie. Int. Ed.* **2015**, *54*, 9249-9252. © 2015 WILEY-VCH Verlag GmbH & Co.

etching is successful in production of alloys of these clusters, including $Au_{24}Pd(SR)_{18}$,[43-44] $Au_{24}Pt(SR)_{18}$,[45] and $Au_{144-x}Ag_x(SR)_{60}$.[46-47] Other examples have been reviewed recently.[48] Etching-type mechanisms also presumably underlie many digestive ripening transformations of noble metal nanoparticles.[49] Furthermore, etching is sometimes used to liberate ligands for downstream analysis.

Despite widespread adoption, the mechanism of thiol-induced etching is obscure, even after theoretical and experimental investigation.[31, 50-53] The literature on magic number gold nanocluster (AuNC) synthesis suggests an overall reaction as shown in Figure 3.1, highlighting the importance of etching in arriving at the final products.[54]

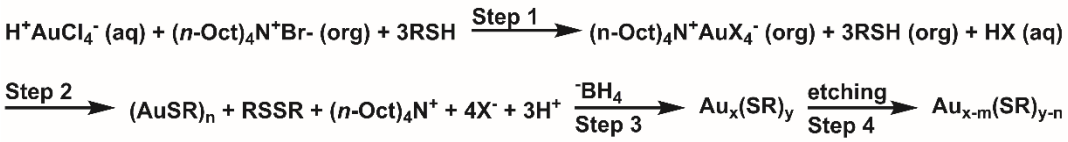

Figure 3.1. Brust synthesis of Au-thiolate clusters

Consistent with Figure 3.1 are recent works showing that larger particles are formed as intermediates before the final synthetic product is formed for Au_{25}.[50] Similarly, etching protocols can convert Au_{40} to Au_{38} or Au_{36}, as well as Au_{102} to Au_{67} and Au_{144} to a variety of smaller clusters.[37, 39, 55-56] Overall, the literature suggests that most synthesis of precisely defined thiolate-protected metal and metal-alloy nanoclusters include a final step in which initially formed polydisperse $Au_x(SR)_y$ nanoparticles are etched to precisely defined $Au_{(x-m)}(SR)_{(y-n)}$ nanoclusters in a mechanistically obscure process.

Gold nanoparticle syntheses are typically performed under ambient atmosphere. We and others observed in, a preliminary way, that synthesis and etching optimized under ambient atmosphere do not work well when performed under inert atmosphere.[3, 57, 58] Intrigued by this observation and the mechanistic obscurity of the process, we endeavoured to clarify the role of oxygen in gold nanocluster etching. We chose to examine role of oxygen in the etching of large (colloidal) gold

nanoparticles, as well as the role of oxygen in the etching based synthesis of Au_{25}. In each case, we observed oxygen was critical for reaction progress.

3.3 Results and Discussion

The colloidal particles we investigated are 5-nm diameter phosphatidylcholine (PC)-coated Au nanoparticles (PC-AuNPs). These were synthesized by a previously reported procedure, yielding products with a characteristic plasmon resonance at 526 nm.[59] Etching of these colloids proceeded in a calculated 500-fold excess of *n*-hexanethiol to gold atoms in methylene chloride. The progress of etching was determined optically by monitoring the surface plasmon resonance peak. As the particles shrink during etching, the surface plasmon becomes less prominent.[42, 60-61]

Figure 3.2 shows the results of etching of colloidal gold in excess *n*-hexanethiol. The black triangle trace and red square trace depict thiol etching of gold in the presence and absence of O_2, respectively. The O_2 atmosphere was maintained with an O_2 balloon, although similar results are observed if the reaction is performed in a vessel open to atmosphere. This result shows clearly that without O_2, the etching of colloidal particles stalls, whereas in the presence of O_2 the etching can proceed until the nanoparticles are largely converted to gold(I)-thiolate polymer products.

Since O_2 can serve as a radical initiator, we hypothesized that etching may proceed through a radical based mechanism. To test this, we attempted the etching experiment in toluene (a radical scavenger, Figure 3.2, blue circle trace). The reactions were sealed and monitored over the course of 90 min. Etching in toluene is minimal – comparable to etching in oxygen-free CH_2Cl_2.

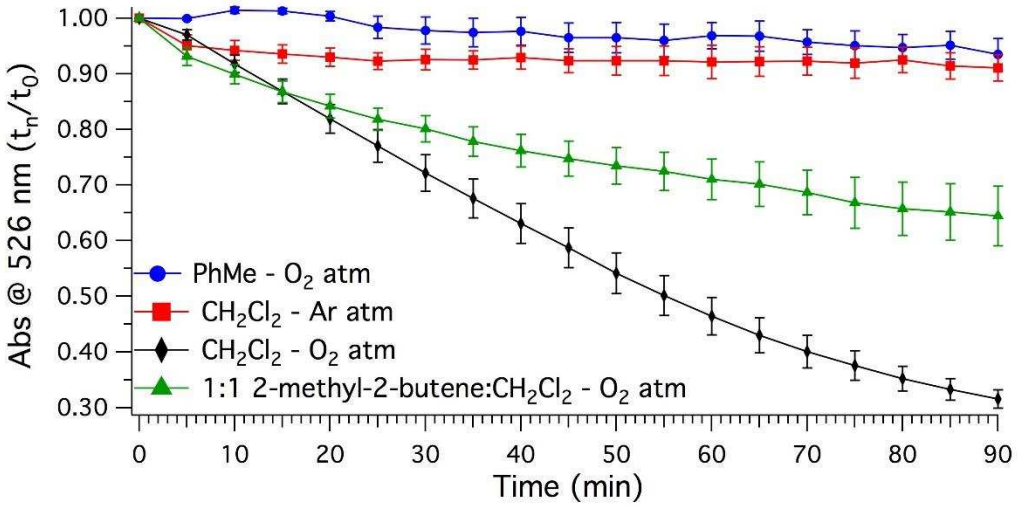

Figure 3.2. Etching of PC-coated AuNPs in organic solvent

Correspondingly, including a radical scavenger, 2-methyl-2-butene, as a co-solvent with methylene chloride inhibits etching (Figure 3.2, green triangle trace). In aggregate, these data suggest that etching of colloidal gold nanoparticles by thiolates proceeds through a radical-based mechanism. To determine if our findings are specific to the colloidal system or generalizable to all thiol etching of gold, we examined the well-developed etching based Au_{25} synthesis in closer detail.[3] We first by investigated whether the Au-thiolate polymer formation (Figure 3.1, step 2) depends on the presence of oxygen. The oligomer / polymer was synthesized by mixing $HAuCl_4 \bullet 3H_2O$ in THF with 1.12 equiv of TOAB, followed by addition of phenylethanethiol (PET) in THF through a syringe. We attempted this synthesis under both ambient atmosphere, and with degassed components under argon atmosphere.

Success of Au(I)-PET oligomer formation in this case was determined by examination of resulting ^{1}H and ^{13}CNMR spectra. These spectra were distinct from the starting materials, and identical (Appendix B, Figures B.16 and B.18) – indicating that oxygen is not involved in the formation of Au(I)-PET oligomers/polymers.

We next determined the O_2 dependence of the simultaneous reduction and etching steps of $Au_{25}(SR)_{18}$ synthesis (Figure 3.1, step 4) All solvents were degassed by 3 cycles of freeze/pump/thaw with an argon atmosphere maintained during the course of the reaction. Success of $Au_{25}(SR)_{18}$ formation was determined by production of a product with a linear optical spectrum consistent with its distinctive spectrum (Appendix B, Figure B.10). When oxygen is excluded from the reduction/etching step, the reaction fails to produce $Au_{25}(SR)_{18}$ (Table 3.1 Entry 6, Appendix B, Figure B.13) consistent with a previous report.[3] The resulting spectrum of this reduction/etching step is featureless indicating particles larger than Au_{25} but too small to be plasmonic (Appendix B, Figure B.13).[62]

Table 3.1. Effect of additives & atmosphere on Au_{25} synthesis

Entry	Atmosphere	Additive	Equiv to Au	Equiv to $NaBH_4$	%Yield $Au_{25}(PET)_{18}$
1	ambient	none	N/A	N/A	60.0
2	ambient	BHT [a]	10.1	1.00	49.3
3	ambient	BHT	20.2	2.00	10.6
4	ambient	BHT	30.2	3.00	7.00
5	ambient	BHT	40.3	4.00	7.45
6	argon[b]	none	N/A	N/A	0.00
7	argon	AIBN[c]	1.00	0.250	40.9

Yields based on Au atoms, [a]3,5-di-tert-butyl-4-hydroxytoluene, [b]all solutions degassed by 3 cycles of freeze/pump/thaw, [c]azobisisobutyronitrile

To test if the radical nature of oxygen is key to the reduction/etching step, we added a radical initiator to the anaerobic synthesis. The particular radical initiator, azobisisobutyronitrile (AIBN, a common initiator in radical polymerizations) was added just prior to the addition of $NaBH_4$ in the previously described anaerobic reaction. Consistent with our hypothesis, this reaction gave $Au_{25}(PET)_{18}$ in 40.9% yield (Table 3.1, Entry 7), consistent with yields typical in aerobic synthesis of $Au_{25}(SR)_{18}$.[2, 63-64]

Conversely, we found that inclusion of a radical scavenger in the aerobic synthesis diminished product yield. We added varying amounts of 3,5-di-tert-butyl-4-hydroxytoluene (BHT, a radical inhibitor) to the reaction under ambient conditions, again just prior to addition of $NaBH_4$. We observed that BHT in excess of borohydride substantially reduced the reaction yield of Au_{25} (Table 3.1, entries 2-5). Notably, 3 and 4 equivalents of BHT to $NaBH_4$ (entries 4 and 5, respectively) gave very nearly the same result. This may be due to saturation of the THF with BHT.

The overall synthesis of thiolate-protected gold nanoparticle synthesis, as depicted in Figure 3.1, proceeds in four steps. Following formation of an oligomer (steps 1 & 2), AuNPs are formed from the oligomer via reduction by sodium borohydride (step 3). This initial mixture of polydisperse nanoparticles is then etched to the final product (step 4). Theoretical study of thiolate protected nanoparticle synthesis so-far focuses on the initial growth.[53, 65] This previous theoretical work suggests that initial growth from the oligomeric species (Figure 3.1, step 3) proceeds by a hydride transfer from $NaBH_4$ to Au(I) to give the large and polydisperse AuNPs reported by Dass.[50]. The mechanism of etching (Figure 3.1, step 4) – which is key to arriving at a magic number cluster – is presently obscure.

We propose that the etching of AuNPs into more focused size distributions is the oxygen dependent portion of the synthesis, and that it is the radical character of oxygen that is important. In Figure 3.3, we propose a radical-based mechanism for etching of AuNPs. After formation of large AuNPs from $NaBH_4$ reduction of the Au(I)-thiolate oligomer, disulfide formed in the initial step of the synthesis and excess $NaBH_4$ remain in solution. We propose that borohydride reduces

the disulfide to the free thiol, from which the O_2 radical abstracts a proton to give a thiyl radical (**1**) and HOO•.

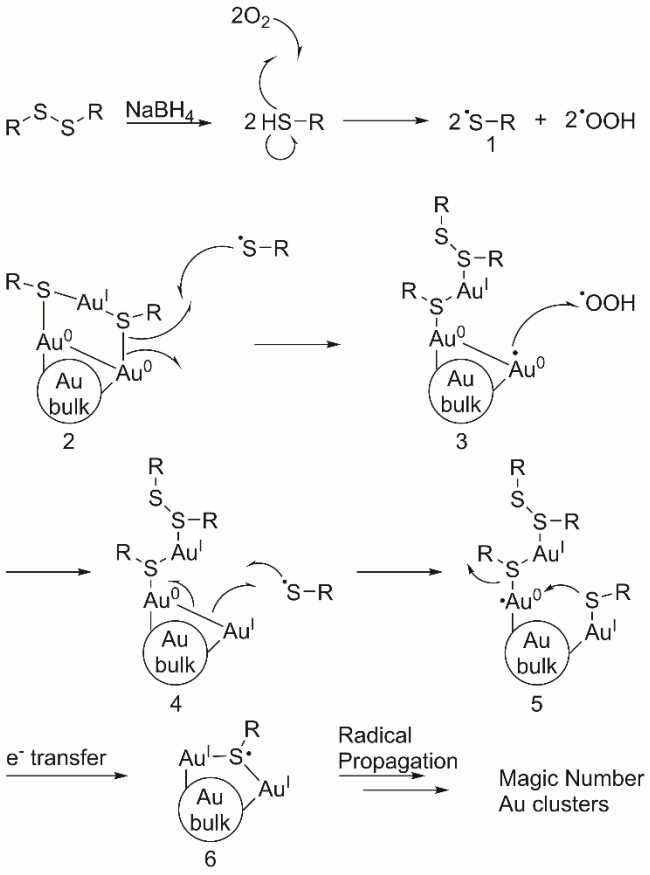

Figure 3.3. Proposed radical etching mechanism

The thiyl radical then homolytically cleaves a sulfur-gold bond on the surface of the initial AuNC to expose core Au (0). This newly exposed Au(0) is oxidized by the peroxy radical formed in the first step, to give a new solvent-exposed Au (I) atom (**3**). Homolytic cleavage of an Au-Au bond gives **5**, in which another equivalent of thiol is now attached to the cluster. Breaking of the Au-S bond in **5** liberates an Au-thiolate monomer and gives another surface-exposed Au (I). Formation of a new Au-S bond gives **6**, in which one layer of Au has been removed from the starting cluster. This cycle can repeat, etching all AuNPs in a preparation to thermodynmically stable magic number AuNCs.

In addition to the radical initiation and scavenging experiments, we performed spin-trapping EPR (ESR) spectroscopy using DMPO[66] as the spin trap. The ESR spectrum (Appendix B, Figure B.21) is consistent with an Au radical as depicted in **3**, this offers further evidence for our mechanistic proposal.

Omission of O_2 makes the mechanism in scheme **2** impossible. Correspondingly, the large, insoluble products observed by Murray would be the expected result of inert synthesis where etching cannot proceed.[3] AIBN can initiate formation of the needed thiyl radical, intercepting the mechanism proposed in Figure 3.3 (Appendix B, Figure B.20).

3.4 Conclusion

Overall our data strongly suggest that the necessity for oxygen in both thiol-etching of colloidal gold and in Brust-type syntheses of AuNCs arises from the O_2 diradical. Although molecular oxygen has been shown to react with thiols to give thiyl radicals,[67-71] to the best of our knowledge this is the first systematic investigation into the role of oxygen and other radicals in AuNC synthesis with thiols. While radicals are known to etch AuNPs under Fenton-like conditions,[72] scheme **2** represents the first proposed atomistic mechanism for thiolate etching of AuNPs so far as we are aware.

Full understanding of this process may allow for better control of reaction outcomes, i.e. size control of particles via changes to the reaction atmosphere. Better control over reproducibility, size and dispersity in these processes will allow for a deeper investigation into the size-dependent properties of Magic Number AuNCs, which in turn will broaden the scope of their applications.

REFERENCES

1. Hakkinen, H. Atomic and electronic structure of gold clusters: understanding flakes, cages and superatoms from simple concepts. *Chem. Soc. Rev.* **2008**, *37*, 1847-1859.

2. Parker, J. F.; Fields-Zinna, C. A.; Murray, R. W. The Story of a Monodisperse Gold Nanoparticle: Au25L18. *Acc. Chem. Res.* **2010**, *43*, 1289-1296.

3. Parker, J. F.; Weaver, J. E. F.; McCallum, F.; Fields-Zinna, C. A.; Murray, R. W. Synthesis of monodisperse [Oct4N+][Au25(SR)18-] nanoparticles, with some mechanistic observations. *Langmuir* **2010**, *26*, 13650-13654.

4. Zhu, Y.; Qian, H.; Zhu, M.; Jin, R. Thiolate-Protected Aun Nanoclusters as Catalysts for Selective Oxidation and Hydrogenation Processes. *Adv. Mater.* **2010**, *22*, 1915-1920.

5. Zhu, Y.; Jin, R.; Sun, Y. Atomically Monodisperse Gold Nanoclusters Catalysts with Precise Core-Shell Structure. *Catalysts* **2011**, *1*, 3-17.

6. Tofanelli, M. A.; Ackerson, C. J. Superatom electron configuration predicts thermal stability of Au25(SR)18 nanoclusters. *J. Am. Chem. Soc.* **2012**, *134*, 16937-16940.

7. Brust, M.; Walker, M.; Bethell, D.; Schiffrin, D. J.; Whyman, R. Synthesis of thiol-derivatised gold nanoparticles in a two-phase liquid-liquid system. *J. Chem. Soc., Chem. Commun.* **1994**, 801-802.

8. Schaaff, T. G.; Knight, G.; Shafigullin, M. N.; Borkman, R. F.; Whetten, R. L. Isolation and selected properties of a 10.4 kDa gold:glutathione cluster compound. *J. Phys. Chem. B* **1998**, *102*, 10643-10646.

9. Schaaff, T. G.; Whetten, R. L. Controlled Etching of Au:SR Cluster Compounds. *J. Phys. Chem. B* **1999**, *103*, 9394-9396.

10. Yao, Q.; Yu, Y.; Yuan, X.; Yu, Y.; Xie, J.; Lee, J. Y. Two-Phase Synthesis of Small Thiolate-Protected Au15 and Au18 Nanoclusters. *Small* **2013**, *9*, 2696-2701.

11. Das, A.; Liu, C.; Byun, H. Y.; Nobusada, K.; Zhao, S.; Rosi, N.; Jin, R. Structure Determination of [Au18(SR)14]. *Angew. Chem. Int. Ed.* **2015**, Ahead of Print.

12. Tang, Q.; Jiang, D.-e. Revisiting Structural Models for Au18(SR)14. *J. Phys. Chem. C* **2015**, *119*, 2904-2909.

13. Pei, Y.; Gao, Y.; Shao, N.; Zeng, X. C. Thiolate-Protected Au20(SR)16 Cluster: Prolate Au8 Core with New [Au3(SR)4] Staple Motif. *J. Am. Chem. Soc.* **2009**, *131*, 13619-13621.

14. Meng, X.; Liu, Z.; Zhu, M.; Jin, R. Controlled reduction for size selective synthesis of thiolate-protected gold nanoclusters Aun(n = 20, 24, 39, 40). *Nanoscale Res. Lett.* **2012**, *7*, 277.

15. Zhu, X.; Jin, S.; Wang, S.; Meng, X.; Zhu, C.; Zhu, M.; Jin, R. One-Pot Synthesis of Phenylmethanethiolate-Protected Au20(SR)16 and Au24(SR)20 Nanoclusters and Insight into the Kinetic Control. *Chem. - Asian J.* **2013**, *8*, 2739-2745.

16. Muhammed, M. A. H.; Verma, P. K.; Pal, S. K.; Kumar, R. C. A.; Paul, S.; Omkumar, R. V.; Pradeep, T. Bright, NIR-emitting Au23 from Au25: characterization and applications including biolabeling. *Chem. Eur. J.* **2009**, *15*, 10110-10120.

17. Das, A.; Li, T.; Nobusada, K.; Zeng, C.; Rosi, N. L.; Jin, R. Nonsuperatomic [Au23(SC6H11)16]- Nanocluster Featuring Bipyramidal Au15 Kernel and Trimeric Au3(SR)4 Motif. *J. Am. Chem. Soc.* **2013**, *135*, 18264-18267.

18. Hesari, M.; Workentin, M. S. Facile synthesis of Au23(SC(CH3)3)16 clusters. *J. Mater. Chem. C* **2014**, *2*, 3631-3638.

19. Zhu, M.; Qian, H.; Jin, R. Thiolate-Protected Au24(SC2H4Ph)20 Nanoclusters: Superatoms or Not? *J. Phys. Chem. Lett.* **2010**, *1*, 1003-1007.

20. Crasto, D.; Barcaro, G.; Stener, M.; Sementa, L.; Fortunelli, A.; Dass, A. Au24(SAdm)16 nanomolecules: X-ray crystal Structure, theoretical analysis, adaptability of adamantane ligands to form Au23(SAdm)16 and Au25(SAdm)16, and its relation to Au25(SR)18. *J. Am. Chem. Soc.* **2014**, *136*, 14933-14940.

21. Das, A.; Li, T.; Li, G.; Nobusada, K.; Zeng, C.; Rosi, N. L.; Jin, R. Crystal structure and electronic properties of a thiolate-protected Au24 nanocluster. *Nanoscale* **2014**, *6*, 6458-6462.

22. Tang, Q.; Ouyang, R.; Tian, Z.; Jiang, D.-e. The ligand effect on the isomer stability of Au24(SR)20 clusters. *Nanoscale* **2015**, *7*, 2225-2229.

23. Wu, Z.; Suhan, J.; Jin, R. One-pot synthesis of atomically monodisperse, thiol-functionalized Au25 nanoclusters. *J. Mater. Chem.* **2009**, *19*, 622-626.

24. Knoppe, S.; Malola, S.; Lehtovaara, L.; Bürgi, T.; Häkkinen, H. Electronic Structure and Optical Properties of the Thiolate-Protected Au28(SMe)20 Cluster. *The Journal of Physical Chemistry A* **2013**, *117*, 10526-10533.

25. Zeng, C.; Li, T.; Das, A.; Rosi, N. L.; Jin, R. Chiral Structure of Thiolate-Protected 28-Gold-Atom Nanocluster Determined by X-ray Crystallography. *J. Am. Chem. Soc.* **2013**, *135*, 10011-10013.

26. Chevrier, D. M.; Zeng, C.; Jin, R.; Chatt, A.; Zhang, P. Role of Au4 Units on the Electronic and Bonding Properties of Au28(SR)20 Nanoclusters from X-ray Spectroscopy. *J. Phys. Chem. C* **2015**, *119*, 1217-1223.

27. Nimmala, P. R.; Dass, A. Au36(SPh)23 Nanomolecules. *J. Am. Chem. Soc.* **2011**, *133*, 9175-9177.

28. Zeng, C.; Qian, H.; Li, T.; Li, G.; Rosi, N. L.; Yoon, B.; Barnett, R. N.; Whetten, R. L.; Landman, U.; Jin, R. Total Structure and Electronic Properties of the Gold Nanocrystal Au36(SR)24. *Angew. Chem. Int. Ed.* **2012**, *51*, 13114-13118.

29. Nimmala, P. R.; Knoppe, S.; Jupally, V. R.; Delcamp, J. H.; Aikens, C. M.; Dass, A. Au36(SPh)24 Nanomolecules: X-ray Crystal Structure, Optical Spectroscopy, Electrochemistry, and Theoretical Analysis. *J. Phys. Chem. B* **2014**, *118*, 14157-14167.

30. Das, A.; Liu, C.; Zeng, C.; Li, G.; Li, T.; Rosi, N. L.; Jin, R. Cyclopentanethiolato-protected Au36(SC5H9)24 nanocluster: crystal structure and implications for the steric and electronic effects of ligand. *J. Phys. Chem. A* **2014**, *118*, 8264-8269.

31. Qian, H.; Zhu, Y.; Jin, R. Size-focusing synthesis, optical and electrochemical properties of monodisperse Au38(SC2H4Ph)24 nanoclusters. *ACS Nano* **2009**, *3*, 3795-3803.

32. Qian, H.; Zhu, M.; Andersen, U. N.; Jin, R. Facile, Large-Scale Synthesis of Dodecanethiol-Stabilized Au38 Clusters†. *The Journal of Physical Chemistry A* **2009**, *113*, 4281-4284.

33. Qian, H.; Eckenhoff, W. T.; Zhu, Y.; Pintauer, T.; Jin, R. Total Structure Determination of Thiolate-Protected Au38 Nanoparticles. *J. Am. Chem. Soc.* **2010**, *132*, 8280-8281.

34. Theivendran, S.; Antony Sami, A. D. *Large-scale synthesis of Au38(SR)24thiolate gold nanomolecules*, Presented at the 2014; SERMACS-686.

35. Qian, H. Thiolate-protected Au38(SR)24 nanocluster: size-focusing synthesis, structure determination, intrinsic chirality, and beyond. *Pure Appl. Chem.* **2014**, *86*, 27-37.

36. Jiang, D.-e.; Walter, M. Au40: a large tetrahedral magic cluster. *Phys. Rev. B: Condens. Matter Mater. Phys.* **2011**, *84*, 193402/1-193402/4.

37. Nimmala, P. R.; Jupally, V. R.; Dass, A. Core size conversion: route for exclusive synthesis of Au38 or Au40 nanomolecules. *Langmuir* **2014**, *30*, 2490-2497.

38. Dass, A. Mass Spectrometric Identification of Au68(SR)34 Molecular Gold Nanoclusters with 34-Electron Shell Closing. *J. Am. Chem. Soc.* **2009**, *131*, 11666-11667.

39. Nimmala, P. R.; Dass, A. Au99(SPh)42 Nanomolecules: Aromatic Thiolate Ligand Induced Conversion of Au144(SCH2CH2Ph)60. *J. Am. Chem. Soc.* **2014**, *136*, 17016-17023.

40. Qian, H.; Jin, R. Ambient synthesis of Au144(SR)60 nanoclusters in methanol. *Chem. Mater.* **2011**, *23*, 2209-2217.

41. Qian, H.; Zhu, Y.; Jin, R. Atomically precise gold nanocrystal molecules with surface plasmon resonance. *Proc. Natl. Acad. Sci. U. S. A.* **2012**, *109*, 696-700, S696/1-S696/3.

42. Kumara, C.; Zuo, X.; Ilavsky, J.; Chapman, K. W.; Cullen, D. A.; Dass, A. Super-Stable, Highly Monodisperse Plasmonic Faradaurate-500 Nanocrystals with 500 Gold Atoms: Au~500(SR)~120. *J. Am. Chem. Soc.* **2014**, *136*, 7410-7417.

43. Negishi, Y.; Kurashige, W.; Niihori, Y.; Iwasa, T.; Nobusada, K. Isolation, structure, and stability of a dodecanethiolate-protected Pd1Au24 cluster. *Phys. Chem. Chem. Phys.* **2010**, *12*, 6219-6225.

44. Yang, A.; Wei, F.; Dong, J. Magnetic Properties of Transition-Metal-Doped Tubular Gold Clusters: M@Au24 (M = V, Cr, Mn, Fe, Co, and Ni). *J. Phys. Chem. A* **2010**, *114*, 4031-4035.

45. Qian, H.; Jiang, D.-e.; Li, G.; Gayathri, C.; Das, A.; Gil, R. R.; Jin, R. Monoplatinum Doping of Gold Nanoclusters and Catalytic Application. *J. Am. Chem. Soc.* **2012**, *134*, 16159-16162.

46. Malola, S.; Hakkinen, H. Electronic Structure and Bonding of Icosahedral Core-Shell Gold-Silver Nanoalloy Clusters Au144-xAgx(SR)60. *J. Phys. Chem. Lett.* **2011**, *2*, 2316-2321.

47. Kumara, C.; Dass, A. (AuAg)144(SR)60 alloy nanomolecules. *Nanoscale* **2011**, *3*, 3064-3067.

48. Jin, R. Atomically precise metal nanoclusters: stable sizes and optical properties. *Nanoscale* **2015**, *7*, 1549-1565.

49. Prasad, B. L. V.; Stoeva, S. I.; Sorensen, C. M.; Klabunde, K. J. Digestive-Ripening Agents for Gold Nanoparticles: Alternatives to Thiols. *Chem. Mater.* **2003**, *15*, 935-942.

50. Dharmaratne, A. C.; Krick, T.; Dass, A. Nanocluster Size Evolution Studied by Mass Spectrometry in Room Temperature Au25(SR)18 Synthesis. *J. Am. Chem. Soc.* **2009**, *131*, 13604-13605.

51. Jin, R.; Qian, H.; Wu, Z.; Zhu, Y.; Zhu, M.; Mohanty, A.; Garg, N. Size focusing: a methodology for synthesizing atomically precise gold nanoclusters. *J. Phys. Chem. Lett.* **2010**, *1*, 2903-2910.

52. Guidez, E. B.; Hadley, A.; Aikens, C. M. Initial Growth Mechanisms of Gold-Phosphine Clusters. *J. Phys. Chem. C* **2011**, *115*, 6305-6316.

53. Barngrover, B. M.; Aikens, C. M. The Golden Pathway to Thiolate-Stabilized Nanoparticles: Following the Formation of Gold(I) Thiolate from Gold(III) Chloride. *J. Am. Chem. Soc.* **2012**, *134*, 12590-12595.

54. Perala, S. R. K.; Kumar, S. On the mechanism of metal nanoparticle synthesis in the Brust–Schiffrin method. *Langmuir* **2013**, *29*, 9863-9873.

55. Jupally, V. R.; Dass, A. Synthesis of Au130(SR)50 and Au130-xAgx(SR)50 nanomolecules through core size conversion of larger metal clusters. *Phys. Chem. Chem. Phys.* **2014**, *16*, 10473-10479.

56. Nimmala, P. R.; Yoon, B.; Whetten, R. L.; Landman, U.; Dass, A. Au67(SR)35 Nanomolecules: Characteristic Size-Specific Optical, Electrochemical, Structural Properties and First-Principles Theoretical Analysis. *J. Phys. Chem. A* **2013**, *117*, 504-517.

57. Wong, O. A.; Compel, W. S.; Ackerson, C. J. Combinatorial discovery of cosolvent systems for production of narrow dispersion thiolate-protected gold nanoparticles. *ACS Comb. Sci.* **2015**, *17*, 11-18.

58. Personal communication with Roger D. Kornberg

59. Sitaula, S.; Mackiewicz, M. R.; Reed, S. M. Gold nanoparticles become stable to cyanide etch when coated with hybrid lipid bilayers. *Chem. Commun.* **2008**, 3013-3015.

60. Philip, R.; Chantharasupawong, P.; Qian, H.; Jin, R.; Thomas, J. Evolution of nonlinear optical properties: from gold atomic clusters to plasmonic nanocrystals. *Nano Lett* **2012**, *12*, 4661-7.

61. Malola, S.; Lehtovaara, L.; Enkovaara, J.; Hakkinen, H. Birth of the Localized Surface Plasmon Resonance in Monolayer-Protected Gold Nanoclusters. *ACS Nano* **2013**, *7*, 10263-10270.

62. Malola, S.; Lehtovaara, L.; Enkovaara, J.; Häkkinen, H. Birth of the Localized Surface Plasmon Resonance in Monolayer-Protected Gold Nanoclusters. *ACS Nano* **2013**, *7*, 10263-10270.

63. Yuan, X.; Zhang, B.; Luo, Z.; Yao, Q.; Leong, D. T.; Yan, N.; Xie, J. Balancing the Rate of Cluster Growth and Etching for Gram-Scale Synthesis of Thiolate-Protected Au25 Nanoclusters with Atomic Precision. *Angew. Chem. Int. Ed.* **2014**, *53*, 4623-4627.

64. Yuan, X.; Yu, Y.; Yao, Q.; Zhang, Q.; Xie, J. Fast synthesis of thiolated Au25 nanoclusters via protection-deprotection method. *J. Phys. Chem. Lett.* **2012**, *3*, 2310-2314.

65. Barngrover, B. M.; Aikens, C. M. Electron and Hydride Addition to Gold(I) Thiolate Oligomers: Implications for Gold-Thiolate Nanoparticle Growth Mechanisms. *J. Phys. Chem. Lett.* **2011**, *2*, 990-994.

66. 5,5-dimethyl-pyrroline-N-oxide

67. Beckwith, A. L. J.; Low, B. S. Thiyl radicals. I. Reactions of anthracene with oxygen and thiols. *J. Chem. Soc.* **1961**, 1304-11.

68. Banchereau, E.; Lacombe, S.; Ollivier, J. Solution reactivity of thiyl radicals with molecular oxygen: unsensitized photooxidation of dimethyl disulfide. *Tet. Lett.* **1995**, *36*, 8197-200.

69. Baucherel, X.; Uziel, J.; Juge, S. Unexpected Catalyzed C:C Bond Cleavage by Molecular Oxygen Promoted by a Thiyl Radical. *J. Org. Chem.* **2001**, *66*, 4504-4510.

70. Tan, K. J.; Wille, U. Activation of molecular oxygen by S-radicals: experimental and computational studies on a novel oxidation of alkynes to α-diketones. *Chem. Commun.* **2008**, 6239-6241.

71. Nauser, T.; Koppenol, W. H.; Schoneich, C. Reversible Hydrogen Transfer Reactions in Thiyl Radicals From Cysteine and Related Molecules: Absolute Kinetics and Equilibrium Constants Determined by Pulse Radiolysis. *J. Phys. Chem. B* **2012**, *116*, 5329-5341.

72. Zhang, Z.; Chen, Z.; Pan, D.; Chen, L. Fenton-like Reaction-Mediated Etching of Gold Nanorods for Visual Detection of Co2+. *Langmuir* **2015**, *31*, 643-650.

CHAPTER 4: OXYGEN'S ROLE IN AQUEOUS GOLD CLUSTER SYNTHESIS*

4.1 Synopsis

The presence of oxygen in thiolate-protected gold nanoparticle synthesis influences product distribution. Oxygen's diradical nature underlies this effect, and oxygen can be replaced with radical initiators in the synthesis of organosoluble gold nanoclusters. The role of O_2 in the synthesis of water-soluble clusters such as $Au_{102}(p\text{-MBA})_{44}$, $Au_{25}(SR)_{18}$, as well as the thiol etching of water-soluble colloidal gold particles is not yet established. Herein it is shown that radicals, either from O_2 or from radical initiators such as 4-hydroxy-TEMPO are necessary components for synthesis of water-soluble thiolate-protected gold nanoclusters, as well as the etching of aqueous colloidal gold by thiols. Furthermore, air-free synthetic routes to water-soluble gold nanoclusters $Au_{102}(SR)_{44}$ and $Au_{25}(SR)_{18}$ are described. Overall, the understanding of the role of radicals in the synthesis of water-soluble gold clusters will allow standardization of often difficult to reproduce syntheses that attract increasing attention for biological applications.

4.2 Introduction

Water-soluble gold nanoparticles are used or investigated in bio-imaging, drug adjuvant, and antimicrobial applications.[1-9] The bioavailability, biocompatibility, and cytotoxicity of water-soluble gold particles is extensively investigated.[8, 10-14] In contrast to clusters soluble in organic solvents (e.g. $Au_{25}(SCH_2CH_2Ph)_{18}$, $Au_{38}(SCH_2CH_2Ph)_{24}$, $Au_{144}(SCH_2CH_2Ph)_{60}$, etc.) the synthesis of atomically precise water-soluble clusters, is not as well developed. [3, 15-35] [36-37]

* The work presented herein is published in the *Journal of Physical Chemistry C*. Timothy A. Dreier's contributions include experimental design, data gathering & interpretation, and preparation of the manuscript. *J. Phys. Chem. C* **2016**, *120*, 28288–28294.

Gold and silver clusters ligated by water-soluble thiols (e.g. 4-mercaptobenzoic acid, *p*-MBA) are synthetically well established.[38-42] While the synthesis is remarkably tunable giving, for instance, $Au_{25}(SR)_{18}$, $Au_{102}(p\text{-MBA})_{44}$, and $Au_{144}(p\text{-MBA})_{60}$, it is exceptionally sensitive to minor procedural changes. For example, the established synthesis of Au_{102} ligated by 4-mercaptobenzoic acid, $Au_{102}(p\text{-MBA})_{44}$, varies with slight changes in ambient atmosphere, supplier of $HAuCl_4 \cdot 3H_2O$ starting material, $NaBH_4$ quality, and solvent composition.[43-44] The difficulty in synthesis means that, on a practical basis, investigation of $Au_{102}(p\text{-MBA})_{44}$ is limited compared to Au_{25} and Au_{144}.[36, 38, 44] While somewhat more robust, the synthesis of Au_{25} protected by glutathione, $Au_{25}(SG)_{18}$, also presents practical challenges.[45-48]

We have investigated many routes for improved synthesis of water-soluble clusters. [14, 36, 40, 43, 49-56] Here we report an attempt to better understand the role of oxygen and radicals in the synthesis of water-soluble clusters. Our recent investigation of radical processes involved in the formation of organic-soluble $Au_{25}(SR)_{18}$ revealed that the etching or size-focusing process involved in the last step in the Brust-Schiffrin method is oxygen dependent.[57] Additionally, we found no oxygen dependence for either the Au(I)-SR oligo/polymer formation or the initial growth steps in the generally accepted reaction scheme.[58-61] Herein, we evaluate the role of oxygen and radical initiators in aqueous solvent mixtures, and if that could be exploited to further our synthetic goals.

4.3 Results

We tested the role of oxygen in thiol-based etching commercially available 5 nm AuNPs protected by tannic acid in water. Figure 4.1 shows that the 5 nm nanoparticles initially etch in the presence of thioglycolic acid (1000 equiv to Au). When air or argon atmospheres are present, the concentration of 5 nm AuNPs stabilizes after an hour. As can be seen under an oxygen atmosphere etching continues over the course of the experiment. When the etching experiment was conducted for 24 hrs (1440 min) under Ar and O_2 atmospheres, the concentration of AuNPs remained stable

in the former case, while diminishing to approximately 50% of its initial value in the latter. These results are broadly consistent with our prior study of phosphatidylcholine-protected AuNPs in

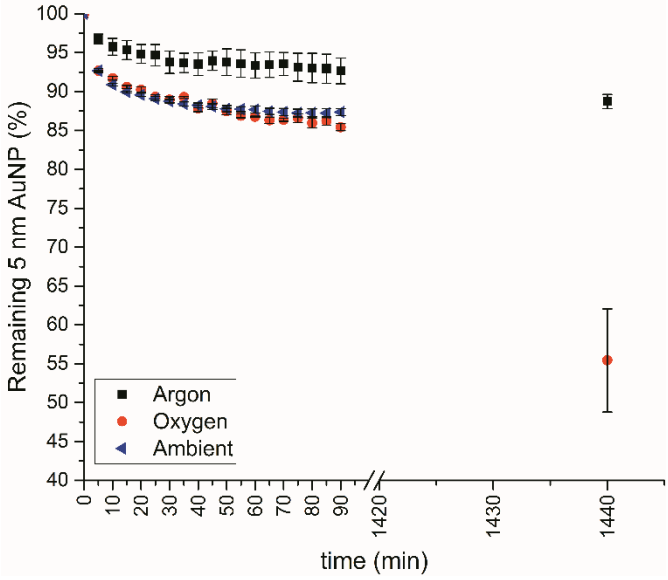

Figure 4.1. Etching of colloidal AuNPs using thioglycolic acid in water. Average of three runs, error bars showing standard error. Y-axis is the AuNP concentration at t_n as a percentage of concentration at t_0. Full details in Appendix C.

organic solvents.[57]

Considering the notable similarity to our previously reported result (*vide* supra), we hypothesized that the diradical nature of $^3O_2$ underlies the observation. Inspired by the problem of reproducible synthesis of $Au_{102}(pMBA)_{44}$,[14, 32, 38, 44, 49, 54, 62] we undertook a series of experiments to explore the role of atmospheric composition on $Au_{102}(p\text{-MBA})_{44}$ synthesis. Figure 4.2 shows that when $NaBH_4$ reduction is performed under oxygen-containing atmosphere (Figure 4.2, lanes 4-9), significant $Au_{102}(p\text{-MBA})_{44}$ is produced, as judged by electrophoretic mobility relative to the standard $Au_{102}(pMBA)_{44}$ synthesis. Exclusion of oxygen during $NaBH_4$ reduction (Figure 4.2, lanes 1-3) stops $Au_{102}(p\text{-MBA})_{44}$ synthesis, producing much larger products. In each experiment we separated the initial formation of the Au(I)-pMBA oligo/polymer from the subsequent $NaBH_4$

reduction step. As can be seen, only exclusion of oxygen from the reduction step results in a change in the reaction's behavior. Overall, this result is consistent with our previous results for the synthesis of $Au_{25}(SR)_{18}$ in organic solvents and the earlier observations of Murray.[21, 57]

Polymer Formation	Ar	O_2	Air	Ar	O_2	Air	Ar	O_2	Air	-
Reduction	Ar	Ar	Ar	O_2	O_2	O_2	Air	Air	Air	-
Lane Number	**1**	**2**	**3**	**4**	**5**	**6**	**7**	**8**	**9**	**10**

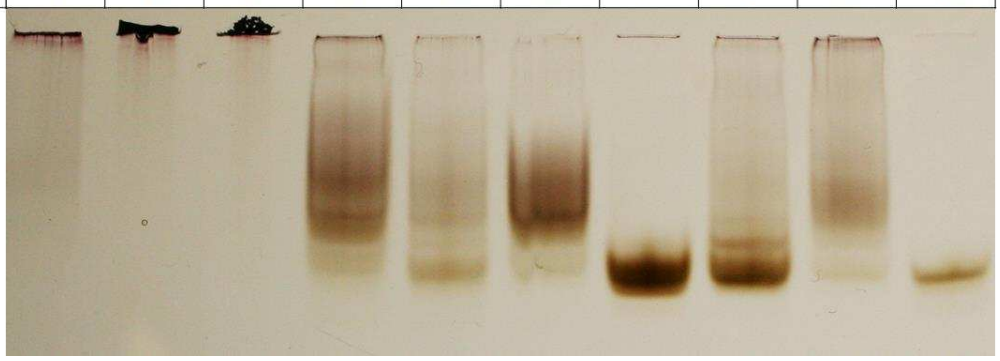

Figure 4.2. Effect of atmosphere on Au_{102} synthesis. Crossover experiments showing the effect of oxygenated vs inert atmosphere on the synthesis of Au_{102}(*p*-MBA)$_{44}$. Lanes 4-9 show that the reduction step requires oxygen. Lane 10 is an Au_{102} standard for reference.

We hypothesized that the oxygen may be replaced with a radical initiator in the water-soluble Brust-type synthesis. We screened several radical initiators in an attempt to synthesize Au_{102}(*p*-MBA)$_{44}$ under inert atmosphere (i.e., more carefully controlled conditions than typical). Figure 4.3 summarizes the products that result from inclusion of differing amounts of 4 different radical initiators. The molar equivalents of radical initiator are shown on the x-axis, with the ratio of distance travelled to Au_{102}(*p*-MBA)$_{44}$ standard on the y-axis. Values of 1.0 indicate perfect alignment with Au_{102}(p-MBA)$_{44}$.

Figure 4.3 shows that Oxone, 4-hydroxy-TEMPO, and sodium persulfate delivered products with electrophoretic mobility similar to that of Au_{102}(*p*-MBA)$_{44}$ under the reaction conditions.

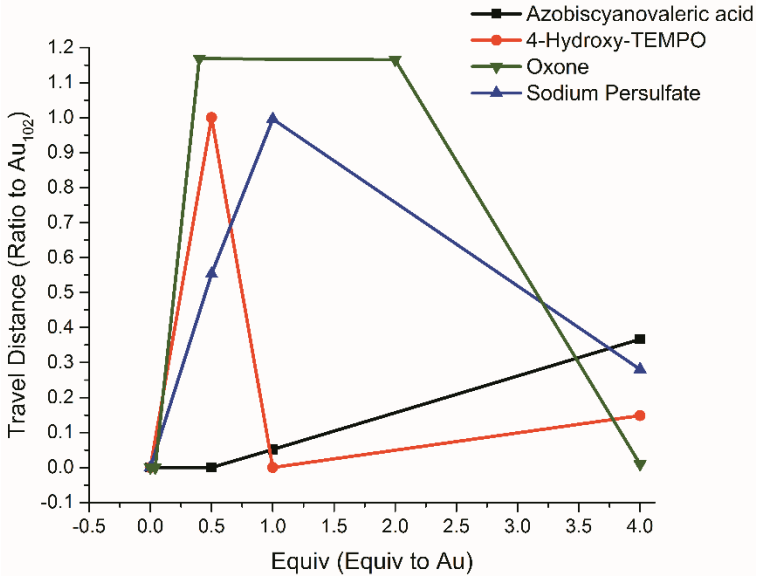

Figure 4.3. Radical initiators in Au_{102} synthesis. Effect of changing radical initiator concentration on product mobility in PAGE compared to $Au_{102}(p\text{-MBA})_{44}$ standard. All reactions were performed under inert atmosphere with degassed solvents.

Azobiscyanovaleric acid (ABCVA), chosen for its structural similarity to the 2,2'-azobisisobutryonitrile (AIBN), effective in our prior work,[57] only gave quite large particles as judged by their electrophoretic mobility even in large excess to Au. Curiously, in the cases of Oxone, and sodium persulfate large excesses of initiator resulted in the formation of larger products as judged by electrophoretic mobility. Interestingly, 4-hydroxy-TEMPO exhibited similar behavior, but more than 0.5 equivalents to Au atoms favors larger products. This may be best understood by viewing etching and growth as simultaneous, competing processes, and could result from additional radical initiator allowing enough gold surface exposure to favor growth.

Our results are entirely empirical, and with judicious screening it may be possible to find initiators that favor products of specific sizes. The full experimental details and PAGE gels for each of these experiments is available in Appendix C.

MALDI-Mass spec validates our assignments made on the basis of gel electrophoretic mobility. As can be seen in Figure 4.4, the radically initiated conditions deliver a product with a

similar mass and envelope shape, with both spectra consistent with the MALDI-MS reported by Kornberg previously.[38]

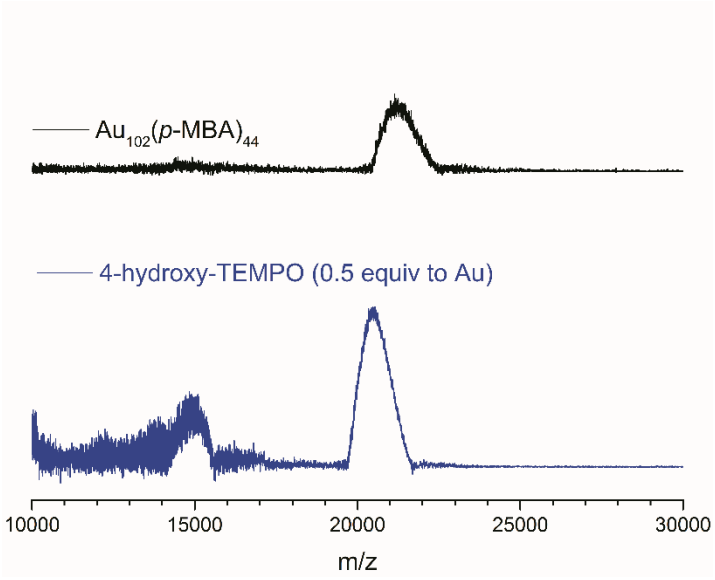

Figure 4.4. MALDI spectrum of Au_{102}(*p*-MBA)$_{44}$ (top) and results of using 0.5 equiv. of 4-hydroxy-TEMPO to Au under air-free conditions.

It should be noted that the position of the radically initiated envelope is at M/Z of 20502, while the Au_{102} standard is centered about 21139. This difference in mean mass is likely attributable to slight differences in actual product distribution, owing to the difficulty in separating Au_{102} from other clusters of similar size. [24, 38-39, 63] Even after repeated fractional precipitation and gel purification, Au_{102}(*p*-MBA)$_{44}$ often contains impurities with 103 or 104 Au atoms. The MALDI-MS sample for the 4-hydroxy-TEMPO reaction was not purified beyond an initial precipitation, and as such is likely to contain a higher proportion of impurities such as Au_{99} and Au_{100}. Taken together with the identical electrophoretic mobility, these data indicate that a radical initiation strategy is viable for the synthesis of Au_{102}(*p*-MBA)$_{44}$.

The *p*-MBA ligand is unusual in gold nanocluster synthesis. In the case of most ligands, increasing ligand concentration results in the formation of smaller products, presumably by favoring etching over growth.[32, 64-68] However, in the case of *p*-MBA, increasing concentration of

ligand tends toward larger products.[40] We hypothesized that the thiyl radical formed from *p*-MBA may be stable enough to inhibit the etching of particles, leading to the seemingly paradoxical result. Under this hypothesis, increasing radical concentration initiation would result in higher concentrations of *p*-MBA giving smaller products. We performed a screen of *p*-MBA concentration using 500 mg Oxone in each experiment (Appendix C, Figure C.44). Results suggest that even in air-free, radical initiation conditions increased concentration of *p*-MBA gives larger particles. This indicates that the origin of *p*-MBA's unusual behavior is separate from the etching mechanism.

Having demonstrated that Au_{102}(*p*-MBA)$_{44}$ can be synthesized under air-free conditions we sought to understand if our prior method for the air-free synthesis of $Au_{25}(SR)_{18}$ using radical initiation would translate to aqueous Au_{25} systems.[57] The two ligands used most commonly for the synthesis of water soluble Au_{25} are glutathione (GSH) and captopril (Capt).[25, 69-70] We began our investigation into the Au_{25} system using captopril as the ligand. We first performed a screen of radical initiators, taking inspiration from our prior work and the results from the Au_{102}(*p*-MBA)$_{44}$ system evaluated above. Figure 4.5 shows the results of these experiments. 4-hydroxy-TEMPO and azobiscyanovaleric acid (ABCVA) resulted in formation of $Au_{25}(Capt)_{18}$. Similar to the

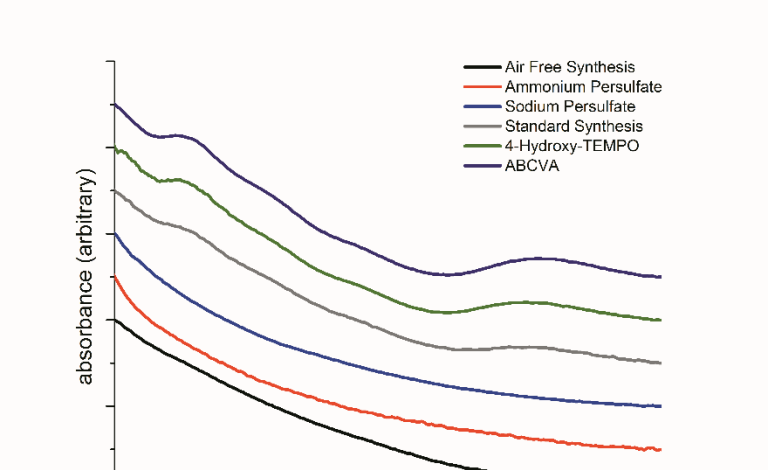

Figure 4.5. Evaluation of radical initiators for Air-free synthesis of $Au_{25}(Capt)_{18}$.

Au_{102}(*p*-MBA)$_{44}$ synthesis conditions, other radical initiators or oxygen sources gave no yield of the desired product.

To complete our evaluation of radical initiation as a strategy for air-free synthesis, we used a subset of radical initiators in the synthesis of $Au_{25}(SG)_{18}$ under inert conditions. Rather than repeat the entire screen with all of the on-hand initiators, we used those which had given promising results in either the Au_{102}(*p*-MBA)$_{44}$ or $Au_{25}(Capt)_{18}$ experiments. Figure 4.6 shows the optical spectra from these experiments. As can be seen in each case the optical spectra match those of the known $Au_{25}(SG)_{18}$ compound.[25]

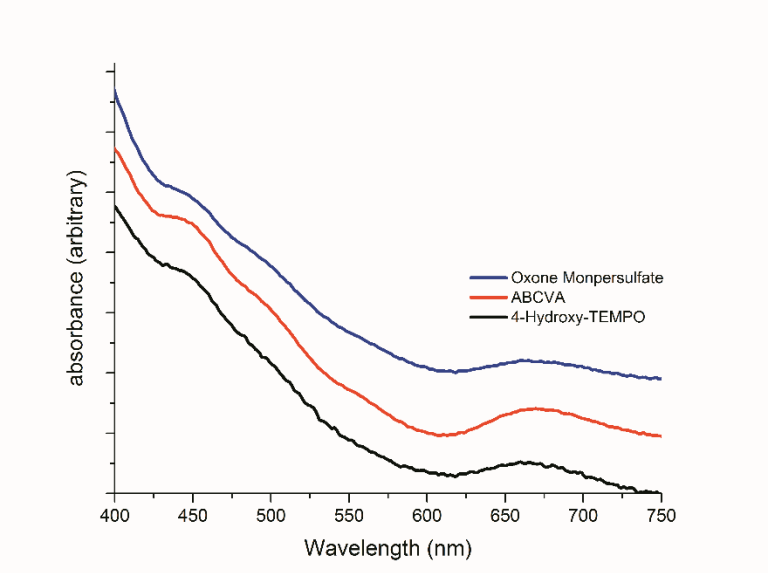

Figure 4.6. Evaluation of radical initiators for synthesis of $Au_{25}(SG)_{18}$ under air-free conditions.

4.4 Discussion

For many years in nanoparticle synthesis, etching (also called size-focusing or digestive ripening) was used as a strategy for shape and size control of inorganic nanoparticles.[71-75] Previous reports often note that oxygen plays a role in this process, although the exact role is obscure.[76-81] In some cases, notably by Xia, oxygen is added explicitly.[82] Oxygen may also be necessary in the core-size conversion syntheses of nanoclusters reported by Dass.[83-84]

Previously we showed radicals as a necessary component for etching in organic solvent. Here we show the general necessity of oxygen in aqueous etching of gold nanoparticles by thioglycolic acid. As can be seen in Figure 4.1, the oxygen and air atmospheres show similar curves for the first 85 minutes of the experiment. After this period etching in air stalls, whereas etching under oxygen atmosphere continues. Over the course of a 24 h experiment, the concentration of AuNPs under argon atmosphere remains constant after 90 minutes, but etching continues in an oxygen environment. The initial etching under argon is likely due to the difficulty of entirely degrassing solutions of AuNPs. For instance, if solutions of AuNPs were sparged with argon longer than c.a. 5 min, the solutions would turn purple, indicating growth of the particles. This agglomeration is caused by the physical disturbance of the solution, rather than by any interaction of the Ar directly with the nanoparticles. Sparging with oxygen for prolonged periods in an attempt to ensure consistent O_2 concentration in the solution for our experiments gave rapid destruction of the 5 nm AuNPs, as indicated by the solutions turning from red to colorless. This is attributable to the particles being directly oxidized by oxygen to Au(I) species which are colorless in solution. Because the particles are protected by tannic acid, rather than thiolates, the surface is fairly easy to expose.[85] Once the etching was allowed to proceed for 24 hours a large divergence in outcome could be observed (Figure 4.1, 1440 min). It should be noted that the error on the 24 h experiment is much larger than on any other observations, this is likely due to differences in dissolved oxygen content due to the considerations noted above. These results are consistent with our prior observations, and indicate that the likely mechanism of oxygen involvement is the same between aqueous and organic systems of 5 nm AuNPs.

Our results from the syntheses of Au_{102}(p-MBA)$_{44}$ under inert conditions, while consistent with our previous results, do not wholly solve the problem of synthetic variability. We were able to

synthesize a limited amount of Au_{102}(p-MBA)$_{44}$ using 4-hydroxy-TEMPO or sodium persulfate under inert atmosphere (Figure 4.3), but these reactions remained inconsistent and poorly behaved, without the concomitant increase in yield that would justify the increased procedural complexity. However, the results do indicate that with further optimization, consistent synthesis of Au_{102}(p-MBA)$_{44}$ under inert conditions should be possible, allowing for its further use as a chemical and biological tool.[14, 44, 86] Figure 4.2 does indicate one intriguing possibility, however. If the precursor formation step is run under argon, but the reduction is performed under air (Figure 4.2, lane 7) the product mixture appears to have much lower dispersity. While we have no concrete explanation for this, it is possible that, much like the results from Figure 4.3, there is an optimal O_2 concentration for Au_{102}(p-MBA)$_{44}$ formation, which is achieved at slightly lower than atmospheric oxygen content, which arises from degassing the initial precursor formation step. Given the large body of literature surrounding precursor influence on nanocluster formation,[60-61, 87-90] it is also possible that the atmospheric change influences the nature of precursor involved, favoring formation of Au_{102}(p-MBA)$_{44}$ sized particles. It may be possible to use this strategy to cleanly form Au_{102}(p-MBA)$_{44}$ without addition of too much procedural complexity, despite the difficulties of degassing aqueous solutions.

Our results with water-soluble $Au_{25}(SR)_{18}$ are much more promising. Using several radical initiators, it is possible to produce reasonable amounts of $Au_{25}(SR)_{18}$ ligated by either captopril or glutathione. Coupled with our results from organic-soluble $Au_{25}(SR)_{18}$,[57] this appears to be a general feature of the $Au_{25}(SR)_{18}$ synthesis. Much progress has been made in synthesizing quantum-confined Au clusters over the past several decades,[28, 32, 38, 91-94] however each advance has thus far been fundamentally limited that the ligand be stable to air and the highly reducing

reaction environment. This work opens the possibility to synthesize clusters containing more air-sensitive moieties.

A further, and perhaps more intriguing possibility to the nanoparticle community, is the potential to directly synthesize noncanonical charge states of quantum-confined Au clusters. Work in our lab has interrogated the effect of changing charge state on the structural, magnetic, and electronic properties of Au clusters.[50, 95] A fundamental challenge to this work is the difficulty in accessing the (+1) charge state of $Au_{25}(SR)_{18}$, which can only be generated by electrochemical methods.[50] With a general strategy for the air-free synthesis of thiolated Au clusters now available, a new area of chemical space should be open for exploration.

4.5 Conclusion

Since the advent of the Brust synthesis, the role of oxygen in its performance has been noted, but until recently was mechanistically obscure. In our previous work we demonstrated that it is likely the diradical nature of O_2 that underlies the need for oxygen in the synthesis using organic solvents. Given the results presented above, it is likely that the same process is operative: oxygen allows for the formation of a thiyl radical, which can etch the gold surface.[57] Here we extend the work to address water-soluble synthesis of $Au_{102}(p\text{-MBA})_{44}$, $Au_{25}(Capt)_{18}$, and $Au_{25}(SG)_{18}$ in aqueous solvent. By using radical initatiors under inert atmosphere, we have synthesized each of these clusters under argon atmosphere. This opens up new possibilities for the entire field – use of air-sensitive ligands, direct synthesis of unstable charge states, and a new variable by which synthesis can be optimized. With a new method by which thiolate Au cluster synthesis can be modified, and the additional mechanistic insight brought about by our work, we may soon enter a new golden age of cluster synthesis.

REFERENCES

1. Arachchige, I. U.; Szymanski, P. L.; Ivanov, S. A. *Electrochemical routes to luminescent gold nanoclusters,* Presented at the National Meeting of the American Chemical Society, 2010; INOR-985.

2. Habeeb, M. M. A.; Verma, P. K.; Pal, S. K.; Retnakumari, A.; Koyakutty, M.; Nair, S.; Pradeep, T. Luminescent quantum clusters of gold in bulk by albumin-induced core etching of nanoparticles: metal ion sensing, metal-enhanced luminescence, and biolabeling. *Chem. Eur. J.* **2010**, *16*, 10103-10112.

3. Shibu, E. S.; Radha, B.; Verma, P. K.; Bhyrappa, P.; Kulkarni, G. U.; Pal, S. K.; Pradeep, T. Functionalized Au22 clusters: synthesis, characterization, and patterning. *ACS Appl. Mater. Interfaces* **2009**, *1*, 2199-2210.

4. Stover, R.; Murthy, A.; Gourisankar, S.; Nie, G.; Martinez, M.; Truskett, T.; Sokolov, K.; Johnston, K. Plasmonic biodegradable gold nanoclusters with high NIR-absorbance for biomedical imaging. *Proc. SPIE* **2014**, *8955*, 89550T/1-89550T/7.

5. Zhou, R.; Shi, M.; Chen, X.; Wang, M.; Chen, H. Atomically monodispersed and fluorescent sub-nanometer gold clusters created by biomolecule-assisted etching of nanometer-sized gold particles and rods. *Chem. Eur. J.* **2009**, *15*, 4944-4951.

6. Agbasi-Porter, C.; Ryman-Rasmussen, J.; Franzen, S.; Feldheim, D. Transcription inhibition using oligonucleotide-modified gold nanoparticles. *Bioconjugate Chem.* **2006**, *17*, 1178-1183.

7. Bowman, M.-C.; Ballard, T. E.; Ackerson, C. J.; Feldheim, D. L.; Margolis, D. M.; Melander, C. Inhibition of HIV fusion with multivalent gold nanoparticles. *J. Am. Chem. Soc.* **2008**, *130*, 6896-6897.

8. Bresee, J.; Bond, C. M.; Worthington, R. J.; Smith, C. A.; Gifford, J. C.; Simpson, C. A.; Carter, C. J.; Wang, G.; Hartman, J.; Osbaugh, N. A., et al. Nanoscale structure-activity relationships, mode of action, and biocompatibility of gold nanoparticle antibiotics. *J. Am. Chem. Soc.* **2014**, *136*, 5295-5300.

9. Gifford, J. C.; Bresee, J.; Carter, C. J.; Wang, G.; Melander, R. J.; Melander, C.; Feldheim, D. L. Thiol-modified gold nanoparticles for the inhibition of Mycobacterium smegmatis. *Chem. Commun.* **2014**, *50*, 15860-15863.

10. Simpson, C. A.; Salleng, K. J.; Cliffel, D. E.; Feldheim, D. L. In vivo toxicity, biodistribution, and clearance of glutathione-coated gold nanoparticles. *Nanomedicine* **2013**, *9*, 257-263.

11. Simpson, C. A.; Agrawal, A. C.; Balinski, A.; Harkness, K. M.; Cliffel, D. E. Short-chain PEG mixed monolayer protected gold clusters cncrease clearance and red blood cell counts. *ACS Nano* **2011**, *5*, 3577-3584.

12. Simpson, C. A.; Huffman, B. J.; Cliffel, D. E. In vivo testing for gold nanoparticle toxicity. *Methods. Mol. Biol.* **2013**, *1026*, 175-186.

13. Simpson, C. A.; Huffman, B. J.; Gerdon, A. E.; Cliffel, D. E. Unexpected toxicity of monolayer protected gold clusters eliminated by PEG-thiol place exchange reactions. *Chem. Res. Toxicol.* **2010**, *23*, 1608-1616.

14. Wong, O. A.; Hansen, R. J.; Ni, T. W.; Heinecke, C. L.; Compel, W. S.; Gustafson, D. L.; Ackerson, C. J. Structure-activity relationships for biodistribution, pharmacokinetics, and excretion of atomically precise nanoclusters in a murine model. *Nanoscale* **2013**, *5*, 10525-10533.

15. Dass, A.; Stevenson, A.; Dubay, G. R.; Tracy, J. B.; Murray, R. W. Nanoparticle MALDI-TOF mass spectrometry without fragmentation: Au25(SCH2CH2Ph)18 and mixed monolayer Au25(SCH2CH2Ph)18-x(L)x. *J. Am. Chem. Soc.* **2008**, *130*, 5940-5946.

16. Farrag, M.; Tschurl, M.; Dass, A.; Heiz, U. Infra-red spectroscopy of size selected Au25, Au38 and Au144 ligand protected gold clusters. *Phys. Chem. Chem. Phys.* **2013**, *15*, 12539-12542.

17. Jin, S.; Meng, X.; Jin, S.; Zhu, M. High yield synthesis of Au25 nanoclusters by controlling the reduction process. *J. Nanosci. Nanotechnol.* **2013**, *13*, 1282-1285.

18. MacDonald, M. A.; Chevrier, D. M.; Zhang, P.; Qian, H.; Jin, R. The structure and bonding of Au25(SR)18 nanoclusters from EXAFS: the interplay of metallic and molecular behavior. *J. Phys. Chem. C* **2011**, *115*, 15282-15287.

19. Meng, X.; Liu, Z.; Zhu, M.; Jin, R. Controlled reduction for size selective synthesis of thiolate-protected gold nanoclusters Aun(n = 20, 24, 39, 40). *Nanoscale Res. Lett.* **2012**, *7*, 277.

20. Meng, X.; Xu, Q.; Wang, S.; Zhu, M. Ligand-exchange synthesis of selenophenolate-capped Au25 nanoclusters. *Nanoscale* **2012**, *4*, 4161-4165.

21. Parker, J. F.; Weaver, J. E. F.; McCallum, F.; Fields-Zinna, C. A.; Murray, R. W. Synthesis of monodisperse [Oct4N+][Au25(SR)18-] nanoparticles, with some mechanistic observations. *Langmuir* **2010**, *26*, 13650-13654.

22. Qian, H.; Jin, R. Ambient synthesis of Au144(SR)60 nanoclusters in methanol. *Chem. Mater.* **2011**, *23*, 2209-2217.

23. Qian, H.; Zhu, M.; Lanni, E.; Zhu, Y.; Bier, M. E.; Jin, R. Conversion of polydisperse Au nanoparticles into monodisperse Au25 nanorods and nanospheres. *J. Phys. Chem. C* **2009**, *113*, 17599-17603.

24. Qian, H.; Zhu, M.; Wu, Z.; Jin, R. Quantum sized gold nanoclusters with atomic precision. *Acc. Chem. Res.* **2012**, *45*, 1470-1479.

25. Shichibu, Y.; Negishi, Y.; Tsukuda, T.; Teranishi, T. Large-scale synthesis of thiolated Au25 clusters via ligand Exchange reactions of phosphine-stabilized Au11 clusters. *J. Am. Chem. Soc.* **2005**, *127*, 13464-13465.

26. Yu, Y.; Chen, X.; Yao, Q.; Yu, Y.; Yan, N.; Xie, J. Scalable and precise synthesis of thiolated Au10-12, Au15, Au18, and Au25 nanoclusters via pH controlled CO reduction. *Chem. Mater.* **2013**, *25*, 946-952.

27. Yuan, X.; Yu, Y.; Yao, Q.; Zhang, Q.; Xie, J. Fast synthesis of thiolated Au25 nanoclusters via protection-deprotection method. *J. Phys. Chem. Lett.* **2012**, *3*, 2310-2314.

28. Beqa, L.; Deschamps, D.; Perrio, S.; Gaumont, A.-C.; Knoppe, S.; Burgi, T. Ligand exchange reaction on Au38(SR)24, separation of Au38(SR)23(SR')1 regioisomers, and migration of thiolates. *J. Phys. Chem. C* **2013**, *117*, 21619-21625.

29. Chevrier, D. M.; Chatt, A.; Zhang, P.; Zeng, C.; Jin, R. Unique bonding properties of the Au36(SR)24 nanocluster with FCC-like core. *J. Phys. Chem. Lett.* **2013**, *4*, 3186-3191.

30. Das, A.; Liu, C.; Zeng, C.; Li, G.; Li, T.; Rosi, N. L.; Jin, R. Cyclopentanethiolato-protected Au36(SC5H9)24 nanocluster: crystal structure and implications for the steric and electronic effects of ligand. *J. Phys. Chem. A* **2014**, *118*, 8264-8269.

31. Donkers, R. L.; Lee, D.; Murray, R. W. Synthesis and isolation of the molecule-like cluster Au38(PhCH2CH2S)24. *Langmuir* **2004**, *20*, 1945-1952.

32. Jin, R. Atomically precise metal nanoclusters: stable sizes and optical properties. *Nanoscale* **2015**, *7*, 1549-1565.

33. Jung, J.; Kang, S.; Han, Y.-K. Ligand effects on the stability of thiol-stabilized gold nanoclusters: Au25(SR)18-, Au38(SR)24, and Au102(SR)44. *Nanoscale* **2012**, *4*, 4206-4210.

34. Knoppe, S.; Burgi, T. Chirality in thiolate-protected gold clusters. *Acc. Chem. Res.* **2014**, *47*, 1318-1326.

35. Knoppe, S.; Michalet, S.; Burgi, T. Stabilization of thiolate-protected gold clusters against thermal inversion: diastereomeric Au38(SCH2CH2Ph)24-2x(R-BINAS)x. *J. Phys. Chem. C* **2013**, *117*, 15354-15361.

36. Wong, O. A.; Heinecke, C. L.; Simone, A. R.; Whetten, R. L.; Ackerson, C. J. Ligand symmetry-equivalence on thiolate protected gold nanoclusters determined by NMR spectroscopy. *Nanoscale* **2012**, *4*, 4099-4102.

37. Jadzinsky, P. D.; Calero, G.; Ackerson, C. J.; Bushnell, D. A.; Kornberg, R. D. Structure of a thiol monolayer-protected gold ganoparticle at 1.1 Å resolution. *Science* **2007**, *318*, 430-433.

38. Levi-Kalisman, Y.; Jadzinsky, P. D.; Kalisman, N.; Tsunoyama, H.; Tsukuda, T.; Bushnell, D. A.; Kornberg, R. D. Synthesis and characterization of Au102(p-MBA)44 nanoparticles. *J. Am. Chem. Soc.* **2011**, *133*, 2976-2982.

39. Alvarez, M. M.; Chen, J.; Plascencia-Villa, G.; Black, D. M.; Griffith, W. P.; Garzon, I. L.; Jose-Yacaman, M.; Demeler, B.; Whetten, R. L. Hidden components in aqueous gold-144 Fractionated by PAGE: high-resolution orbitrap ESI-MS identifies the gold-102 and higher all-aromatic Au-pMBA cluster compounds. *J. Phys. Chem. B* **2016**, Ahead of Print.

40. Tvedte, L. M.; Ackerson, C. J. Size-focusing synthesis of gold nanoclusters with p-mercaptobenzoic acid. *The Journal of Physical Chemistry A* **2014**, *118*, 8124-8128.

41. Black, D. M.; Bach, S. B. H.; Whetten, R. L. Capillary liquid chromatography mass spectrometry analysis of intact monolayer-protected gold clusters in complex mixtures. *Anal. Chem.* **2016**, *88*, 5631-5636.

42. Plascencia-Villa, G.; Demeler, B.; Whetten, R. L.; Griffith, W. P.; Alvarez, M.; Black, D. M.; Jose-Yacaman, M. Analytical characterization of size-dependent properties of larger aqueous gold nanoclusters. *J. Phys. Chem. C* **2016**, *120*, 8950-8958.

43. Wong, O. A.; Compel, W. S.; Ackerson, C. J. Combinatorial discovery of cosolvent systems for production of narrow dispersion thiolate-protected gold nanoparticles. *ACS Comb. Sci.* **2015**, *17*, 11-18.

44. Hulkko, E.; Lopez-Acevedo, O.; Koivisto, J.; Levi-Kalisman, Y.; Kornberg, R. D.; Pettersson, M.; Hakkinen, H. Electronic and vibrational signatures of the Au102(p-MBA)44 cluster. *J. Am. Chem. Soc.* **2011**, *133*, 3752-3755.

45. Schaaff, T. G.; Knight, G.; Shafigullin, M. N.; Borkman, R. F.; Whetten, R. L. Isolation and selected properties of a 10.4 kDa gold:glutathione cluster compound. *J. Phys. Chem. B* **1998**, *102*, 10643-10646.

46. Negishi, Y.; Takasugi, Y.; Sato, S.; Yao, H.; Kimura, K.; Tsukuda, T. Magic-numbered Aun clusters protected by glutathione monolayers (n = 18, 21, 25, 28, 32, 39): isolation and spectroscopic characterization. *J. Am. Chem. Soc.* **2004**, *126*, 6518-6519.

47. Shibu, E. S.; Muhammed, M. A. H.; Tsukuda, T.; Pradeep, T. Ligand exchange of Au25SG18 leading to functionalized gold clusters: spectroscopy, kinetics, and luminescence. *J. Phys. Chem. C* **2008**, *112*, 12168-12176.

48. Muhammed, M. A. H.; Verma, P. K.; Pal, S. K.; Kumar, R. C. A.; Paul, S.; Omkumar, R. V.; Pradeep, T. Bright, NIR-emitting Au23 from Au25: characterization and applications including biolabeling. *Chem. Eur. J.* **2009**, *15*, 10110-10120.

49. Walter, M.; Akola, J.; Lopez-Acevedo, O.; Jadzinsky, P. D.; Calero, G.; Ackerson, C. J.; Whetten, R. L.; Gronbeck, H.; Hakkinen, H. A unified view of ligand-protected gold clusters as superatom complexes. *Proc. Natl. Acad. Sci. U. S. A.* **2008**, *105*, 9157-9162.

50. Tofanelli, M. A.; Ackerson, C. J. Superatom electron configuration predicts thermal stability of Au25(SR)18 nanoclusters. *J. Am. Chem. Soc.* **2012**, *134*, 16937-16940.

51. Heinecke, C. L.; Ni, T. W.; Malola, S.; Mäkinen, V.; Wong, O. A.; Häkkinen, H.; Ackerson, C. J. Structural and theoretical basis for ligand exchange on thiolate monolayer protected gold nanoclusters. *J. Am. Chem. Soc.* **2012**, *134*, 13316-13322.

52. Yi, C.; Tofanelli, M. A.; Ackerson, C. J.; Knappenberger, K. L. Optical properties and electronic energy relaxation of metallic Au144(SR)60 nanoclusters. *J. Am. Chem. Soc.* **2013**, *135*, 18222-18228.

53. Heinecke, C. L.; Ackerson, C. J. Preparation of gold nanocluster bioconjugates for electron microscopy. *Methods. Mol. Biol.* **2013**, *950*, 293-311.

54. Knoppe, S.; Wong, O. A.; Malola, S.; Häkkinen, H.; Bürgi, T.; Verbiest, T.; Ackerson, C. J. Chiral phase transfer and enantioenrichment of thiolate-protected Au102 clusters. *J. Am. Chem. Soc.* **2014**, *136*, 4129-4132.

55. Ni, T. W.; Tofanelli, M. A.; Phillips, B. D.; Ackerson, C. J. Structural basis for ligand exchange on Au25(SR)18. *Inorg. Chem.* **2014**, *53*, 6500-6502.

56. Dreier, T. A.; Wong, O. A.; Ackerson, C. J. Oxidative decomposition of Au25(SR)18 clusters in a catalytic context. *Chem. Commun.* **2015**, *51*, 1240-1243.

57. Dreier, T. A.; Ackerson, C. J. Radicals are required for thiol etching of gold particles. *Angew. Chem. Int. Ed.* **2015**, *54*, 9249-9252.

58. Brust, M.; Walker, M.; Bethell, D.; Schiffrin, D. J.; Whyman, R. Synthesis of thiol-derivatised gold nanoparticles in a two-phase liquid-liquid system. *J. Chem. Soc., Chem. Commun.* **1994**, 801-802.

59. Brust, M.; Fink, J.; Bethell, D.; Schiffrin, D. J.; Kiely, C. Synthesis and reactions of functionalized gold nanoparticles. *J. Chem. Soc., Chem. Commun.* **1995**, 1655-6.

60. Goulet, P. J. G.; Lennox, R. B. New insights into Brust−Schiffrin metal manoparticle synthesis. *J. Am. Chem. Soc.* **2010**, *132*, 9582-9584.

61. Li, Y.; Zaluzhna, O.; Xu, B.; Gao, Y.; Modest, J. M.; Tong, Y. Y. J. Mechanistic insights into the Brust-Schiffrin two-phase synthesis of organo-chalcogenate-protected metal nanoparticles. *J. Am. Chem. Soc.* **2011**, *133*, 2092-2095.

62. Jiang, D.-e.; Whetten, R. L.; Luo, W.; Dai, S. The smallest thiolated gold superatom complexes. *J. Phys. Chem. C* **2009**, *113*, 17291-17295.

63. Salorinne, K.; Malola, S.; Wong, O. A.; Rithner, C. D.; Chen, X.; Ackerson, C. J.; Hakkinen, H. Conformation and dynamics of the ligand shell of a water-soluble Au102 nanoparticle. *Nat. Commun.* **2016**, *7*, 10401.

64. Jin, R.; Qian, H.; Wu, Z.; Zhu, Y.; Zhu, M.; Mohanty, A.; Garg, N. Size focusing: a methodology for synthesizing atomically precise gold nanoclusters. *J. Phys. Chem. Lett.* **2010**, *1*, 2903-2910.

65. Qian, H.; Zhu, Y.; Jin, R. Size-focusing synthesis, optical and electrochemical properties of monodisperse Au38(SC2H4Ph)24 nanoclusters. *ACS Nano* **2009**, *3*, 3795-3803.

66. Aguila, A.; Murray, R. W. Monolayer-protected clusters with fluorescent dansyl ligands. *Langmuir* **2000**, *16*, 5949-5954.

67. Chen, S.; Templeton, A. C.; Murray, R. W. Monolayer-protected cluster growth dynamics. *Langmuir* **2000**, *16*, 3543-3548.

68. Cliffel, D. E.; Hicks, J. F.; Templeton, A. C.; Murray, R. W. *The Electrochemistry of Monolayer Protected Au Clusters*, Presented at the 2002; 297-317.

69. Kumar, S.; Jin, R. *Synthesis of water soluble Au25 cluster with high thermal stability*, Presented at the 2012; INOR-581.

70. Kumar, S.; Jin, R. Water-soluble Au25(Capt)18 nanoclusters: synthesis, thermal stability, and optical properties. *Nanoscale* **2012**, *4*, 4222-4227.

71. Alex, S.; Tiwari, A. Functionalized gold nanoparticles: synthesis, properties and applications-a review. *J. Nanosci. Nanotechnol.* **2015**, *15*, 1869-1894.

72. Adams, J.; Tizazu, G.; Janusz, S.; Brueck, S. R. J.; Lopez, G. P.; Leggett, G. J. Large-area nanopatterning of self-assembled monolayers of alkanethiolates by interferometric lithography. *Langmuir* **2010**, *26*, 13600-13606.

73. Banerjee, I.; Kumaran, V.; Santhanam, V. Synthesis and characterization of Au@Pt nanoparticles with ultrathin platinum overlayers. *J. Phys. Chem. C* **2015**, *119*, 5982-5987.

74. Dishner, M. H.; Hemminger, J. C.; Feher, F. J. *Ordered monolayers on Au(111) formed by gas- and liquid-phase deposition of thiophene, methanethiol, and benzeneselenol: understanding the chemisorption mechanism*, Presented at the National Meeting of the American Chemical Society, 1997; PHYS-375.

75. Ducker, R. E.; Leggett, G. J. A mild etch for the fabrication of three-dimensional nanostructures in gold. *J. Am. Chem. Soc.* **2006**, *128*, 392-393.

76. Hou, W.; Dasog, M.; Scott, R. W. J. Probing the relative stability of thiolate- and dithiolate-protected Au monolayer-protected clusters. *Langmuir* **2009**, *25*, 12954-12961.

77. Kumar, A.; Whitesides, G. M. Features of gold having micrometer to centimeter dimensions can be formed through a combination of stamping with an elastomeric stamp and an alkanethiol "ink" followed by chemical etching. *Appl. Phys. Lett.* **1993**, *63*, 2002-4.

78. Matsumoto, T.; Nickut, P.; Sawada, T.; Tsunoyama, H.; Watanabe, K.; Tsukuda, T.; Al-Shamery, K.; Matsumoto, Y. Deposition and fabrication of alkanethiolate gold nanocluster films on TiO2(110) and the effects of plasma etching. *Surf. Sci.* **2007**, *601*, 5121-5126.

79. Langille, M. R.; Personick, M. L.; Zhang, J.; Mirkin, C. A. Defining rules for the shape evolution of gold nanoparticles. *J. Am. Chem. Soc.* **2012**, *134*, 14542-14554.

80. Personick, M. L.; Langille, M. R.; Wu, J.; Mirkin, C. A. Synthesis of gold hexagonal bipyramids directed by planar-twinned silver triangular nanoprisms. *J. Am. Chem. Soc.* **2013**, *135*, 3800-3803.

81. Zhang, Y.; Salaita, K.; Lim, J.-H.; Mirkin, C. A. Electrochemical whittling of organic nanostructures. *Nano Lett.* **2002**, *2*, 1389-1392.

82. Cho, E. C.; Cobley, C. M.; Rycenga, M.; Xia, Y. Fine tuning the optical properties of Au-Ag nanocages by selectively etching Ag with oxygen and a water-soluble thiol. *J. Mater. Chem.* **2009**, *19*, 6317-6320.

83. Nimmala, P. R.; Jupally, V. R.; Dass, A. Core size conversion: route for exclusive synthesis of Au38 or Au40 nanomolecules. *Langmuir* **2014**, *30*, 2490-2497.

84. Yu, Y.; Yao, Q.; Luo, Z.; Yuan, X.; Lee, J. Y.; Xie, J. Precursor engineering and controlled conversion for the synthesis of monodisperse thiolate-protected metal nanoclusters. *Nanoscale* **2013**, *5*, 4606-4620.

85. Alkilany, A. M.; Abulateefeh, S. R.; Mills, K. K.; Bani Yaseen, A. I.; Hamaly, M. A.; Alkhatib, H. S.; Aiedeh, K. M.; Stone, J. W. Colloidal Stability of Citrate and Mercaptoacetic Acid Capped Gold Nanoparticles upon Lyophilization: Effect of Capping Ligand Attachment and Type of Cryoprotectants. *Langmuir* **2014**, *30*, 13799-13808.

86. Yi, C.; Zheng, H.; Tvedte, L. M.; Ackerson, C. J.; Knappenberger, K. L. Nanometals: identifying the onset of metallic relaxation dynamics in monolayer-protected gold clusters using femtosecond spectroscopy. *J. Phys. Chem. C* **2015**, *119*, 6307-6313.

87. Li, Y.; Zaluzhna, O.; Tong, Y. Y. J. Critical role of water and the structure of inverse micelles in the Brust-Schiffrin synthesis of metal nanoparticles. *Langmuir* **2011**, *27*, 7366-7370.

88. Zaluzhna, O.; Li, Y.; Zangmeister, C.; Allison, T. C.; Tong, Y. Y. J. Mechanistic insights on one-phase vs. two-phase Brust-Schiffrin method synthesis of Au nanoparticles with dioctyl-diselenides. *Chem. Commun.* **2012**, *48*, 362-364.

89. Perala, S. R. K.; Kumar, S. On the mechanism of metal nanoparticle synthesis in the Brust–Schiffrin method. *Langmuir* **2013**, *29*, 9863-9873.

90. Uehara, A.; Booth, S. G.; Chang, S. Y.; Schroeder, S. L. M.; Imai, T.; Hashimoto, T.; Mosselmans, J. F. W.; Dryfe, R. A. W. Electrochemical insight into the Brust-Schiffrin synthesis of Au nanoparticles. *J. Am. Chem. Soc.* **2015**, *137*, 15135-15144.

91. Chen, J.; Zhang, Q.-F.; Williard, P. G.; Wang, L.-S. Synthesis and structure determination of a new Au20 nanocluster protected by tripodal tetraphosphine ligands. *Inorg. Chem.* **2014**, *53*, 3932-3934.

92. Jiang, D.-e.; Walter, M. Au40: a large tetrahedral magic cluster. *Phys. Rev. B: Condens. Matter Mater. Phys.* **2011**, *84*, 193402/1-193402/4.

93. Crasto, D.; Barcaro, G.; Stener, M.; Sementa, L.; Fortunelli, A.; Dass, A. Au24(SAdm)16 nanomolecules: X-ray crystal Structure, theoretical analysis, adaptability of adamantane ligands to form Au23(SAdm)16 and Au25(SAdm)16, and its relation to Au25(SR)18. *J. Am. Chem. Soc.* **2014**, *136*, 14933-14940.

94. Dainese, T.; Antonello, S.; Gascón, J. A.; Pan, F.; Perera, N. V.; Ruzzi, M.; Venzo, A.; Zoleo, A.; Rissanen, K.; Maran, F. Au25(SEt)18, a nearly naked thiolate-protected Au25 cluster: structural analysis by single crystal X-ray crystallography and electron nuclear double resonance. *ACS Nano* **2014**, *8*, 3904-3912.

95. Tofanelli, M. A.; Ni, T. W.; Phillips, B. D.; Ackerson, C. J. Crystal structure of the [PdAu24(SR)18]0 superatom. *Inorg. Chem.* **2016**, *55*, 999-1001.

CHAPTER 5: ALLOY CLUSTER SYNTHESIS

5.1 Synopsis

Recently many alloy clusters containing gold and at least one heterometal (e.g. Ag, Pd, Hg) have been synthesized. Commonly, this is done through either co-reduction of the heterometal salt along with the Au-thiolate precursor or by metal atom exchange with a heterometal precursor and intact $Au_{25}(SR)_{18}$. However, the reported alloy clusters have only thus far incorporated metals with full d-orbitals. Herein we report our efforts toward incorporation of open d-orbital heterometals into Au-thiolate clusters.

5.2 Introduction

Over the past decade, as the structures of AuNCs have been solved, interest in forming new structures has greatly expanded. In particular, synthesis and evaluation of heterometallic clusters has been an area of active inquiry.[1-10] However, as far as we are aware, all published reports of heterometallic Au clusters involve late transition metals with closed d-shells. We have recently begun an inquiry into incorporating metals with vacant d-orbitals into AuNCs. Owing to the expected interesting electronic and structural properties of such alloy clusters,[3] we expect this to be a fruitful area going forward.

Unfortunately, our efforts have, to this point, provided a fairly comprehensive picture of those strategies which will fail. Our synthetic strategy has largely taken the same approaches as other alloy cluster syntheses involving Pd, Pt, Ag, Cu, Cd, and Hg.[9-13] It has become clear, however, that alternate strategies will be required to achieve long-term success on this project. This chapter is, therefore, organized by which metal we have attempted to dope into the Au cluster. In each case the experimental procedure is indexed to a particular notebook page, and the spectra follow the experimental procedure. These data are presented in a manner akin to a laboratory notebook, with

each procedure identified by the notebook in which it appears. This approach serves to make reference back to the original source material simple for any future members of the Ackerson lab pursuing this or a similar project.

In the cases of Fe, Mn, and Co, co-reduction strategies in organic solvents have universally failed to give anything other than $Au_{25}(SR)_{18}$ or colloidal gold products. This may be due to the redox properties of the relevant salts. In the case of Fe, the reduction of Fe(III) to Fe(II) is favorable by 0.77 V (vs SHE), but further reduction of Fe(II) to Fe(0) or direct reduction of Fe(III) to Fe(0) are unfavorable by 0.41 and 0.04 V, respectively. Similarly, reducing Mn(II) to Mn(0) is unfavorable by 1.18 V, and reduction of Co(II) to Co(0) is unfavorable by 0.29 V. By contrast, reduction of $[AuCl_4]^-$ to Au(I) (in the form of $[AuCl_2]^-$ is favorable by 0.926 V, and further reduction to Au(0) favorable by 1.15 V.[14] What this means synthetically is that the standard Brust procedure used to synthesize Au_{25} and $Au_{25-x}M_x$ with coinage metal dopants may not contain a reductant strong enough to get early transition metals into the correct oxidation state for cluster formation.

In $Au_{25}(SR)_{18}$, the 13 Au atoms comprising the icosahedral core are formally Au(0), while those in the semirings are Au(I). In order for a dopant metal atom to occupy the icosahedral core, it seems reasonable that it would also be formally in the (0) oxidation state, having only metal-metal bonds. As such, while the thiol to disulfide oxidation is sufficient to reduce Au(III) to Au(I) and NaBH4 is strong enough to further reduce Au(I) to Au(0), initiating growth, these mild reductants may leave early transition metal salts in their native oxidation state.

Another strategy we have employed is separate synthesis of M-thiolate precursors and introduction of those into the Au_{25} synthesis once the Au-thiolate is fully formed, followed by reduction. These procedures have also failed to give the desired result, either forming $Au_{25}(SR)_{18}$

or larger Au particles. This could again be due to a redox issue, if the metal-thiolates are formed as simple ligand exchange products rather than the metal being reduced by the thiolate. If the metal-thiolate cannot be reduced by sodium borohydride and participate in nucleation, $Au_{25}(SR)_{18}$ would be the expected product. Additionally, it may be necessary that the heterometal be incorporated into the same thiolate polymer as the Au atoms, meaning that phase-segregated mixtures of Au/M thiolates will not form alloy clusters regardless of redox chemistry. As there is little if any mechanistic data for the alloy-forming co-reduction reactions in the literature, this analysis is largely speculative.

We have also attempted co-reduction syntheses with Ir, Rh, Ru, and Re as the dopant metals. These reactions have met with the same fate as those with earlier transition metals. In the case of Re, it is still likely that unfavorable redox chemistry is again the likely culprit.[14] Ir, Rh, and Ru, however, all have favorable potentials for reduction to their (0) oxidation state (*vide supra*). These metals, then, in principle should be amenable to co-reduction with Au to form alloy clusters, but these products have not been observed. In these cases, there is the possibility that the products have been formed in small amount, then destroyed by the reaction conditions over time. It may be possible to synthesize Ir, Ru, and Rh-doped Au clusters via co-reduction with fine-tuning of the reaction conditions.

When co-reduction approaches hit a dead-end, we began examining metal exchange reactions using both metal salts and metal-thiolate complexes. In each case the desired product did not form, with the reactions either returning starting material or decomposing the clusters. Details of each of these experiments can be found below. Given that metal exchange has been successful in other cases,[15-17] it may be possible to again optimize reaction conditions to give the desired products. While we have so far tried many approaches of this kind, the work is by no means exhaustive.

In sum, co-reduction strategies with early transition metals seem unlikely to be viable as a strategy for the formation of alloy clusters. It may be possible to make co-reduction effective, but it will require use of more powerful reductants than are typically employed in the Brust-Schiffrin synthesis. Metal exchange may be a more viable strategy, but empirical screening to identify the optimal conditions will be required.

5.2 General Experimental Procedures

All reactions were performed with commercially purchased starting materials used without further purification. UV/Visible spectra were collected on a ThermoFisher Nanodrop UV/Vis spectrophotometer. Data were exported to XML files, imported into Microsoft Excel, and analyzed. Spectra appearing in this chapter were generated using OriginPro software. All normalized UV/Vis spectra were normalized such that absorbance of the sample at 300 nm is equal to 1. MALDI-MS were collected on a Bruker Microflex MALDI-TOF instrument operating in linear mode, using a protein calibrant. Clusters for MALDI were prepared in DCTB matrix in CH_2Cl_2, the calibrant was prepared in a sinapinic acid matrix in water. Mass spectra were exported from Bruker's FlexAnalysis package as ASCII text files, then analyzed in MMass. Mass spectra appearing in this chapter were directly exported from MMass.

5.3 Attempts to Synthesize Au/Mn Alloy Clusters

Td-002-103

$HAuCl_4 \cdot 3H_2O$ (100 mg, 0.254 mmol, 1.00 equiv) was dissolved in a solution of TOAB (155.6 mg, 0.284 mmol, 1.12 equiv) in 7 mL of THF. After the solution was homogeneous, 2-phenylethanethiol (179.6 μL, 1.34 mmol, 5.28 equiv) was added and the solution was stirred at room temperature until colorless. At this point $Mn(OAc)_2 \cdot 4H_2O$ (6.22 mg, 0.0254 mmol, 0.100 equiv) was added, followed immediately by an ice cold solution of $NaBH_4$ (96.9 mg, 2.56 mmol, 10.08 equiv) in 2.5 mL of water was added in one portion. The reaction was allowed to stir at room

temperature for 48 hrs, the aqueous layer was removed, and the products were precipitated by the addition of methanol to the organic layer. The organic MeOH/THF phase was centrifuged to isolate the precipitate, which was then washed with methanol to remove excess thiol. Products were purified by size-exclusion chromatography in toluene, and the fractions were analyzed by UV/Visible spectroscopy.

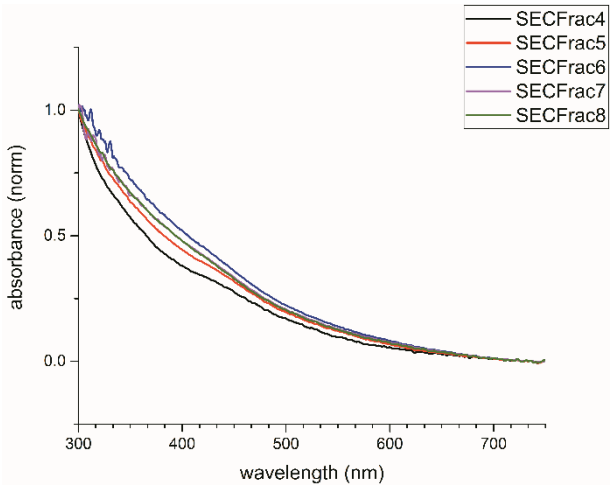

Figure 5.1. Normalized spectra of SEC fractions 4-8

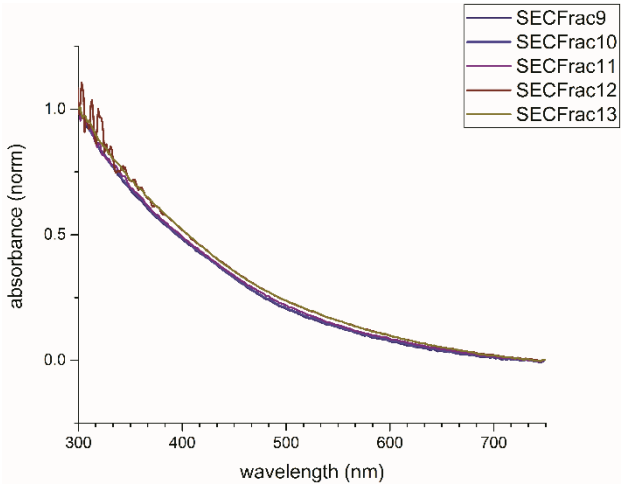

Figure 5.2. Normalized spectra of SEC fractions 9-13

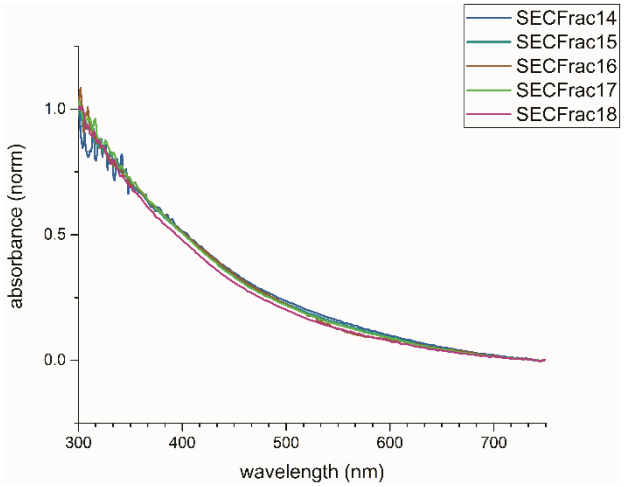

Figure 5.3. Normalized spectra of SEC fractions 14-18

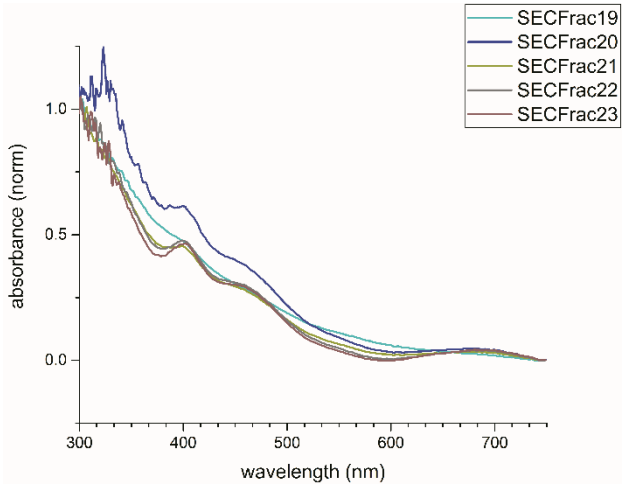

Figure 5.4. Normalized spectra of SEC fractions 19-22

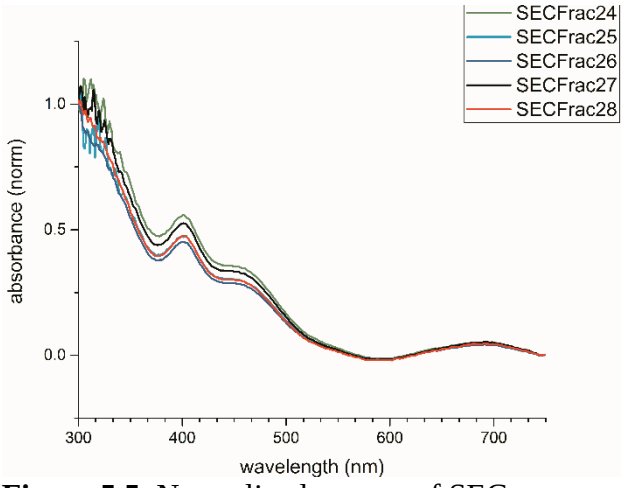

Figure 5.5. Normalized spectra of SEC fractions 24-28

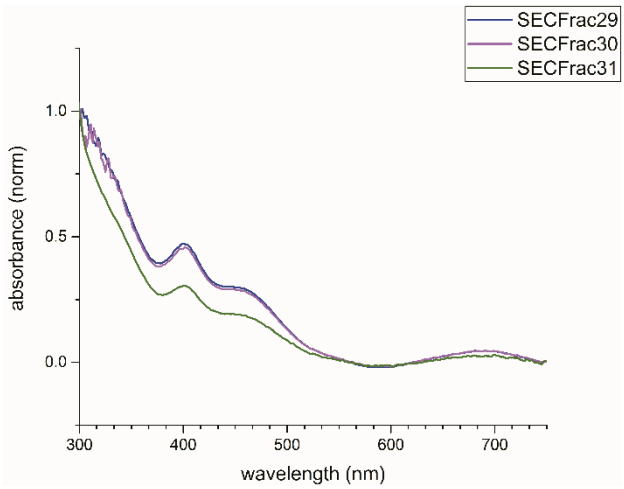

Figure 5.6. Normalized spectra of SEC fractions 29-31

Td-002-105

$HAuCl_4 \cdot 3H_2O$ (100 mg, 0.254 mmol, 1.00 equiv) was dissolved in a solution of TOAB (155.6 mg, 0.284 mmol, 1.12 equiv) in 7 mL of THF. After the solution was homogeneous, 2-phenylethanethiol (179.6 µL, 1.34 mmol, 5.28 equiv) was added and the solution was stirred at room temperature until colorless. The solution was then concentrated and the solid was washed three times with 15 mL portions of MeOH to remove excess thiol. The solids were then resuspended in 7 mL THF. At this point $Mn(OAc)_2 \cdot 4H_2O$ (6.22 mg, 0.0254 mmol, 0.100 equiv) was added, followed immediately by an ice cold solution of NaBH4 (96.9 mg, 2.56 mmol, 10.08 equiv) in 2.5 mL of water was added in one portion. After addition of reductant, 2-phenylethanethiol (77 µL, 0.580 mmol, 2.28 equiv) were added and the reaction was allowed to stir at room temperature for 48 hrs. The aqueous layer was removed, and the products were precipitated by the addition of methanol to the organic layer. The organic MeOH/THF phase was centrifuged to isolate the precipitate, which was then washed with methanol to remove excess thiol. Products were purified by size-exclusion chromatography in toluene, and the fractions were analyzed by UV/Visible spectroscopy.

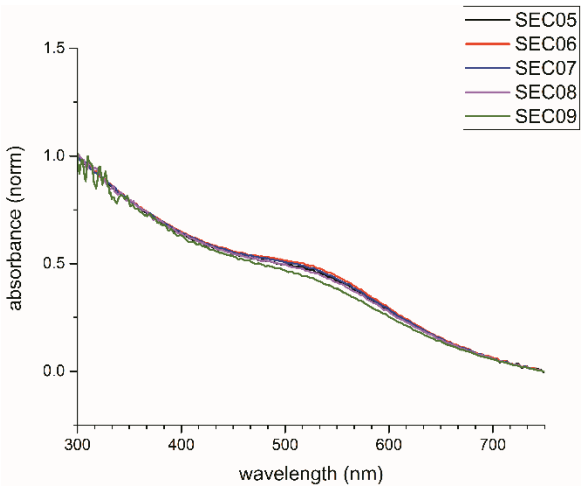

Figure 5.7. Normalized spectra of SEC fractions 6-9

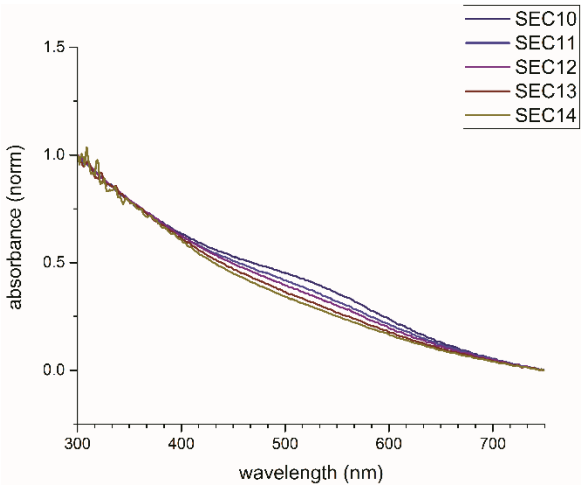

Figure 5.8. Normalized spectra of SEC fractions 10-14

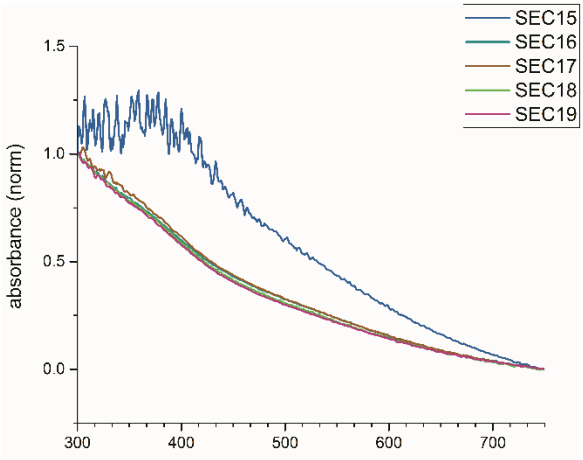

Figure 5.9. Normalized spectra of SEC fractions 15-19

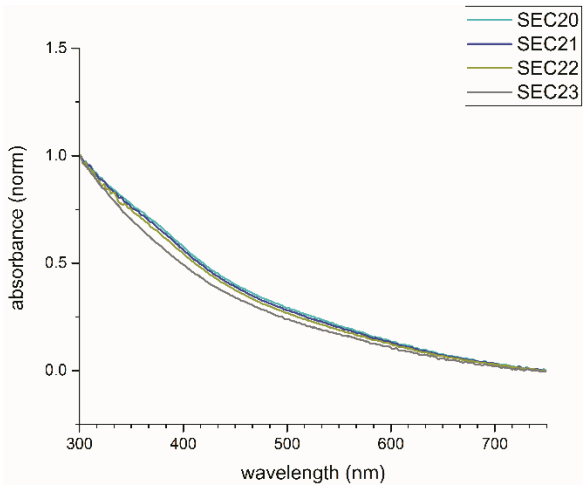

Figure 5.10. Normalized spectra of SEC fractions 20-23

Td-002-107

$HAuCl_4•3H_2O$ (100 mg, 0.254 mmol, 1.00 equiv) was dissolved in a solution of TOAB (155.6 mg, 0.284 mmol, 1.12 equiv) in 7 mL of THF. To this solution Mn(OAc)2•$_4H_2O$ (6.22 mg, 0.0254 mmol, 0.100 equiv) was added and the reaction was allowed to until homogeneous. 2-phenylethanethiol (179.6 µL, 1.34 mmol, 5.28 equiv) was added and the solution was stirred at room temperature until colorless. An ice cold solution of $NaBH_4$ (96.9 mg, 2.56 mmol, 10.08 equiv) in 2.5 mL of water was added in one portion. The reaction was allowed to stir at room temperature for approximately 3 hrs and then the aqueous layer was removed. The products were precipitated by the addition of methanol to the organic layer. The organic MeOH/THF phase was centrifuged to isolate the precipitate, which was then washed with methanol to remove excess thiol. Products were purified by size-exclusion chromatography in toluene, and the fractions were analyzed by UV/Visible spectroscopy.

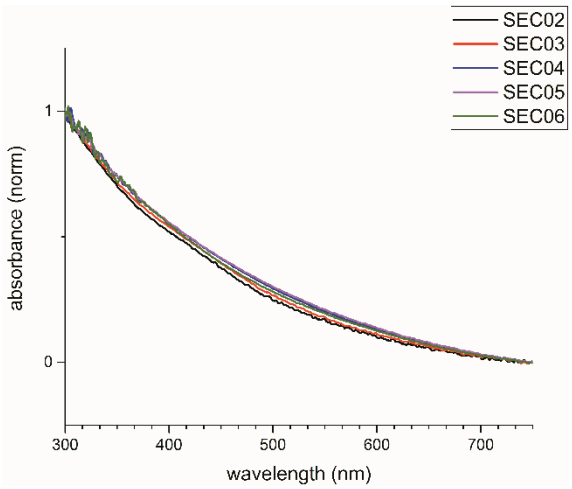

Figure 5.11. Normalized spectra of SEC fractions 2-6

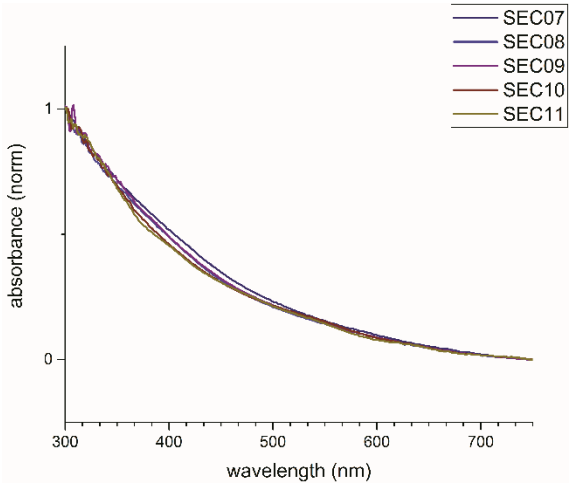

Figure 5.12. Normalized spectra of SEC fractions 7-11

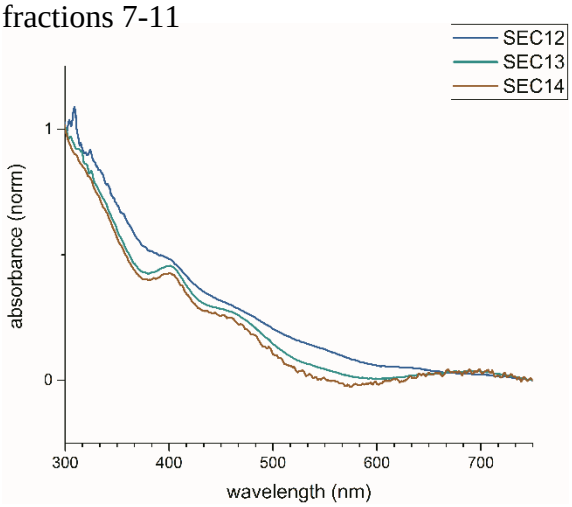

Figure 5.13. Normalized spectra of SEC fractions 12-14

Td-002-114

$HAuCl_4 \cdot 3H_2O$ (100 mg, 0.254 mmol, 1.00 equiv) was dissolved in a solution of TOAB (155.6 mg, 0.284 mmol, 1.12 equiv) in 7 mL of THF. To this solution $Mn(OAc)_2 \cdot 4H_2O$ (31.3 mg, 0.127 mmol, 0.500 equiv) was added and the reaction was allowed to until homogeneous. 2-phenylethanethiol (179.6 µL, 1.34 mmol, 5.28 equiv) was added and the solution was stirred at room temperature until colorless. An ice cold solution of $NaBH_4$ (96.9 mg, 2.56 mmol, 10.08 equiv) in 2.5 mL of water was added in one portion. The reaction was allowed to stir at room temperature for approximately 3 hrs and then the aqueous layer was removed. The products were precipitated by the addition of methanol to the organic layer. The organic MeOH/THF phase was centrifuged to isolate the precipitate, which was then washed with methanol to remove excess thiol. Products were purified by size-exclusion chromatography in toluene, and the fractions were analyzed by UV/Visible spectroscopy.

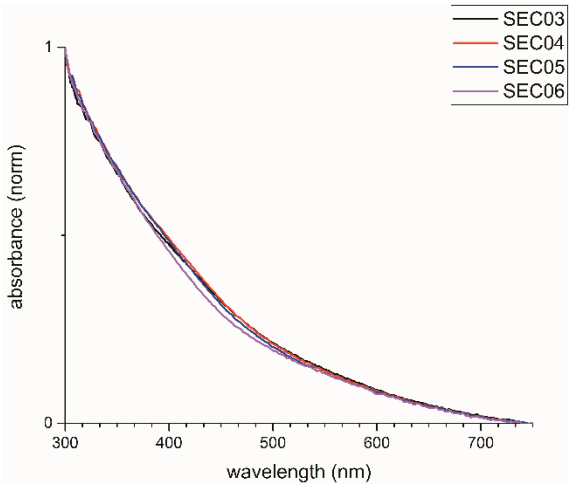

Figure 5.14. Normalized spectra of SEC fractions 3-6

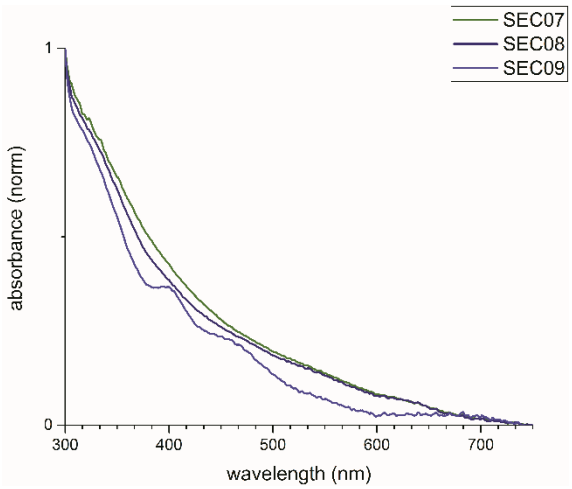

Figure 5.15. Normalized spectra of SEC fractions 7-9

Td-002-118

$HAuCl_4 \cdot 3H_2O$ (100 mg, 0.254 mmol, 1.00 equiv) was dissolved in a solution of TOAB (155.6 mg, 0.284 mmol, 1.12 equiv) in 7 mL of THF. After the solution was homogeneous, 2-phenylethanethiol (179.6 µL, 1.34 mmol, 5.28 equiv) was added and the solution was stirred at room temperature until colorless. At this point $Mn(OAc)_2 \cdot 4H_2O$ (6.22 mg, 0.0254 mmol, 0.100 equiv) was added, followed immediately by an ice cold solution of $NaBH_4$ (96.9 mg, 2.56 mmol,

10.08 equiv) in 2.5 mL of water was added in one portion. The reaction was allowed to stir at room temperature for 24 hrs, the aqueous layer was removed, and the products were precipitated by the addition of methanol to the organic layer. The organic MeOH/THF phase was centrifuged to isolate the precipitate, which was then washed with methanol to remove excess thiol. Products were purified by size-exclusion chromatography in toluene, and the fractions were analyzed by UV/Visible spectroscopy.

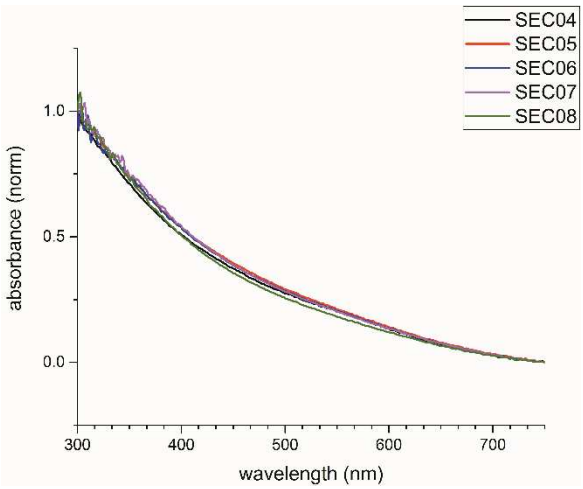

Figure 5.16. Normalized spectra of SEC fractions 4-8

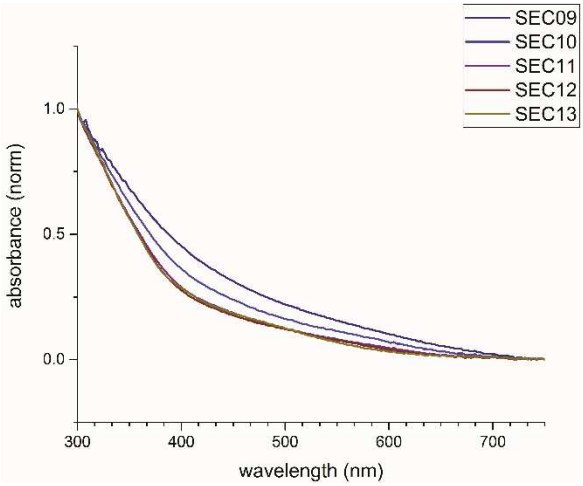

Figure 5.17. Normalized spectra of SEC fractions 9-12

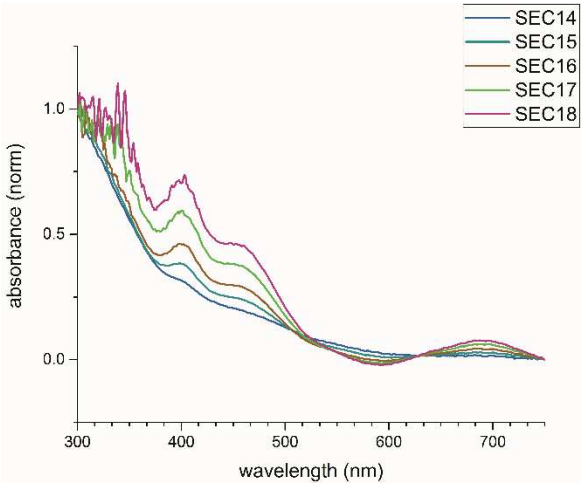

Figure 5.18. Normalized spectra of SEC fractions 14-18

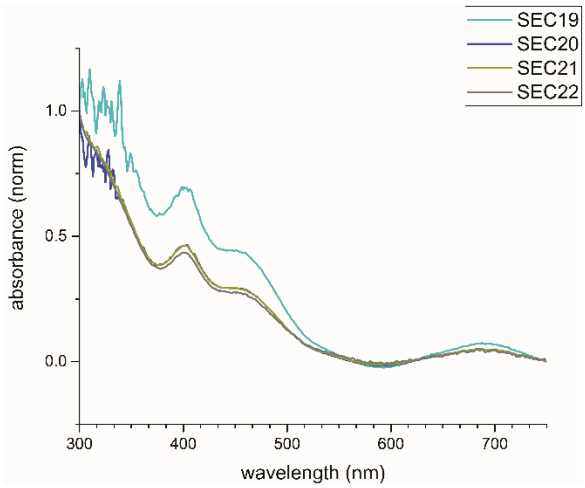

Figure 5.19. Normalized spectra of SEC fractions 19-22

Td-002-123

$HAuCl_4•3H_2O$ (100 mg, 0.254 mmol, 1.00 equiv) was dissolved in a solution of TOAB (155.6 mg, 0.284 mmol, 1.12 equiv) in 7 mL of THF. To this solution $Mn(OAc)_2•_4H2O$ (31.3 mg, 0.127 mmol, 0.500 equiv) was added and the reaction was allowed to until homogeneous. 2-phenylethanethiol (179.6 µL, 1.34 mmol, 5.28 equiv) was added and the solution was stirred at room temperature until colorless. An ice cold solution of $NaBH_4$ (96.9 mg, 2.56 mmol, 10.08 equiv) in 2.5 mL of water was added in one portion. The reaction was allowed to stir at room temperature for approximately 24 hrs and then the aqueous layer was removed. The products were precipitated by the addition of methanol to the organic layer. The organic MeOH/THF phase was centrifuged to isolate the precipitate, which was then washed with methanol to remove excess thiol. Products were purified by size-exclusion chromatography in toluene, and the fractions were analyzed by UV/Visible spectroscopy.

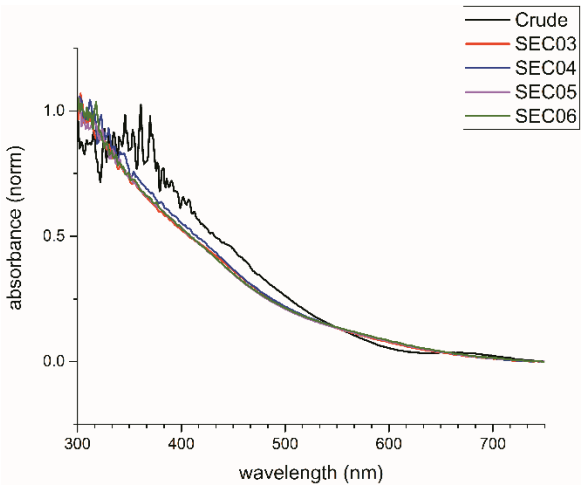

Figure 5.20. Normalized spectra of crude product at SEC fractions 3-6

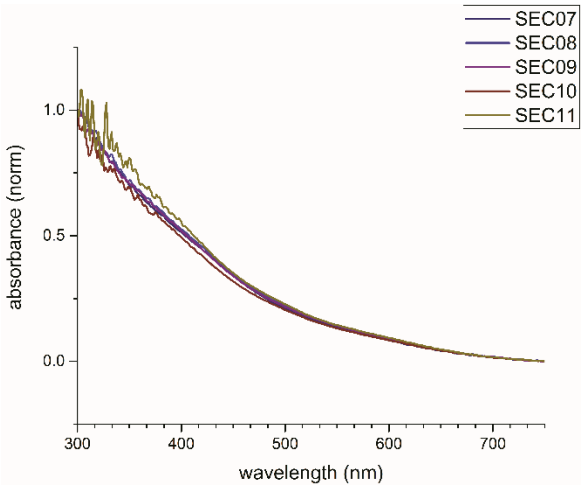

Figure 5.21. Normalized spectra of SEC fractions 7-11

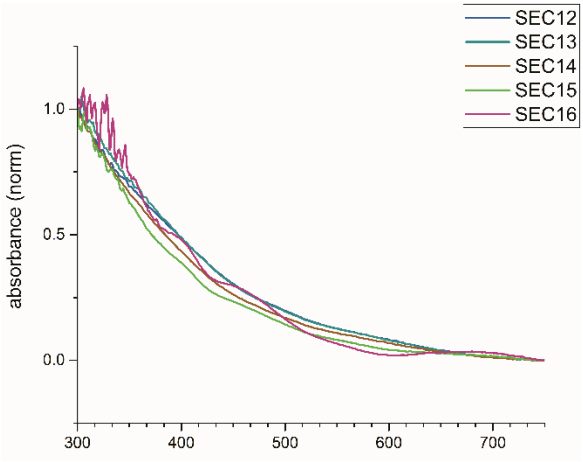

Figure 5.22. Normalized spectra of SEC fractions 12-16

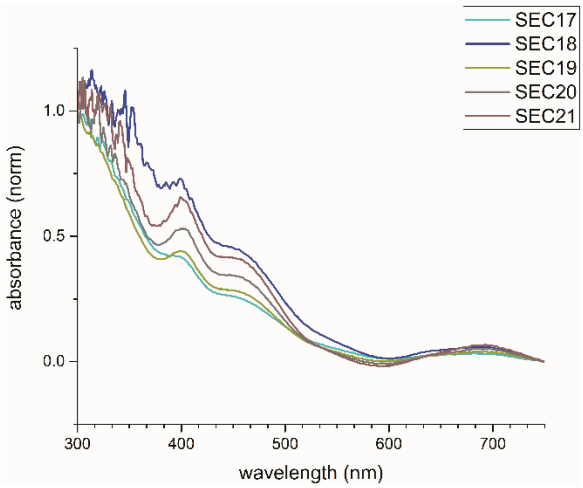

Figure 5.23. Normalized spectra of SEC fractions 17-21

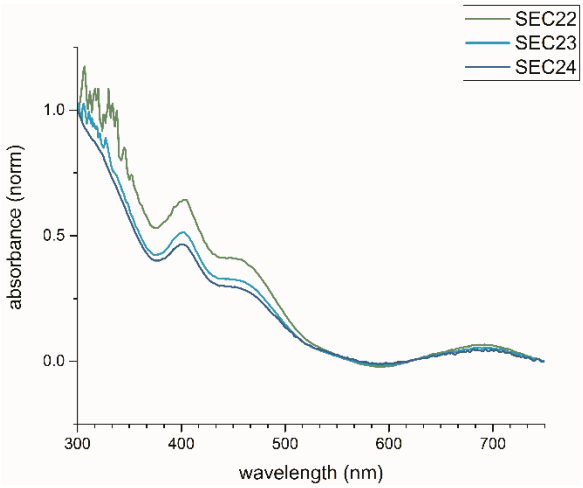

Figure 5.24. Normalized spectra of SEC fractions 22-24

Td-002-134[18]

$[Au_{25}(PET)_{18}]^{-}TOA^{+}$ (24 mg, 0.003 mol, 1.00 equiv) were dissolved in 8 mL acetonitrile, then an aqueous solution of $Mn(OAc)_2 \cdot 4H_2O$ (3.00 µL, 0.003 mmol, 1.00 equiv) was added. The reaction was allowed to stir for 90 minutes, and then 2-phenylethanethiol (10 µL, 0.0746 mmol, 24.8 equiv) in 300 µL acetonitrile was added while the solution was vigorously stirred. The precipitate was collected & analyzed. Recovered starting material.

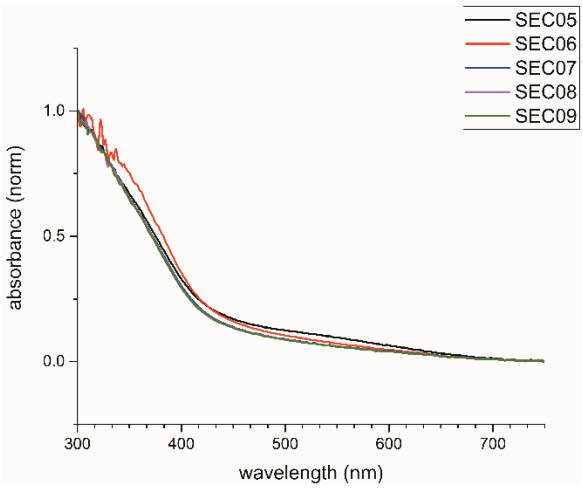

Figure 5.25. Normalized spectra of SEC fractions 5-9

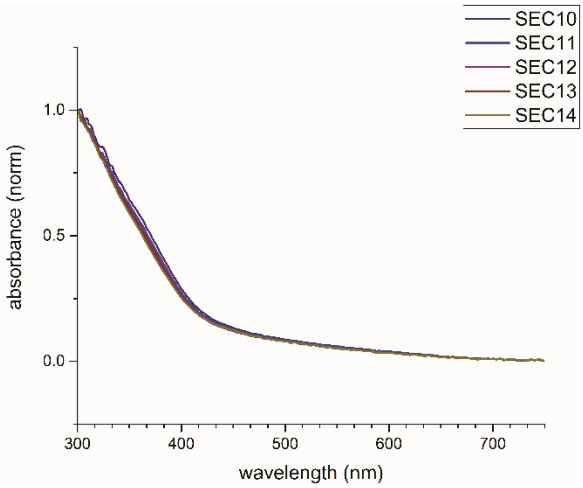

Figure 5.26. Normalized spectra of SEC fractions 10-14

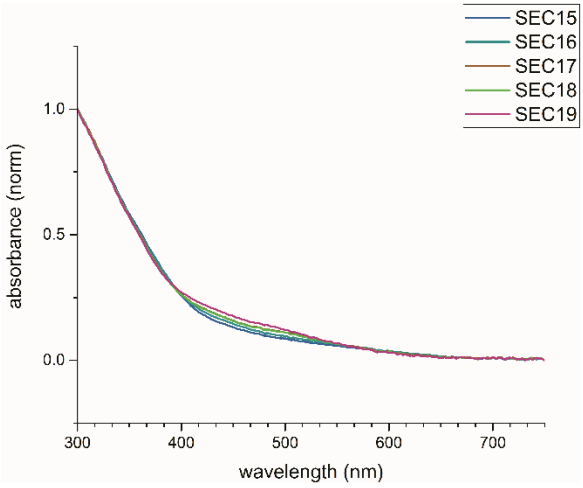

Figure 5.27. Normalized spectra of SEC fractions 15-19

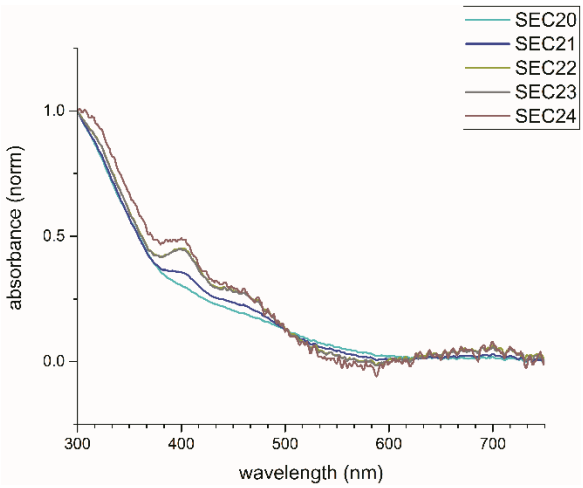

Figure 5.28. normalized spectra of SEC fractions 20-24

Td-002-136

$HAuCl_4 \cdot 3H_2O$ (100 mg, 0.254 mmol, 1.00 equiv) was dissolved in a solution of TOAB (155.6 mg, 0.284 mmol, 1.12 equiv) in 7 mL of THF. To this was added $Mn(OAc)_2 \cdot {}_4H2O$ (62.3 mg, 0.254 mmol, 1.00 equiv). After the solution was homogeneous, ethanethiol (96.7 µL, 1.34 mmol, 5.28 equiv) was added and the solution was stirred at room temperature until colorless. At this point an ice cold solution of $NaBH_4$ (96.9 mg, 2.56 mmol, 10.08 equiv) in 2.5 mL of water was added in one portion. The reaction was allowed to stir at room temperature for 48 hrs, the aqueous layer was removed, and the products were precipitated by the addition of methanol to the organic layer. The organic MeOH/THF phase was centrifuged to isolate the precipitate, which was then washed with methanol to remove excess thiol. Gave exclusively large, insoluble particles.

Td-002-138[15]

$HAuCl_4 \cdot 3H_2O$ (100 mg, 0.254 mmol, 1.00 equiv) was dissolved in 30 mL MeOH, and 2-phenylethanethiol (179.6 µL, 1.34 mmol, 5.28 equiv) was added in one portion. Reaction was stirred at room temperature for ~30 minutes, and the resultant precipitate was collected by centrifugation and washed with MeOH (20 mL portions, 3x) to remove excess thiol. $Mn_{12}(OAc)_{16}$

was dissolved in 4 mL CH_2Cl_2 to give an 8 μM solution. 10.7 mg Au(I)-thiolate was dissolved in 6 mL PhMe and added to the $Mn_{12}(OAc)_{16}$ solution in one portion. This was then stirred at room temperature overnight. The resulting reaction was filtered to remove large precipitates then purified by size-exclusion chromatography in PhMe to give an orange product. Repeated crystallization gave orange crystals which did not defract and then decomposed upon further attempts to purify and recrystallize.

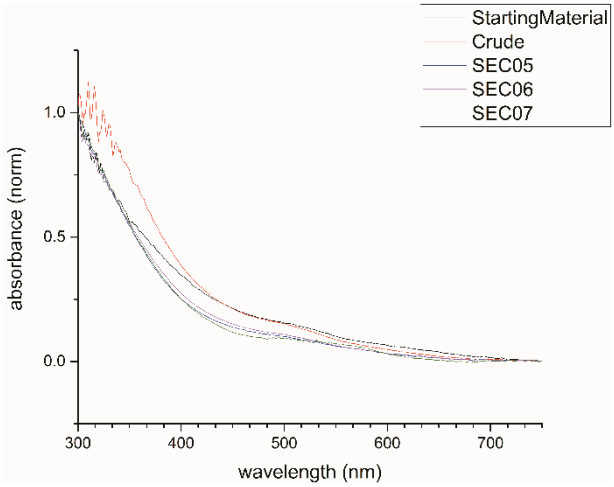

Figure 5.29. Normalized spectra of starting material, crude product, and SEC fractions 5-7

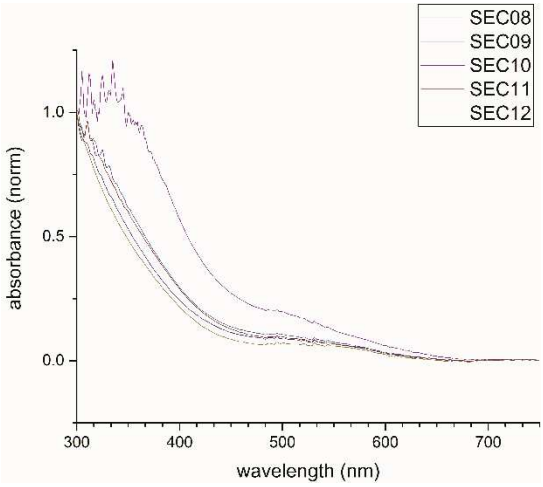

Figure 5.30. Normalized spectra of SEC fractions 8-12

Td-002-139

To a solution of $Mn(OAc)_2•4H_2O$ (62.3 mg, 0.254 mmol, 1.00 equiv) in 7 mL MeOH, 2-phenylethanethiol (179.6 μL, 1.34 mmol, 5.28 equiv) was added at room temperature. The reaction was stirred for ~1 hr, then dried under vacuum. Resulting product was washed with 3 portions of PhMe (20 mL each) to remove excess thiol, and then redissolved in MeOH to a concentration of 1 M in Mn.

A solution of $[Au_{25}(SCH_2CH_2Ph)_{18}]^-TOA^+$ (52 mg, 0.0066 mmol, 1.00 equiv) in THF (5 mL) was prepared, and to this Mn-thiolate was added (164 μL 1 M in MeOH, 0.164 mmol, 25 equiv). Reaction was allowed to stir at room temperature overnight, then evaluated by UV/Vis. Gave exclusively decomposition of the starting material.

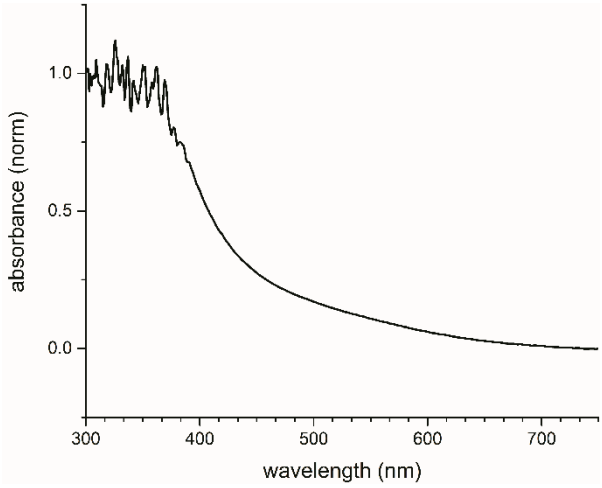

Figure 5.31. Normalized spectrum of the crude product.

Td-002-141

$HAuCl_4•3H_2O$ (100 mg, 0.254 mmol, 1.00 equiv) was dissolved in a solution of TOAB (155.6 mg, 0.284 mmol, 1.12 equiv) in 7 mL of THF. After the solution was homogeneous, 2-phenylethanethiol (179.6 μL, 1.34 mmol, 5.28 equiv) was added and the solution was stirred at room temperature until colorless. At this point, $Mn_{12}(OAc)_{16}$ (58.2 mg, 0.0212 mmol, 0.0833 equiv) was added and the reaction was stirred until homogeneous. At this point an ice solution of

$NaBH_4$ (96.9 mg, 2.56 mmol, 10.08 equiv) in 2.5 mL of water was added in one portion and the reaction was stirred overnight then separated on SEC.

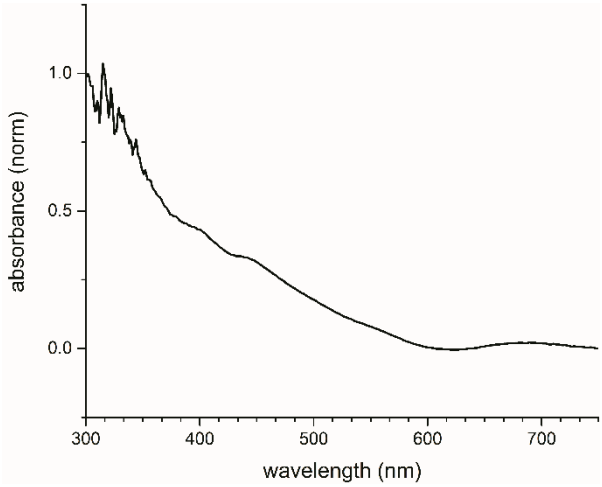

Figure 5.32. Normalized absorbance of the only isoloble product, corresponds with Au_{25}.

Td-003-5 – Synthesis of manganese thiolate

$Mn(OAc)_2 \cdot 4H_2O$ (122.5 mg, 0.525 mmol, 1.00 equiv) was dissolved in 2.5 mL nanopure water, and 2.5 mL EtOH was added. A second solution of 2-phenylethanethiol (0.300 mL, 2.24 mmol, 4.27 equiv) in 3.05 mL EtOH with Et_3N (1.00 mL, 7.17 mmol, 13.7 equiv) was prepared. The solutions were combined and stirred vigorously at room temperature for 30 minutes. After stirring the reaction mixture was centrifuged to collect the precipitate. The supernatant was discarded, and the pellet was washed several times with EtOH to remove excess thiol. The resulting manganese-thiolate was carried into the next step without further purification.

Td-003-10

10 mg $[Au_{25}(SCH_2CH_2Ph)]^-TOA^+$ dissolved in 10 mL PhMe. 10 mg Mn-PET thiolate added as a powder and the reaction was stirred at room temperature for 3 hrs. The solids were removed, and the product was precipitated from the supernatant by addition of MeOH followed by

centrifugation. The resulting pellet was dissolved in minimal PhMe and purified by size-exclusion chromatography.

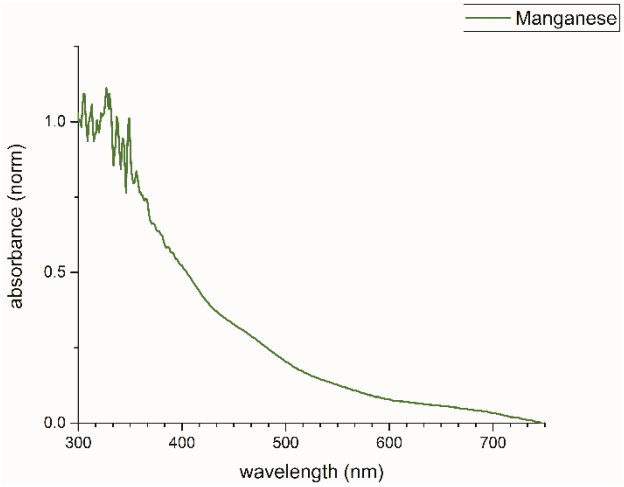

Figure 5.33. Normalized spectrum of the product. Appears to be low concentration Au_{25}

Td-003-49

10 mg $Mn(OAc)_2•4H_2O$ were dissolved in 1 mL EtOH and 16.5 μL 2-phenylethanethiol were added. This was allowed to stir for 10 minutes at room temperature, and then added to a solution of 10 mg $[Au_{25}(SCH_2CH_2Ph)]^-TOA^+$ in 10 mL PhMe. Reaction stirred 2 hrs at room temperature. Reaction was then transferred to a centrifuge tube, and the precipitate was removed. The supernatant was placed in a 50 mL centrifuge tube, diluted to 50 mL with MeOH, and centrifuged to isolate the precipitate. The resulting pellet was dissolved in 1 mL PhMe and separated by size-exclusion chromatography. Resulting product spectra below, appears to be a non-Au_{25} cluster of indeterminate composition which could not be crystallized.

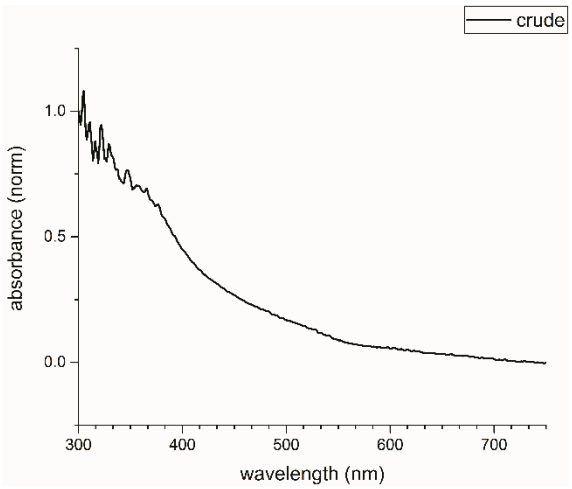

Figure 5.34. Normalized spectrum of the crude product.

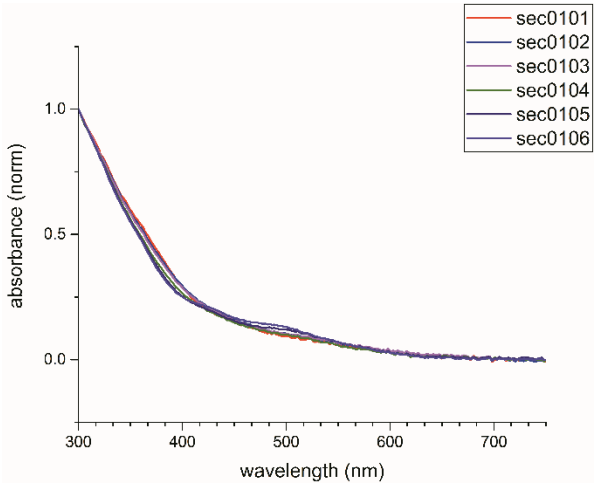

Figure 5.35. Normalized spectra of SEC fractions 1-6.

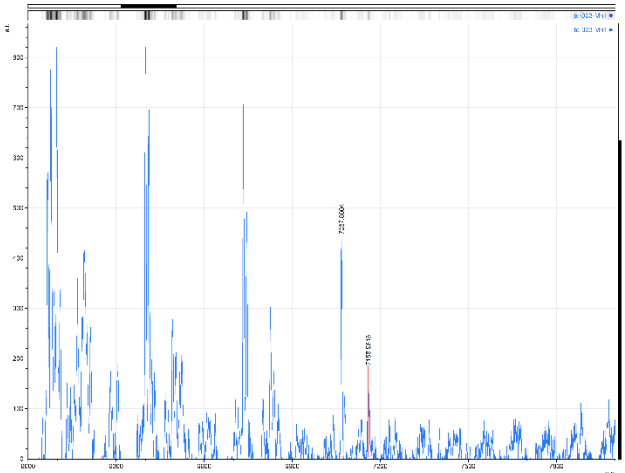

Figure 5.36. MALDI mass spectrum of isolated product. Labeled peaks are 7158.98 & 7067.80 M/Z

Td-003-95

$HAuCl_4 \cdot 3H_2O$ (100 mg, 0.254 mmol, 1.00 equiv) was dissolved in 7 mL THF along with TOAB (311.2 mg, 0.570 mmol, 2.24 equiv). This was followed by the addition of $Mn(OAc)_2 \cdot 4H_2O$ (62.3 mg, 0.254 mmol, 1.00 equiv). This mixture was allowed to stir for 10 min until homogeneous then 2-phenylethanethiole (180 µL, 1.34 mmol, 5.30 equiv) was added and the reaction was stirred for 2 hrs at room temperature. NaBH4 (97 mg, 2.56 mmol, 10.08 equiv) dissolved in 2.5 mL cold nanopure water was added in one portion and the reaction was stirred overnight at room temperature. The aqueous layer was removed, and the products precipitated from THF by dilution to 50 mL with MeOH then collected by centrifugation. The resulting pellet was dissolved in minimal PhMe and purified by size-exclusion chromatography.

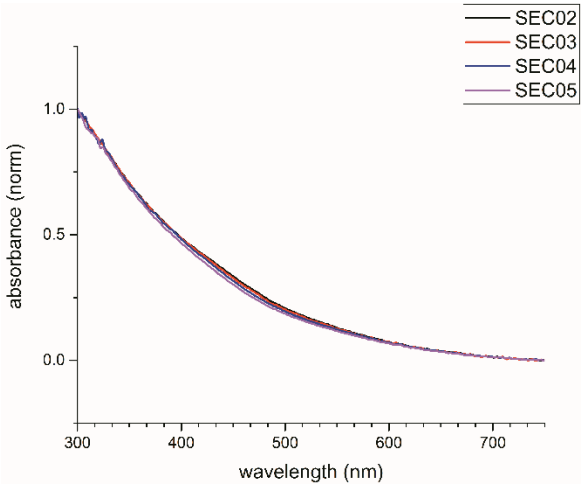

Figure 5.37. Normalized spectra of SEC fractions 2-5

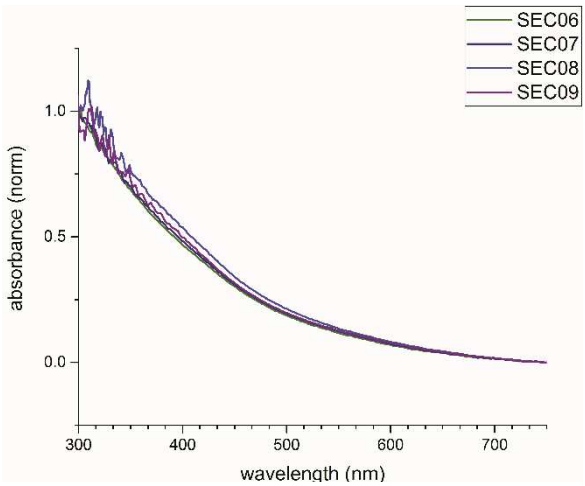

Figure 5.38. Normalized spectra of SEC fractions 6-9

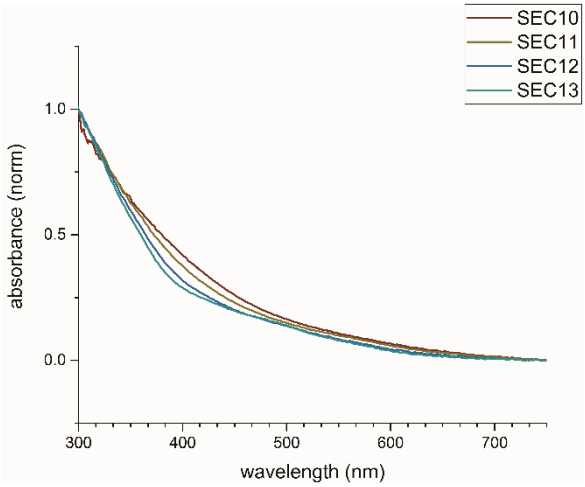

Figure 5.39. Normalized spectra of SEC fractions 10-13

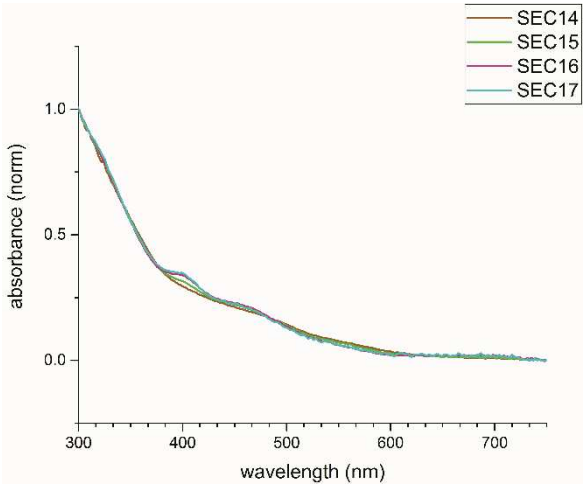

Figure 5.40. Normalized spectra of SEC fractions 14-17

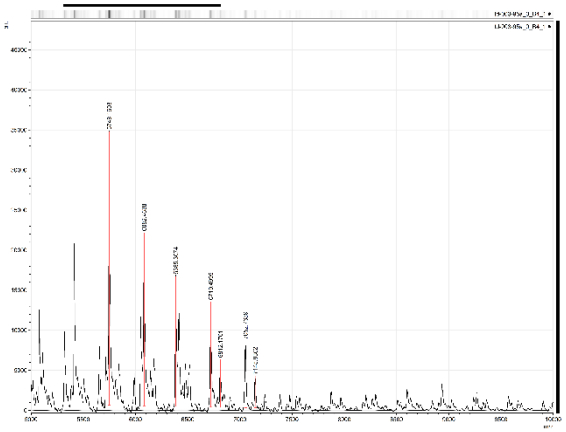

Figure 5.41. MALDI Mass Spectrum 1 - 7145.8302, 7052.7639, 6812.1701, 6719.4995, 6385.3074, 6082.4638, 5748.1603 M/Z

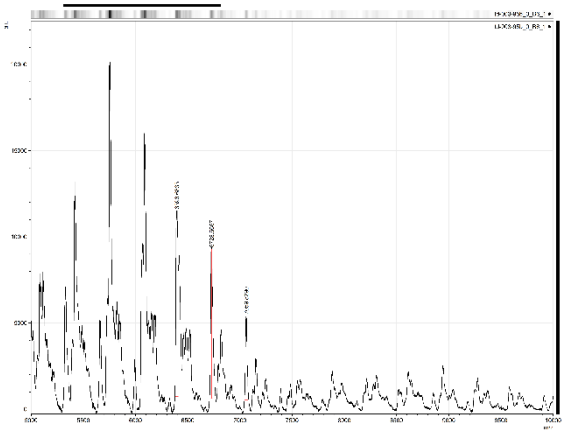

Figure 5.42. MALDI Mass Spectrum 2 - 7059.8290, 6728.6667, 6396.6833 M/Z

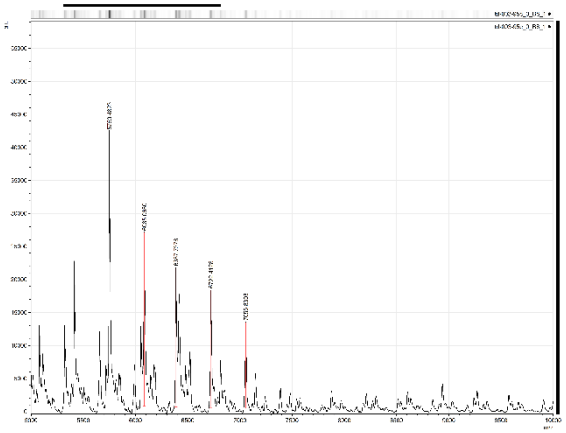

Figure 5.43. MALDI Mass Spectrum 3 - 7055.8393, 6722.4128, 6387.7376, 6085.0680, 5750.4823 M/Z

Td-003-101

42.5 mg $[Au_{25}(SCH_2CH_2Ph)]^-TOA^+$ was dissolved in 5 mL CH_2Cl_2. 3.3 mg of $Mn(CO)_5Br$ was added as a powder and the reaction was stirred overnight at room temperature. Resulted in cluster decomposition.

5.4 Attempts to Synthesize Au/Fe Alloy Clusters

Td-003-4 – Synthesis of iron thiolate

$FeCl_3$ (81.1 mg, 0.500 mmol, 1.00 equiv) was dissolved in 2.5 mL nanopure water, and 2.5 mL EtOH was added. A second solution of 2-phenylethanethiol (0.300 mL, 2.24 mmol, 4.27 equiv) in 3.05 mL EtOH with Et_3N (1.00 mL, 7.17 mmol, 13.7 equiv) was prepared. The solutions were combined and stirred vigorously at room temperature for 30 minutes. After stirring the reaction mixture was centrifuged to collect the precipitate. The supernatant was discarded, and the pellet was washed several times with EtOH to remove excess thiol. The resulting iron-thiolate was carried into the next step without further purification.

Td-003-9

10 mg $[Au_{25}(SCH_2CH_2Ph)]^-TOA^+$ dissolved in 10 mL PhMe. 10 mg Fe-PET thiolate added as a powder and the reaction was stirred at room temperature for 3 hrs. The solids were removed, and the product was precipitated from the supernatant by addition of MeOH followed by centrifugation. The resulting pellet was dissolved in minimal PhME and purified by size-exclusion chromatography. Gave decomposition of Au_{25} as indicated by the featureless spectrum of the resulting product.

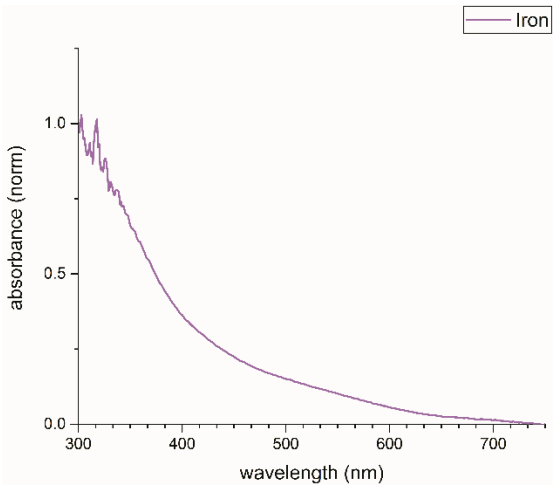

Figure 5.44. Normalized UV/Visible spectrum of the product.

Td-003-31

Two separate solutions of TOAB (78 mg, 0.284 mmol, 1.12 equiv) dissolved in 3.5 mL THF were prepared. To the first solution $HAuCl_4 \bullet 3H_2O$ (100 mg, 0.254 mmol, 1.00 equiv) was added. To the other, $FeCl_3$ (41.2 mg, 0.254 mmol, 1.00 equiv) was added. 2-phenyethanethiol (180 μL, 1.34 mmol, 5.28 equiv) was added to each solution and they were stirred at room temperature until the Au solution was colorless. The two solutions where then combined, stirred for 5 min, and reduced with $NaBH_4$ (97 mg, 2.56 mmol, 10.08 equiv) dissolved in 2.5 mL cold nanopure water. The reaction was stirred overnight, the products precipitated with MeOH, collected by centrifugation, and separated by size-exclusion chromatography. Gave exclusively $Au_{25}(SCH_2CH_2Ph)_{18}$.

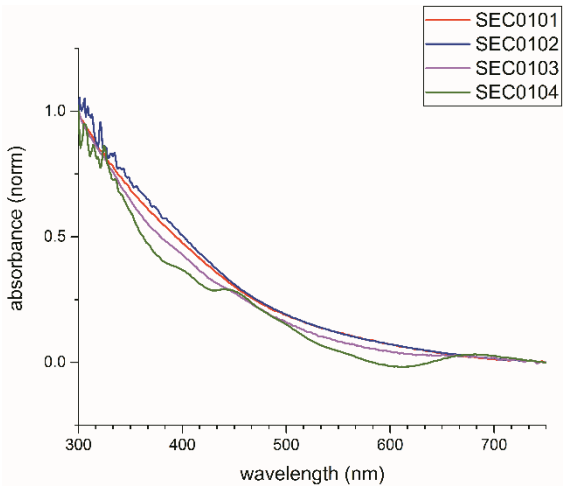

Figure 5.45. Normalized spectra of SEC fractions 1-4

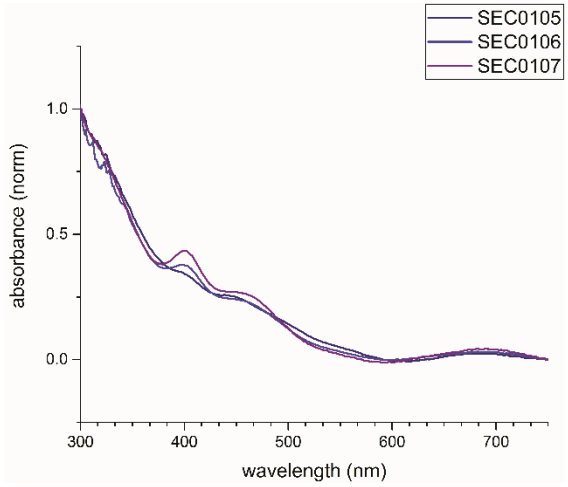

Figure 5.46. Normalized spectra of SEC fractions 5-7

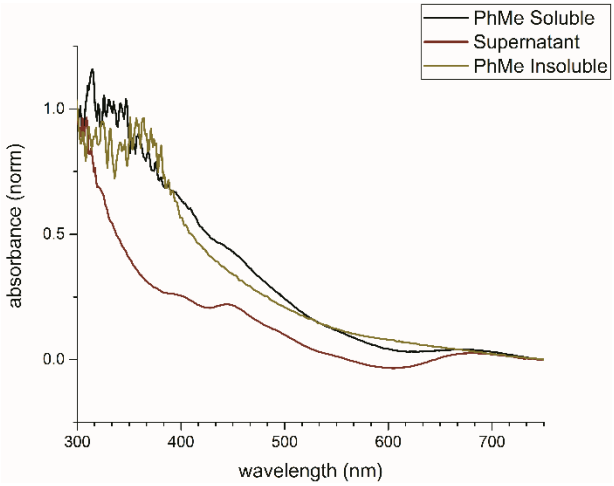

Figure 5.47. Normalized spectra of crude reaction products

Td-003-32

10 mg $[Au_{25}(SCH_2CH_2Ph)]^-TOA^+$ was dissolved in 10 mL of PhMe. 10 mg of $FeCl_3$ was dissolved in 1 mL EtOH. The ethanol solution of $FeCl_3$ was added to the solution of $[Au_{25}(SCH_2CH_2Ph)]^-TOA^+$ and the reaction was stirred for 2 hrs at room temperature. Returned starting material as evidenced by MALDI.

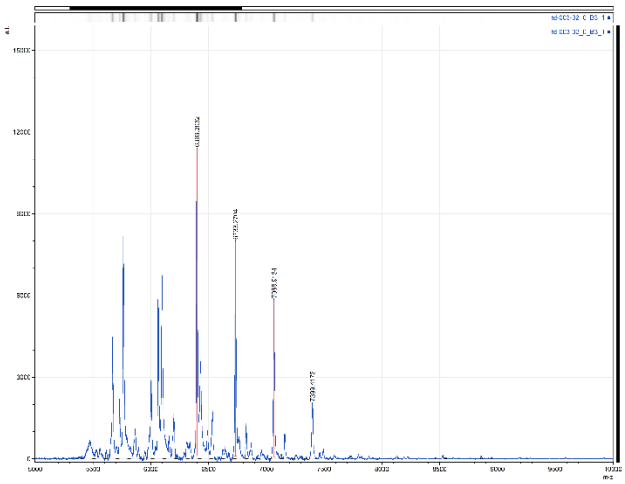

Figure 5.48. MALDI Mass Spectrum, 7399.4172, 7066.6134, 6733.2704, 6399.2632 M/Z

Td-003-33

10 mg $FeCl_3$ were dissolved in 1 mL EtOH and 25 μL 2-phenylethanethiol were added. This was allowed to stir for 10 minutes at room temperature, and then added to a solution of 10 mg $[Au_{25}(SCH_2CH_2Ph)]^-TOA^+$ in 10 mL PhMe. Reaction stirred 2 hrs at room temperature. Reaction was then transferred to a centrifuge tube, and the precipitate was removed. The supernatant was placed in a 50 mL centrifuge tube, diluted to 50 mL with MeOH, and centrifuged to isolate the precipitate. The resulting pellet was dissolved in 1 mL PhMe and separated by size-exclusion chromatography. Resulting product spectra below, appears to be a non-Au_{25} cluster of indeterminate composition which could not be crystallized.

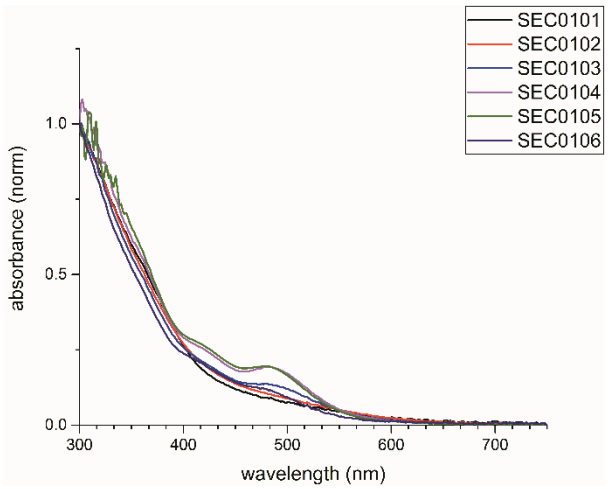

Figure 5.49. Normalized spectra of SEC fractions.

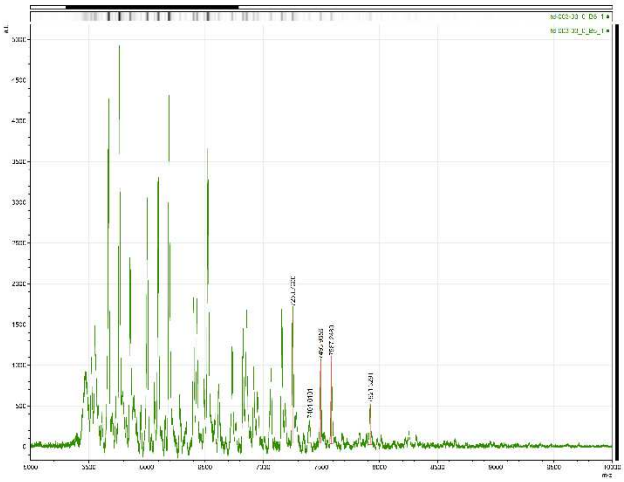

Figure 5.50. MALDI Mass Spectrum, 7921.3291, 7587.2480, 7493.9659, 7401.0101, 7253.7000 M/Z

Td-003-103[10]

$HAuCl_4 \bullet 3H_2O$ (212 mg, 0.538 mmol, 1.00 equiv) was dissolved in 15 mL THF along with TOAB (464 mg, 0.849 mmol, 1.58 equiv). This mixture was allowed to stir for 10 min until homogeneous then 2-phenylethanethiol (553 µL, 4.13 mmol, 7.67 equiv) was added and the reaction was stirred for 15 min at room temperature. This was followed by the addition of $FeCl_2$ (27.1 mg, 0.214 mmol, 0.397 equiv) as a solution in 5 mL THF. $NaBH_4$ (264 mg, 6.98 mmol, 12.97 equiv) dissolved in 5 mL cold nanopure water was added in one portion and the reaction

was stirred overnight at room temperature. The aqueous layer was removed, and the products precipitated from THF by dilution to 50 mL with MeOH then collected by centrifugation. The initial purple reaction mixture turns brown upon standing in MeOH for several minutes. The isolated pellet was redissolved in minimal PhMe then purified by size-exclusion chromatography. Gave a mixture of several clusters which could not be separated and decomposed upon repeated attempts to recrystallize.

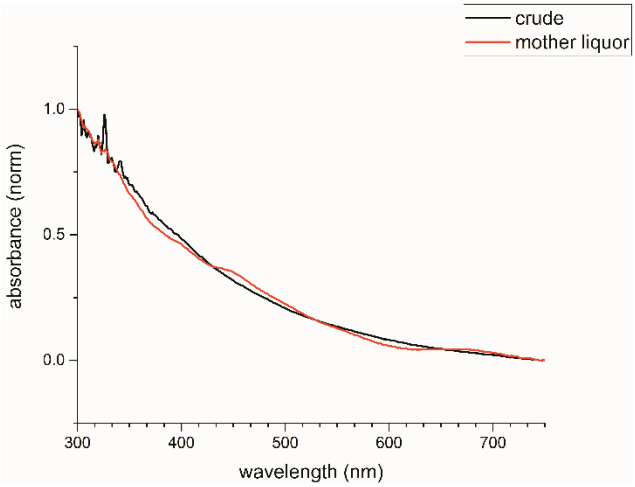

Figure 5.51. Normalized spectra of the crude product and the supernatant from precipitation.

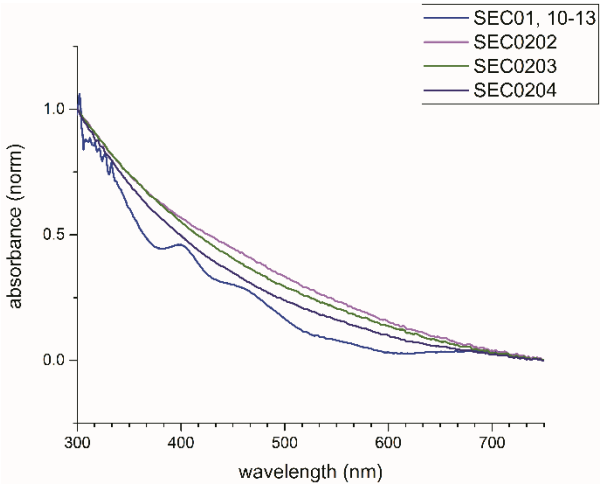

Figure 5.52. Normalized spectra of fractions 10-13 from precipitate, 2-4 from concentrated supernatant.

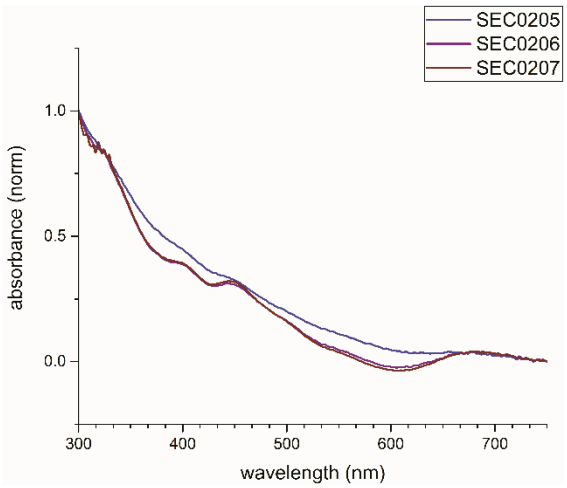

Figure 5.53. Normalized spectra of SEC fractions 5-7 from concentrated supernatant.

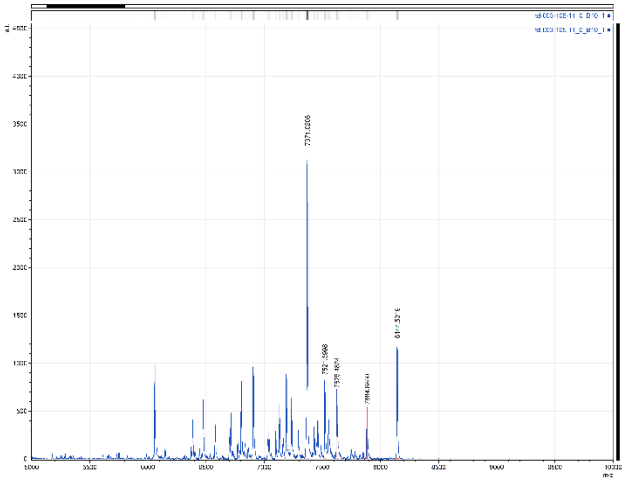

Figure 5.54. MALDI Mass Spectrum of SEC combined fractions. 8144.5319, 7884.8850, 7625.4824, 7521.3998, 7371.0205 M/Z

Td-003-106

$HAuCl_4 \cdot 3H_2O$ (212 mg, 0.538 mmol, 1.00 equiv) was dissolved in 15 mL THF along with TOAB (464 mg, 0.849 mmol, 1.58 equiv). This mixture was allowed to stir for 10 min until homogeneous then 2-phenylethanethiol (553 µL, 4.13 mmol, 7.67 equiv) was added and the reaction was stirred for 15 min at room temperature. This was followed by the addition of $Fe(OAc)_2$ (37.2 mg, 0.214 mmol, 0.397 equiv) as a solution in 5 mL THF. $NaBH_4$ (264 mg, 6.98

mmol, 12.97 equiv) dissolved in 5 mL cold nanopure water was added in one portion and the reaction was stirred overnight at room temperature. The aqueous layer was removed, and the products precipitated from THF by dilution to 50 mL with MeOH then collected by centrifugation. The initial purple reaction mixture turns brown upon standing in MeOH for several minutes. The isolated pellet was redissolved in minimal PhMe then purified by size-exclusion chromatography. Gave a mixture of several clusters, which when separated decomposed upon attempts to crystallize.

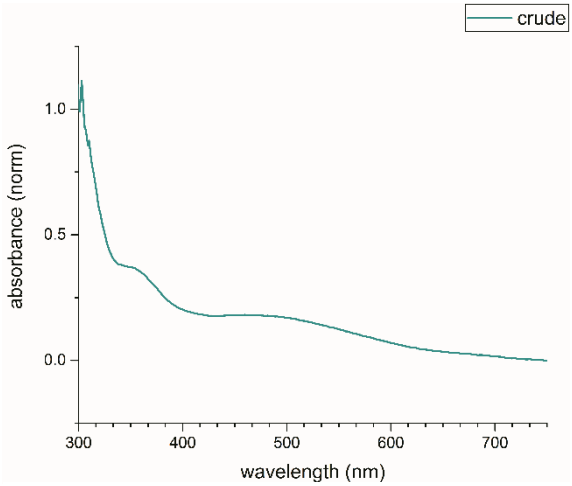

Figure 5.55. Normalized spectrum of the crude reaction product.

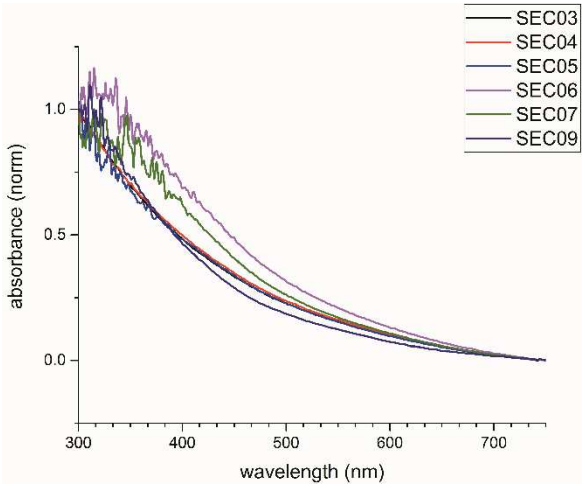

Figure 5.56. Normalized spectrum of SEC fractions

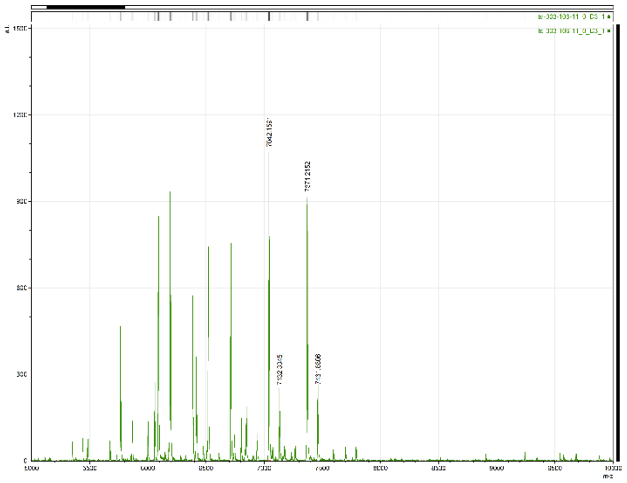

Figure 5.57. MALDI Mass Spectrum of SEC fraction 11, 7461.8806, 7371.2152, 7132.3345, 7042.1591 M/Z

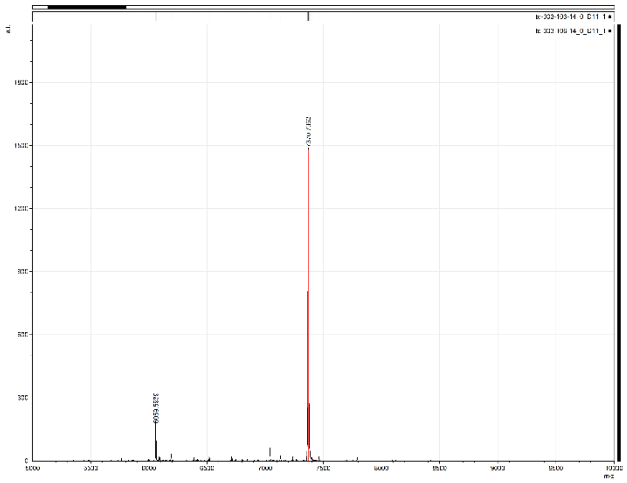

Figure 5.58. Maldi Mass Spectrum of SEC fraction 14, 7370.7362, 6059.5939 M/Z

5.5 Attempts to Synthesize Au/Co

Td-003-3 – Synthesis of cobalt thiolate

$CoCl_2 \cdot 6H_2O$ (119 mg, 0.500 mmol, 1.00 equiv) was dissolved in 2.38 mL nanopure water, and 2.5 mL EtOH was added. A second solution of 2-phenylethanethiol (0.286 mL, 2.14 mmol, 4.27 equiv) in 3.5 mL EtOH with Et_3N (0.953 mL, 6.84 mmol, 13.7 equiv) was prepared. The solutions were combined and stirred vigorously at room temperature for 30 minutes. After stirring the reaction mixture was centrifuged to collect the precipitate. The supernatant was discarded, and the

pellet was washed several times with EtOH to remove excess thiol. The resulting cobalt-thiolate was carried into the next step without further purification.

Td-003-8

10 mg $[Au_{25}(SCH_2CH_2Ph)]^-TOA^+$ dissolved in 10 mL PhMe. 10 mg Co-PET thiolate added as a powder and the reaction was stirred at room temperature for 3 hrs. The solids were removed, and the product was precipitated from the supernatant by addition of MeOH followed by centrifugation. The resulting pellet was dissolved in minimal PhME and purified by size-exclusion chromatography. Returned only Au_{25}.

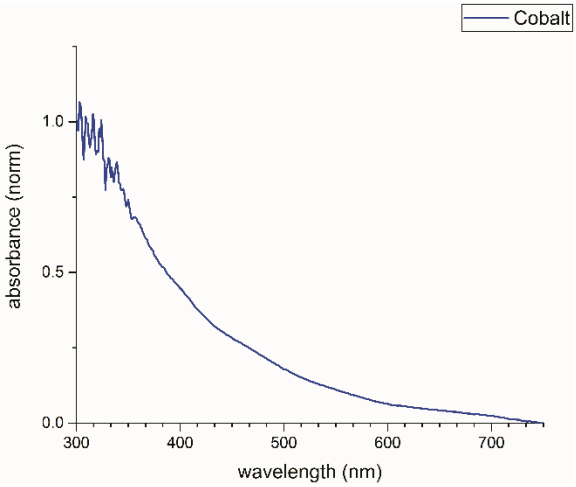

Figure 5.59. Normalized spectrum of the crude reaction. Low concentration of Au_{25} can be seen.

Td-003-109

$HAuCl_4•3H_2O$ (212 mg, 0.538 mmol, 1.00 equiv) was dissolved in 15 mL THF along with TOAB (464 mg, 0.849 mmol, 1.58 equiv). This mixture was allowed to stir for 10 min until homogeneous then 2-phenylethanethiol (553 µL, 4.13 mmol, 7.67 equiv) was added and the reaction was stirred for 15 min at room temperature. This was followed by the addition of $CoCl_2•6H_2O$ (27.8 mg, 0.214 mmol, 0.397 equiv) as a solution in 5 mL THF. $NaBH_4$ (264 mg, 6.98 mmol, 12.97 equiv) dissolved in 5 mL cold nanopure water was added in one portion and the

reaction was stirred overnight at room temperature. The aqueous layer was removed, and the products precipitated from THF by dilution to 50 mL with MeOH then collected by centrifugation. The initial purple reaction mixture turns brown upon standing in MeOH for several minutes. The isolated pellet was redissolved in minimal PhMe then purified by size-exclusion chromatography. Gave only Au_{25}.

Td-003-116

$HAuCl_4 \cdot 3H_2O$ (212 mg, 0.538 mmol, 1.00 equiv) was placed in a mortar and pestle, to which $CoCl_2 \cdot 6H_2O$ (60.4 mg, 0.254 mmol, 1.00 equiv) and TOAB (347.2 mg, 0.635 mmol, 2.5 equiv) were added. The mixture was ground until homogeneously mixed, turning green/blue in the process. 2-phenylethanethiol (180 μL, 1.34 mmol, 5.38 equiv) were added and the mixture was ground manually for 10 minutes until the metal salts had formed a solution in the minimal amount of PET. $NaBH_4$ (96.9 mg, 2.56 mmol, 10.08 equiv) was added and the paste was ground for a further 10 minutes. 7 mL THF was then added and the reaction mixture was dissolved into solution. The products were then precipitated by addition of MeOH to the THF, and isolated by centrifugation. The resulting pellet was redissolved in minimal PhMe and purified by size-exclusion chromatography. The isolated product decomposed upon attempts to isolate it from PhMe after column.

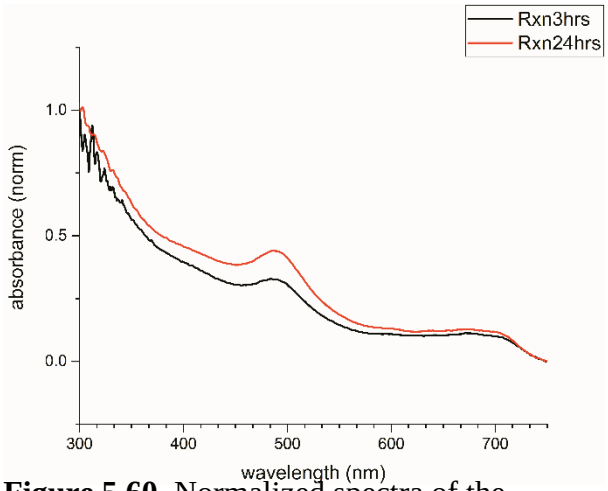

Figure 5.60. Normalized spectra of the reaction at 3 hrs and 24 hrs after reduction

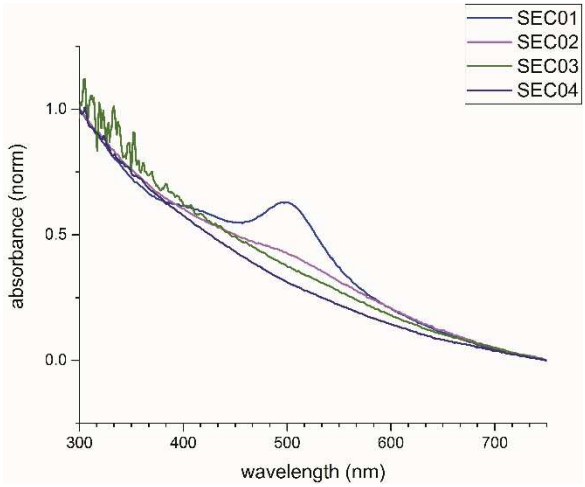

Figure 5.61. Normalized spectra of SEC fractions 1-4

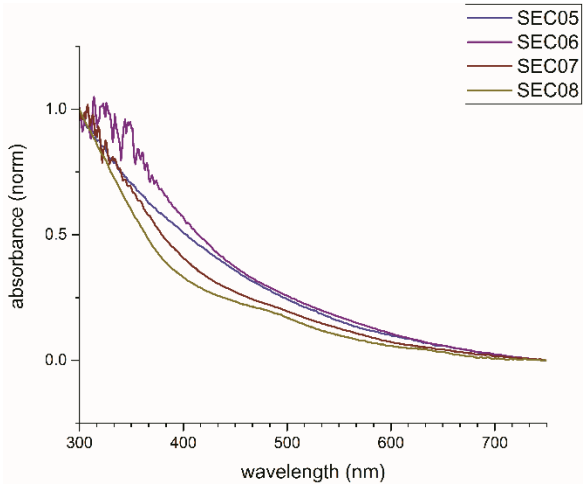

Figure 5.62. Normalized spectra of SEC fractions 5-8

Td-003-119

$HAuCl_4 \cdot 3H_2O$ (1.00 g, 2.54 mmol, 1.00 equiv), $CoCl_2 \cdot 6H_2O$ (60.4 mg, 0.254 mmol, 1.00 equiv) and TOAB (347.2 mg, 0.635 mmol, 2.5 equiv) were dissolved in 136 mL THF. The solution was allowed to stir at room temperature for 15 minutes and 2-phenylethanethiol (1.43 mL, 10.58 mmol, 4.17 equiv) was added. The reaction was stirred for approximately 2.5 hrs at room temperature and $NaBH_4$ (1.54 g, 40.7 mmol, 16.02 equiv) as a solution in 20 mL ice cold nanopure water was added all in one portion. The reaction turned dark, and was allowed to stir at room temperature for 3 hrs. The aqueous phase was removed, and the organic phase concentrated, with the solids being redissolved in minimal CH_2Cl_2. To the redissolved solids, MeOH was added, and the resulting precipitate was isolated by centrifugation. The product was then redissolved in PhMe and purified by size-exclusion chromatography. This gave only $Au_{25}(SCH_2CH_2Ph)_{18}$.

5.6 Attempts to Synthesize Au/Rh Alloy Clusters

Td-002-144

$HAuCl_4 \cdot 3H_2O$ (100 mg, 0.254 mmol, 1.00 equiv) was dissolved in a solution of TOAB (157.0 mg, 0.287 mmol, 1.13 equiv) in 7 mL THF. To this $RhCl_3 \cdot H_2O$ (6.6 mg, 0.0254 mmol, 0.100 equiv) was added and the reaction stirred for 5 min. After this time, 2-phenylethanethiol (180.1 μL, 1.35 mmol, 5.31 equiv) was added and the reaction was stirred at room temperature until colorless. At this point an ice solution of $NaBH_4$ (96.9 mg, 2.56 mmol, 10.08 equiv) in 2.5 mL of water was added in one portion and the reaction was stirred overnight and separated by SEC. Gave exclusively Au_{25}.

Td-002-145 A – Synthesis of rhodium thiolate

$RhCl_3 \cdot H_2O$ (270.1 mg, 1.05 mmol, 1.00 equiv) was dissolved in 5 mL EtOH. A second solution of 2-phenylethanethiol (0.600 mL, 4.48 mmol, 4.27 equiv) in 7 mL EtOH with Et_3N (2 mL, 14.34 mmol, 13.7 equiv) was prepared. The solutions were combined and stirred vigorously at room

temperature for 30 minutes. After stirring the reaction mixture was centrifuged to collect the precipitate. The supernatant was discarded, and the pellet was washed several times with EtOH to remove excess thiol. The resulting rhodium-thiolate was carried into the next step without further purification.

Td-002-146 A

Rh-thiolate (10 mg) was added to a solution of 10 mg $[Au_{25}(SCH2CH2Ph)_{18}]^{-}TOA^{+}$ in 10 mL PhMe. The reaction was stirred for two hours at room temperature, then the reaction was centrifuged and the supernatant collected. The supernatant was concentrated under vacuum, and the resulting solid was washed with MeOH, and the product extracted from the resultant solid using a 1:6 mixture of CH_2Cl_2/ACN.

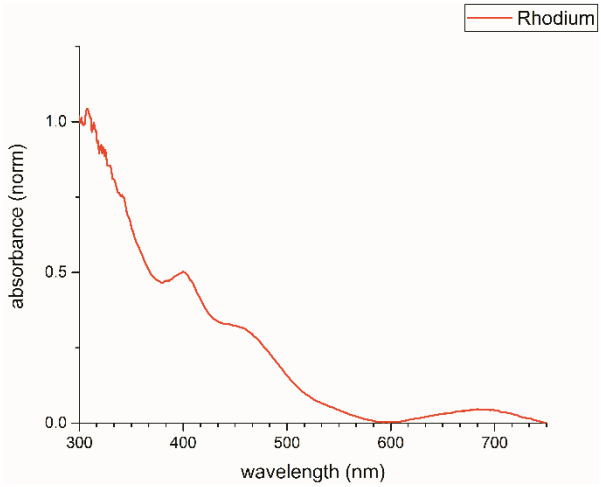

Figure 5.63. Normalized spectrum, shows that reaction gave only Au_{25}.

5.7 Attempts to Synthesize Au/Re Alloy Clusters

Td-003-2 – Synthesis of rhenium thiolate

ReI_3 (250 mg, 0.440 mmol, 1.00 equiv) was dissolved in 2.10 mL nanopure water, and 2.0 mL of EtOH was added. A second solution of 2-phenylethanethiol (0.251 mL, 1.88 mmol, 4.27 equiv) in 3.5 mL EtOH with Et_3N (0.838 mL, 6.01 mmol, 13.7 equiv) was prepared. The solutions were

combined and stirred vigorously at room temperature for 30 minutes. After stirring the reaction mixture was centrifuged to collect the precipitate. The supernatant was discarded, and the pellet was washed several times with EtOH to remove excess thiol. The resulting rhenium-thiolate was carried into the next step without further purification.

Td-002-145 B – Synthesis of rhenium thiolate

ReI_3 (250.0 mg, 0.440 mmol, 1.00 equiv) was dissolved in 2 mL EtOH. A second solution of 2-phenylethanethiol (0.251 mL, 1.88 mmol, 4.27 equiv) in 3 mL EtOH with Et_3N (0.838 mL, 6.01 mmol, 13.7 equiv) was prepared. The solutions were combined and stirred vigorously at room temperature for 30 minutes. After stirring the reaction mixture was centrifuged to collect the precipitate. The supernatant was discarded, and the pellet was washed several times with EtOH to remove excess thiol. The resulting rhenium-thiolate was carried into the next step without further purification.

Td-002-146 B

Re-thiolate (10 mg) was added to a solution of 10 mg $[Au_{25}(SCH2CH2Ph)_{18}]^{-}TOA^{+}$ in 10 mL PhMe. The reaction was stirred for two hours at room temperature, then the reaction was centrifuged and the supernatant collected. The supernatant was concentrated under vacuum, and the resulting solid was washed with MeOH, and the product extracted from the resultant solid using a 1:6 mixture of CH_2Cl_2/ACN. This resulted in large, but not plasmonic products.

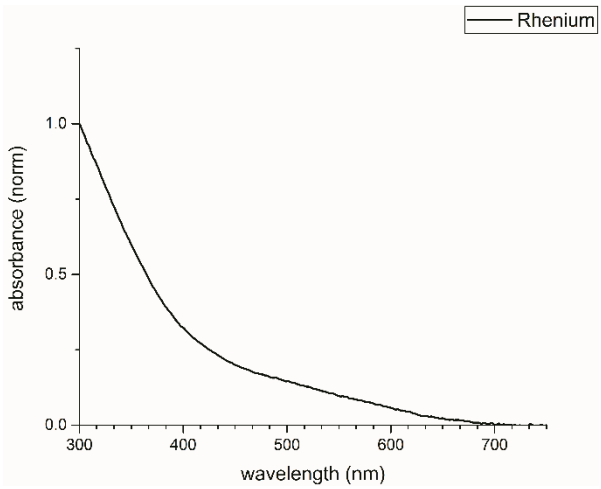

Figure 5.64. Normalized spectrum of product.

Td-003-7

10 mg $[Au_{25}(SCH_2CH_2Ph)]^-TOA^+$ dissolved in 10 mL PhMe. 10 mg Re-PET thiolate added as a powder and the reaction was stirred at room temperature for 3 hrs. The solids were removed, and the product was precipitated from the supernatant by addition of MeOH followed by centrifugation. Resulted in cluster decomposition.

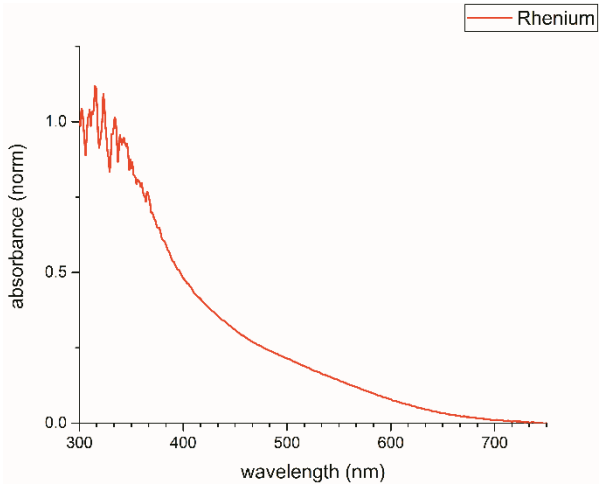

Figure 5.65. Normalized spectrum of the product.

5.8 Attempts to Synthesize Au/Ir Alloy Clusters

Td-002-145 C – Synthesis of iridium thiolate

$IrCl_3$•1.5H_2O (171 mg, 0.525 mmol, 1.00 equiv) was dissolved in 2.5 mL EtOH. A second solution of 2-phenylethanethiol (0.300 mL, 2.24 mmol, 4.27 equiv) in 3.5 mL EtOH with Et_3N (1.00 mL, 7.17 mmol, 13.7 equiv) was prepared. The solutions were combined and stirred vigorously at room temperature for 30 minutes. After stirring the reaction mixture was centrifuged to collect the precipitate. The supernatant was discarded, and the pellet was washed several times with EtOH to remove excess thiol. The resulting iridium-thiolate was carried into the next step without further purification.

Td-003-1 – Synthesis of iridium thiolate.

$IrCl_3$•1.5H_2O (171 mg, 0.525 mmol, 1.00 equiv) was dissolved in 2.5 mL nanopure water, and 2.5 mL EtOH was added. A second solution of 2-phenylethanethiol (0.300 mL, 2.24 mmol, 4.27 equiv) in 3.0 mL EtOH with Et_3N (1.00 mL, 7.17 mmol, 13.7 equiv) was prepared. The solutions were combined and stirred vigorously at room temperature for 30 minutes. After stirring the reaction mixture was centrifuged to collect the precipitate. The supernatant was discarded, and the pellet was washed several times with EtOH to remove excess thiol. The resulting iridium-thiolate was carried into the next step without further purification.

Td-003-40

10 mg $IrCl_3$•1.5H_2O were dissolved in 1 mL EtOH and 25 μL 2-phenylethanethiol were added. This was allowed to stir for 10 minutes at room temperature, and then added to a solution of 10 mg $[Au_{25}(SCH_2CH_2Ph)]^-TOA^+$ in 10 mL PhMe. Reaction stirred 2 hrs at room temperature. Reaction was then transferred to a centrifuge tube, and the precipitate was removed. The supernatant was placed in a 50 mL centrifuge tube, diluted to 50 mL with MeOH, and centrifuged to isolate the precipitate. The resulting pellet was dissolved in 1 mL PhMe and separated by size-

exclusion chromatography. Resulting product spectra below, appears to be a non-Au_{25} cluster of indeterminate composition which could not be crystallized.

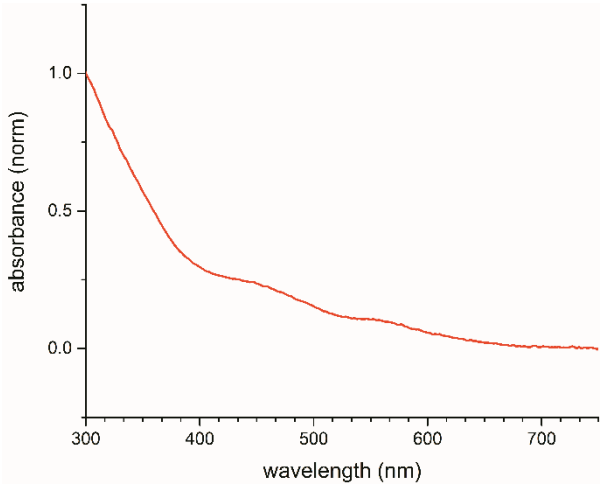

Figure 5.66. Normalized spectrum of product.

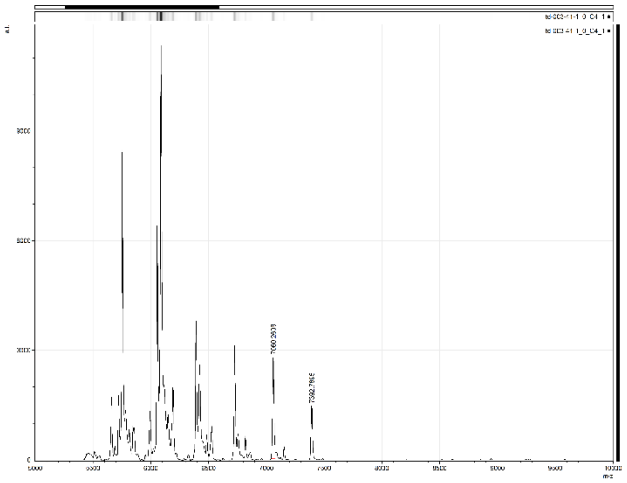

Figure 5.67. MALDI Mass Spectrum, 7392.7895, 7060.2606 M/Z

Td-002-146 C

Ir-thiolate (10 mg) was added to a solution of 10 mg $[Au_{25}(SCH2CH2Ph)_{18}]^{-}TOA^{+}$ in 10 mL PhMe. The reaction was stirred for two hours at room temperature, then the reaction was centrifuged and the supernatant collected. The supernatant was concentrated under vacuum, and

the resulting solid was washed with MeOH, and the product extracted from the resultant solid using a 1:6 mixture of CH_2Cl_2/ACN. Returned Au_{25}.

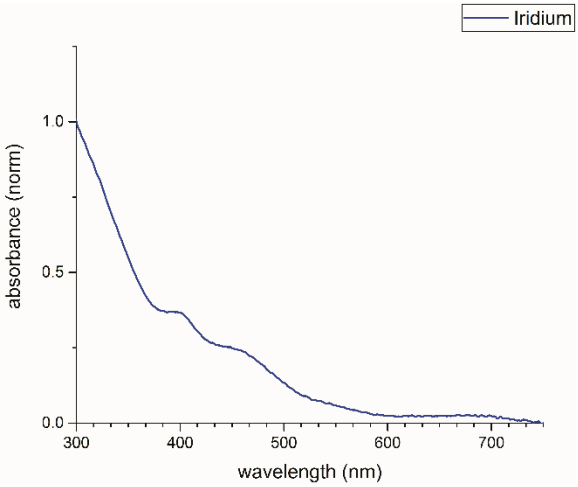

Figure 5.68. Normalized spectrum of product.

5.9 Conclusion

The above experiments illustrate the difficulty in synthesizing alloy clusters of approximately 25 metal atoms containing gold and transition metals with open d-orbitals. Over the course of many months and numerous attempts, we were able to make none of the desired clusters, although some reaction conditions showed promise. However, these experiments were not particularly well-behaved and tended to give different product mixtures upon repetition or increases in scale. Given the unfavorable redox chemistry involved, co-reduction strategies seem the least promising approach. Going forward this project may require new synthetic strategies involving extension of other work from the Ackerson laboratory.[19]

REFERENCES

1. Kacprzak, K. A.; Lehtovaara, L.; Akola, J.; Lopez-Acevedo, O.; Haekkinen, H. A density functional investigation of thiolate-protected bimetal PdAu24(SR)18z clusters: doping the superatom complex. *Phys. Chem. Chem. Phys.* **2009**, *11*, 7123-7129.

2. Negishi, Y.; Kurashige, W.; Niihori, Y.; Iwasa, T.; Nobusada, K. Isolation, structure, and stability of a dodecanethiolate-protected Pd1Au24 cluster. *Phys. Chem. Chem. Phys.* **2010**, *12*, 6219-6225.

3. Yang, A.; Wei, F.; Dong, J. Magnetic Properties of Transition-Metal-Doped Tubular Gold Clusters: M@Au24 (M = V, Cr, Mn, Fe, Co, and Ni). *J. Phys. Chem. A* **2010**, *114*, 4031-4035.

4. Negishi, Y.; Igarashi, K.; Munakata, K.; Ohgake, W.; Nobusada, K. Palladium doping of magic gold cluster Au38(SC2H4Ph)24: formation of Pd2Au36(SC2H4Ph)24 with higher stability than Au38(SC2H4Ph)24. *Chem. Commun.* **2012**, *48*, 660-662.

5. Christensen, S. L.; MacDonald, M. A.; Chatt, A.; Zhang, P.; Qian, H.; Jin, R. Dopant Location, Local Structure, and Electronic Properties of Au24Pt(SR)18 Nanoclusters. *J. Phys. Chem. C* **2012**, *116*, 26932-26937.

6. Tlahuice-Flores, A. Optical properties of thiolate-protected AgnAu25-n(SCH3)18- clusters. *J. Nanopart. Res.* **2013**, *15*, 1771/1-1771/7.

7. Yamazoe, S.; Kurashige, W.; Nobusada, K.; Negishi, Y.; Tsukuda, T. Preferential Location of Coinage Metal Dopants (M = Ag or Cu) in [Au25-xMx(SC2H4Ph)18]- (x ∼ 1) As Determined by Extended X-ray Absorption Fine Structure and Density Functional Theory Calculations. *J. Phys. Chem. C* **2014**, *118*, 25284-25290.

8. Yan, J.; Su, H.; Yang, H.; Malola, S.; Lin, S.; Hakkinen, H.; Zheng, N. Total Structure and Electronic Structure Analysis of Doped Thiolated Silver [MAg24(SR)18]2- (M = Pd, Pt) Clusters. *J. Am. Chem. Soc.* **2015**, *137*, 11880-11883.

9. Kwak, K.; Tang, Q.; Kim, M.; Jiang, D.-e.; Lee, D. Interconversion between Superatomic 6-Electron and 8-Electron Configurations of M@Au24(SR)18 Clusters (M = Pd, Pt). *J. Am. Chem. Soc.* **2015**, *137*, 10833-10840.

10. Tofanelli, M. A.; Ni, T. W.; Phillips, B. D.; Ackerson, C. J. Crystal structure of the [PdAu24(SR)18]0 superatom. *Inorg. Chem.* **2016**, *55*, 999-1001.

11. Peng, Y.; Wu, X.; Qiu, L.; Liu, C.; Wang, S.; Yan, F. Synthesis of carbon-PtAu nanoparticle hybrids originating from triethoxysilane-derivatized ionic liquids for methanol electrooxidation and the catalytic reduction of 4-nitrophenol. *J. Mater. Chem. A* **2013**, *1*, 9257-9263.

12. Zhou, T.-y.; Lin, L.-p.; Rong, M.-c.; Jiang, Y.-q.; Chen, X. Silver-Gold Alloy Nanoclusters as a Fluorescence-Enhanced Probe for Aluminum Ion Sensing. *Anal. Chem.* **2013**, *85*, 9839-9844.

13. Liao, L.; Zhou, S.; Dai, Y.; Liu, L.; Yao, C.; Fu, C.; Yang, J.; Wu, Z. Mono-Mercury Doping of Au25 and the HOMO/LUMO Energies Evaluation Employing Differential Pulse Voltammetry. *J. Am. Chem. Soc.* **2015**, *137*, 9511-9514.

14. Atkins, P.; Overton, T.; Rourke, J.; Weller, M.; Armstrong, F. *Inorganic Chemistry*. 4th Edition ed.; W.H. Freeman and Company: New York, NY, 2006; p 822.

15. Shon, Y.-S.; Dawson, G. B.; Porter, M.; Murray, R. W. Monolayer-Protected Bimetal Cluster Synthesis by Core Metal Galvanic Exchange Reaction. *Langmuir* **2002**, *18*, 3880-3885.

16. Song, Y.; Huang, T.; Murray, R. W. Heterophase Ligand Exchange and Metal Transfer between Monolayer Protected Clusters. *J. Am. Chem. Soc.* **2003**, *125*, 11694-11701.

17. Wang, S.; Song, Y.; Jin, S.; Liu, X.; Zhang, J.; Pei, Y.; Meng, X.; Chen, M.; Li, P.; Zhu, M. Metal Exchange Method Using Au25 Nanoclusters as Templates for Alloy Nanoclusters with Atomic Precision. *J. Am. Chem. Soc.* **2015**, *137*, 4018-4021.

18. Liao, L.; Zhou, S.; Dai, Y.; Liu, L.; Yao, C.; Fu, C.; Yang, J.; Wu, Z. Mono-Mercury Doping of Au25 and the HOMO/LUMO Energies Evaluation Employing Differential Pulse Voltammetry. *J. Am. Chem. Soc.* **2015**, *137*, 9511-9514.

19. Compel, W. S. Metallogels through glyme coordination. *Dalton Transactions* **2016**, *45*, 4509-4512.

APPENDIX A: SUPPLEMENTAL TO CHAPTER 2

A.1 Synthesis of $[Au_{25}(SCH_2CH_2Ph)_{18}]^0$

To a 500 mL roundbottom flask equipped with a magnetic stirbar $HAuCl_4 \bullet 3H_2O$ (>49%, 1.00 g, 2.54 mmol, 1.00 equiv) was added to 70.6 mL of dry tetrahydrofuran and stirred at ambient temperature to give an orange solution. To this tetra-*n*-octylammonium bromide (1.55 g, 2.82 mmol, 1.12 equiv) was added and the reaction was stirred for 10 minutes. After 10 minutes of stirring phenylethanethiol (1.80 mL, 13.41 mmol, 5.28 equiv) was added all in one portion. The resultant dark orange solution was stirred for 1.5 hrs at room temperature until the solution was clear. When the solution was no longer colored, sodium borohydride (0.969 g, 25.60 mmol, 10.08 equiv) dissolved in 24 mL of nanopure water was chilled to 0 °C and then added to the gold solution in three portions over the course of five minutes. The resulting dark brown solution was covered with a plastic cap and allowed to stir at ambient temperature for 48 hrs.

After 48 hrs, 50 mL of PhMe was added, the reaction was poured into a separatory funnel, and the aqueous layer was removed. The organic phase was concentrated *in vacuo* and azeotroped with three 25 mL portions of PhMe to remove residual water. The resultant residue was washed three times with 10 mL portions of MeOH, then dissolved in CH_2Cl_2 and purified by flash chromatography on silica gel (20% to 50% CH_2Cl_2 in hexanes) to give 171.2 mg of the desired product as a nearly black solid. UV/Vis spectrum consistent with literature reports.

$[Au_{25}(S\textit{n}\text{-Hex})_{18}]^0$, and $[Au_{25}(S\textit{n}\text{-Oct})_{18}]^0$ were synthesized via the same procedure. $[Au_{25}(SCH_2CH_2Ph)_{18}]^{-1}$ was prepared as above, with omission of flash chromatography.

A.2 Synthesis of *N*-heterocyclic carbene (NHC) catalyst poison

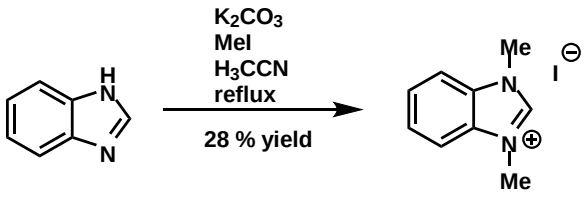

Figure A.1. NHC Synthesis

Synthesis adapted from literature reports.[1] Briefly: To a round bottom flask, Acetonitrile (ACN, 10 mL) was added, followed by benzimidazole (1.004 g, 8.5 mmol, 1 equiv) and K_2CO_3. MeI (2.1 mL, 33.7 mmol, 4 equiv) was added, the flask was fitted with a condenser, and heated to reflux overnight. Volatile components were removed *in vaccuo*, and the residue repeatedly washed with CH_2Cl_2. Recrystallization from EtOAc gave pure product (0.645 g, 285 yield) whose NMR spectra were consistent with literature reports.

A.3 Oxidative Cleavage Starting from Cluster, using PhMe as solvent

$[Au_{25}(SCH_2CH_2Ph)_{18}]^0$ was prepared as a stock solution (11.61 mg/mL) in PhMe and used immediately. To a flame-dried 2-dram vial equipped with a stir bar, 1 mL of $[Au_{25}(SCH_2CH_2Ph)_{18}]^0$ stock solution (1 mol% cluster) was added, followed by an additional 1 mL of PhMe, 17.98 μL styrene (0.157 mmol, 1 equiv) and TBHP (50 μL, 5.5 M in decane, 0.275 mmol, 1.75 equiv). The vessel was then sealed and heated to 75 °C in a sand bath attached to a variac. 50 μL aliquots were taken at the times noted and analyzed by the GC/MS methods outlined below. Experiments with $[Au_{25}(S\textit{n}\text{-Hex})_{18}]^0$ and $[Au_{25}(S\textit{n}\text{-Oct})_{18}]^0$ were performed similarly, also with 1 mol % loading of cluster.

A.4 Oxidative Cleavage Starting from Cluster, using ACN as solvent

$[Au_{25}(SCH_2CH_2Ph)_{18}]^0$ was prepared as a stock solution (5.7 mg/mL) in THF and used immediately. To a flame-dried 2-dram vial equipped with a stir bar, 2.03 mL of $[Au_{25}(SCH_2CH_2Ph)_{18}]^0$ stock solution (1 mol% cluster) was added, and the solvent was removed

in vacuo. This was followed by an addition of 2 mL of ACN, 17.98 μL styrene (0.157 mmol, 1 equiv) and TBHP (50 μL, 5.5 M in decane, 0.275 mmol, 1.75 equiv). The vessel was then sealed and heated to 75 °C in a sand bath attached to a variac. 50 μL aliquots were taken at the times noted and analyzed by the GC/MS methods outlined below. Experiments with $[Au_{25}(S\textit{n}\text{-Hex})_{18}]^0$ and $[Au_{25}(S\textit{n}\text{-Oct})_{18}]^0$ were performed similarly, also with 1 mol % loading of cluster.

A.5 Oxidative Cleavage using cluster decomposition products (PhMe as solvent):

$[Au_{25}(SCH_2CH_2Ph)_{18}]^0$ was prepared as a stock solution (11.61 mg/mL) in PhMe and used immediately. To a flame-dried 2-dram vial equipped with a stir bar, 1 mL of $[Au_{25}(SCH_2CH_2Ph)_{18}]^0$ stock solution (1 mol% cluster) was added followed by an additional 1 mL PhMe. To this solution TBHP (50 μL, 5.5 M in decane, 1.75 equiv to styrene) was added, and the vessel was sealed then heated to 75 °C for 10 minutes. After heating the vessel was allowed to cool to room temperature and 17.98 μL styrene (0.157 mmol, 1 equiv) was added. The vessel was then sealed and heated to 75 °C for 1 h at which time a 50 μL aliquot was taken. The reaction result was then analyzed by GC/MS as described below.

A.6 Oxidative Cleavage using cluster decomposition products (ACN as solvent):

$[Au_{25}(SCH_2CH_2Ph)_{18}]^0$ was prepared as a stock solution (5.7 mg/mL) in THF and used immediately. To a flame-dried 2-dram vial equipped with a stir bar, 2.03 mL of $[Au_{25}(SCH_2CH_2Ph)_{18}]^0$ stock solution (1 mol% cluster, 25 mol % Au atoms) was added, and the solvent removed *in vacuo*. This was followed by addition of 2 mL ACN. To this suspension, TBHP (50 μL, 5.5 M in decane, 1.75 equiv to styrene) was added, and the vessel was sealed then heated to 75 °C for 10 minutes. After heating, the vessel was allowed to cool to room temperature and 17.98 μL styrene (0.157 mmol, 1 equiv) was added. The vessel was then sealed and heated to 75 °C for 1 h at which time a 50 μL aliquot was taken. The reaction result was then analyzed by

GC/MS as described below. Experiments with $[Au_{25}(S\textit{n}\text{-Hex})_{18}]^0$ and $[Au_{25}(S\textit{n}\text{-Oct})_{18}]^0$ were performed similarly, also with 1 mol % loading of cluster (25 mol % Au atoms).

A.7 Oxidative Cleavage using cluster precursors (PhMe as solvent):

To a flame-dried 2 dr vial equipped with stir bar were added $HAuCl_4 \cdot 3H_2O$ (1 mol% Au, 0.618 mg, 0.00157) mmol), 2 mL PhMe, and $(\textit{n}\text{-Oct})_4NBr$ (0.963 mg, 1.12 equiv to Au, 0.00175 mmol). This solution was allowed to stir for several minutes at ambient temperature until homogeneous. When the solution was homogeneous, 2phenylethanethiol (1.18 μL, 5.28 equiv to Au, 0.00829 mmol) was added and the reaction was allowed to stir at ambient temperature until the orange solution turned clear. Once the solution was clear, styrene (17.98 μL 0.157 mmol, 1 equiv) was added followed by TBHP (50 μL, 5.5 M in decane, 1.75 equiv to styrene). The vessel was sealed and heated to 75 °C for 1 h at which time a 50 μL aliquot was taken. The reaction result was then analyzed by GC/MS as described below. Experiments with $[Au_{25}(S\textit{n}\text{-Hex})_{18}]^0$ and $[Au_{25}(S\textit{n}\text{-Oct})_{18}]^0$ were performed similarly.

A.8 Oxidative Cleavage using cluster precursors (ACN as solvent):

To a flame-dried 2 dr vial equipped with stir bar were added $HAuCl_4 \cdot 3H_2O$ (1 mol% Au, 0.618 mg, 0.00157) mmol), 2 mL THF, and $(\textit{n}\text{-Oct})_4NBr$ (0.963 mg, 1.12 equiv to Au, 0.00175 mmol). This solution was allowed to stir for several minutes at ambient temperature until homogeneous. When the solution was homogeneous, 2phenylethanethiol (1.18 μL, 5.28 equiv to Au, 0.00829 mmol) was added and the reaction was allowed to stir at ambient temperature until the orange solution turned clear. Once the solution was clear the solvent was removed *in vacuo* and replaced with 2 mL ACN, then styrene (17.98 μL 0.157 mmol, 1 equiv) was added followed by TBHP (50 μL, 5.5 M in decane, 1.75 equiv to styrene). The vessel was sealed and heated to 75 °C for 1 h at which time a 50 μL aliquot was taken. The reaction result was then analyzed by GC/MS as

described below. Experiments with $[Au_{25}(S\textit{n}\text{-Hex})_{18}]^0$ and $[Au_{25}(S\textit{n}\text{-Oct})_{18}]^0$ were performed similarly.

A.9 Kinetic Poisoning Experiments with Phosphines

All kinetic poisoning experiments using phosphine poisons were performed with the same general procedure as follows. $[Au_{25}(PET)_{18}]^0$ (0.00157 mmol, 11.6 mg) was dissolved in 2 mL dry PhMe at room temperature in a 2-dram vial fitted with a Teflon-lined cap and magnetic stir bar. To this the selected poison was added, and the vessel was stirred at room temperature for 5 minutes. After this short incubation period, styrene (0.157 mmol, 18 μL) and TBHP (5.5 M in decane, 50 μL) were added, and the vessel was heated to 75 °C for 60 minutes then analyzed by GC/MS as described below.

A.10 Kinetic Poisoning Experiments with 1,3-dimethylbenzimidazolium iodide (NHC)

All poisoning experiments with the NHC poison were performed with the same general procedure. $[Au_{25}(PET)_{18}]^{-1}$ $[TOA]^+$ (10.6 mg, 0.00135 mmol) was dissolved in 2 mL $CHCl_3$ at room temperature in a 2-dram vial fitted with a magnetic stir bar and Teflon-lined cap. 1,3-dimethylbenzimidazolium iodide and an equimolar amount of triethylamine were added, and the solution was allowed to stir for 5 min at room temperature. After this brief period, styrene (0.135 mmol, 15.5 μL) was added followed by TBHP (5.5 M in decane, 0.236 mmol, 43 μL). The vessel was sealed and heated to 75 °C for 75 minutes then analyzed by GC/MS as described below.

A.11 GC/MS Data Collection

All gas chromatograph mass spectroscopy (GC/MS) data were collected on an Agilent 6890 GC equipped with an agilent 5973N MSD as the detector and fitted with an Agilent 7683 autoinjector. GC experiments were run using a Phenomenex Zebron ZB-5HT Inferno column (30 m, 0.25 mm ID, 0.25 μm film thickness) using He as the carrier gas and a 0.2 μL injection with a 1:50 split. Injection temperature was 275 °C, with a 320 °C transfer line. Method began at 100 °C

and ramped at 10 °C per minute to 210 °C then held for 2 minutes, a 2 minute solvent delay was used in order to preserve the MSD, this gave a total run time of 15 minutes with 13 minutes of data collection. Decane present in all cases results from TBHP being added as a solution in decane.

A.12 GC/MS Data Analysis

GC traces were exported as CSV files using Agilent ChemStation, then recreated in Microsoft Excel 2007. GC Integrations were calculated using Agilent ChemStation, then exported and worked-up in Microsoft Excel. Product concentrations were calculated using external 2- or 3-point calibration curves for each substance. Calibration curves were constructed using known samples of product and starting material from commercial vendors, with samples prepared via serial dilution. Trendline was constructed using the built-in linear regression analysis in Microsoft Excel and manually setting the intercept to 0. It should be noted that Figure 1 in the main body was constructed in Igor. In the case of experiments with $Au_{25}SR_{18}$, sampling was performed as follows: At the indicated reaction time the vessel was allowed to cool to room temperature and a 50 μL aliquot was taken using a calibrated micropipette. This aliquot was diluted by addition of 1000 μL of HPLC grade acetonitrile to give a total GC sample volume of 1050 μL. Concentrations of the GC samples were calculated using the previously constructed calibration curves for each compound, which allowed for calculation of the reaction concentration. All calculations were done in Microsoft Excel. Conversions are shown as a percentage of the starting amount of styrene (0.157 mmol). Conversions are reported as an average of three runs, plus or minus the standard error where N = 3, for $Au_{25}(PET)_{18}$ experiments. Conversions for experiments with $Au_{25}(S\textit{n}\text{-Hex})_{18}$ and Au25SnOct18 were calculated similarly unless otherwise noted.

Representative GC traces are shown starting on page 125. Area data for each run follow the representative trace immediately in each case.

A.13 UV/VIS Data Collection

All UV/VIS spectra were collected on a Thermo Fisher NanoDrop 2000c spectrophotometer using its native software. All spectra were exported as Excel files and then reconstructed using Microsoft Excel 2007. All spectra were trimmed to show 300 nm to 800 nm wavelengths for clarity. No further processing was required. It should be noted that Figure 2.4 in the main body was constructed in Igor. Spectra begin on page 156.

A.14 Oxidative Decay of $[Au_{25}(SCH_2CH_2Ph)_{18}]^0$ Observed by UV/VIS

11.61 mg (0.00157 mmol) $[Au_{25}(SCH_2CH_2Ph)_{18}]^0$ was dissolved in 2 mL PhMe at room temperature. To this 50 μL TBHP was added and the solution was shaken to mix. A 50 μL aliquot was taken, diluted to 1 mL using additional PhMe, and placed in a cuvette. The instrument was set to heat the holder to 37 °C. Spectra were taken at regular intervals until characteristic absorbance for $[Au_{25}(SCH_2CH_2Ph)_{18}]^0$ was no longer detected (Fig. 2.3, Chapter 2, raw data presented below).

A.15 X-ray Photoelectron Spectroscopy (XPS)

A PHI 5800 system was used to measure X-ray photoelectron spectra. Samples were dissolved in $CDCl_3$ and spotted onto a high purity aluminum substrate. Charge was referenced to adventitious C1s at 284.4 eV

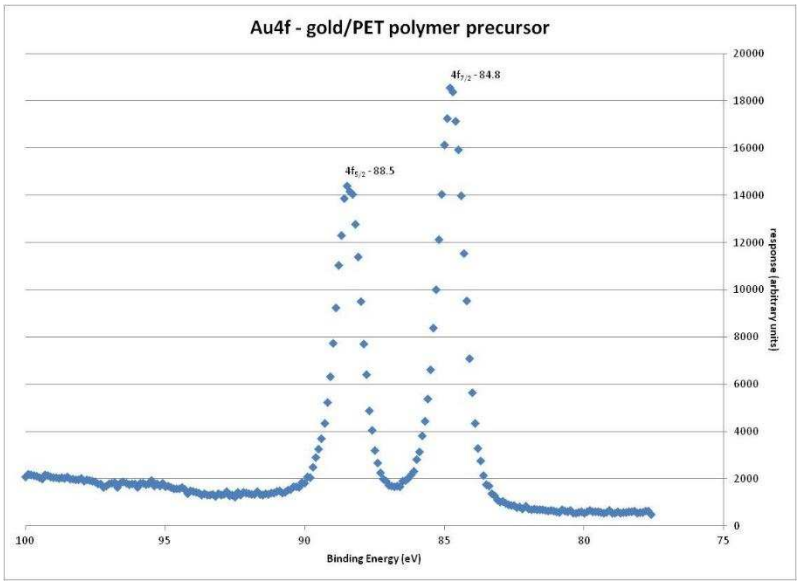

Figure A.2. XPS of Au_{25} precursor

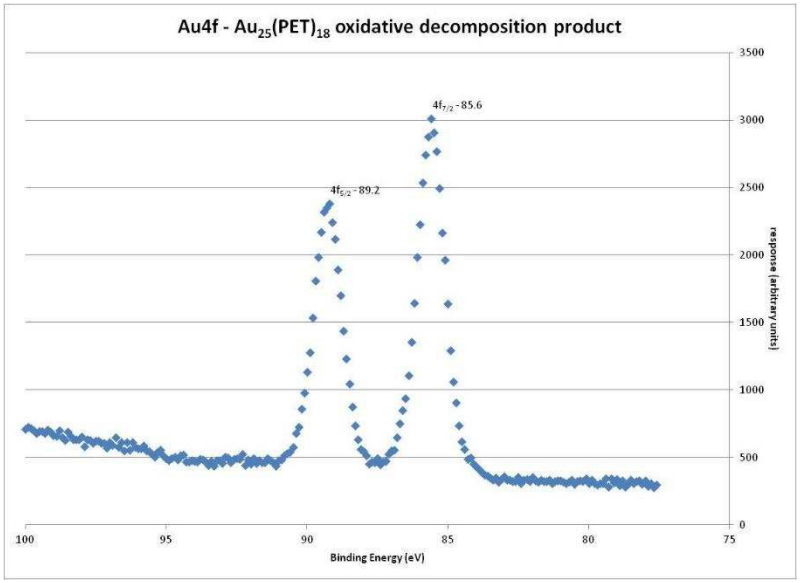

Figure A.3. XPS of Au_{25} oxidative decomposition products

A.16 Gas Chromatograms

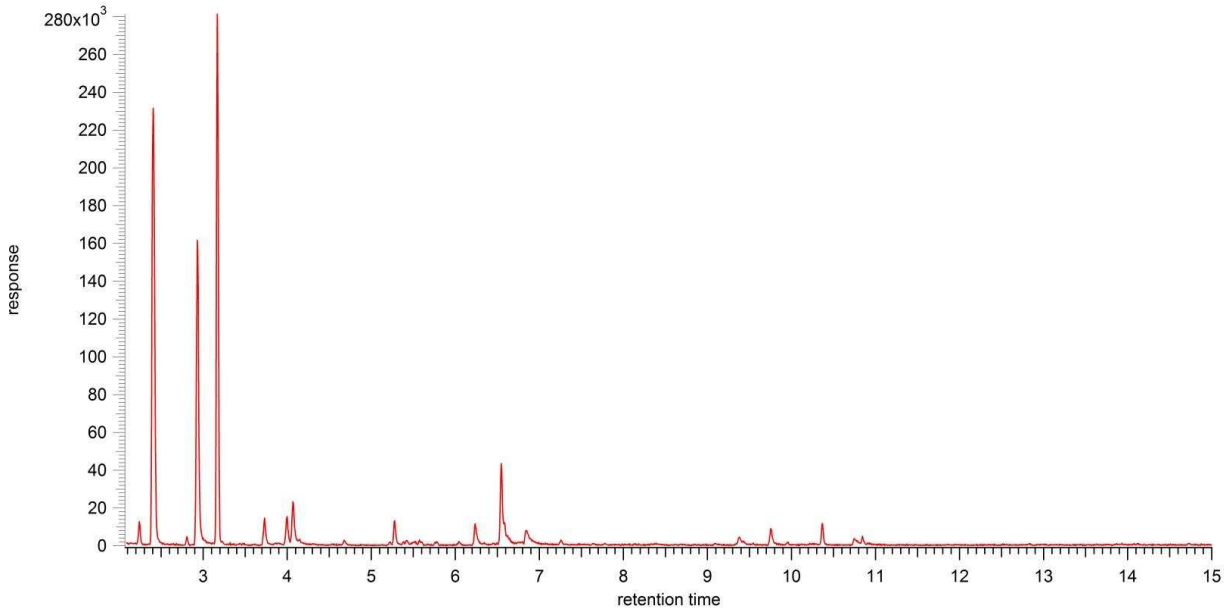

Figure A.4. Chapter 2, Figure 2.2, full spectrum

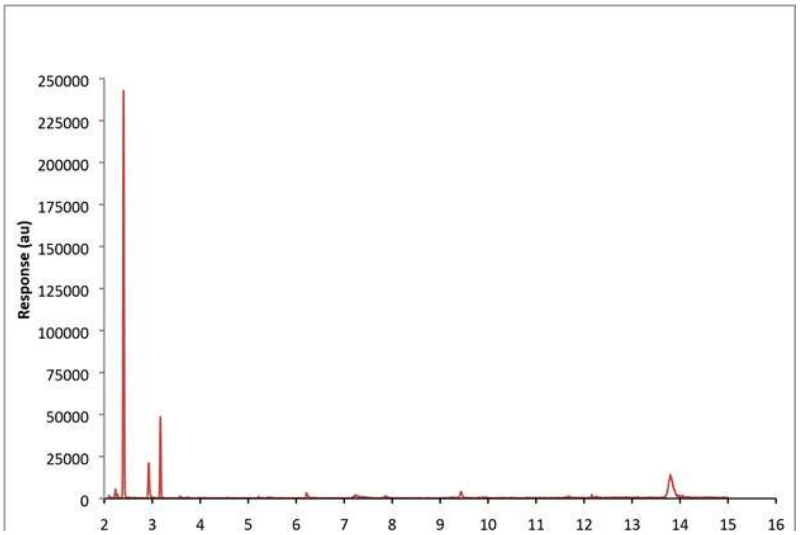

Figure A.5. GC/MS, Chapter 2, Table 2.1, Entry 1, run 1

Table A.1. GC/MS Data Chapter 2, Table 2.1, Entry 1, run 1

Header=	Peak	R.T.	First	Max	Last	PK TY	Height	Area	Pct Max	Pct Total	Compound
1=	1	2.236	23	33	37	BV 3	5197	77992	2.01	1.305	
2=	2	2.405	60	69	86	PV	239897	3888266	100	65.045	styrene
3=	3	2.927	168	180	190	BV 3	20355	383601	9.87	6.417	benzaldehyde
4=	4	3.171	216	232	245	PV	47223	712071	18.31	11.912	decane
5=	5	9.439	1541	1565	1578	BV 7	3695	109514	2.82	1.832	
6=	6	13.8	2467	2492	2494	PV 8	12844	411311	10.58	6.881	
7=	7	13.82	2494	2496	2518	VV 7	11620	395032	10.16	6.608	

Table A.2. GC/MS Data Chapter 2, Table 2.1, Entry 1, run 2

Header=	Peak	R.T.	First	Max	Last	PK TY	Height	Area	Pct Max	Pct Total	Compound
1=	1	2.235	26	33	38	PV 4	3728	51880	1.41	0.844	
2=	2	2.405	56	69	86	BV	206325	3667862	100	59.673	styrene
3=	3	2.931	168	181	200	BV 5	21498	451328	12.3	7.343	benzaldehyde
4=	4	3.171	222	232	242	BV	47663	748790	20.41	12.182	decane
5=	5	13.808	2474	2494	2496	PV 5	11517	346577	9.45	5.639	
6=	6	13.822	2496	2497	2521	VV 6	10212	309681	8.44	5.038	
7=	7	14.847	2672	2715	2734	PV 3	13453	570435	15.55	9.281	

Table A.3. GC/MS Data Chapter 2, Table 2.1, Entry 1, run 3

Header=	Peak	R.T.	First	Max	Last	PK TY	Height	Area	Pct Max	Pct Total	Compound
1=	1	2.24	13	34	38	BV 4	3770	67266	1.81	0.933	
2=	2	2.405	52	69	81	PV	202944	3707759	100	51.417	styrene
3=	3	2.932	157	181	196	PV 2	22972	469608	12.67	6.512	benzaldehyde
4=	4	3.171	219	232	242	PV 2	45077	716261	19.32	9.933	decane
5=	5	13.789	2465	2490	2517	VV 5	30782	1836087	49.52	25.462	
6=	6	14.617	2646	2666	2667	PV 7	7504	212308	5.73	2.944	
7=	7	14.631	2667	2669	2689	VV 6	7458	201805	5.44	2.799	

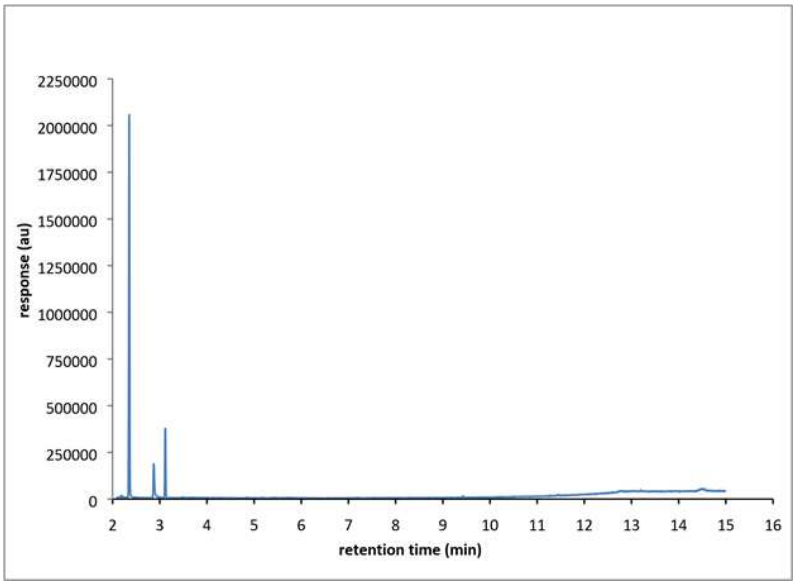

Figure A.6. GC/MS, Chapter 2, Table 2.1, Entry 2, run 1

Table A.4. GC/MS Data, Chapter 2, Table 2.1, Entry 2, run 1

Peak	R.T.	First	Max	Last	PK TY	Height	Area	Pct Max	Pct Total	Compound
1	2.184	16	22	27	PV	20120	232200	0.5	0.265	
2	2.222	27	30	36	VV	11685	135356	0.29	0.154	
3	2.353	50	58	72	PV	4327172	46906220	100	53.499	styrene
4	2.424	72	73	81	VV 6	5967	101358	0.22	0.116	
5	2.645	114	120	131	PV 6	4260	79675	0.17	0.091	
6	2.87	161	168	201	PV	490575	7783712	16.59	8.878	benzaldehyde
7	3.035	201	203	212	VV 9	6727	134749	0.29	0.154	
8	3.12	212	221	234	VV	684529	8270378	17.63	9.433	decane

Table A.5. GC/MS Data, Chapter 2, Table 2.1, Entry 2, run 2

Peak	R.T.	First	Max	Last	PK TY	Height	Area	Pct Max	Pct Total	Compound
1	2.184	16	22	27	VV	10242	111061	0.52	0.224	
2	2.222	27	30	35	VV 2	6409	68338	0.32	0.138	
3	2.306	46	48	49	PV 2	1620	8411	0.04	0.017	
4	2.353	49	58	77	VV	1977294	21518729	100	43.404	styrene
5	2.447	77	78	86	VV 8	1739	32255	0.15	0.065	
6	2.875	157	169	190	PV	178547	3197471	14.86	6.449	benzaldehyde
7	2.983	190	192	193	VV 2	4640	33455	0.16	0.067	
8	2.997	193	195	197	VV 3	4244	44199	0.21	0.089	
9	3.016	197	199	201	VV 3	4075	36997	0.17	0.075	
10	3.12	212	221	235	VV	356363	4213366	19.58	8.499	decane

Table A.6. GC/MS Data, Chapter 2, Table 2.1, Entry 2, run 3

Peak	R.T.	First	Max	Last	PK TY	Height	Area	Pct Max	Pct Total	Compound
1	2.184	17	22	27	PV 2	9850	124184	0.5	0.257	
2	2.222	27	30	42	VV 3	6840	89696	0.36	0.186	
3	2.353	49	58	75	PV	2259938	24603341	100	50.935	styrene
4	2.443	75	77	80	VV 4	3273	46110	0.19	0.095	
5	2.875	162	169	197	VV	144651	2719007	11.05	5.629	benzaldehyde
6	3.012	197	198	200	VV 2	3592	28326	0.12	0.059	
7	3.04	200	204	211	VV 10	3653	84045	0.34	0.174	
8	3.12	214	221	228	VV	390776	4606450	18.72	9.536	decane

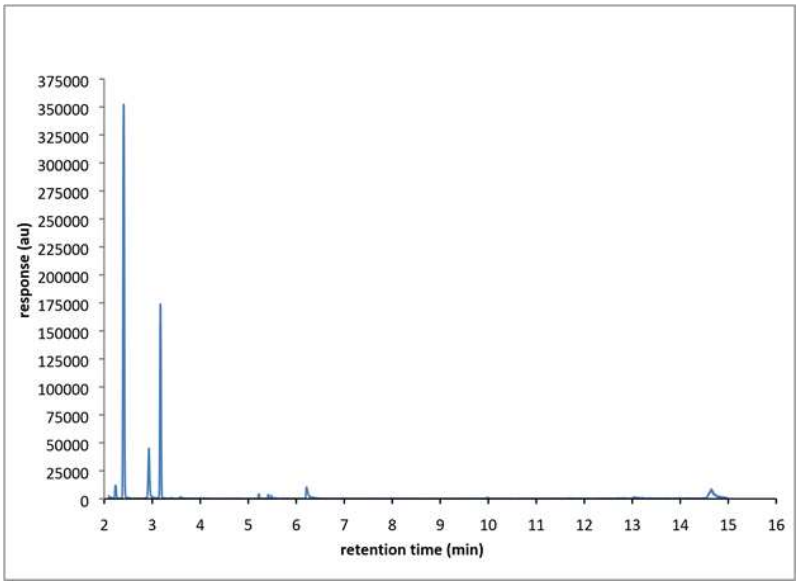

Figure A.7. GC/MS, Chapter 2, Table 2.1, Entry 3, run 1

Table A.7. GC/MS Data, Chapter 2, Table 2.1, Entry 3, run 1

Peak	R.T.	First	Max	Last	PK TY	Height	Area	Pct Max	Pct Total	Compound
1	2.24	19	34	39	BV 2	5487	91589	1.3	1.007	
2	2.409	60	70	90	PV	373839	7018473	100	77.193	styrene
3	2.931	172	181	213	PV 2	29204	705729	10.06	7.762	benzaldehyde
4	3.171	221	232	245	BV	75782	1276316	18.19	14.038	decane

Table A.8. GC/MS Data, Chapter 2, Table 2.1, Entry 3, run 2

Peak	R.T.	First	Max	Last	PK TY	Height	Area	Pct Max	Pct Total	Compound
1	2.235	23	33	50	BV 4	11548	227972	3.52	2.052	
2	2.405	58	69	84	BV 2	349558	6474269	100	58.288	styrene
3	2.931	171	181	200	VV 3	43529	942286	14.55	8.483	benzaldehyde
4	3.171	223	232	251	VV	170789	2775370	42.87	24.987	decane
5	5.221	652	668	678	VV 4	4001	73000	1.13	0.657	
6	5.419	703	710	719	PV 4	3424	57239	0.88	0.515	
7	6.218	868	880	906	BV 2	9801	290775	4.49	2.618	
8	14.645	2640	2672	2674	PV 6	6031	175186	2.71	1.577	
9	14.659	2674	2675	2688	VV 6	4571	91265	1.41	0.822	

Table A.9. GC/MS Data, Chapter 2, Table 2.1, Entry 3, run 3

Peak	R.T.	First	Max	Last	PK TY	Height	Area	Pct Max	Pct Total	Compound
1	2.24	25	34	39	PV 3	4828	66923	0.92	0.725	
2	2.405	53	69	86	BV	401090	7296356	100	79.061	styrene
3	2.932	166	181	201	PV 4	36485	795022	10.9	8.615	benzaldehyde
4	3.171	222	232	243	BV 2	66585	1070461	14.67	11.599	decane

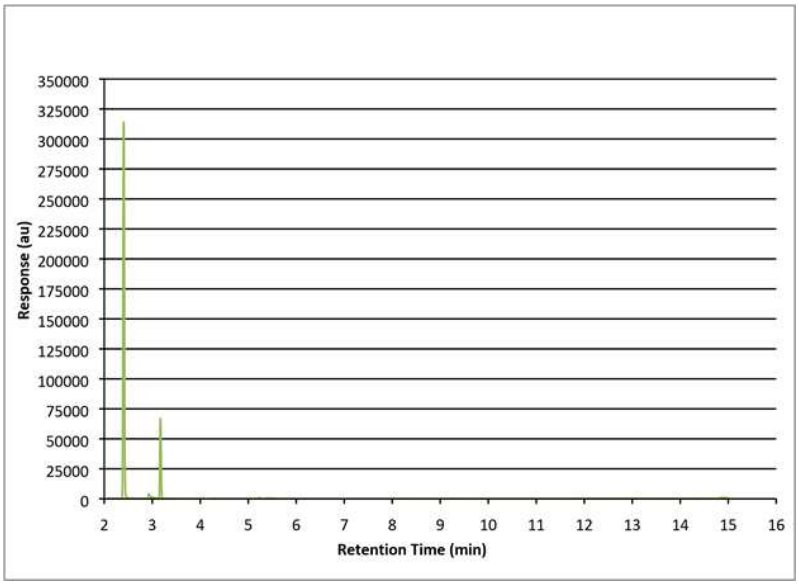

Figure A.8. GC/MS, Chapter 2, Table 2.1, Entry 4, run 1

Table A.10. GC/MS, Chapter 2, Table 2.1, Entry 4, run 1

Peak	R.T.	First	Max	Last	PK TY	Height	Area	Pct Max	Pct Total	Compound
1	2.405	60	69	84	rBB2	314003	591420	100	84.479	styrene
2	2.932	173	181	189	rBB5	3275	6627	1.12	0.947	benzaldehyde
3	3.171	222	232	243	rBB	62470	102035	17.25	14.575	decane

Table A.11. GC/MS, Chapter 2, Table 2.1, Entry 4, run 2

Peak	R.T.	First	Max	Last	PK TY	Height	Area	Pct Max	Pct Total	Compound
1	2.405	59	69	86	BV	291057	5E+06	100	84.022	styrene
2	2.936	165	182	190	BV 6	4701	83721	1.57	1.32	benzaldehyde
3	3.171	222	232	254	PB 2	58161	929903	17.45	14.658	decane

Table A.12. GC/MS, Chapter 2, Table 2.1, Entry 4, run 3

Peak	R.T.	First	Max	Last	PK TY	Height	Area	Pct Max	Pct Total	Compound
1	2.41	59	70	83	PV	312274	6E+06	100	83.277	styrene
2	2.932	171	181	192	PV 6	4317	101432	1.72	1.43	benzaldehyde
3	3.171	224	232	248	BV 2	66276	1E+06	18.36	15.293	decane

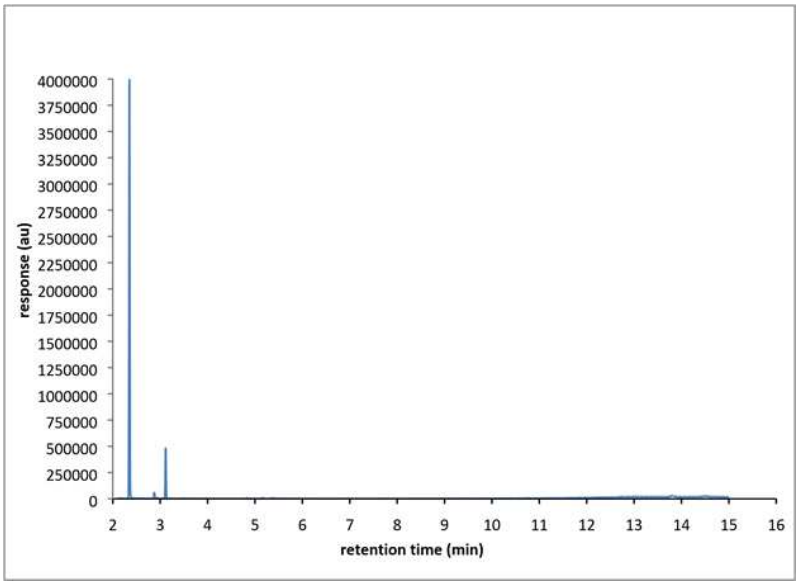

Figure A.9. GC/MS, Chapter 2, Table 2.1, Entry 5, run 1

Table A.13. GC/MS, Chapter 2, Table 2.1, Entry 5, run 1

Peak	R.T.	First	Max	Last		PK TY	Height	Area	Pct Max	Pct Total	compound
1	2.353	50	58		80	PV	2151470	23261966	100	67.484	styrene
2	2.88	161	170		186	VV 3	23216	491051	2.11	1.425	benzaldehyde
3	2.965	186	188		193	VV 5	2228	23772	0.1	0.069	
4	3.12	212	221		228	VV	330662	3845897	16.53	11.157	decane

Table A.14. GC/MS, Chapter 2, Table 2.1, Entry 5, run 2

Peak	R.T.	First	Max	Last		PK TY	Height	Area	Pct Max	Pct Total	Compound
1	2.189	19	23		25	PV 5	1728	18742	0.05	0.033	
2	2.353	50	58		70	PV	3881427	40454478	100	71.663	styrene
3	2.414	70	71		78	VV 5	5866	84905	0.21	0.15	
4	2.457	78	80		82	VV 3	3209	32349	0.08	0.057	
5	2.645	115	120		127	VV 7	2182	42199	0.1	0.075	
6	2.875	160	169		185	PV	54801	974348	2.41	1.726	benzaldehyde
7	2.96	185	187		193	VV 6	2642	39270	0.1	0.07	
8	3.035	197	203		208	VV 9	2462	43617	0.11	0.077	
9	3.115	212	220		231	VV	460383	5334305	13.19	9.449	decane

Table A.15. GC/MS, Chapter 2, Table 2.1, Entry 5, run 3

Peak	R.T.	First	Max	Last		PK TY	Height	Area	Pct Max	Pct Total	Compound
1	2.184	19	22		29	PV 9	1733	22142	0.06	0.043	
2	2.353	51	58		79	VV	3781486	40017897	100	77.955	styrene
3	2.461	79	81		99	VV	2818	92261	0.23	0.18	
4	2.649	114	121		125	PV 9	2294	40564	0.1	0.079	
5	2.88	162	170		192	VV 3	22861	503570	1.26	0.981	benzaldehyde
6	3.04	200	204		212	VV 9	2198	33461	0.08	0.065	
7	3.115	212	220		231	VV	470468	5504748	13.76	10.723	decane

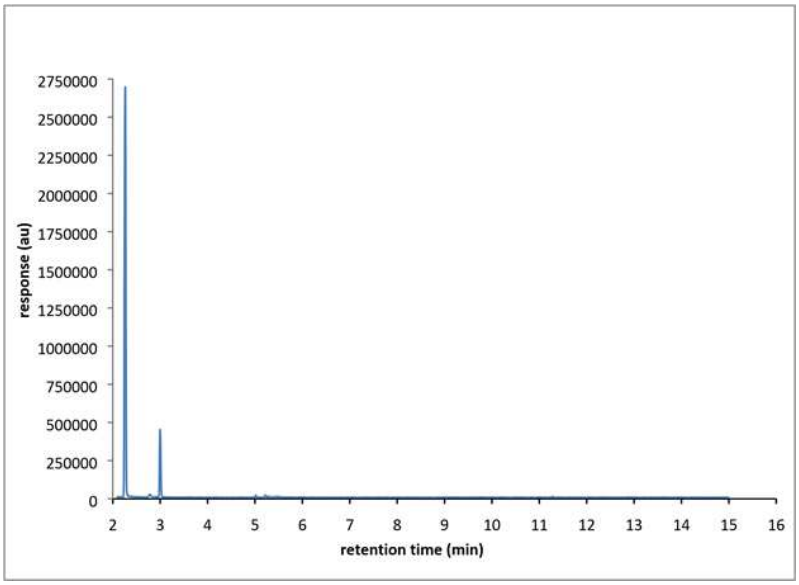

Figure A.10. GC/MS, Chapter 2, Table 2.1, Entry 6, run 1

Table A.16. GC/MS, Chapter 2, Table 2.1, Entry 6, run 1

Peak	R.T.	First	Max	Last	PK TY	Height	Area	Pct Max	Pct Total	Compound
1	2.264	25	39	57	PV	2670858	52982297	100	79.186	styrene
2	2.363	57	60	65	VV 7	5533	110064	0.21	0.164	
3	2.391	65	66	81	VV 7	4799	118737	0.22	0.177	
4	2.607	109	112	114	VV 4	2755	26871	0.05	0.04	
5	2.781	138	149	161	VV 6	19802	601889	1.14	0.9	benzaldehyde
6	2.847	161	163	169	VV 7	4748	93541	0.18	0.14	
7	2.913	174	177	180	VV 4	4272	51899	0.1	0.078	
8	2.936	180	182	185	VV 4	4154	48160	0.09	0.072	
9	2.997	185	195	208	VV	439299	7822583	14.76	11.691	decane

Table A.17. GC/MS, Chapter 2, Table 2.1, Entry 6, run 2

Peak	R.T.	First	Max	Last	PK TY	Height	Area	Pct Max	Pct Total	Compound
1	2.17	17	19	21	PV 3	1877	11205	0.02	0.017	
2	2.188	21	23	24	VV 2	2614	12623	0.02	0.019	
3	2.264	24	39	65	PV	2655142	52501757	100	78.092	styrene
4	2.395	65	67	73	VV 6	4449	77651	0.15	0.115	
5	2.433	73	75	83	VV 8	3597	70059	0.13	0.104	
6	2.551	98	100	108	VV 8	2794	45003	0.09	0.067	
7	2.631	115	117	119	VV 3	2992	22411	0.04	0.033	
8	2.659	119	123	125	VV 5	2689	27851	0.05	0.041	
9	2.781	138	149	158	VV 5	18739	554504	1.06	0.825	benzaldehyde
10	2.828	158	159	169	VV 9	6607	144206	0.27	0.214	
11	2.88	169	170	175	VV 5	3931	60084	0.11	0.089	
12	2.913	175	177	179	VV 3	4279	42584	0.08	0.063	
13	2.997	183	195	210	VV	461229	8161281	15.54	12.139	decane

Table A.18. GC/MS, Chapter 2, Table 2.1, Entry 6, run 3

Peak	R.T.	First	Max	Last	PK TY	Height	Area	Pct Max	Pct Total	Compound
1	2.17	15	19	22	PV 6	1807	14967	0.03	0.021	
2	2.193	22	24	25	VV 2	1774	8144	0.01	0.011	
3	2.264	28	39	59	VV	2787766	55412852	100	76.119	styrene
4	2.367	59	61	72	VV	5186	138228	0.25	0.19	
5	2.593	107	109	111	VV 3	2675	19710	0.04	0.027	
6	2.682	126	128	130	VV 3	2276	8264	0.01	0.011	
7	2.781	135	149	159	VV 3	20901	589330	1.06	0.81	benzaldehyde
8	2.833	159	160	164	VV 4	5845	75563	0.14	0.104	
9	2.861	164	166	169	VV 4	4072	48141	0.09	0.066	
10	3.002	185	196	206	VV	433891	7752282	13.99	10.649	decane

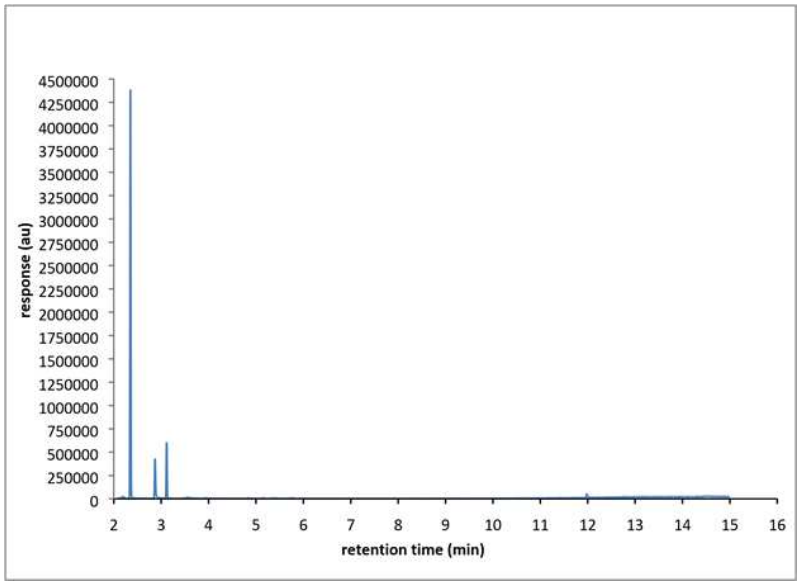

Figure A.11. GC/MS, Chapter 2, Table 2.1, Entry 7, run 1

Table A.19. GC/MS, Chapter 2, Table 2.1, Entry 7, run 1

Peak	R.T.	First	Max	Last	PK TY	Height	Area	Pct Max	Pct Total	Compound
1	2.184	16	22	26	PV	12098	141731	0.49	0.267	
2	2.221	26	30	36	VV	9227	102220	0.35	0.192	
3	2.353	43	58	82	PV	2732831	29193255	100	54.939	styrene
4	2.649	112	121	126	VV 9	2233	38737	0.13	0.073	
5	2.87	159	168	199	PV	338161	5218907	17.88	9.821	benzaldehyde
6	3.026	199	201	210	VV 9	3809	106258	0.36	0.2	
7	3.115	213	220	235	VV	535091	6318739	21.64	11.891	decane

Table A.20. GC/MS, Chapter 2, Table 2.1, Entry 7, run 2

Peak	R.T.	First	Max	Last	PK TY	Height	Area	Pct Max	Pct Total	Compound
1	2.184	17	22	26	PV 2	16205	165540	0.38	0.247	
2	2.222	26	30	34	VV 2	10638	110297	0.25	0.164	
3	2.353	51	58	70	PV	4211840	44115783	100	65.765	styrene
4	2.414	70	71	78	VV 6	4479	66975	0.15	0.1	
5	2.64	112	119	133	VV 6	2133	50643	0.11	0.075	
6	2.87	156	168	192	PV	408939	6053340	13.72	9.024	benzaldehyde
7	2.988	192	193	199	VV 6	5005	92693	0.21	0.138	
8	3.04	199	204	211	VV 10	4557	109469	0.25	0.163	
9	3.115	211	220	233	VV	572830	6712821	15.22	10.007	decane

Table A.21. GC/MS, Chapter 2, Table 2.1, Entry 7, run 3

Peak	R.T.	First	Max	Last	PK TY	Height	Area	Pct Max	Pct Total	Compound
1	2.184	16	22	26	PV	11676	119282	0.39	0.25	
2	2.226	26	31	47	VV	7324	88840	0.29	0.186	
3	2.353	47	58	73	PV	2937245	30728404	100	64.354	styrene
4	2.428	73	74	79	VV 5	3240	38384	0.12	0.08	
5	2.645	115	120	124	VV 6	2140	27794	0.09	0.058	
6	2.875	161	169	196	PV	140390	2392179	7.78	5.01	benzaldehyde
7	3.035	196	203	209	VV 9	2853	83777	0.27	0.175	
8	3.119	209	221	232	VV	453065	5289672	17.21	11.078	decane

Table A.22. GC/MS, Chapter 2, Table 2.1, Entry 8, run 1

Peak	R.T.	First	Max	Last	PK TY	Height	Area	Pct Max	Pct Total	Compound
1	2.104	3	5	20	BV 3	7888	134971	0.26	0.163	
2	2.264	20	39	51	PV	2569855	51185507	100	61.857	styrene
3	2.33	51	53	61	VV 9	7197	118741	0.23	0.143	
4	2.377	61	63	73	VV 10	3536	98037	0.19	0.118	
5	2.546	93	99	110	PV	32404	446130	0.87	0.539	
6	2.616	110	114	122	VV	2948	60816	0.12	0.073	
7	2.772	137	147	164	VV	249871	5320609	10.39	6.43	benzaldehyde
8	2.861	164	166	175	VV 9	7225	165199	0.32	0.2	
9	2.913	175	177	179	VV 3	4229	42167	0.08	0.051	
10	3.002	188	196	210	VV	461859	8529192	16.66	10.307	decane

Table A.23. GC/MS, Chapter 2, Table 2.1, Entry 8, run 2

Peak	R.T.	First	Max	Last	PK TY	Height	Area	Pct Max	Pct Total	Compound
1	2.137	3	12	22	BV 3	6592	55708	0.1	0.07	
2	2.193	22	24	25	PV 2	1753	9480	0.02	0.012	
3	2.264	25	39	56	VV	2693422	53524015	100	66.931	styrene
4	2.353	56	58	63	VV 6	5123	87011	0.16	0.109	
5	2.391	63	66	79	VV 6	3561	116800	0.22	0.146	
6	2.461	79	81	86	VV 6	2651	36096	0.07	0.045	
7	2.518	89	93	94	VV 3	2846	21222	0.04	0.027	
8	2.546	94	99	109	VV	27651	401205	0.75	0.502	
9	2.602	109	111	125	VV	3167	97775	0.18	0.122	
10	2.771	136	147	176	VV	213366	4798402	8.96	6	benzaldehyde
11	2.922	176	179	182	VV 5	5594	79857	0.15	0.1	
12	2.945	182	184	188	VV 4	4565	58594	0.11	0.073	
13	3.002	188	196	210	VV	469906	8607105	16.08	10.763	decane

Table A.24. GC/MS, Chapter 2, Table 2.1, Entry 8, run 3

Peak	R.T.	First	Max	Last	PK TY	Height	Area	Pct Max	Pct Total	Compound
1	2.104	3	5	9	BV	10928	82315	0.15	0.104	
2	2.137	9	12	19	PV 2	9560	124896	0.23	0.158	
3	2.264	26	39	61	PV	2688363	53225948	100	67.283	styrene
4	2.377	61	63	73	VV	4120	89673	0.17	0.113	
5	2.546	90	99	110	PV	33374	498555	0.94	0.63	
6	2.612	110	113	121	VV 10	3303	75734	0.14	0.096	
7	2.706	131	133	137	VV 4	1946	19121	0.04	0.024	
8	2.772	137	147	175	VV 2	292219	6221462	11.69	7.865	benzaldehyde
9	2.922	175	179	186	VV 10	4963	110111	0.21	0.139	
10	3.002	186	196	207	VV	446144	8183483	15.37	10.345	decane

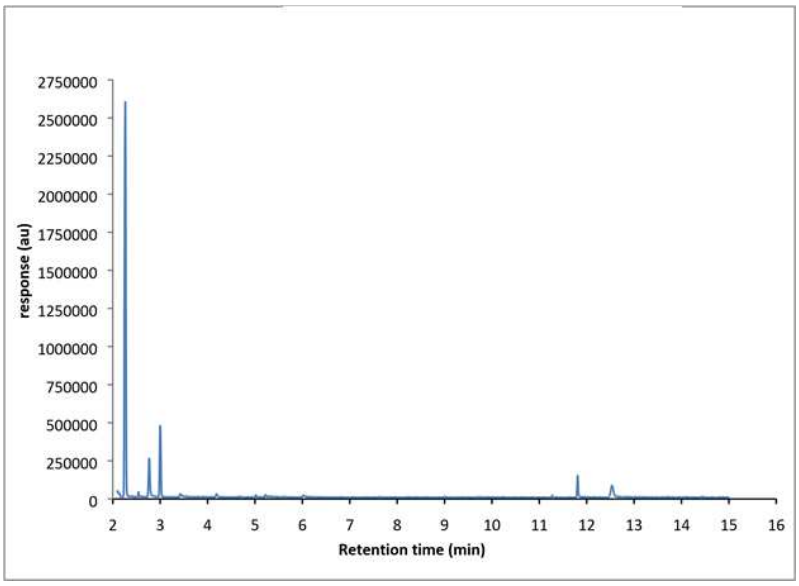

Figure A.12. GC/MS, Chapter 2, Table 2.1, Entry 8, run 1

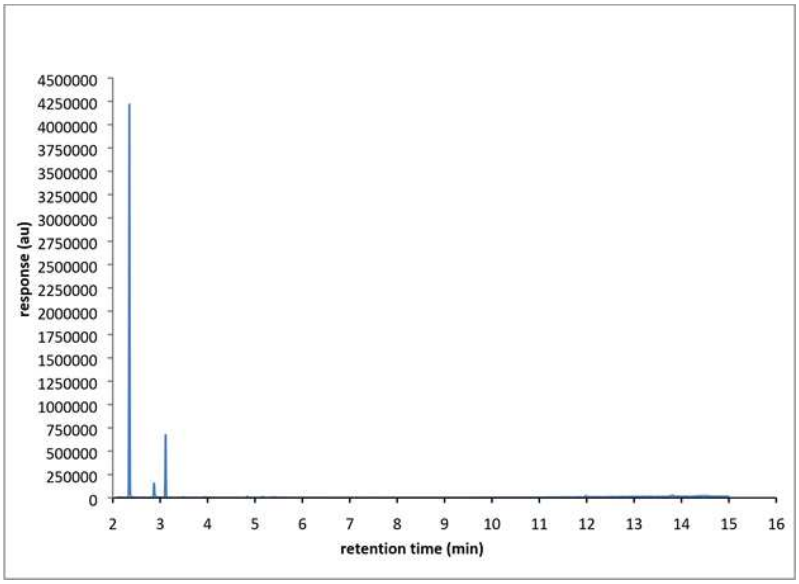

Figure A.13. GC/MS, Chapter 2, Table 2.1, Entry 9, run 1

Table A.25. GC/MS, Chapter 2, Table 2.1, Entry 9, run 1

Peak	R.T.	First	Max	Last	PK TY	Height	Area	Pct Max	Pct Total	Compound
1	2.353	46	58	82	PV	1727070	18620125	100	64.618	styrene
2	2.875	160	169	196	PV	129899	2238299	12.02	7.768	benzaldehyde
3	3.007	196	197	205	VV 5	2222	48522	0.26	0.168	
4	3.12	213	221	235	VV	290257	3440661	18.48	11.94	decane

Table A.26. GC/MS, Chapter 2, Table 2.1, Entry 9, run 2

Peak	R.T.	First	Max	Last	PK TY	Height	Area	Pct Max	Pct Total	Compound
1	2.353	50	58	76	PV	1771038	18885597	100	69.664	styrene
2	2.447	76	78	87	VV 6	2345	40746	0.22	0.15	
3	2.88	157	170	192	PV	31687	717527	3.8	2.647	benzaldehyde
4	2.988	192	193	195	VV 2	2160	17910	0.09	0.066	
5	3.12	210	221	239	VV	248684	2929061	15.51	10.805	decane

Table A.27. GC/MS, Chapter 2, Table 2.1, Entry 9, run 3

Peak	R.T.	First	Max	Last	PK TY	Height	Area	Pct Max	Pct Total	Compound
1	2.353	50	58	74	PV	4045479	42748920	100	70.05	styrene
2	2.438	74	76	85	VV 9	2927	55046	0.13	0.09	
3	2.64	115	119	120	PV 4	1531	10567	0.02	0.017	
4	2.649	120	121	125	VV 4	1792	12689	0.03	0.021	
5	2.87	156	168	195	PV	149547	2494163	5.83	4.087	benzaldehyde
6	3.035	195	203	211	VV	2720	72571	0.17	0.119	
7	3.115	211	220	236	VV	649833	7658284	17.91	12.549	decane

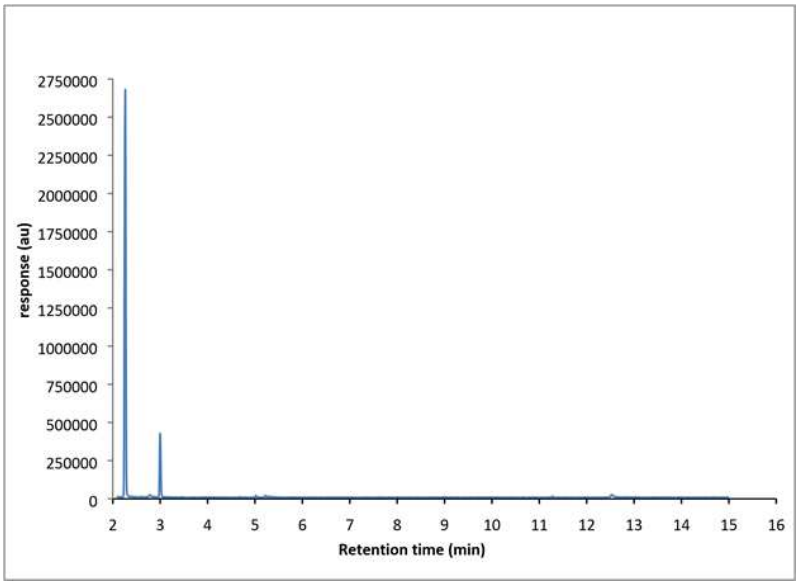

Figure A.14. GC/MS, Chapter 2, Table 2.1, Entry 10, run 1

Table A.28. GCMS, Chapter 2, Table 2.1, Entry 10, run 1

Peak	R.T.	First	Max	Last	PK TY	Height	Area	Pct Max	Pct Total	Compound
1	2.264	28	39	60	VV	2714719	53590404	100	80.253	styrene
2	2.372	60	62	79	VV	4231	135816	0.25	0.203	
3	2.546	92	99	104	VV	2661	46346	0.09	0.069	
4	2.776	137	148	159	PV 6	16768	523291	0.98	0.784	benzaldehyde
5	2.837	159	161	175	VV 6	5075	173400	0.32	0.26	
6	2.922	175	179	187	VV 6	3309	84506	0.16	0.127	
7	2.997	187	195	218	VV	401921	7115721	13.28	10.656	decane

Table A.29. GCMS, Chapter 2, Table 2.1, Entry 10, run 2

Peak	R.T.	First	Max	Last	PK TY	Height	Area	Pct Max	Pct Total	Compound
1	2.264	25	39	57	PV	2652919	52854683	100	77.461	styrene
2	2.372	57	62	66	VV 8	5913	121068	0.23	0.177	
3	2.395	66	67	69	VV 2	4515	32680	0.06	0.048	
4	2.414	69	71	76	VV 6	4146	59321	0.11	0.087	
5	2.461	79	81	94	VV 6	2926	82033	0.16	0.12	
6	2.621	108	115	117	VV 8	3022	57191	0.11	0.084	
7	2.706	130	133	138	VV 7	2577	34112	0.06	0.05	
8	2.781	138	149	163	VV 8	15844	562870	1.06	0.825	benzaldehyde
9	2.856	163	165	171	VV 7	4954	92350	0.17	0.135	
10	2.894	171	173	177	VV 5	3816	51243	0.1	0.075	
11	3.002	187	196	223	VV	412445	7543231	14.27	11.055	decane

Table A.30. GCMS, Chapter 2, Table 2.1, Entry 10, run 3

Peak	R.T.	First	Max	Last	PK TY	Height	Area	Pct Max	Pct Total	Compound
1	2.146	10	14	16	PV 5	2233	22292	0.04	0.033	
2	2.212	22	28	29	PV 6	2196	28949	0.05	0.043	
3	2.264	29	39	54	VV	2678815	53245455	100	79.672	styrene
4	2.344	54	56	60	VV 5	6076	91214	0.17	0.136	
5	2.372	60	62	70	VV 8	5772	126194	0.24	0.189	
6	2.532	92	96	101	VV 7	3554	63646	0.12	0.095	
7	2.588	106	108	110	VV 3	3195	26644	0.05	0.04	
8	2.616	110	114	119	VV 8	3550	66178	0.12	0.099	
9	2.72	134	136	138	VV 3	2558	18615	0.03	0.028	
10	2.781	138	149	164	VV 7	15855	575554	1.08	0.861	benzaldehyde
11	2.861	164	166	172	VV 6	4754	83157	0.16	0.124	
12	2.997	188	195	214	VV 2	363643	6536684	12.28	9.781	decane
13	3.204	236	239	246	VV 8	2797	48949	0.09	0.073	

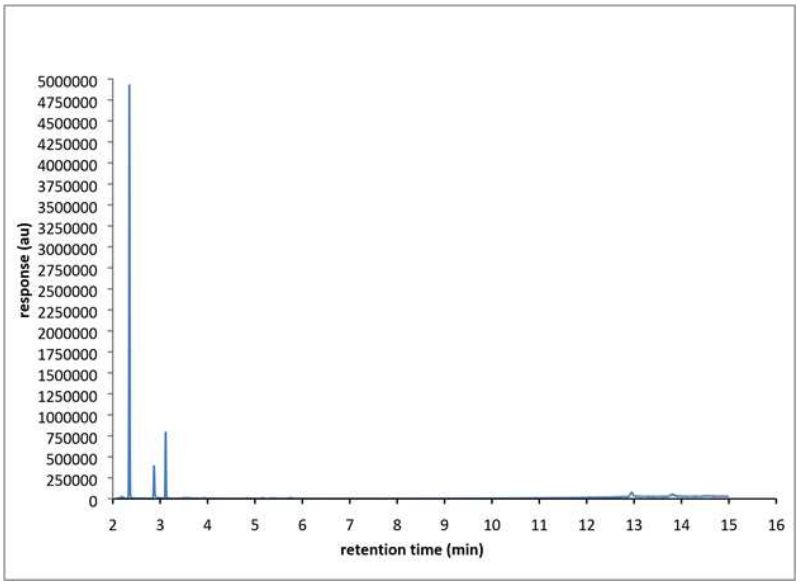

Figure A.15. GCMS, Chapter 2, Table 2.1, Entry 11, run 1

Table A.31. GCMS, Chapter 2, Table 2.1, Entry 11, run 1

Peak	R.T.	First	Max	Last	PK TY	Height	Area	Pct Max	Pct Total	Compound
1	2.184	16	22	27	PV	9186	99236	0.52	0.263	
2	2.222	27	30	40	VV 2	5672	62189	0.33	0.165	
3	2.353	51	58	89	PV	1797519	18904902	100	50.151	styrene
4	2.875	161	169	202	PV	161205	2836727	15.01	7.525	benzaldehyde
5	3.04	202	204	208	VV 5	2911	41262	0.22	0.109	
6	3.12	208	221	227	VV	315915	3659637	19.36	9.708	decane

Table A.32. GCMS, Chapter 2, Table 2.1, Entry 11, run 2

Peak	R.T.	First	Max	Last	PK TY	Height	Area	Pct Max	Pct Total	Compound
1	2.184	17	22	26	PV	18202	196186	0.39	0.239	
2	2.221	26	30	36	VV	12456	137866	0.27	0.168	
3	2.353	47	58	77	PV	4744829	50570569	100	61.493	styrene
4	2.452	77	79	81	VV 3	2656	21853	0.04	0.027	
5	2.649	116	121	126	VV 8	2848	39077	0.08	0.048	
6	2.87	161	168	199	VV	377208	5854774	11.58	7.119	benzaldehyde
7	3.04	199	204	213	VV 9	5296	135986	0.27	0.165	
8	3.115	213	220	244	VV	757620	9156079	18.11	11.134	decane

Table A.33. GCMS, Chapter 2, Table 2.1, Entry 11, run 3

Peak	R.T.	First	Max	Last	PK TY	Height	Area	Pct Max	Pct Total	Compound
1	2.183	16	22	26	PV	18767	199433	0.39	0.241	
2	2.221	26	30	41	VV	12003	143935	0.28	0.174	
3	2.353	49	58	87	VV	4827430	51465768	100	62.082	styrene
4	2.503	87	90	96	VV 7	2542	24460	0.05	0.03	
5	2.644	116	120	126	VV 8	3043	36927	0.07	0.045	
6	2.87	160	168	186	PV	337537	4968411	9.65	5.993	benzaldehyde
7	2.959	186	187	190	VV 3	6251	52841	0.1	0.064	
8	2.978	190	191	199	VV 6	5094	96971	0.19	0.117	
9	3.039	199	204	210	VV 6	3860	81717	0.16	0.099	
10	3.119	213	221	228	VV	680033	8083639	15.71	9.751	decane

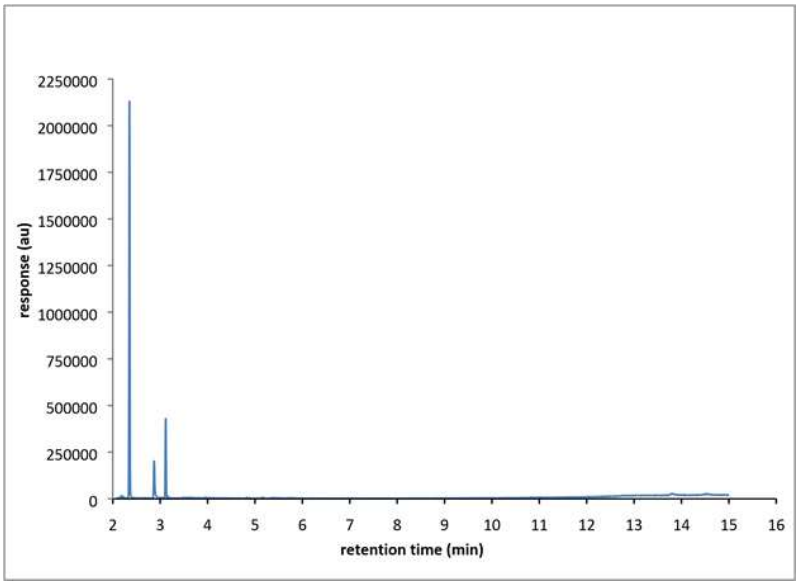

Figure A.16. GCMS, Chapter 2, Table 2.1, Entry 12, run 1

Table A.34. GCMS, Chapter 2, Table 2.1, Entry 12, run 1

Peak	R.T.	First	Max	Last	PK TY	Height	Area	Pct Max	Pct Total	Compound
1	2.184	14	22	26	PV	17347	188337	0.34	0.223	
2	2.221	26	30	38	VV	11611	135591	0.25	0.161	
3	2.353	49	58	85	PV	5178168	54780856	100	64.933	styrene
4	2.645	117	120	125	VV 6	3832	48107	0.09	0.057	
5	2.87	159	168	199	PV	489941	7211747	13.16	8.548	benzaldehyde
6	3.044	199	205	210	VV 10	3968	87491	0.16	0.104	
7	3.115	210	220	226	VV	845319	9847312	17.98	11.672	decane

Table A.35. GCMS, Chapter 2, Table 2.1, Entry 12, run 2

Peak	R.T.	First	Max	Last	PK TY	Height	Area	Pct Max	Pct Total	Compound
1	2.184	16	22	26	PV	8783	100520	0.63	0.328	
2	2.226	26	31	44	VV 2	5992	85802	0.54	0.28	
3	2.353	50	58	77	PV	1509562	15995103	100	52.205	styrene
4	2.645	118	120	123	VV 3	1673	13495	0.08	0.044	
5	2.875	159	169	189	VV	146171	2410120	15.07	7.866	benzaldehyde
6	2.978	189	191	194	VV 3	3544	43892	0.27	0.143	
7	3.002	194	196	199	VV 3	2865	29941	0.19	0.098	
8	3.119	212	221	227	VV	313916	3639699	22.76	11.879	decane

Table A.36. GCMS, Chapter 2, Table 2.1, Entry 12, run 3

Peak	R.T.	First	Max	Last	PK TY	Height	Area	Pct Max	Pct Total	Compound
1	2.184	18	22	27	VV	10894	116403	0.54	0.313	
2	2.221	27	30	36	VV 3	8047	85232	0.4	0.229	
3	2.353	50	58	75	VV	2036109	21421360	100	57.524	styrene
4	2.654	115	122	124	PV 7	1575	16518	0.08	0.044	
5	2.875	155	169	198	VV	194646	3231200	15.08	8.677	benzaldehyde
6	3.016	198	199	201	VV 2	2771	24037	0.11	0.065	
7	3.03	201	202	211	VV 7	2846	58314	0.27	0.157	
8	3.119	211	221	227	VV	408747	4757267	22.21	12.775	decane

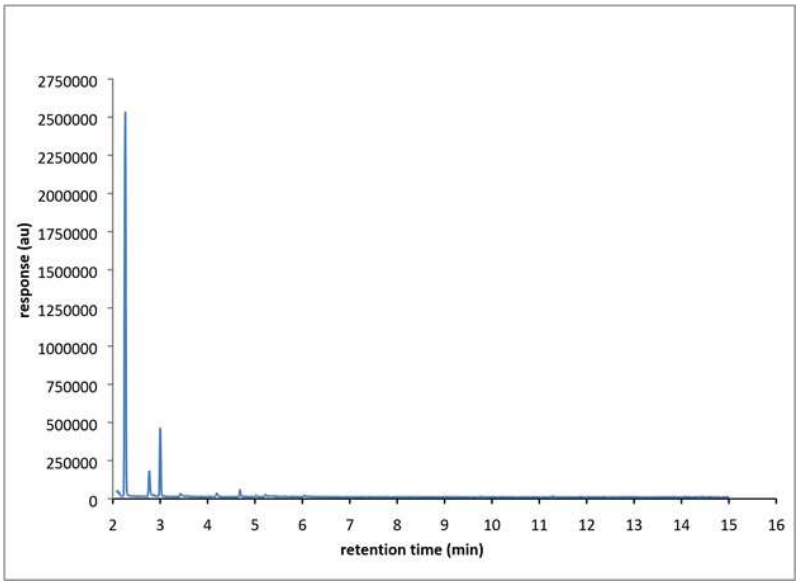

Figure A.17. GCMS, Chapter 2, Table 2.1, Entry 13, run 1

Table A.37. GCMS, Chapter 2, Table 2.1, Entry 13, run 1

Peak	R.T.	First	Max	Last	PK TY	Height	Area	Pct Max	Pct Total	Compound
1	2.198	22	25	27	PV 4	1705	11808	0.02	0.016	
2	2.264	27	39	59	VV	2478853	49379806	100	66.835	styrene
3	2.362	59	60	72	VV	3179	90946	0.18	0.123	
4	2.616	110	114	116	VV 5	2904	21911	0.04	0.03	
5	2.771	137	147	164	VV	167952	3625267	7.34	4.907	benzaldehyde
6	2.87	164	168	175	VV 7	8195	182392	0.37	0.247	
7	2.931	175	181	185	VV 9	4471	102158	0.21	0.138	
8	3.002	185	196	209	VV	456455	8234494	16.68	11.145	decane
9	3.148	225	227	230	VV 3	2835	30876	0.06	0.042	
10	3.213	239	241	250	VV 10	2525	43896	0.09	0.059	

Table A.48. GCMS, Chapter 2, Table 2.1, Entry 13, run 2

Peak	R.T.	First	Max	Last	PK TY	Height	Area	Pct Max	Pct Total	Compound
1	2.264	19	39	65	BV	2495530	50035601	100	67.54	styrene
2	2.395	65	67	74	VV 8	2917	46859	0.09	0.063	
3	2.461	78	81	83	VV 4	2526	24205	0.05	0.033	
4	2.513	88	92	95	PV 6	2406	25556	0.05	0.034	
5	2.555	95	101	107	VV 6	2383	47999	0.1	0.065	
6	2.612	107	113	116	PV 8	3091	44039	0.09	0.059	
7	2.649	116	121	128	VV 8	2360	51526	0.1	0.07	
8	2.696	128	131	138	VV 8	2366	31408	0.06	0.042	
9	2.772	138	147	162	VV	164961	3644274	7.28	4.919	benzaldehyde
10	2.875	162	169	175	VV 6	10325	278570	0.56	0.376	
11	2.931	175	181	186	VV 10	5058	121020	0.24	0.163	
12	3.002	186	196	206	VV	442045	8127017	16.24	10.97	decane

Table A.49. GCMS, Chapter 2, Table 2.1, Entry 13, run 3

Peak	R.T.	First	Max	Last	PK TY	Height	Area	Pct Max	Pct Total	Compound
1	2.264	28	39	55	PV	2493287	49118050	100	63.711	styrene
2	2.344	55	56	63	VV 6	4528	74639	0.15	0.097	
3	2.381	63	64	67	VV 3	3698	35054	0.07	0.045	
4	2.405	67	69	76	VV 8	3545	55737	0.11	0.072	
5	2.471	80	83	84	PV 3	2366	13328	0.03	0.017	
6	2.546	98	99	108	VV 9	2470	35856	0.07	0.047	
7	2.635	112	118	123	VV 10	2853	47621	0.1	0.062	
8	2.711	132	134	137	VV 4	1605	16559	0.03	0.021	
9	2.772	137	147	163	VV	262531	5463905	11.12	7.087	benzaldehyde
10	2.856	163	165	170	VV 6	8530	142878	0.29	0.185	
11	2.885	170	171	179	VV 8	6136	128505	0.26	0.167	
12	2.932	179	181	184	VV 4	4870	55217	0.11	0.072	
13	3.002	184	196	213	VV	456332	8373553	17.05	10.861	decane

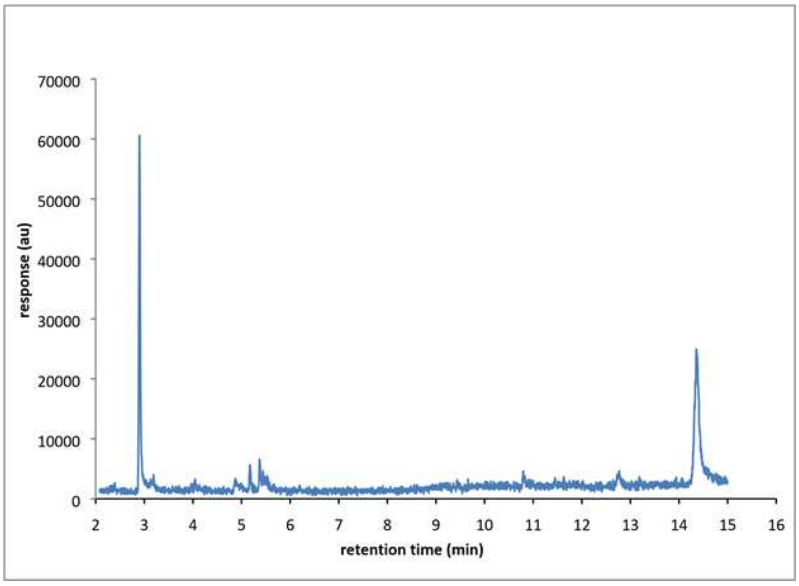

Figure A.18. GCMS, Chapter 2, Table 2.1, Entry 14, run 1

Table A.50. GCMS, Chapter 2, Table 2.1, Entry 14, run 1

Peak	R.T.	First	Max	Last	PK TY	Height	Area	Pct Max	Pct Total	Compound
1	2.386	60	65	68	VV 5	1939	31340	1.34	0.62	
2	2.899	162	174	189	PV	124466	2343644	100	46.58	benzaldehyde
3	2.974	189	190	198	VV 4	4439	84482	3.6	1.68	
4	3.124	212	222	232	VV 8	3736	135988	5.8	2.7	
5	3.961	392	400	409	VV 7	4141	92195	3.93	1.83	
6	4.027	409	414	416	VV 3	3379	45545	1.94	0.91	
7	4.041	416	417	430	VV 2	3646	63440	2.71	1.26	
8	4.878	577	595	598	VV 7	2129	64901	2.77	1.29	
9	5.174	652	658	665	VV 5	6829	128606	5.49	2.56	
10	5.372	688	700	708	PV 4	6063	122841	5.24	2.44	
11	5.442	708	715	724	VV 2	3218	67767	2.89	1.35	
12	5.494	724	726	729	VV 3	958	5886	0.25	0.12	
13	9.439	1559	1565	1575	VV 5	2049	43362	1.85	0.86	
14	10.803	1848	1855	1857	PV 4	1000	13900	0.59	0.28	
15	12.745	2250	2268	2272	PV 6	2477	50483	2.15	1	
16	12.778	2272	2275	2280	VV 3	2101	31824	1.36	0.63	
17	12.961	2309	2314	2324	VV 9	1891	42563	1.82	0.85	
18	14.363	2588	2612	2632	VV 5	23458	1477875	63.06	29.37	
19	14.466	2632	2634	2640	VV 5	4886	79651	3.4	1.58	
20	14.499	2640	2641	2649	VV 7	3107	68667	2.93	1.37	
21	14.645	2667	2672	2674	VV 4	2275	30389	1.3	0.6	
22	14.823	2708	2710	2712	PV 3	1226	5899	0.25	0.12	

Table A.51. GCMS, Chapter 2, Table 2.1, Entry 14, run 2

Peak	R.T.	First	Max	Last	PK TY	Height	Area	Pct Max	Pct Total	Compound
1	2.903	165	175	197	PV 2	57950	1246573	100	39.56	benzaldehyde
2	3.011	197	198	201	VV 2	1772	17071	1.37	0.54	
3	3.19	232	236	245	VV 7	2142	37380	3	1.19	
4	4.046	411	418	423	VV 6	2015	35831	2.87	1.14	
5	4.874	583	594	596	PV 6	870	18631	1.49	0.59	
6	5.174	650	658	667	PV 6	4226	90288	7.24	2.87	
7	5.372	692	700	709	PV 7	4926	106551	8.55	3.38	
8	5.442	709	715	720	VV 5	2724	47865	3.84	1.52	
9	5.49	720	725	730	VV 4	1582	26935	2.16	0.86	
10	5.527	730	733	736	VV 3	1421	15151	1.22	0.48	
11	9.439	1558	1565	1569	PV 7	1477	22906	1.84	0.73	
12	10.798	1848	1854	1867	VV 2	2852	77386	6.21	2.46	
13	12.736	2245	2266	2268	VV 6	2462	67566	5.42	2.14	
14	12.769	2268	2273	2288	VV 9	2963	101526	8.14	3.22	
15	13.182	2352	2361	2363	PV 4	1316	13666	1.1	0.43	
16	14.358	2588	2611	2613	PV 4	20768	654827	52.53	20.78	
17	14.377	2613	2615	2637	VV 3	19415	570682	45.78	18.11	

Table A.52. GCMS, Chapter 2, Table 2.1, Entry 14, run 3

Peak	R.T.	First	Max	Last	PK TY	Height	Area	Pct Max	Pct Total	Compound
1	2.372	55	62	64	VV 3	1692	20305	0.92	0.69	
2	2.903	161	175	194	PV	116552	2204828	100.00	74.38	benzaldehyde
3	3.007	194	197	212	VV 9	2785	97927	4.44	3.30	
4	3.124	212	222	229	VV 9	3053	98835	4.48	3.33	
5	3.957	393	399	409	PV 6	3776	82794	3.76	2.79	
6	4.027	409	414	420	PV 4	2286	33615	1.52	1.13	
7	5.17	647	657	665	PV 7	4953	86121	3.91	2.91	
8	5.381	694	702	709	PV 6	4906	95848	4.35	3.23	
9	5.438	709	714	723	VV 6	3428	67801	3.08	2.29	
10	5.49	723	725	731	VV 4	1933	22616	1.03	0.76	
11	12.74	2262	2267	2276	PV 4	1653	37005	1.68	1.25	
12	12.957	2303	2313	2315	VV 6	2212	47537	2.16	1.60	
13	13.789	2475	2490	2493	PV 6	2177	38397	1.74	1.30	
14	13.817	2493	2496	2503	VV 7	1896	30546	1.39	1.03	

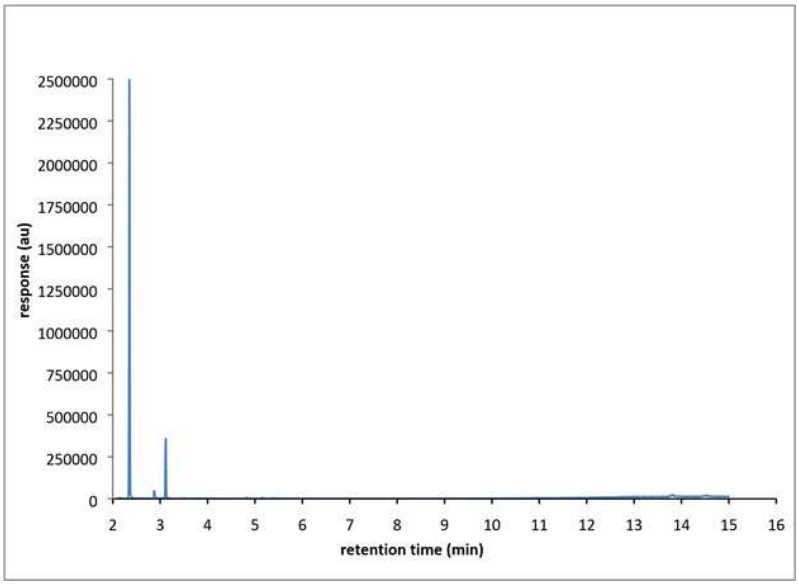

Figure A.19. GCMS, Chapter 2, Table 2.1, Entry 15, run 1

Table A.53. GCMS, Chapter 2, Table 2.1, Entry 15, run 1

Peak	R.T.	First	Max	Last	PK TY	Height	Area	Pct Max	Pct Total	Compound
1	2.353	48	58	75	PV	2446968	25948127	100.00	69.52	styrene
2	2.442	75	77	81	VV 4	2523	29007	0.11	0.08	
3	2.875	158	169	186	VV	43626	822038	3.17	2.20	benzaldehyde
4	3.119	212	221	227	VV	340606	3982716	15.35	10.67	decane

Table A.54. GCMS, Chapter 2, Table 2.1, Entry 15, run 2

Peak	R.T.	First	Max	Last	PK TY	Height	Area	Pct Max	Pct Total	Compound
1	2.353	50	58	84	PV	1836244	19748842	100.00	72.11	styrene
2	2.649	116	121	123	PV 5	1662	19603	0.10	0.07	
3	2.88	161	170	186	VV 2	33395	668205	3.38	2.44	benzaldehyde
4	2.965	186	188	199	VV 8	2369	55540	0.28	0.20	
5	3.12	212	221	227	VV	293832	3378330	17.11	12.34	decane

Table A.55. GCMS, Chapter 2, Table 2.1, Entry 15, run 3

Peak	R.T.	First	Max	Last	PK TY	Height	Area	Pct Max	Pct Total	Compound
1	2.353	51	58	77	PV	1129925	11944512	100.00	58.61	styrene
2	2.875	156	169	189	PV	80200	1397722	11.70	6.86	benzaldehyde
3	2.979	189	191	195	VV 4	2883	36934	0.31	0.18	
4	3.12	214	221	232	VV	222380	2566018	21.48	12.59	decane

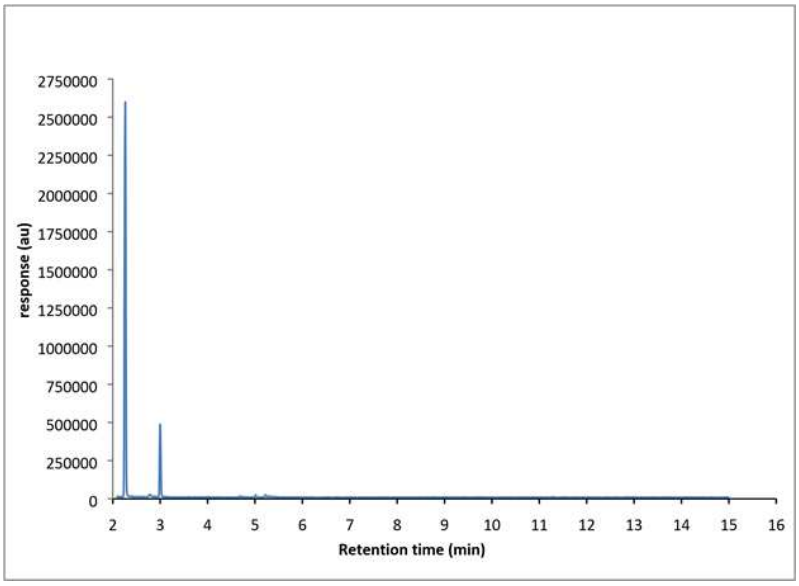

Figure A.20. GCMS, Chapter 2, Table 2.1, Entry 16, run 1

Table A.56. GCMS, Chapter 2, Table 2.1, Entry 16, run 1

Peak	R.T.	First	Max	Last	PK TY	Height	Area	Pct Max	Pct Total	Compound
1	2.264	27	39	61	PV	2617122	52142150	100.00	78.37	styrene
2	2.377	61	63	78	VV	4153	125921	0.24	0.19	
3	2.541	96	98	106	PV 9	2837	35983	0.07	0.05	
4	2.607	106	112	116	VV 9	2975	37685	0.07	0.06	
5	2.781	137	149	162	VV 5	17144	535108	1.03	0.80	benzaldehyde
6	2.847	162	163	165	VV 2	4744	25147	0.05	0.04	
7	2.861	165	166	175	VV 9	4508	92679	0.18	0.14	
8	3.002	186	196	206	VV	440684	7920399	15.19	11.91	decane

Table A.57. GCMS, Chapter 2, Table 2.1, Entry 16, run 2

Peak	R.T.	First	Max	Last	PK TY	Height	Area	Pct Max	Pct Total	Compound
1	2.165	13	18	23	PV 9	2416	30590	0.06	0.05	
2	2.264	23	39	59	PV	2390454	47955226	100.00	76.97	styrene
3	2.367	59	61	74	VV	4656	164048	0.34	0.26	
4	2.438	74	76	83	VV 8	3535	62136	0.13	0.10	
5	2.48	83	85	88	VV 4	3481	34760	0.07	0.056	
6	2.701	130	132	135	VV 4	2420	21073	0.04	0.03	
7	2.781	135	149	162	VV 3	15659	510063	1.06	0.82	benzaldehyde
8	2.847	162	163	166	VV 3	5005	48708	0.10	0.08	
9	2.866	166	167	174	VV 7	4143	87181	0.18	0.14	
10	2.913	174	177	179	VV 4	4062	46716	0.10	0.08	
11	3.002	186	196	205	VV	405837	7340111	15.31	11.78	decane

Table A.58. GCMS, Chapter 2, Table 2.1, Entry 16, run 3

Peak	R.T.	First	Max	Last	PK TY	Height	Area	Pct Max	Pct Total	Compound
1	2.188	21	23	26	PV 4	1746	12352	0.02	0.02	
2	2.212	26	28	29	VV 2	2131	10223	0.02	0.02	
3	2.264	29	39	56	VV	2567751	51101512	100.00	75.58	styrene
4	2.348	56	57	58	VV	4927	35512	0.07	0.05	
5	2.362	58	60	62	VV 3	4597	37656	0.07	0.056	
6	2.395	66	67	71	VV 4	4778	42351	0.08	0.06	
7	2.428	71	74	79	VV 6	3717	48064	0.09	0.07	
8	2.518	90	93	94	VV 3	2805	18328	0.04	0.03	
9	2.546	94	99	101	VV 6	2800	40056	0.08	0.06	
10	2.565	101	103	108	VV 6	2776	32486	0.06	0.05	
11	2.607	108	112	119	PV 10	2387	51160	0.10	0.08	
12	2.645	119	120	124	VV 4	2142	23691	0.05	0.04	
13	2.781	137	149	164	VV 6	18026	608936	1.19	0.90	benzaldehyde
14	2.866	164	167	176	VV 6	4912	123932	0.24	0.18	
15	2.931	176	181	185	VV 8	4635	86582	0.17	0.128	
16	3.002	185	196	207	VV	470117	8438877	16.51	12.481	decane

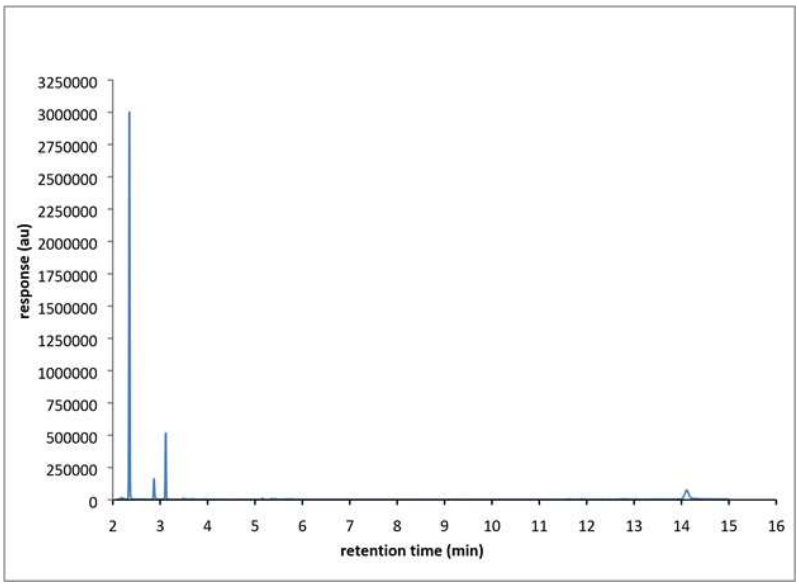

Figure A.21. GCMS, Chapter 2, Table 2.2, Entry 1, run 1

Table A.59. GCMS, Chapter 2, Table 2.2, Entry 1, run 1

Peak	R.T.	First	Max	Last	PK TY	Height	Area	Pct Max	Pct Total	Compound
1	2.184	14	22	27	PV 3	11448	151845	0.45	0.32	
2	2.222	27	30	35	VV 2	8203	91184	0.27	0.19	
3	2.353	47	58	81	PV	2898902	33515377	100.00	69.62	styrene
4	2.87	160	168	187	VV	155683	2442984	7.29	5.07	benzaldehyde
5	3.12	208	221	229	VV	495641	6102413	18.21	12.676	decane

Table A.60. GCMS, Chapter 2, Table 2.2, Entry 1, run 2

Peak	R.T.	First	Max	Last	PK TY	Height	Area	Pct Max	Pct Total	Compound
1	2.184	16	22	26	PV	18402	209909	0.43	0.30	
2	2.221	26	30	36	VV	11244	129063	0.27	0.18	
3	2.353	48	58	74	VV	4553683	48643215	100.00	69.45	styrene
4	2.87	160	168	188	PV	365564	4979181	10.24	7.11	benzaldehyde
5	2.969	188	189	196	VV 6	2724	38082	0.08	0.054	
6	3.115	211	220	230	BV	758591	8954335	18.41	12.79	decane

Table A.61. GCMS, Chapter 2, Table 2.2, Entry 1, run 3

Peak	R.T.	First	Max	Last	PK TY	Height	Area	Pct Max	Pct Total	Compound
1	2.184	13	22	26	PV 2	12312	169018	0.50	0.33	
2	2.222	26	30	36	VV 4	7896	99256	0.29	0.20	
3	2.353	45	58	75	PV	2949011	34033673	100.00	67.26	styrene
4	2.87	161	168	191	PV	210651	3436180	10.10	6.79	benzaldehyde
5	2.983	191	192	200	VV 6	4417	81309	0.24	0.161	
6	3.12	210	221	231	VV	478075	5659218	16.63	11.19	decane

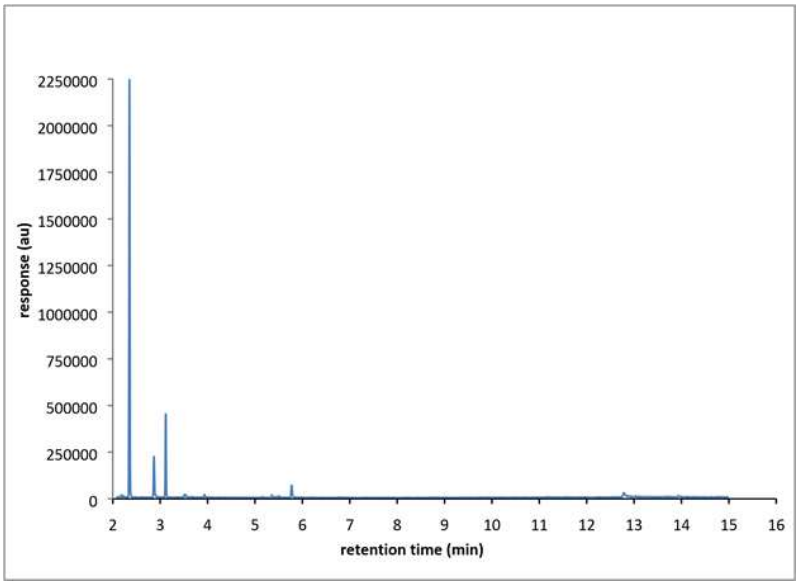

Figure A.22. GCMS, Chapter 2, Table 2.2, Entry 2, run 1

Table A.62. GCMS, Chapter 2, Table 2.2, Entry 2, run 1

Peak	R.T.	First	Max	Last	PK TY	Height	Area	Pct Max	Pct Total	Compound
1	2.353	49	58	68	BB	2178343	24113563	100.00	75.24	styrene
2	2.87	160	168	180	BB	212679	2988801	12.39	9.33	benzaldehyde
3	3.12	213	221	231	BB	427130	4948288	20.52	15.44	decane

Table A.63. GCMS, Chapter 2, Table 2.2, Entry 2, run 2

Peak	R.T.	First	Max	Last	PK TY	Height	Area	Pct Max	Pct Total	Compound
1	2.353	50	58	71	BB	3927503	43594597	100.00	77.12	styrene
2	2.87	160	168	183	BB	372788	5090263	11.68	9.00	benzaldehyde
3	3.115	213	220	229	BB	670936	7846106	18.00	13.88	decane

Table A.64. GCMS, Chapter 2, Table 2.2, Entry 2, run 3

Peak	R.T.	First	Max	Last	PK TY	Height	Area	Pct Max	Pct Total	Compound
1	2.353	50	58	71	BB	3570418	39247387	100.00	82.43	styrene
2	2.87	160	168	179	BB	167994	2311431	5.89	4.86	benzaldehyde
3	3.12	214	221	231	BB	515740	6051993	15.42	12.71	decane

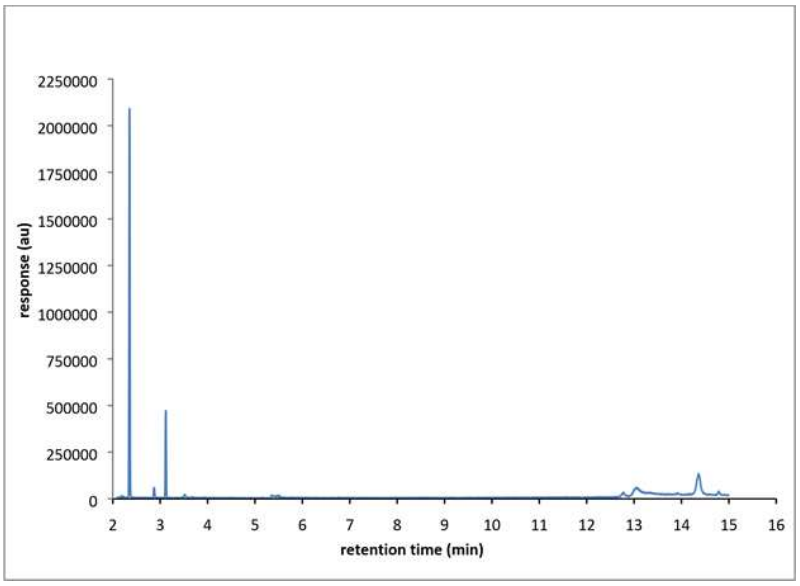

Figure A.23. GCMS, Chapter 2, Table 2.2, Entry 3, run 2

Table A.65. GCMS, Chapter 2, Table 2.2, Entry 3, run 1

Peak	R.T.	First	Max	Last	PK TY	Height	Area	Pct Max	Pct Total	Compound
1	2.353	43	58	83	BV	2011808	21908284	100.00	56.60	styrene
2	2.87	162	168	185	PB	53489	839361	3.83	2.17	benzaldehyde
3	3.12	211	221	235	PV	446832	5115981	23.35	13.22	decane
4	3.524	302	307	321	VV 4	16182	344840	1.57	0.89	
5	5.363	681	698	703	PV 6	8148	78256	0.36	0.202	
6	12.778	2259	2275	2296	PV 5	22115	894590	4.08	2.31	
7	13.051	2303	2333	2336	PV 7	36667	1680706	7.67	4.34	
8	13.07	2336	2337	2364	VV 6	34033	1248943	5.70	3.23	
9	14.363	2584	2612	2638	PV 2	107467	6027939	27.51	15.57	
10	14.786	2689	2702	2715	PV 2	19875	566813	2.59	1.46	

Table A.66. GCMS, Chapter 2, Table 2.2, Entry 3, run 2

Peak	R.T.	First	Max	Last	PK TY	Height	Area	Pct Max	Pct Total	Compound
1	2.184	18	22	26	BV	14068	157917	0.41	0.25	
2	2.353	50	58	72	PV	3371951	38701411	100.00	59.94	styrene
3	2.87	160	168	188	PV	127232	1918437	4.96	2.97	benzaldehyde
4	3.119	213	221	236	PV	587321	7088420	18.32	10.98	decane
5	3.524	302	307	330	VV 2	21113	457570	1.18	0.709	
6	5.381	689	702	717	PV 4	64881	2622082	6.78	4.06	
7	5.461	717	719	725	VV 3	29789	542923	1.40	0.84	
8	5.508	725	729	742	VV 2	22818	500298	1.29	0.78	
9	10.441	1773	1778	1785	VV 2	6359	129581	0.33	0.20	
10	12.778	2248	2275	2297	PV 4	28466	1070832	2.77	1.66	
11	13.027	2297	2328	2330	PV 5	64805	2513093	6.49	3.89	
12	13.055	2330	2334	2345	VV 9	61896	2208079	5.71	3.42	
13	13.112	2345	2346	2375	VV 9	31485	1046425	2.70	1.62	
14	14.353	2587	2610	2635	PV 3	83699	4932398	12.74	7.64	
15	14.786	2691	2702	2715	PV 2	26772	681243	1.76	1.055	

Table A.67. GCMS, Chapter 2, Table 2.2, Entry 3, run 3

Peak	R.T.	First	Max	Last	PK TY	Height	Area	Pct Max	Pct Total	Compound
1	2.353	48	58	81	BV	2201348	25209847	100.00	51.29	styrene
2	2.87	145	168	187	PV	75133	1179982	4.68	2.40	benzaldehyde
3	3.12	208	221	234	PV	394866	4804855	19.06	9.78	decane
4	5.381	682	702	716	PV 2	66390	2344743	9.30	4.77	
5	5.461	716	719	725	VV 3	22806	494449	1.96	1.006	
6	5.508	725	729	738	VV 4	16940	343272	1.36	0.70	
7	10.314	1720	1751	1784	BV 8	67534	6651613	26.38	13.53	
8	10.474	1784	1785	1789	VV 4	20706	236506	0.94	0.48	
9	10.498	1789	1790	1801	VV 4	11784	217962	0.86	0.44	
10	12.773	2246	2274	2286	PV 4	22087	992143	3.94	2.02	
11	13.041	2298	2331	2353	VV 7	40141	3538146	14.03	7.20	
12	13.154	2353	2355	2379	VV 7	13084	459976	1.82	0.94	
13	14.363	2582	2612	2646	PV 4	32304	2038652	8.09	4.15	
14	14.786	2692	2702	2713	PV 2	24280	636138	2.52	1.29	

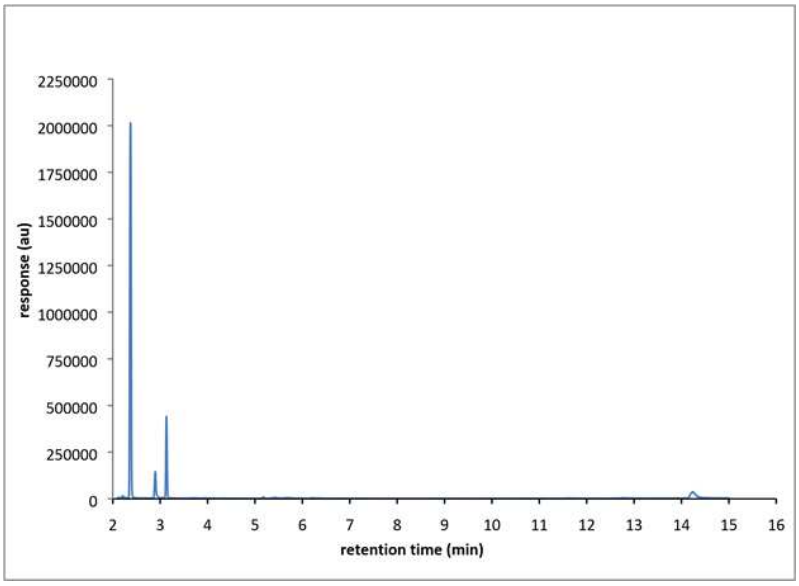

Figure A.24. GCMS, Chapter 2, Table 2.2, Entry 4

Table A.68. GCMS, Chapter 2, Table 2.2, Entry 4

Peak	R.T.	First	Max	Last	PK TY	Height	Area	Pct Max	Pct Total	Compound
1	2.377	45	63	94	BV	1996117	38263476	100.00	75.05	styrene
2	2.899	159	174	201	VV	140864	3196631	8.35	6.27	benzaldehyde
3	3.134	214	224	247	VV	430846	7322505	19.14	14.36	decane
4	14.24	2556	2586	2614	BV 4	31483	2202867	5.76	4.32	

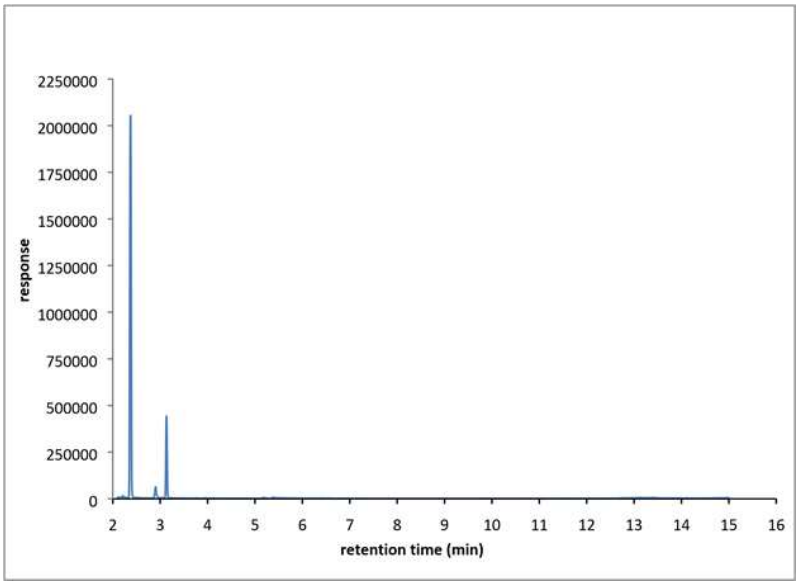

Figure A.25. GCMS, Chapter 2, Table 2.2, Entry 5

Table A.69. GCMS, Chapter 2, Table 2.2, Entry 5

Peak	R.T.	First	Max	Last	PK TY	Height	Area	Pct Max	Pct Total	Compound
1	2.207	16	27	31	PV 3	9615	196594	0.01	0.00	
2	2.245	31	35	43	VV 4	5893	107874	0.00	0.00	
3	2.377	53	63	85	VV	2030502	38804771	1.00	0.80	styrene
4	2.903	160	175	204	PV	58776	1431985	0.04	0.03	benzaldehyde
5	3.059	204	208	211	VV 4	1498	16862	0.00	0.000	
6	3.134	216	224	234	VV	433121	7230247	0.19	0.15	decane

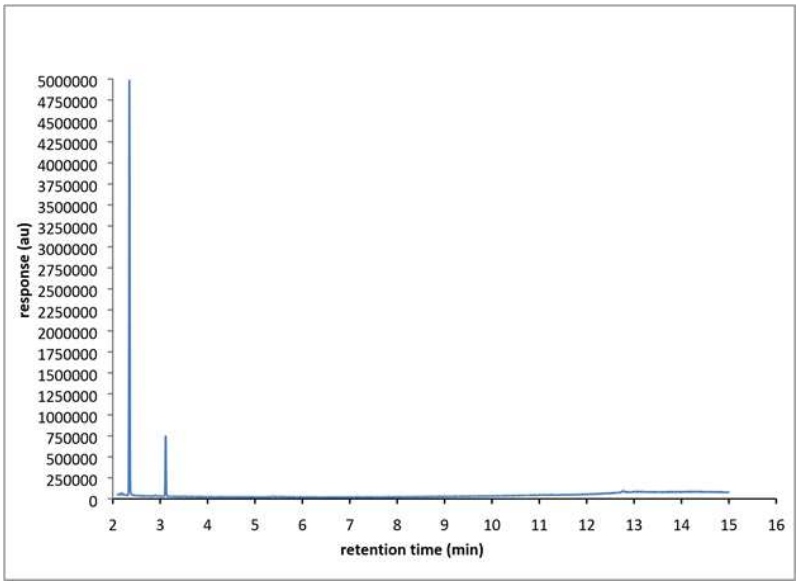

Figure A.26. GCMS, Chapter 2, Table 2.2, Entry 6

Table A.70. GCMS, Chapter 2, Table 2.2, Entry 6

Peak	R.T.	First	Max	Last	PK TY	Height	Area	Pct Max	Pct Total	Compound
1	2.184	12	22	27	VV	18481	201737	0.39	0.21	
2	2.222	27	30	36	VV 3	11300	134714	0.26	0.14	
3	2.353	51	58	75	PV	4767616	51749344	100.00	53.48	styrene
4	2.443	75	77	85	VV 9	5767	82428	0.16	0.09	
5	2.565	101	103	112	PV 10	2907	48244	0.09	0.050	
6	2.626	112	116	119	PV 6	2420	31083	0.06	0.03	
7	2.649	119	121	125	VV 5	2712	31438	0.06	0.03	
8	2.809	152	155	158	PV 5	4065	32472	0.06	0.03	
9	2.828	158	159	163	VV 4	2562	24271	0.05	0.03	
10	2.866	163	167	170	VV 6	6683	96009	0.19	0.10	
11	2.899	170	174	177	VV 5	10008	134129	0.26	0.14	benzaldehyde
12	2.917	177	178	187	VV 9	6909	141714	0.27	0.15	
13	2.988	191	193	195	VV 3	4627	44395	0.09	0.05	
14	3.007	195	197	200	VV 4	4270	44851	0.09	0.05	
15	3.035	200	203	208	VV 7	4459	65094	0.13	0.067	
16	3.115	208	220	235	VV	689160	8284837	16.01	8.562	decane

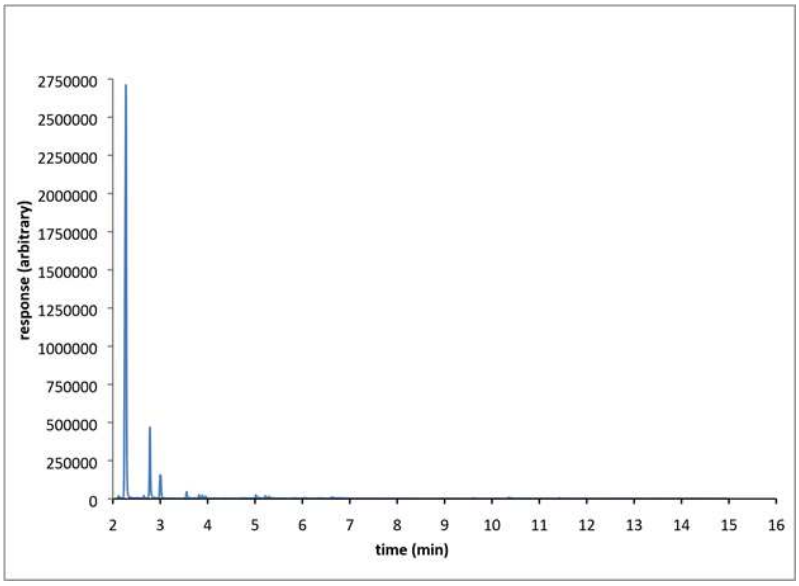

Figure A.27. GCMS, Chapter 2, Table 2.2, Entry 7

Table A.71. GCMS, Chapter 2, Table 2.2, Entry 7

Peak	R.T.	First	Max	Last	PK TY	Height	Area	Pct Max	Pct Total	Compound
1	2.123	3	9	25	BV 3	13808	256389	0.45	0.35	
2	2.278	25	42	68	PV	2666195	57246531	100.00	77.83	styrene
3	2.405	68	69	76	VV 7	4208	66374	0.12	0.09	
4	2.522	91	94	103	VV 9	4158	70822	0.12	0.10	
5	2.659	114	123	133	VV 4	17578	369137	0.64	0.502	
6	2.781	139	149	171	VV	455094	6991334	12.21	9.51	benzaldehyde
7	2.889	171	172	184	VV 9	4977	120192	0.21	0.16	
8	3.007	184	197	207	VV	153152	3281935	5.73	4.46	decane
9	3.228	242	244	250	VV 4	2712	36586	0.06	0.05	
10	3.557	302	314	332	PV 2	43240	913614	1.60	1.24	
11	3.646	332	333	335	VV 2	2468	21245	0.04	0.03	
12	3.731	347	351	355	VV 7	3356	60529	0.11	0.08	
13	3.82	361	370	378	VV 5	23153	460427	0.80	0.63	
14	3.886	378	384	393	VV 2	20268	460671	0.80	0.63	
15	3.957	393	399	406	VV 4	15327	336409	0.59	0.457	
16	4.366	475	486	492	VV 6	3065	83377	0.15	0.113	
17	4.709	549	559	561	VV 6	3171	48011	0.08	0.065	
18	4.732	561	564	569	VV 5	3344	60632	0.11	0.082	
19	5.019	617	625	632	VV 2	22130	372492	0.65	0.506	
20	5.076	632	637	647	VV 3	8285	187156	0.33	0.254	

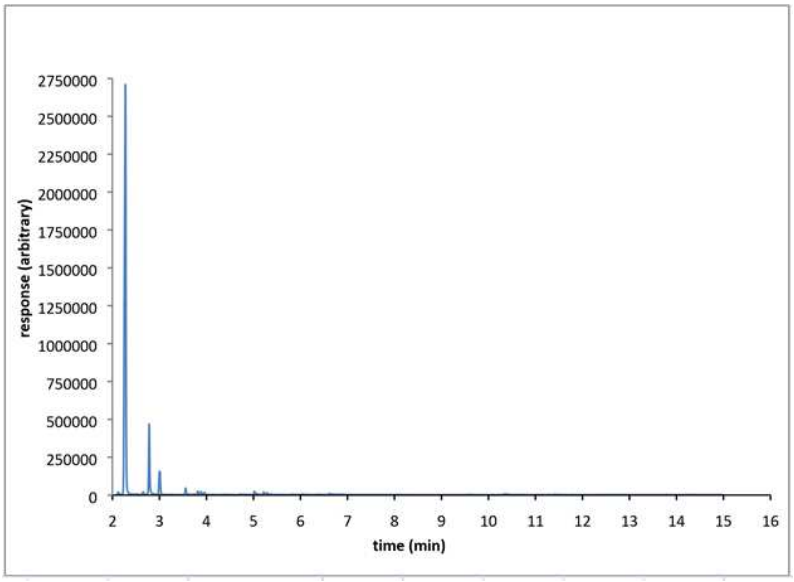

Figure A.28. GCMS, Chapter 2, Table 2.2, Entry 8

Table A.72. GCMS, Chapter 2, Table 2.2, Entry 8

Peak	R.T.	First	Max	Last	PK TY	Height	Area	Pct Max	Pct Total	Compound
1	2.278	23	42	74	BB	2486548	55650509	100.00	82.60	styrene
2	2.781	130	149	149	PB	439121	6689447	12.02	9.93	benzaldehyde
3	3.002	180	196	196	BV 2	156940	3435383	6.17	5.10	decane
2	3.548	298	312	312	BB	94156	1597552	2.87	2.37	

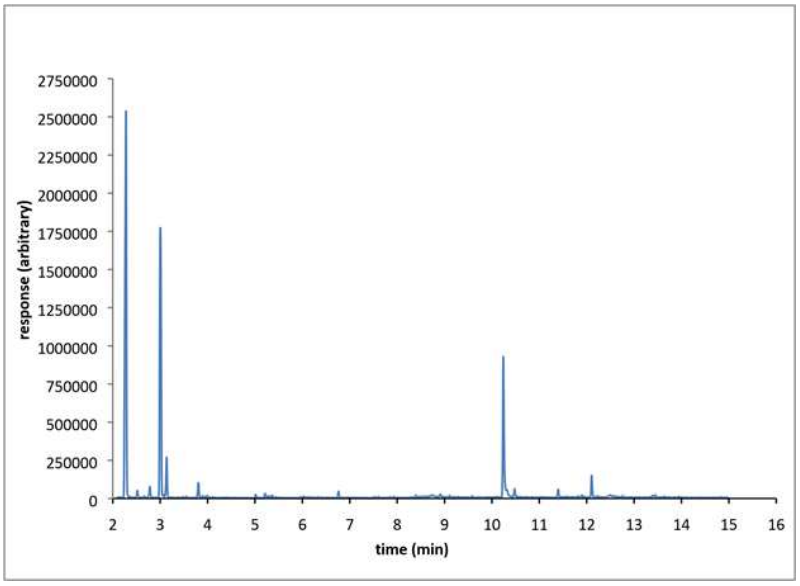

Figure A.29. GCMS, Chapter 2, Table 2.2, Entry 9

Table A.73. GCMS, Chapter 2, Table 2.2, Entry 9

Peak	R.T.	First	Max	Last	PK TY	Height	Area	Pct Max	Pct Total	Compound
1	2.278	30	42	55	PV	2482553.00	53007330.00	100	38.144	styrene
2	2.349	55	57	65	VV 9	7713.00	131938.00	0.25	0.095	
3	2.518	84	93	105	VV	45023.00	822419.00	1.55	0.592	
4	2.659	114	123	132	VV	9605.00	232574.00	0.44	0.167	
5	2.781	132	149	166	PV	70869.00	1308172.000	2.47	0.941	benzaldehyde
6	3.007	184	197	207	VV	1759293.00	37246971.00	70.27	26.803	decane
75	10.24	1724	1736	1773	BV	904103	18458030	34.82	13.282	NHC

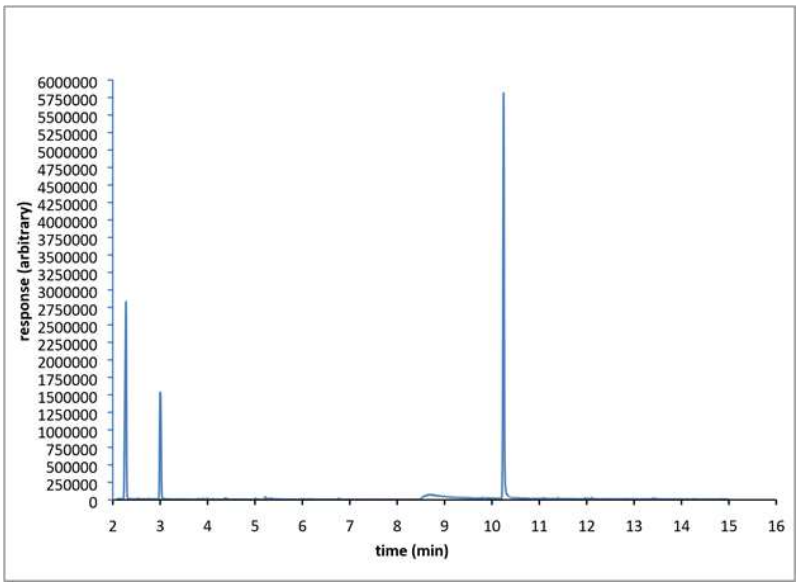

Figure A.30. GCMS, Chapter 2, Table 2.2, Entry 10

Table A.74. GCMS, Chapter 2, Table 2.2, Entry 10

Peak	R.T.	First	Max	Last	PK TY	Height	Area	Pct Max	Pct Total	Compound
1	2.278	29	42	56	PV	2756448.00	58868972	57.41	24.96	Styrene
2	2.353	56	58	61	VV 3	3532.00	40343	0.04	0.017	
3	2.527	83	95	106	VV 3	11196.00	253148	0.25	0.107	
4	2.645	115	120	134	VV 3	3684.00	90481	0.09	0.038	
5	2.753	134	143	160	PV 7	7976.000	243904	0.24	0.103	
6	2.856	160	165	174	VV 7	2508.00	57967	0.06	0.025	
7	2.936	174	182	187	PV 9	2327	49415	0.05	0.021	
8	3.002	187	196	206	VV	1521700	32515026	31.71	13.786	Decane
9	3.063	206	209	220	VV 2	13883	324857	0.32	0.138	
67	10.25	1726	1737	1770	VV	5705138	1.03E+08	100	43.477	NHC

A.17 GCMS Calibration Curves

Calibration curves for benzaldehyde are presented below. It should be noted that on 6/23/2014 the filament in the GCMS used for these experiments was replaced, spectra gathered before that date use the first calibration curve, spectra gathered after that date use the second. First calibration curve applies to Table 2.1 Entries 1, 3, and 4. Second curve applies to all other entries in Tables 2.1 and 2.2.

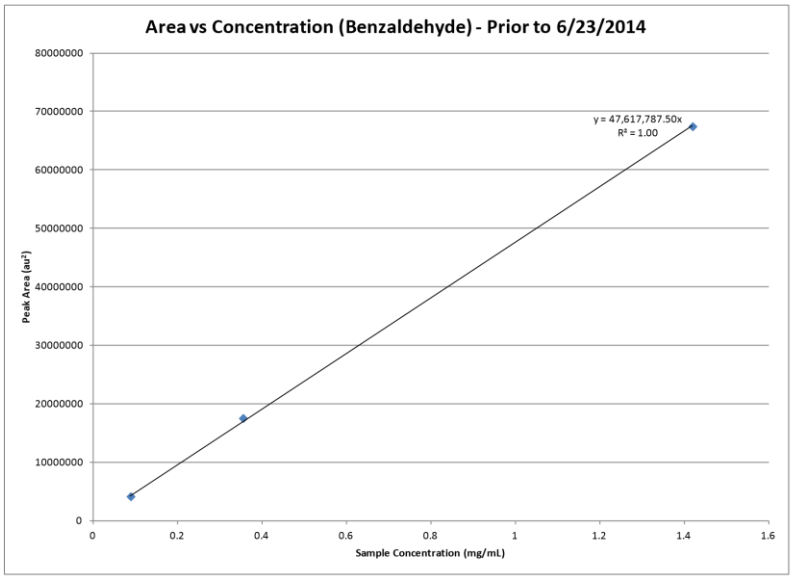

slope = 47,617,787.50

Figure A.75. GCMS Calibration Curve 1

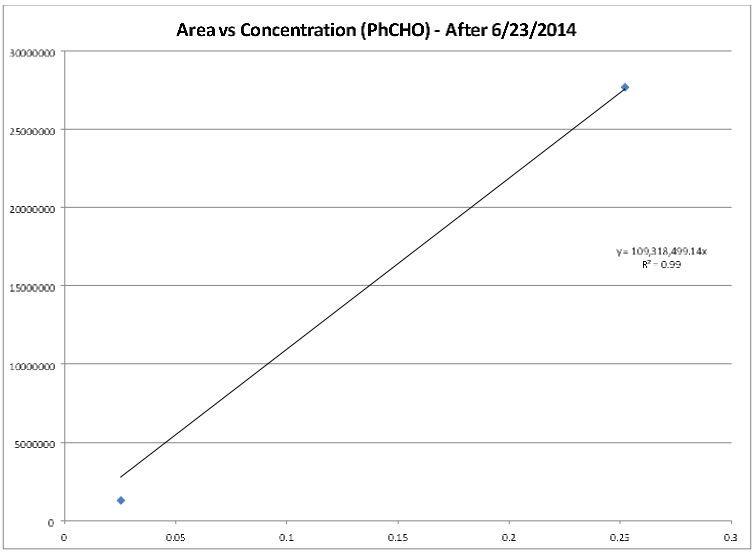

slope = 109,318,499.14

Figure A.76. GCMS Calibration Curve 2

A.18 UV/Visible Spectra

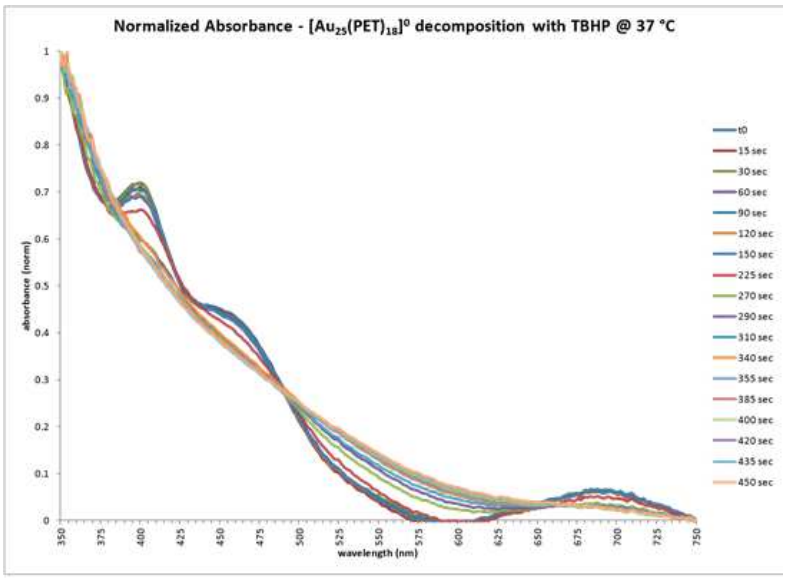

Figure A.77. Normalized UV/Vis, Chapter 2, Figure 2.3

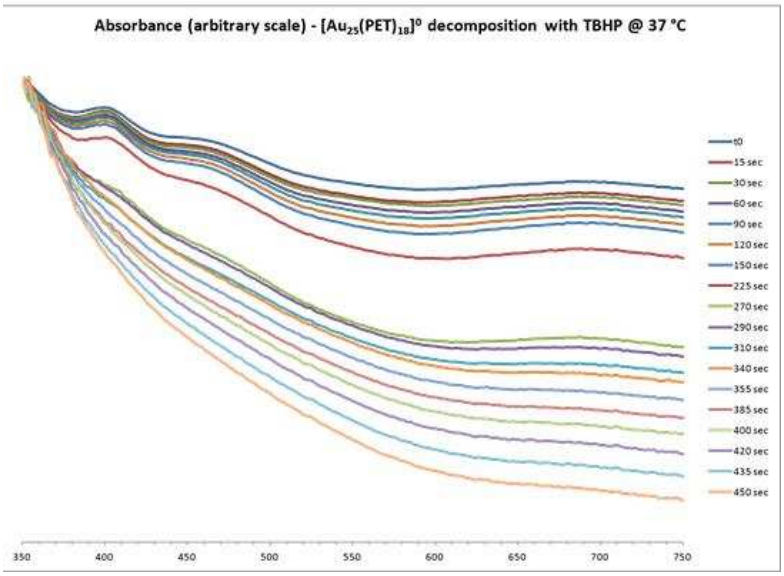

Figure A.78. Arbitrary scale UV/Vis, Chapter 2, Figure 2.3

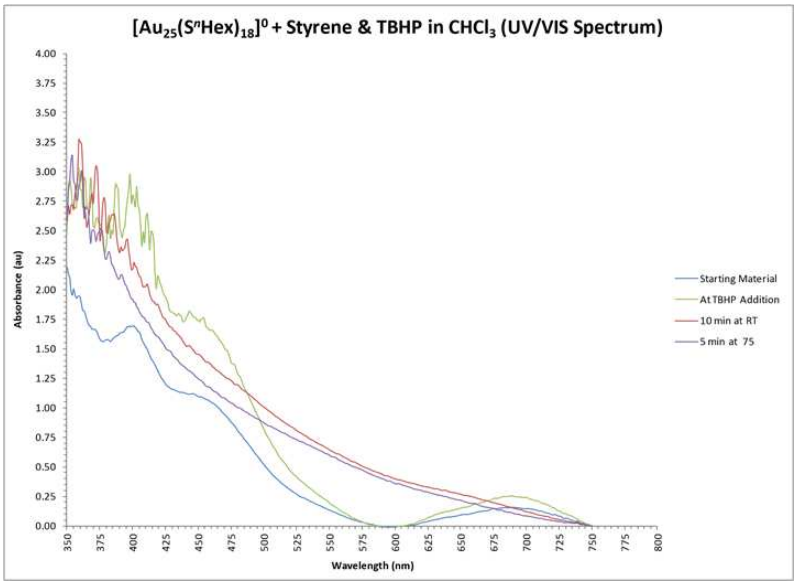

Figure A.79. Initial decomposition experiment

Figure A.79 shows results of the initial decomposition experiment. 11.6 mg of $[Au_{25}(S\textit{n}\text{-}Hex)_{18}]^0$ was dissolved in 2 mL chloroform. To this 18 µL of styrene followed by 50 µL TBHP was added, and the solution was stirred for 30 seconds. A 50 µL aliquot was taken, diluted to 1 mL with chloroform, and evaluated by UV/VIS. The solution was then allowed to stir for 10 minutes at room temperature then evaluated similarly. In a separate experiment 11.6 mg of

$[Au_{25}(Sn\text{-}Hex)_{18}]^0$ was dissolved in 2 mL chloroform. To this 18 µL of styrene followed by 50 µL TBHP was added, and the solution heated to 75 °C for 5 minutes, then evaluated by UV as before. The results were then plotted on the same axes.

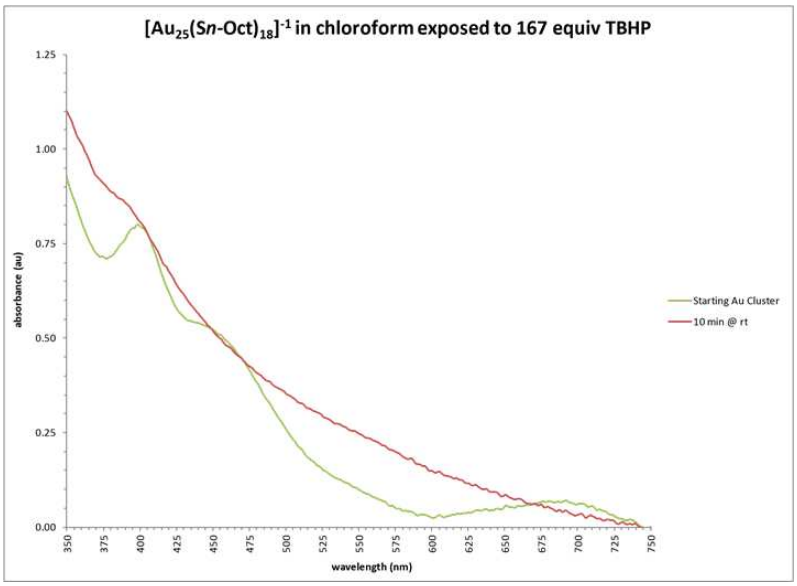

Figure A.80. Decomposition of Octanethiol protected Au_{25}

A.19 Decomposition of Supported Clusters

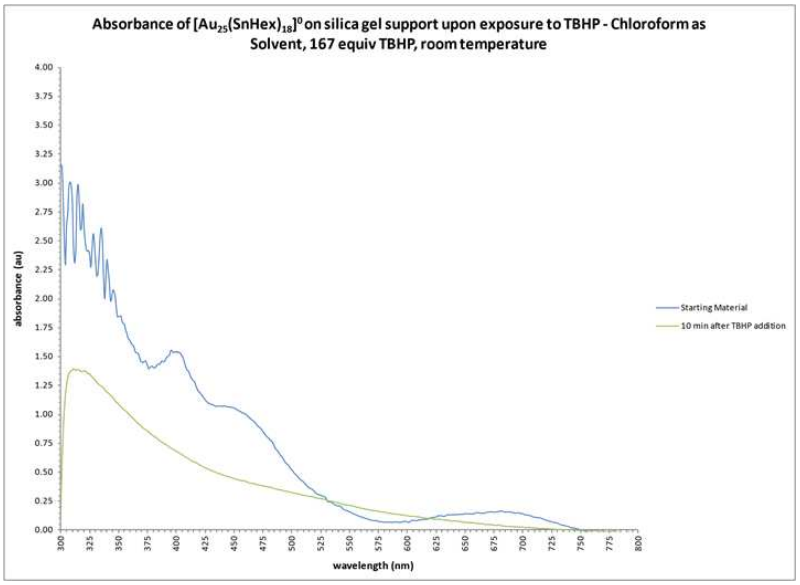

Figure A.81. Decomposition of Au_{25} adsorbed on silica gel

Supported catalyst was prepared by stirring starting cluster in DCM with silica gel for 24 hrs, then concentrating *in vaccuo*. Supported material was not calcinated. UV spectrum was obtained by suspending supported catalyst in chloroform before addition of TBHP. No styrene was added to this decomposition reaction.

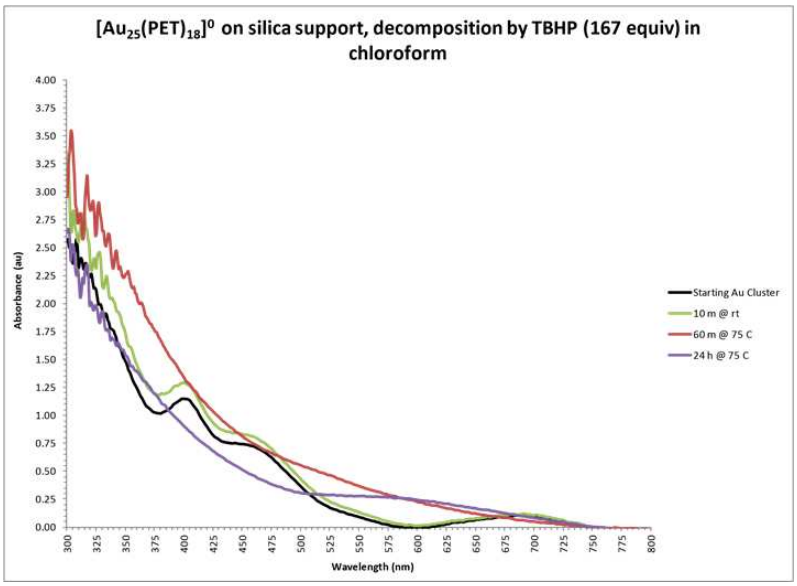

Figure A.82. Decomposition of Au_{25} adsorbed on silica

Supported catalyst was prepared by stirring starting cluster in DCM with silica gel for 24 hrs, then concentrating *in vaccuo*. Supported material was not calcinated. UV spectrum was obtained by dissolving supported catalyst in chloroform before addition of TBHP. No styrene was added to the decomposition experiment.

A.20 Catalysis in Ambient Lighting vs Darkness

General Procedure – These experiments were performed as described above. All reactions were done in chloroform. Those done with exclusion of light were wrapped in aluminum foil. GC traces of experimental results provided below.

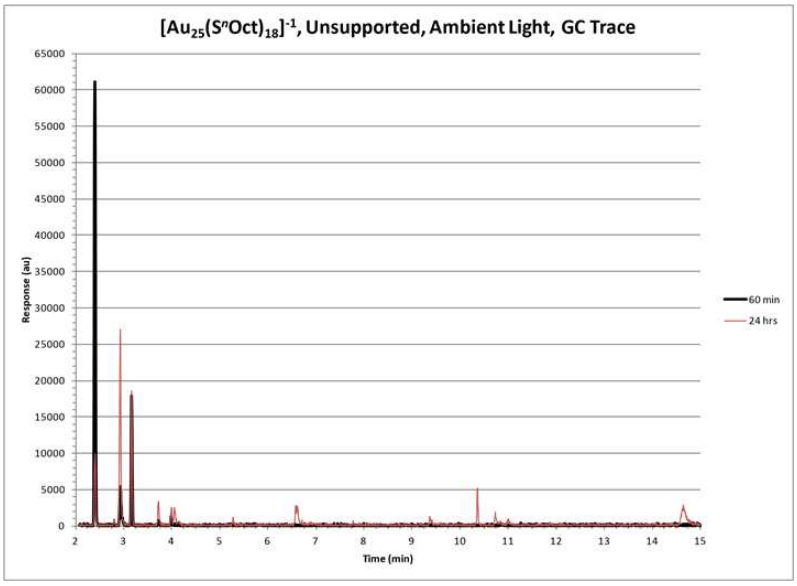

Figure A.83. Unsupported catalyst under ambient lighting

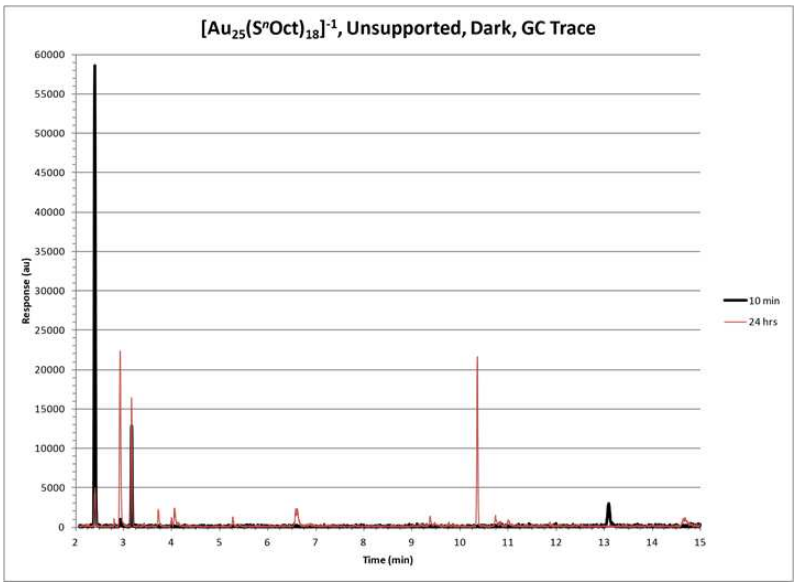

Figure A.84. Unsupported catalyst in darkness

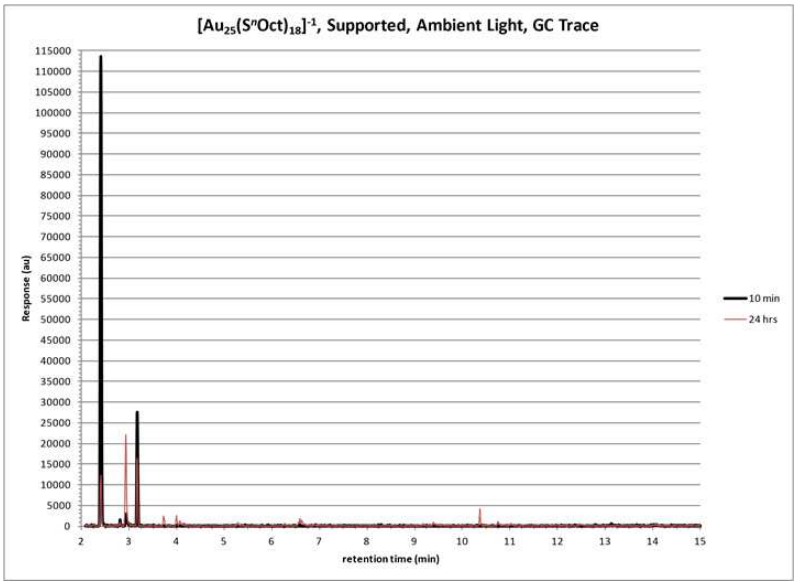

Figure A.85. Supported catalyst under ambient lighting

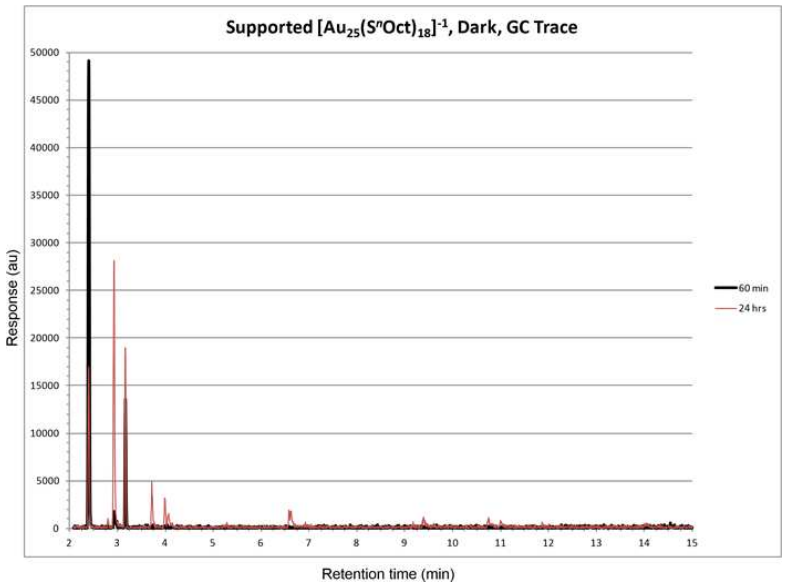

Figure A.86. Supported catalyst in darkness

A.21 Au(PPh$_3$)Cl as Au source for catalysis

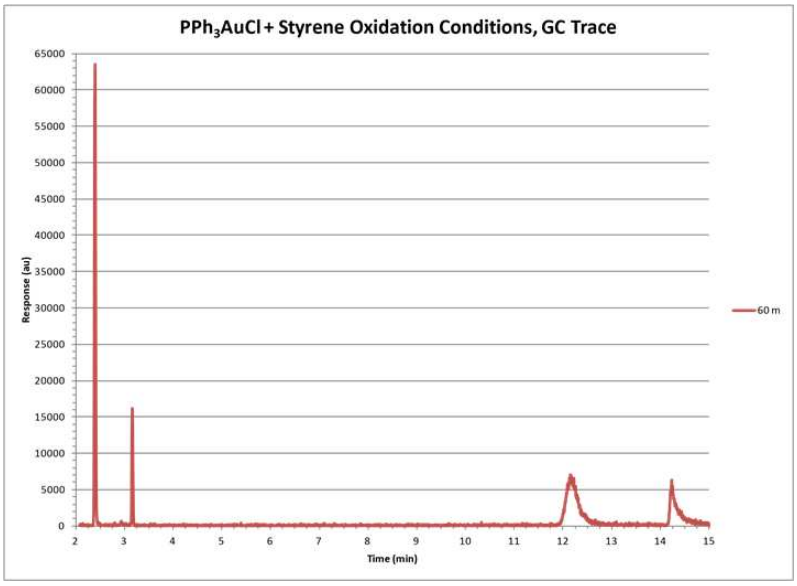

Figure A.87. Au(PPh$_3$)Cl as Au source for catalysis

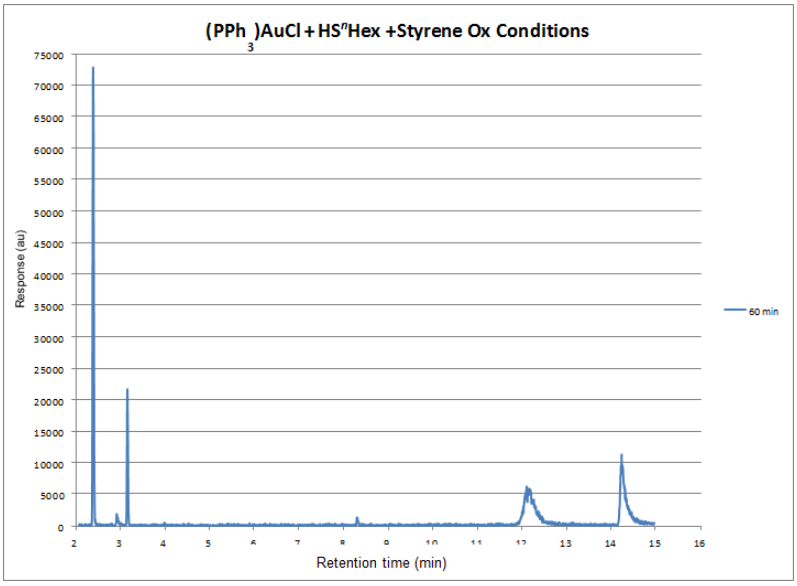

Figure A.88. Au(PPh$_3$)Cl as Au source, with hexanethiol ligand added

In the course of our initial investigation into the active catalyst, we attempted to use PPh$_3$AuCl to catalyze the oxidation of styrene under consideration. This experiment was carried out using 25 mol % catalyst loading on 0.157 mmol styrene, using the procedure described above for the cluster precursor. The last two peaks in this GC trace are triphenylphosphine and triphenylphosphine

oxide. Minimal conversion was observed at 1 hr in either case (with or without the inclusion of thiol). This led us to conclude that phosphines may make for reasonable catalyst poisons in this reaction.

A.22 NMR Spectra

^{1}H NMR spectra were acquired on a Varian 400 MR (at 400 MHz), and are reported relative to $SiMe_4$ (δ 0.00)

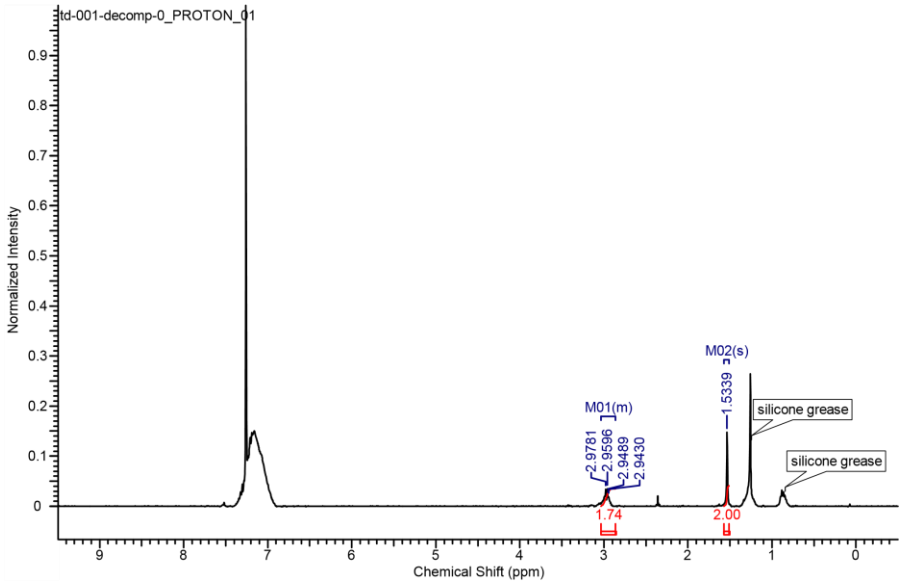

Figure A.89. ^{1}H NMR of $Au_{25}(PET)_{18}$ + TBHP decomposition product

APPENDIX B: SUPPLEMENTARY TO CHAPTER 3

B.1 General Methods

All chemicals were obtained from commercial suppliers and used without further purification unless otherwise noted. UV/Vis spectra were collected on an HP 8452A Diode Array Spectrophotometer. Data were analyzed using Microsoft Excel, with calibration curves constructed using the built-in linear regression function. ^{1}H NMR spectra were acquired on a Varian 400 MR (at 400 MHz), and are reported relative to $SiMe_4$ (δ 0.00). ^{13}C NMR spectra were acquired on a Varian 400 MR (at 400 MHz), and are reported relative to $SiMe_4$ (δ 0.00). Flash chromatography was performed with SiliFlash P60 silica gel (230-400 mesh) purchased from Silicycle. Electron paramagnetic resonance (EPR) spectra were obtained using a continuous-wave X-band Bruker EMX 200U instrument outfitted with a liquid nitrogen cryostat. Compounds were dissolved in a 1:1 mixture of dichloromethane and 1,2-dichloroethane to form a glass at low temperature.

B.2 Synthesis of Phosphatidyl Choline (PC)-Coated 5 nm Au particles

This procedure was adapted from *Chem. Commun.* **2008**, 3013-3015.[1] A solution of PC (0.064 g, 0.084 mmol, 1 equiv) in 10 mL CH_2Cl_2 was added to an aqueous solution of $HAuCl_4$ (0.029g, 0.084 mmol, 1 equiv) in 5 mL of nanopure water. Mixture was stirred rapidly to form an emulsion, and a freshly prepared solution of $NaBH_4$ (0.016 g, 0.42 mmol, 5 equiv) in 5 mL nanopure water was added dropwise at room temperature. The reaction was stirred for 1 h at ambient temperature, then stored overnight at 4 °C. Both solvents were removed by rotary evaporation, and the resultant solid was re-dissolved in a minimal volume of CH_2Cl_2, and washed with water (2 x 5 mL). Remaining solvent was removed by rotary evaporation and the product was dried under vacuum overnight. Resultant purple solid shows optical properties consistent with the previous report.

B.3 Etching of Organic Soluble 5 nm gold colloids in O_2 atmosphere (CH_2Cl_2 solvent)

A suspension of 5 nm colloidal gold, synthesized as noted below, in CH_2Cl_2 (1 mL, 0.40 mg Au / mL) was placed in an air-free cuvette. This solution was sparged for approximately 2 minutes with pure oxygen, and the cuvette was sealed. Separately a solution of HS*n*-Hex (0.296 mL, 1.00 mmol, 500 equiv to Au) in 0.704 mL of CH_2Cl_2 was made and sparged for approximately 90 sec with oxygen, the cuvette was opened under a constant stream of oxygen, the hexane thiol solution was added in one portion and the cuvette was sealed. The cuvette sidearm was fitted with an oxygen balloon and the valve was opened slightly to maintain 1 atm oxygen pressure in the head space. The cuvette was placed in the spectrophotometer and a UV/Vis spectrum was collected every 5 min for a period of 1.5 hr. Spectra were exported to Excel and evaluated therein.

B.4 Etching of Organic Soluble 5 nm gold colloids in O_2 atmosphere (PhMe solvent)

A suspension of 5 nm colloidal gold, synthesized as described above, in PhMe (1 mL, 0.40 mg Au / mL) was placed in an air-free cuvette. This solution was sparged for approximately 2 minutes with pure oxygen, and the cuvette was sealed. Separately a solution of HS*n*-Hex (0.296 mL, 1.00 mmol, 500 equiv to Au) in 0.704 mL of PhMe was made and sparged for approximately 90 sec with oxygen, the cuvette was opened under a constant stream of oxygen, the hexane thiol solution was added in one portion and the cuvette was sealed. The cuvette sidearm was fitted with an oxygen balloon and the valve was opened slightly to maintain 1 atm oxygen pressure in the head space. The cuvette was placed in the spectrophotometer and a UV/Vis spectrum was collected every 5 min for a period of 1.5 hr. Spectra were exported to Excel and evaluated therein.

B.5 Etching of Organic Soluble 5 nm gold colloids in Ar atmosphere (CH_2Cl_2 solvent)

A suspension of 5 nm colloidal gold, synthesized as noted above, in CH_2Cl_2 (1 mL, 0.40 mg Au / mL) was placed in a 2-dram vial and degassed via freeze/pump/thaw (3 cycles). This solution was then transferred to an air-free cuvette that was previously purged with argon. The cuvette was

then sealed. Separately a solution of HS*n*-Hex (0.296 mL, 1.00 mmol, 500 equiv to Au) in 0.704 mL of CH_2Cl_2 was made and degassed via freeze/pump/thaw (3 cycles), the cuvette was opened under a constant stream of argon, the hexane thiol solution was added in one portion and the cuvette was sealed. The cuvette was placed in the spectrophotometer and a UV/Vis spectrum was collected every 5 min for a period of 1.5 hr. Spectra were exported to Excel and evaluated therein.

B.6 Etching of Organic Soluble 5 nm gold colloids in O_2 atmosphere (CH_2Cl_2/2-Me-2-butene solvent)

A suspension of 5 nm colloidal gold, synthesized as noted below, in CH_2Cl_2 (0.704 mL, 0.40 mg Au / mL) was placed in an air-free cuvette. This solution was sparged for approximately 2 minutes with pure oxygen, and the cuvette was sealed. Separately a solution of HS*n*-Hex (0.296 mL, 1.00 mmol, 500 equiv to Au) in 0.704 mL 2-methyl-2-butene was sparged for approximately 2 minutes with pure oxygen in a sealed 2-dram vial. The cuvette was opened under a constant stream of oxygen, and this solution was added via pipette. The cuvette was sealed, the sidearm was fitted with an oxygen balloon, and the valve was opened slightly to maintain 1 atm of oxygen pressure over the course of the experiment. The cuvette was placed in the spectrophotometer and a UV/Vis spectrum was collected every 5 min for a period of 1.5 hr. Spectra were exported to Excel and evaluated therein.

B.7 Synthesis of $Au_{25}(PET)_{18}$

Au_{25} was synthesized by a modified Brust-Schiffrin method. Briefly: A solution of tetraoctylammonium bromide (TOAB, 155 mg, 0.282 mmol, 1.12 equiv) in THF (7 mL) was prepared with stirring in a 50 mL round bottom flask open to the ambient atmosphere. To this $HAuCl_4 \cdot 3H_2O$ (100 mg, 0.254 mmol, 1.00 equiv) was added, and the reaction was stirred until homogeneous. Upon complete dissolution of the gold salt, phenylethane thiol was added (232 µL, 1.341 mmol, 5.28 equiv) and the reaction was allowed to stir at room temperature under ambient

atmosphere until clear (typically 3-4 hours). When the solution was clear, $NaBH_4$ (96.9 mg, 2.56 mmol, 10.1 equiv) was dissolved in nanopure water (2.5 mL) and chilled to 0 °C by freezing in liquid nitrogen then allowing to thaw. This was added all in one portion to the clear Au solution. Upon addition the solution turned from clear to nearly black. This was allowed to stir at room temperature, loosely covered with a cap to prevent evaporation of the solvent, for 48 hrs. After this time, the reaction was transferred to a separatory funnel and the layers were separated. The organic phase was evaporated to near dryness and the concentrate was dissolved in a minimal amount of CH_2Cl_2. This was divided into 5 mL portions in 50 mL conical centrifuge vials, and each was filled with MeOH then spun at 4000 rpm for 10 min at 4 °C. The supernatant was discarded, the vial was refilled with MeOH, sonicated until suspended, then placed in the centrifuge again. This step was repeated twice, and the pellets were allowed to dry. Pellets were then dissolved in minimal CH_2Cl_2 and purified by flash chromatography (gradient 20%-50% CH_2Cl_2 in Hexanes). Product UV/VIS spectrum comports with literature for Au_{25} in the neutral charge state.

B.8 Attempted synthesis of $Au_{25}(PET)_{18}$ under inert atmosphere

As previously reported by Murray,[2] attempting the Brust synthesis of Au_{25} under inert conditions does not deliver the desired product. The inert atmosphere procedure is as follows. To a 50 mL round bottom flask equipped with a magnetic stir bar, tetraoctylammonium bromide (TOAB, 155 mg, 0.282 mmol, 1.12 equiv) and THF (7 mL) were added and stirred until a homogeneous solution formed. $HAuCl_4 \cdot 3H_2O$ (100 mg, 0.254 mmol, 1.00 equiv) was then added, and allowed to stir until the dark orange solution was homogeneous. The flask was then fitted with a septum and the solution was degassed by freeze/pump/thaw (3 cycles) then back-filled with argon. In a separate 2-dram vial, phenylethane thiol (PET, 232 µL, 1.341 mmol, 5.28 equiv) was dissolved in 1 mL of THF and also degassed by 3 cycles of freeze/pump/thaw, then back-filled with argon. The PET solution was transferred by a purged needle to the Au solution and this was

allowed to stir until clear (typically 3-4 hours). A 2-dram vial containing solid $NaBH_4$ (96.9 mg, 2.56 mmol, 10.1 equiv) was placed under vacuum for several minutes then back-filled with argon. Separately, a 50 mL round bottom flask containing ~25 mL of nanopure water was fitted with a septum and a vent needle, and then sparged with argon for approximately 1 hr and left under an argon atmosphere. When the Au solution was clear, 2.5 mL of the sparged nanopure water was added via syringe to the 2-dram vial containing solid $NaBH_4$ and the vial was chilled to 0 °C by freezing in liquid nitrogen then thawing. This solution was then added to the Au solution via syringe and the reaction was allowed to stir 48 hrs under an inert atmosphere at ambient temperature. After 48 hrs stirring the reaction was worked-up as described above, but not purified by flash chromatograph. UV/VIS of the crude product does not show characteristic peaks for Au_{25}, as expected.

B.9 UV/Vis Data – 5 nm PC-AuNP

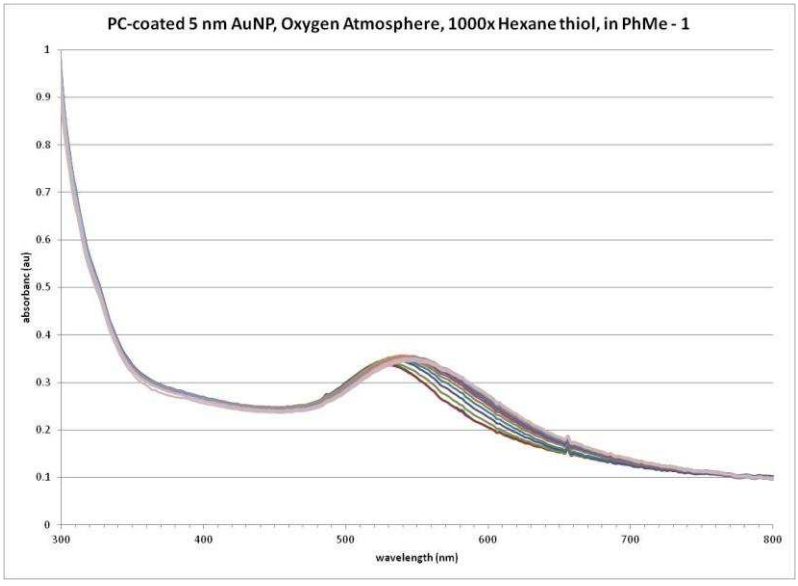

Figure B.1. Etching of 5 nm AuNP in Toluene Run 1

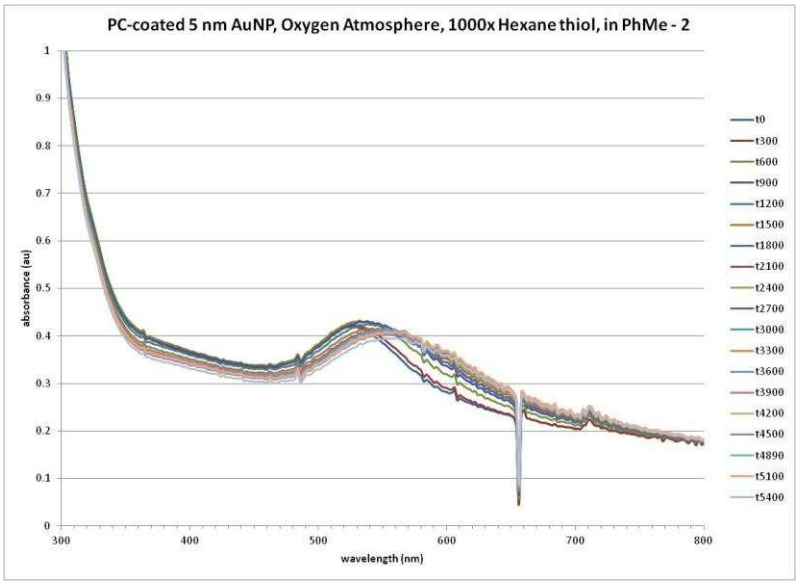

Figure B.2. Etching of 5 nm AuNP in Toluene Run 2

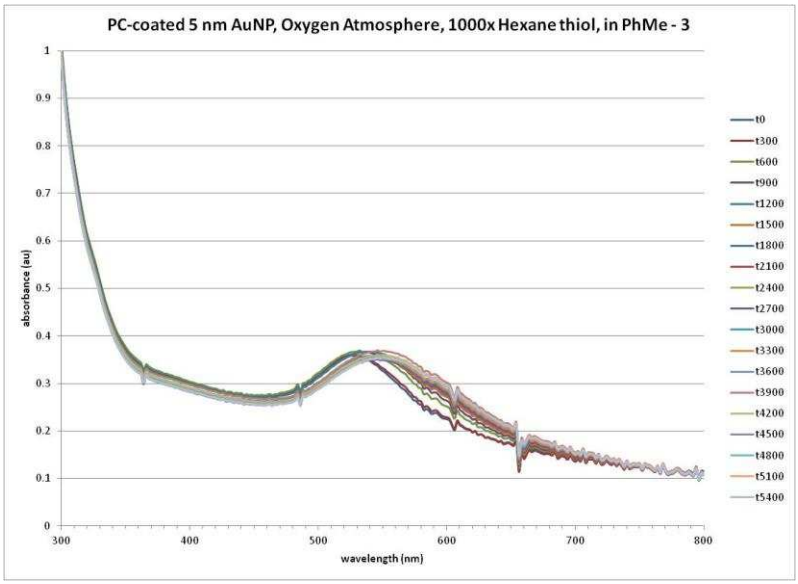

Figure B.3. Etching of 5 nm AuNP in Toluene Run 3

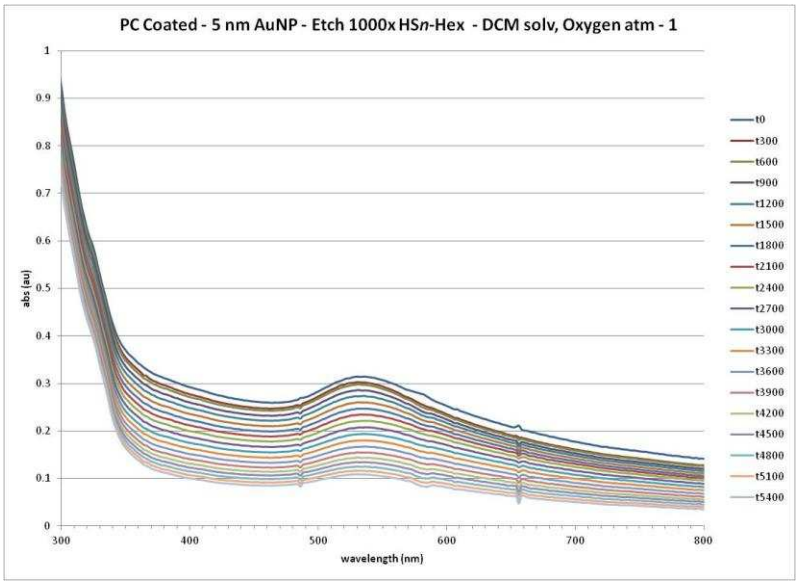

Figure B.4. Etching of 5 nm AuNP in DCM, O_2 atm, Run 1

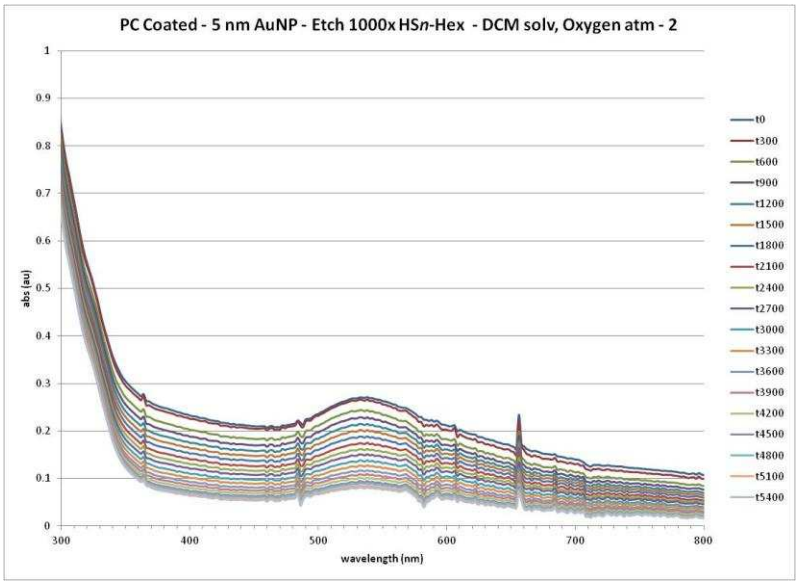

Figure B.5. Etching of 5 nm AuNP in DCM, O_2 atm, Run 2

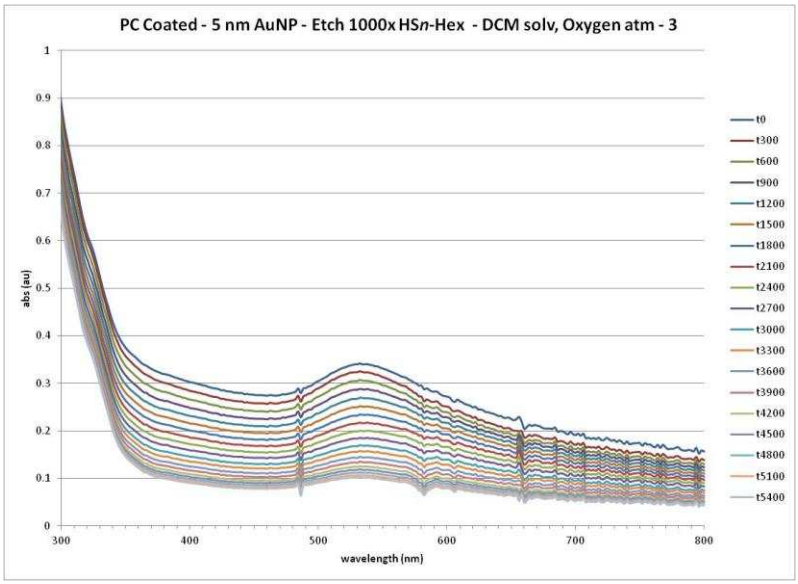

Figure B.6. Etching of 5 nm AuNP in DCM, O_2 atm, Run 3

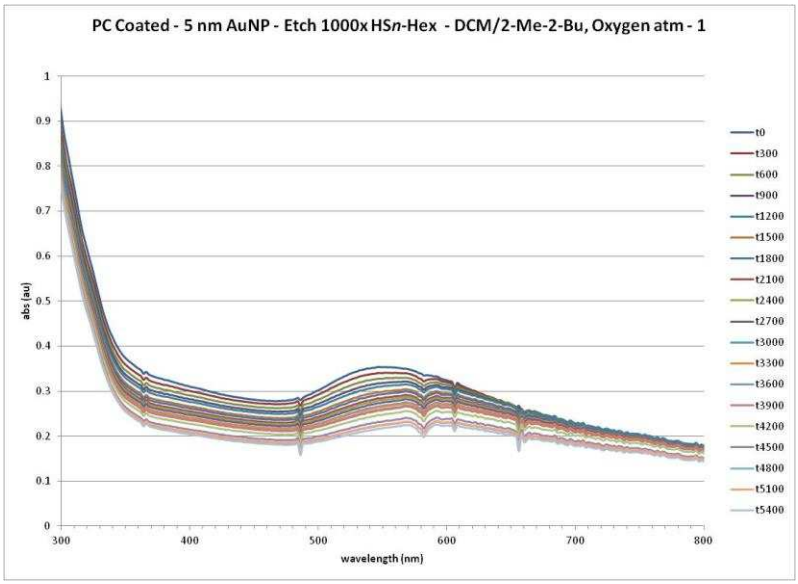

Figure B.7. Etching of 5 nm AuNP in DCM/2-methyl-2-butene, O_2 atm, Run 1

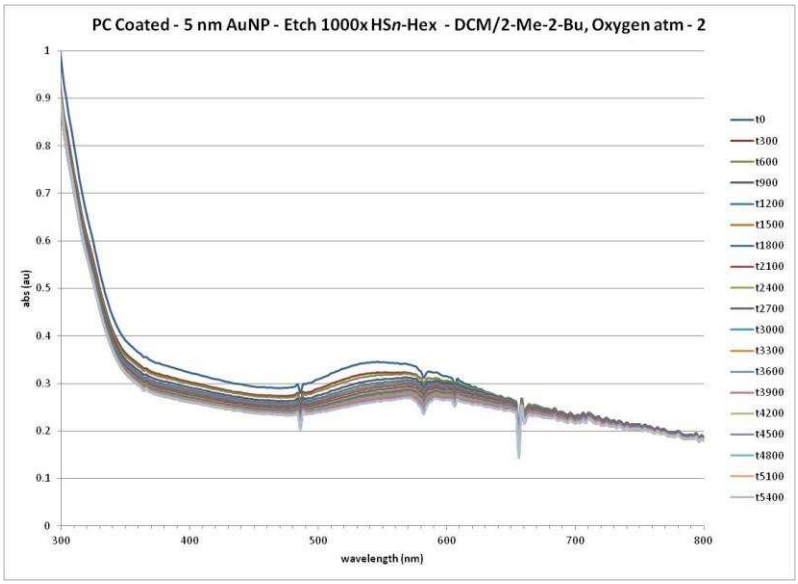

Figure B.8. Etching of 5 nm AuNP in DCM/2-methyl-2-butene, O_2 atm, Run 2

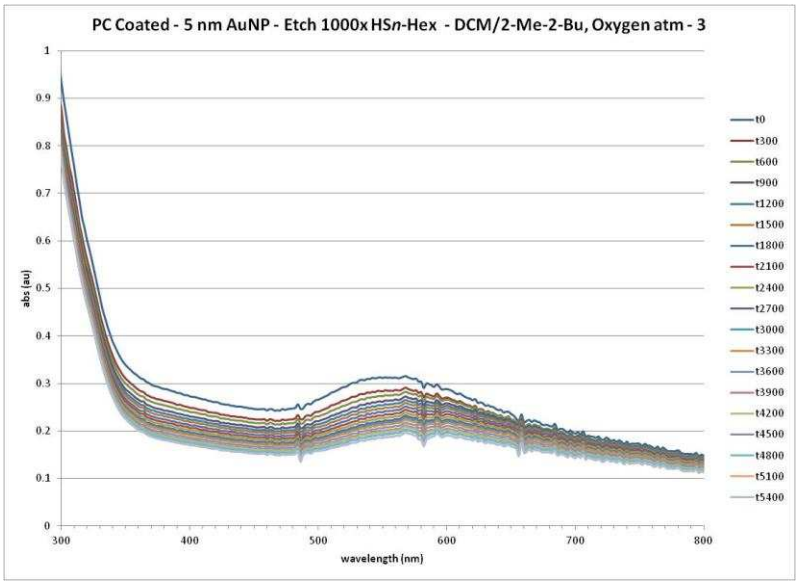

Figure B.9. Etching of 5 nm AuNP in DCM/2-methyl-2-butene, O_2 atm, Run 3

Table B.1. Compiled 5 nm AuNP Etching Data

time (min)	time (s)	DCM Ox Avg	DCM Ox StdErr	DCM Ar Avg	DCM Ar Stderr	Ox 2Me-2Bu Avg	Ox 2Me-2Bu StdErr	Ox PhMe Avg	Ox PhMe StErr
0	0	1	0	1	0	1	0	1	0
5	300	0.969696419	0.009115544	0.950741488	0.019433154	0.931419391	0.016440007	0.999446543	0.002833184
10	600	0.917497341	0.015437524	0.942256766	0.017614019	0.899187592	0.017140564	1.014159616	0.005801966
15	900	0.868351819	0.022416621	0.935478749	0.016554808	0.867306167	0.019455608	1.013086116	0.005083276
20	1200	0.818779987	0.02573818	0.929761849	0.016550222	0.842142578	0.021272944	1.00337886	0.008428211
25	1500	0.77007368	0.029429529	0.922578549	0.014889951	0.818026744	0.020077154	0.983799238	0.020061856
30	1800	0.72148828	0.032546483	0.925859898	0.018491059	0.801253666	0.023923334	0.977733874	0.024307164
35	2100	0.676085821	0.034708726	0.924501836	0.016277015	0.77811246	0.026565411	0.974402256	0.025529255
40	2400	0.630648751	0.035549075	0.928794085	0.020697084	0.762032503	0.029021817	0.976037114	0.025295863
45	2700	0.586939256	0.035593827	0.923214388	0.021758337	0.74722265	0.031617182	0.965194244	0.026658177
50	3000	0.541764958	0.036512811	0.923717972	0.025522439	0.734553049	0.032833508	0.964811106	0.027440995
55	3300	0.501669403	0.035648281	0.92311181	0.026614196	0.724700189	0.034024267	0.960051909	0.029628431
60	3600	0.464430662	0.033470543	0.921454679	0.030154689	0.710400736	0.036335878	0.968400588	0.023820366
65	3900	0.430235456	0.031695091	0.921653482	0.02665579	0.701577766	0.040311889	0.968076639	0.026968599
70	4200	0.400526023	0.029265282	0.922593889	0.025095368	0.686392467	0.040383786	0.957366087	0.022395933
75	4500	0.375254445	0.026318401	0.918966847	0.0274998	0.667910679	0.045973533	0.950726383	0.026577279
80	4800	0.351868845	0.022085194	0.924881908	0.023178259	0.657098055	0.048067827	0.947001988	0.023737312
85	5100	0.332582914	0.019615102	0.913801698	0.0238933	0.65187734	0.050580386	0.95109057	0.024952159
90	5400	0.315562587	0.016491375	0.910184688	0.023442385	0.644216242	0.053838211	0.935182761	0.028450727

Table B.2. Absorbance Data 5 nm AuNP in DCM (t_n/t_0), O_2 atm

time (min)	time (sec)	Ox DCM @526 - 1	Ox DCM @526 - 2	Ox DCM @526 - 3
0	0	1	1	1
5	300	0.986414	0.955039	0.967637
10	600	0.905084	0.899222	0.948186
15	900	0.847156	0.844736	0.913163
20	1200	0.795275	0.790872	0.870194
25	1500	0.743767	0.737628	0.828826
30	1800	0.692819	0.685213	0.786433
35	2100	0.642878	0.639897	0.745482
40	2400	0.594468	0.595735	0.701743
45	2700	0.553038	0.549679	0.6581
50	3000	0.50642	0.504097	0.614778
55	3300	0.466669	0.465377	0.572962
60	3600	0.43136	0.430562	0.53137
65	3900	0.399	0.398083	0.493623
70	4200	0.370446	0.372083	0.459049
75	4500	0.346932	0.350992	0.427839
80	4800	0.327971	0.331647	0.395988
85	5100	0.311287	0.314698	0.371764
90	5400	0.296805	0.301446	0.348436

Table B.3. Absorbance Data 5 nm AuNP in DCM (t_n/t_0), Ar atm

time (min)	time (sec)	Ar DCM @526 - 1	Ar DCM @526 - 2	Ar DCM @526 - 3
0	0	1	1	1
5	300	0.912457	0.964082	0.975685
10	600	0.908308	0.951083	0.967379
15	900	0.903036	0.945976	0.957425
20	1200	0.896988	0.942135	0.950163
25	1500	0.8928	0.937745	0.93719
30	1800	0.890629	0.933736	0.953215
35	2100	0.894002	0.929895	0.949608
40	2400	0.89125	0.93247	0.962663
45	2700	0.882759	0.929557	0.957327
50	3000	0.875703	0.932723	0.962728
55	3300	0.872562	0.933947	0.962826
60	3600	0.864343	0.933229	0.966792
65	3900	0.871903	0.929937	0.96312
70	4200	0.876905	0.927447	0.96343
75	4500	0.871787	0.918077	0.967037
80	4800	0.88303	0.928544	0.963071
85	5100	0.868685	0.92272	0.95
90	5400	0.865661	0.919723	0.94517

Table B.4. Absorbance Data 5 nm AuNP in Toluene (t_n/t_0), O_2 atm

time (min)	time (sec)	Ox PhMe @526 - 1	Ox PhMe @526 - 2	Ox PhMe @526 - 3
0	0	1	1	1
5	300	0.996458715	1.005110044	0.996770871
10	600	1.002626453	1.021034368	1.018818027
15	900	1.023047866	1.009863574	1.006346909
20	1200	1.019181963	0.99039787	1.000556746
25	1500	1.023903677	0.964823882	0.962670156
30	1800	1.02402172	0.941721728	0.967458174
35	2100	1.025408723	0.946903076	0.95089497
40	2400	1.025526766	0.942197081	0.960387495
45	2700	1.018473706	0.940271902	0.936837124
50	3000	1.019683645	0.936492846	0.938256827
55	3300	1.018473706	0.922256025	0.939425994
60	3600	1.014696335	0.935518372	0.954987056
65	3900	1.009059789	0.917217284	0.977952844
70	4200	0.998022782	0.920758663	0.953316817
75	4500	1.001977218	0.912891572	0.937310358
80	4800	0.992681343	0.912962875	0.935361746
85	5100	1	0.918049151	0.935222559
90	5400	0.984565897	0.886010363	0.934972023

Table B.5. Absorbance Data 5 nm AuNP in DCM/2-methyl-2-butene (t_n/t_0), O_2 atm

time (min)	time (sec)	Ox DCM/2Me2Bu @526 - 1	Ox DCM/2Me2Bu @526 - 2	Ox DCM/2Me2Bu @526 - 3
0	0	1	1	1
5	300	0.95899953	0.933131691	0.902126952
10	600	0.921408418	0.910684103	0.865470256
15	900	0.890694804	0.882543071	0.828680625
20	1200	0.864948272	0.861845032	0.79963443
25	1500	0.831677639	0.843904753	0.77849784
30	1800	0.817246649	0.832310293	0.754204055
35	2100	0.789795439	0.81715743	0.727384513
40	2400	0.774688455	0.804762328	0.706646726
45	2700	0.759375735	0.794887762	0.687404453
50	3000	0.741711733	0.787504077	0.674443337
55	3300	0.735039972	0.777777778	0.661282818
60	3600	0.718022572	0.769178306	0.644001329
65	3900	0.710351517	0.766598464	0.627783317
70	4200	0.682430049	0.758236219	0.618511133
75	4500	0.642634611	0.757109391	0.603988036
80	4800	0.620003527	0.752453815	0.598836823
85	5100	0.62182577	0.750556	0.583250249
90	5400	0.600723019	0.751267681	0.580658026

B.10 UV/Vis Data – Au_{25}

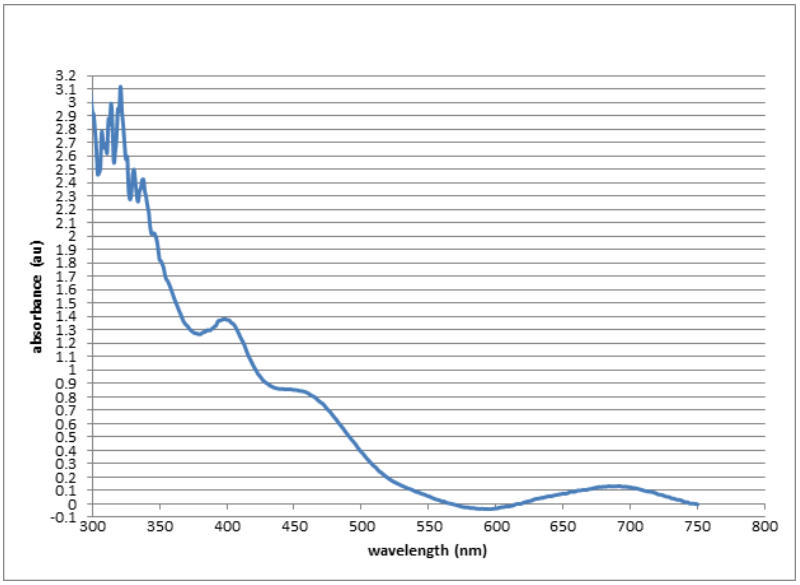

Figure B.10. Chapter 3, Table 3.1, Control, UV/Vis

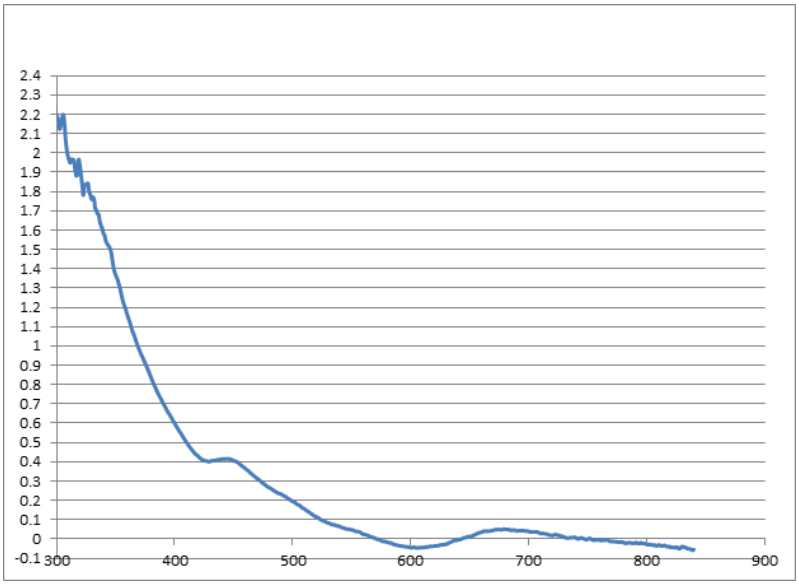

Figure B.11. Chapter 3, Table 3.1, Ambient + BHT, UV/Vis

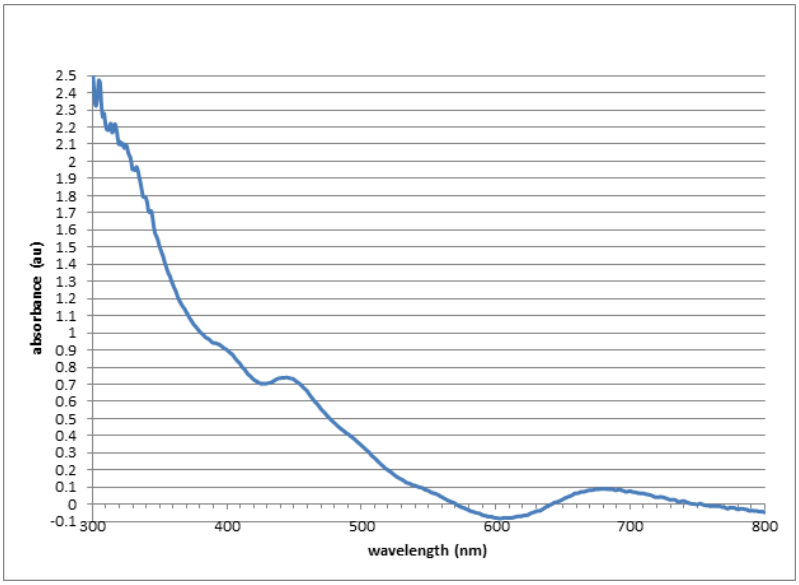

Figure B.12. Chapter 3, Table 3.1, Argon+AIBN, UV/Vis

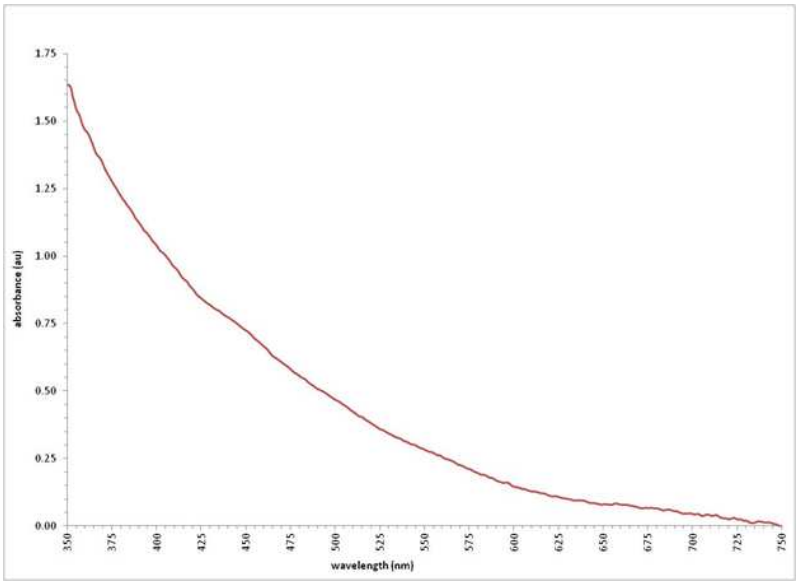

Figure B.13. Chapter 3, Table 3.1, Argon Control, UV/Vis

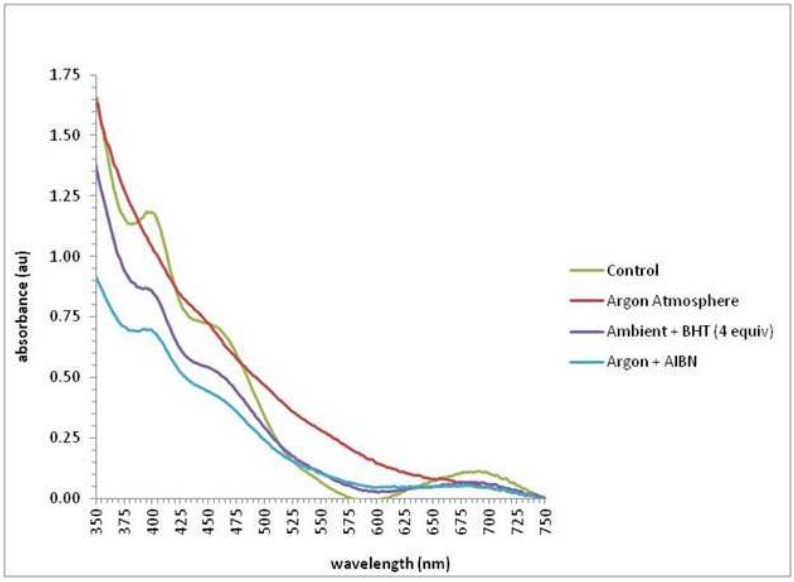

Figure B.15. Chapter 3, Table 3.1, UV/Vis Combined

B.11 NMR Spectra

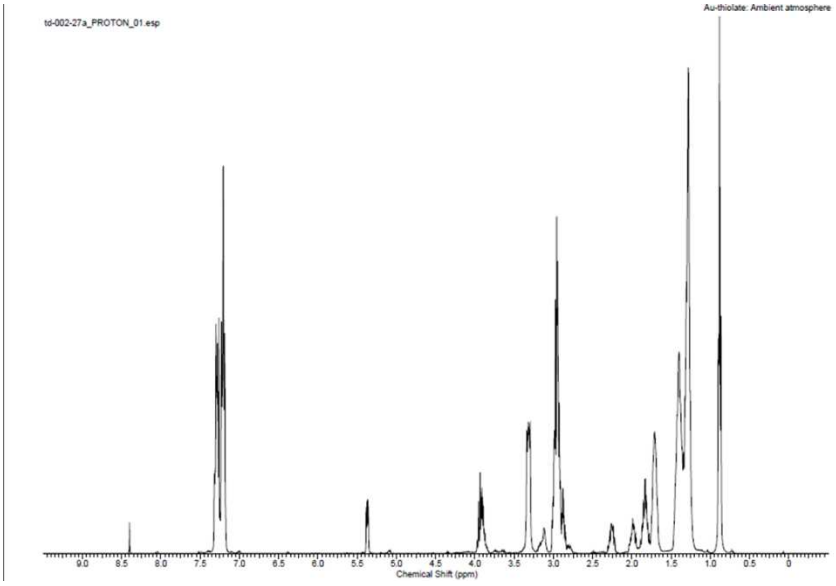

Figure B.16. ^{1}H NMR Spectrum, Au-thiolate polymer made under ambient atmosphere

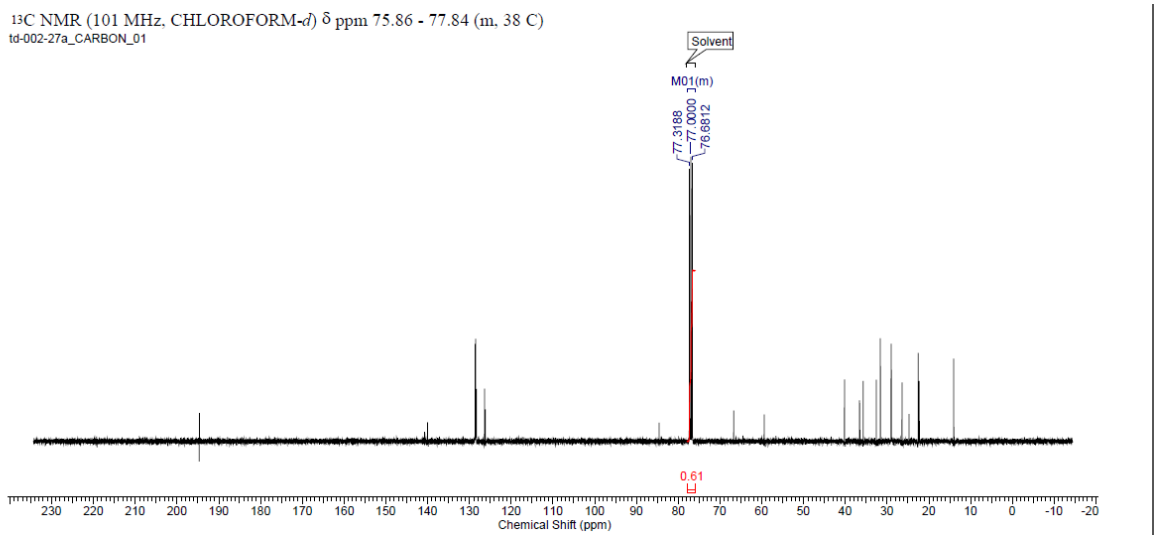

Figure B.17. ^{13}C NMR Spectrum, Au-thiolate polymer made under ambient atmosphere

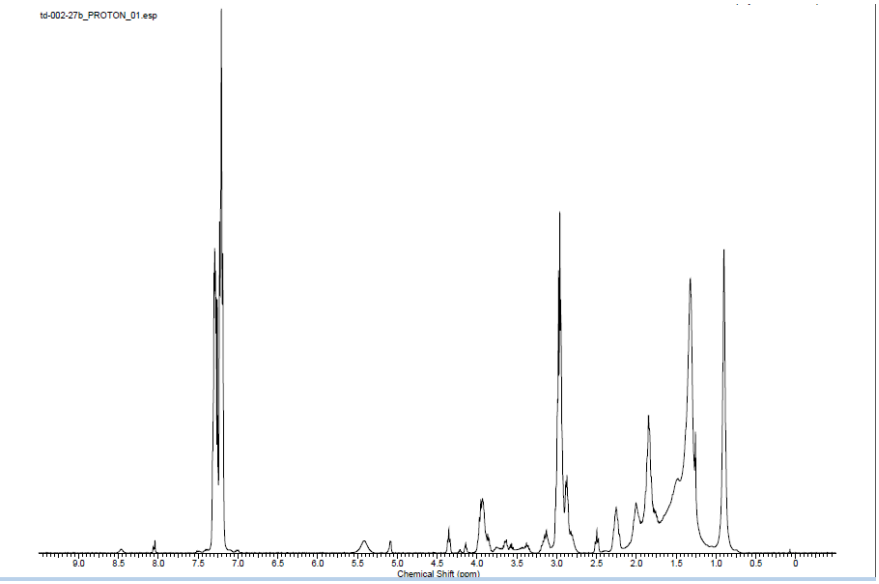

Figure B.18. ^{1}H NMR Spectrum, Au-thiolate generated under inert atmosphere

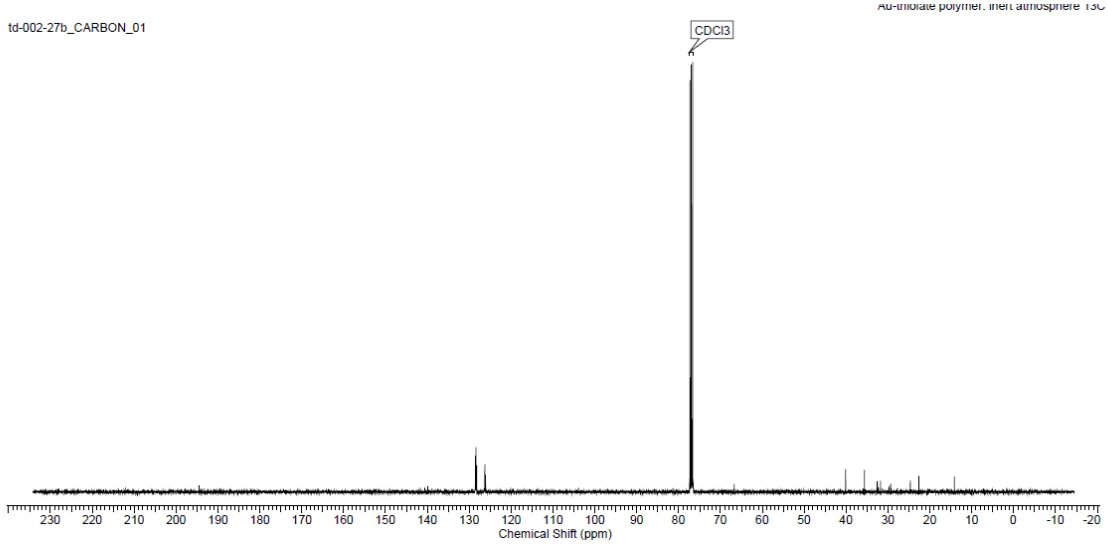

Figure B.19. ^{13}C NMR Spectrum, Au-thiolate generated under inert atmosphere

B.12 Proposed AIBN-initiated etching mechanism

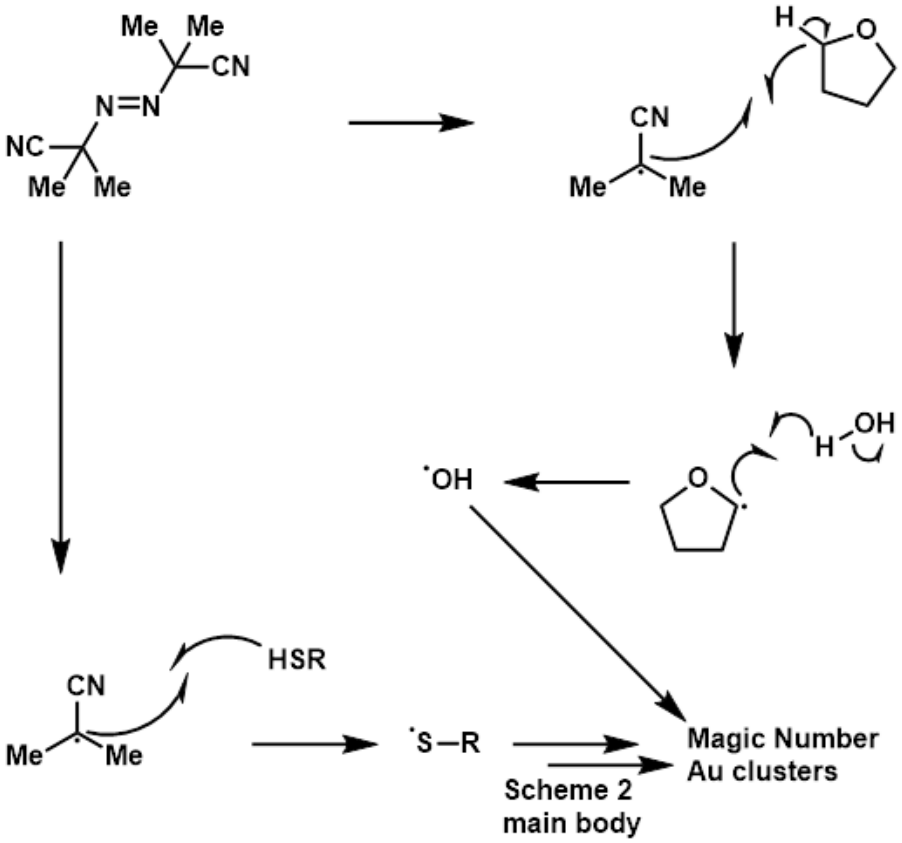

Figure B.20. Proposed AIBN-initated etching mechanism

B.13 ESR Method & Spectrum

ESR Reaction Procedure

The $Au_{25}(PET)_{18}$ synthesis was undertaken as described above on a 100 mg scale. After addition of the aqueous sodium borohydride solution, the reaction was allowed to reduce for 3.5 hrs at which point an aliquot (25% of the organic reaction volume, 1.75 mL) was removed. To this aliquot 0.148 mL of DMPO were added, and the mixture was stirred for 15 minutes at room temperature to allow radical trapping to occur. MeOH was then added to a total volume of 15 mL and in soluble Au-thiol oligomers were removed via centrifugation. The supernatant was

concentrated under vacuum and the residue dissolved in 0.800 mL 1:1 CH_2Cl_2:$ClCH_2CH_2Cl$. Upon solvent addition, more oligomer precipitated, and the sample was filtered into an NMR tube.

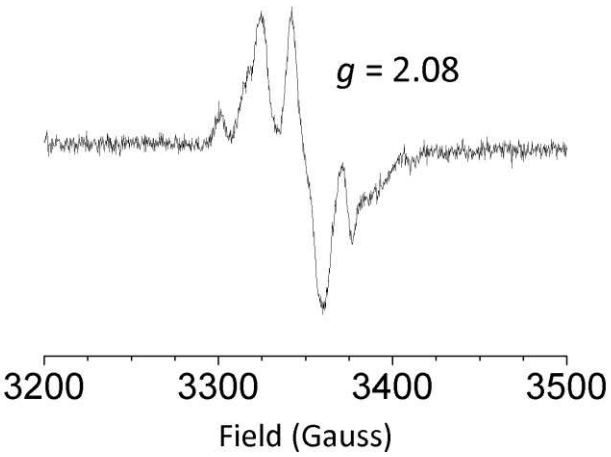

Figure B.21. EPR spectrum of DMPO adduct recorded at 108 K in 1:1 CH_2Cl_2:$ClCH_2CH_2Cl$. A full field scan was performed which did not indicate any other responses.

REFERENCES

1. Sitaula, S.; Mackiewicz, M. R.; Reed, S. M. Gold nanoparticles become stable to cyanide etch when coated with hybrid lipid bilayers. *Chem. Commun.* **2008**, 3013-3015.

2. Parker, J. F.; Weaver, J. E. F.; McCallum, F.; Fields-Zinna, C. A.; Murray, R. W. Synthesis of monodisperse [Oct4N+][Au25(SR)18-] nanoparticles, with some mechanistic observations. *Langmuir* **2010**, *26*, 13650-13654.

APPENDIX C: SUPPLEMENTARY TO CHAPTER 4

C.1 General Procedures

UV/Vis spectra were collected on an HP 8452A Diode Array Spectrophotometer in the case of colloidal nanoparticle etching and on a ThermoFisher NanoDrop spectrophotometer in all other cases, except where otherwise noted. Data were analyzed using Microsoft Excel, with calibration curves constructed using the built-in linear regression function. Spectra were constructed from the raw data in either OriginLab for the main text or Excel for the Supplementary Information. Polyacrylamide Gel Electropheresis was performed on 20% Acrylamide (19:1 acrylamide:bisacrylamide) gel at 125 V for 3 hrs in TBE (1X) buffer except where otherwise noted. Water was degassed by placing in a sealed vessel and sparging for 24-48 hours with Ar. Anyhydrous, degassed methanol was purchased packed under nitrogen in a SureSeal from Sigma-Aldrich. Air-free experiments were performed using standard Schlenk techniques. All materials were purchased from commercial suppliers and used without further purification. 5 nm AuNPs from Ted Pella were used in the etching experiments (Product number: 82150-5).

C.2 Synthesis of Au_{102}(*p*-MBA)$_{44}$

$HAuCl_4 \cdot 3H_2O$ (100 mg, 0.254 mmol, 1.00 equiv) was dissolved in 27.5 mL nanopure water in a 250 mL round-bottom flask equipped with a magnetic stir bar. To this a solution of *para*-mercaptobenzoic acid (*p*-MBA, 119.8 mg, 0.762 mmol, 3.00 equiv) and NaOH (116.6 mg, 2.92 mmol, 11.48 equiv) in 9 mL nanopure water was added at room temperature, followed immediately by 37.5 mL of methanol. The reaction was allowed to stir at room temperature for 1 hr, over the course of which the solution turned from dark orange to light yellow/orange. After 1 hr, powdered $NaBH_4$ (10.4 mg, 0.275 mmol, 1.08 equiv) were added as a solid. Upon addition reaction turned black, accompanied by substantial outgassing. Reaction was stirred overnight after addition of

sodium borohydride (c.a. 12-18 hrs), then poured into a 500 mL Erlenmeyer flask. Reaction was then diluted to ~400 mL total volume by addition of MeOH, followed by addition of ~ 25 mL 5 M aqueous NH_4OAc. This reaction mixture was split equally into to 50 mL conical centrifuge tubes, with each tube diluted to a total volume of 50 mL using MeOH. Resulting solids were isolated by centrifugation (4000 rpm, 10 minutes, 4 ºC) and the supernatant was discarded. The precipitate was then redissolved in a minimal amount of 2 M aqueous NH_4OAc and combined into two 50 mL conical centrifuge tubs. Each tube was diluted to 50 mL total solvent volume with MeOH and resulting solids were again isolated by centrifugation. Product was then dissolved in minimal 1:1 water:glycerol and purified by PAGE under conditions described above. Isolated bands were crushed & soaked from the gel, filtered, then lyophilized to yield Au_{102}(*p*-MBA)$_{44}$. Yield based on Au atoms typically < 30%.[1-3]

C.3 Synthesis of $Au_{25}(Capt)_{18}$

Procedure largely adapted from the literature, but is described briefly here.[4]

$HAuCl_4 \cdot 3H_2O$ (78.7 mg, 0.25 mmol, 1.00 equiv) was dissolved in 10 mL MeOH along with tetraoctylammonium bromide (TOAB, 126.8 mg, 0.23 mmol, 0.92 equiv) in a 250 mL round bottom flask under ambient atmosphere. The resulting red solution was allowed to stir for 20 min at room temperature to ensure complete dissolution of the starting material. A solution of captopril (217.2 mg, 1.00 mmol, 4.00 equiv) in 5 mL MeOH was added in one portion, resulting in a white precipitate almost immediately upon addition. This suspension was stirred a further 30 minutes at room temperature. After this time, a solution of $NaBH_4$ (75.6 mg, 2.00 mmol, 8 equiv) in 5 mL cold, nanopure water was added in one portion. The reaction turned black immediately upon addition of sodium borohydride, and this black reaction mixture was allowed to stir at room temperature overnight (typically 8-12 hours). The crude reaction mixture was then centrifuged (4000 rpm, 10 minutes, 4 ºC) and the supernatant was isolated. Supernatant was then concentrated

to approximately half of its volume, placed in a 50 mL conical centrifuge tube, and diluted to 50 mL total volume with EtOH. Resulting precipitate was again collected by centrifugation, then washed with several portions of EtOH. Resulting product spectra comported with the literature optical spectra.[5] Spectra shown below. Yield typically 40% based on Au atoms.

C.4 Synthesis of $Au_{25}(SG)_{18}$

$HAuCl_4 \cdot 3H_2O$ (100 mg, 0.254 mmol, 1 equiv) were added to a 250 mL round bottom flask under ambient atmosphere and dissolved in 50 mL MeOH with stirring. After complete dissolution of Au salt, the vessel was cooled in an ice bath and glutathione (GSH, 312.24 mg, 1.016 mmol, 4 equiv) was added as a solid. The solution immediately turned from deep red to light yellow and a white suspension resulted. This suspension was allowed to stir at 0 ºC for approximately 30 minutes until it was colorless and homogeneous. $NaBH_4$ (94.6 mg, 2.50 mmol, 9.84 equiv) dissolved in 12.5 mL ice cold nanopure water was added all in one portion, causing the reaction mixture to immediately turn black and vigorously outgas. Reaction was allowed to stir a further hour at 0 ºC, then diluted to a total reaction volume of 100 mL using methanol. Reaction was then split into two 50 mL conical centrifuge tubes and the precipitate was isolated by centrifugation (4000 rpm, 10 minutes, 4 ºC). Resulting black solid was dried under vacuum and purified by PAGE using 22% acrylamide gel (19:1 acrylamide/bisacrylamide) in TBE buffer at 125 V. Isolated orange band was crushed and soaked out of the gel, filtered, then lyophilized to give $Au_{25}(SG)_{18}$ as an orange solid.

C.5 Airfree Attempts at Synthesis of Au_{102}(p-MBA)$_{44}$

$HAuCl_4 \cdot 3H_2O$ (100 mg, 0.254 mmol, 1 equiv) was placed in a 250 mL round bottom flask equipped with a magnetic stir bar. Vessel was sealed with a septum and evacuated for at least 10 minutes. Flask was then backfilled with Ar and 27.5 mL of degassed, nanopure water were added by syringe. In a separate 50 mL round bottom flask, NaOH (116.6 mg, 2.92 mmol, 11.48 equiv)

and *p*-MBA (119.8 mg, 0.762 mmol, 3.00 equiv) were placed under Ar atmosphere similarly. To the solid NaOH & *p*-MBA 9 mL of degassed, nanopure water were added by syringe. The flask was shaken until all solids were in solution, and the resulting basic *p*-MBA solution was transferred to the aqueous Au solution. After addition of *p*-MBA, 37.5 mL of degassed, anhydrous MeOH were added by syringe. The resulting solution was allowed to stir at ambient temperature for approximately 1 hr. $NaBH_4$ (10.6 mg, 0.279 mmol, 1.10 equiv) was added as a powder while the vessel was maintained under a constant stream of argon. After addition of sodium borohydride reaction was allowed to stir at room temperature overnight (12-18 hrs). The airfree synthesis resulted in large colloids after the workup described in the standard synthesis.

C.6 General Procedure for Radical Initiated Synthesis of Au_{102}(*p*-MBA)$_{44}$

Except where otherwise noted, the procedure for air-free Au_{102} synthesis was followed. Radical initiators were added contemporaneously with sodium borohydride as solids. Gel images of the resulting products can be found below in the PAGE section of the ESI. Where noted, in order to achieve clearer gel images, crude products were fractionally precipitated according to a procedure first reported by Kornberg, briefly described below.[6]

Fractional precipitation: Pellets from the work-up described above in the standard Au_{102} synthesis were fractionally precipitated prior to evaluation by PAGE. The pellets were dissolved into a total volume of 18.8 mL nanopure water, followed by addition of 1.2 mL 5 M aqueous NH_4OH to give a total overall concentration of 0.12 M NH_4OH. This 50 mL volume was then centrifuged to give a pellet (0) and the resulting supernatant was split into to 25 mL portions. Sufficient MeOH was added to a total volume of 50 mL and sufficient 5 M aqueous NH_4OH was added to give ~ 0.12 M solutions in NH_4OH. These fractions were again centrifuged to yield pellets (1) and this second splitting & dilution step was repeated until the supernatant was colorless. Each resulting pellet was then dissolved in 1:1 glycerol:water and evaluated on PAGE.

C.7 Radical Initiators Used for Au_{102}(*p*-MBA)$_{44}$ Synthesis

4-hydroxy-TEMPO: 0, 0.5, 1.0 and 4.0 equiv to Au

Azobiscyanovaleric acid (ABCVA): 0, 0.5, 1.0, and 4.0 equiv to Au

Sodum Persulfate (Na2S2O8): 0, 0.5, 1.0, and 4.0 equiv to Au

Oxone: 0, 0.04, 0.40, 2.0, and 4.0 equiv to Au (calculated based on 1.6% oxygen content)

C.8 Inert Atmosphere Polymer Formation

Inert Atmosphere – In a 250 mL round-bottom flask, roughly 200 mL of nanopure water was degassed via freeze/pump/thaw (3 cycles) then back-filled to argon. In a separate 250 mL round-bottom flask, the same volume of methanol was degassed via freeze/pump/thaw (3 cycles) and back-filled to argon. In a third 250 mL round-bottom flask fitted with a septum and equipped with a stir bar $HAuCl_4 \cdot 3H_2O$ (0.209 g, 0.50 mmol) was placed under inert atmosphere by placing the flask under vacuum for 10 min then back-filling with argon. To the flask containing $HAuCl_4 \cdot 3H_2O$ 19.0 mL of the degassed nanopure water was added via syringe and the vessel was stirred at room temperature. In a 100 mL round-bottom flask, *p*-mercaptobenzoic acid (0.292 g, 1.89 mmol) was suspended in 18.43 mL of degassed nanopure water. To this suspension 10 M NaOH (0.57 mL, 5.70 mmol) was added and the flask was again freeze/pump/thawed (3 cycles) then back-filled to inert atmosphere. An additional 51.5 mL of degassed nanopure water was added to the Au solution via syringe, followed by addition of the *p*-MBA solution via syringe. This was followed immediately after by addition of 75 mL degassed MeOH, also by syringe. The solution was allowed to stir at room temperature for approximately 1 hr until the solution color changed from dark to light orange before proceeding to the next step.

C.9 Oxygen Atmosphere Polymer Formation

In a 250 mL round-bottom flask, roughly 200 mL of nanopure water was oxygenated by sparging for 30 minutes, this was then sealed with a septum and equipped with an oxygen-filled

balloon to maintain the oxygen environment. In a separate 250 mL round-bottom flask, roughly the same volume of methanol was oxygenated by sparging for 30 minutes, this was then sealed with a septum and equipped with an oxygen balloon to maintain the atmosphere. In a third 250 mL round-bottom flask fitted with a septum and equipped with a stir bar $HAuCl_4 \cdot 3H_2O$ (0.209 g, 0.50 mmol) was placed under oxygen atmosphere by placing the flask under vacuum for 10 min then back-filling with oxygen, then fitted with an oxygen balloon to maintain the atmosphere. To this flask 19.0 mL of the oxygenated nanopure water were added by syringe. In a 100 mL round-bottom flask, *p*-mercaptobenzoic acid (0.292 g, 1.89 mmol) was suspended in 18.43 mL of oxygenated nanopure water. To this suspension 10 M NaOH (0.57 mL, 5.70 mmol) was added and the flask was again freeze/pump/thawed (3 cycles) then back-filled to inert atmosphere. An additional 51.5 mL of oxygenated nanopure water was added to the Au solution via syringe, followed by addition of the *p*-MBA solution via syringe. This was followed immediately after by addition of 75 mL oxygenated MeOH, also by syringe. The solution was allowed to stir at room temperature for approximately 1 hr until the solution color changed from dark to light orange before proceeding to the next step.

C.10 Ambient Atmosphere Polymer Formation

To form the polymer under ambient atmosphere the standard synthesis described above was followed.

C.11 Crossover Experiments

After 1 hr stirring at room temperature each of the polymers resulting from syntheses described above were divided into four portions of equal volume. One portion was concentrated to solid by lyophylization. The remaining portions were carried on to the borohydride reduction as described below.

Ar polymer – Ar reduction: To the portion of the polymer synthesized under Ar which was left in the inert-atmosphere round-bottom flask, pulverized solid $NaBH_4$ (5.2 mg, 0.14 mmol, 1.1 equiv.) was added all at once as a constant stream of argon ran into the flask. The reaction turned a very dark brown or black immediately, and was allowed to stir at room temperature overnight under inert atmosphere. After stirring over night the reaction was worked-up as described in the Au_{102} synthesis above.

Ar polymer – O_2 reduction: A portion of the Ar-synthesized polymer was removed from the 250 mL round-bottom flask via syringe (this amounted to 25% of the total reaction volume) and placed in 100 mL round-bottom flask which had been purged to an oxygen atmosphere by evacuating under vacuum and back-filling with oxygen, then equipped with a stir bar. The reaction was allowed to stir under oxygen atmosphere for 15 minutes prior to addition of reductant. To this portion of the reaction, pulverized solid $NaBH_4$ (5.2 mg, 0.14 mmol, 1.1 equiv.) was added all at once as a constant stream of oxygen ran into the flask. The vessel was then sealed, fitted with an oxygen balloon, and allowed to stir overnight under an oxygen atmosphere. After overnight stirring, the reaction was worked up as described above. It should be noted that the reaction turned black upon addition of reductant.

Ar polymer – ambient reduction: A portion of the Ar-synthesized polymer was removed from the 250 mL round-bottom flask and placed in a 125 mL erlenmeyer that was open to the ambient atmosphere. This was allowed to stir for 15 minutes under ambient atmosphere prior to addition of reductant. To this pulverized solid $NaBH_4$ (5.2 mg, 0.14 mmol, 1.1 equiv.) was added all at once. The reaction turned black upon borohydride addition, and was allowed to stir open to the ambient atmosphere overnight, then worked-up as described above.

O_2 polymer - O_2 reduction: To the portion of the polymer synthesized under O_2 which was left in the inert-atmosphere round-bottom flask, pulverized solid $NaBH_4$ (5.2 mg, 0.14 mmol, 1.1 equiv.) was added all at once as a constant stream of oxygen ran into the flask. The reaction turned a very dark brown or black immediately, and was allowed to stir at room temperature overnight under an oxygen atmosphere. After stirring over-night the reaction was worked-up as described in the Au_{102} synthesis above.

O_2 polymer – Ar reduction: A portion of the O_2-synthesized polymer was removed from the 250 mL round-bottom flask via syringe (this amounted to 25% of the total reaction volume) and placed in 100 mL round-bottom flask which had been purged to an argon atmosphere by evacuating under vacuum and back-filling with argon, then equipped with a stir bar. The reaction was then sparged for 10 minutes to remove oxygen from solution. To this portion of the reaction, pulverized solid $NaBH_4$ (5.2 mg, 0.14 mmol, 1.1 equiv.) was added all at once as a constant stream of argon ran into the flask. The vessel was then sealed, and allowed to stir over-night under an inert atmosphere. After overnight stirring, the reaction was worked up as described above. It should be noted that the reaction turned black upon addition of reductant.

O_2 polymer – ambient reduction: A portion of the O_2-synthesized polymer was removed from the 250 mL round-bottom flask via syringe (this amounted to 25% of the total reaction volume) and placed in 125 mL Erlenmeyer flask which was open to the ambient atmosphere and equipped with a stir bar. This reaction was allowed to stir for 15 minutes prior to addition of the reductant. To this portion of the reaction, pulverized solid $NaBH_4$ (5.2 mg, 0.14 mmol, 1.1 equiv.) was added all at once and the reaction was allowed to stir overnight under an inert atmosphere. After overnight stirring, the reaction was worked up as described above. It should be noted that the reaction turned black upon addition of reductant.

C.12 Airfree Synthesis of $Au_{25}(Capt)_{18}$

Procedure broadly similar to the $Au_{25}(Capt)_{18}$ synthesis as described above, modified as follows. $HAuCl_4 \cdot 3H_2O$ (78.7 mg, 0.25 mmol, 1.00 equiv) and TOAB (126.8 mg, 0.23 mmol, 0.92 equiv) were added to a 250 mL RBF equipped with a magnetic stir bar, sealed with a septum, and evacuated using a hi-vacuum pump for at least 10 minutes. The flask was then back-filled with Argon. To this flask, 50 mL anhydrous & degassed methanol (purchased from Sigma-Aldrich in a SureSeal) was added via syringe. The resulting red solution was allowed to stir for 20 min at room temperature to ensure complete dissolution of the starting material. Captopril (217.2 mg, 1.00 mmol, 4.00 equiv) was added to a separate 25 mL RBF and degassed similarly to the gold salt above. 5 mL degassed MeOH was added in one portion via syringe and the suspension was sonicated to dissolve the captopril. The resulting captopril solution was added to the solution of gold via cannula. This resulted, almost immediately, in formation of a white precipitate. This suspension was stirred for a further 30 minutes at room temperature. $NaBH_4$ (75.6 mg, 2.00 mmol, 8 equiv) was added to another 25 mL RBF and degassed similarly. Borohydride was then dissolved in 5 mL degassed water, chilled to 0 ºC, and added to the gold-captopril suspension via syringe. The reaction turned black immediately upon addition of sodium borohydride, and this black reaction mixture was allowed to stir at room temperature overnight (typically 8-12 hours). The crude reaction mixture was then centrifuged (4000 rpm, 10 minutes, 4 ºC) and the supernatant was isolated. Supernatant was then concentrated to approximately half of its volume, placed in a 50 mL conical centrifuge tube, and diluted to 50 mL total volume with EtOH. Resulting precipitate was again collected by centrifugation, then washed with several portions of EtOH. Resulting product spectra comported with the literature optical spectra.

C.13 Airfree Synthesis of $Au_{25}(SG)_{18}$

$HAuCl_4 \cdot 3H_2O$ (100 mg, 0.254 mmol, 1 equiv) was added to a 250 mL round bottom flask equipped with magnetic stir bar and the flask was evacuated, then back-filled to argon atmosphere. 25 mL anhydrous & degassed MeOH was added via syringe and the solution was stirred. In a separate RBF glutathione (GSH, 312.24 mg, 1.016 mmol, 4 equiv) was placed under argon atmosphere, then dissolved in 25 mL degassed MeOH. The gold solution was chilled to 0 ºC in an ice bath and the GSH solution was added via cannula. The solution immediately turned from deep red to light yellow and a white suspension resulted. This suspension was allowed to stir at 0 ºC for approximately 30 minutes until it was colorless and homogeneous. $NaBH_4$ (94.6 mg, 2.50 mmol, 9.84 equiv) was placed in a separate RBF, similarly placed under Ar atmosphere, and dissolved in 12.5 mL ice cold nanopure degassed water. The resulting $NaBH_4$ solution was added to the Au-SG solution via syringe, causing the reaction mixture to immediately turn black and vigorously outgas. Reaction was allowed to stir a further hour at 0 ºC, then diluted to a total reaction volume of 100 mL using methanol. Reaction was then split into two 50 mL conical centrifuge tubes and the precipitate was isolated by centrifugation (4000 rpm, 10 minutes, 4 ºC). Resulting black solid was dried under vacuum and purified by PAGE using 22% acrylamide gel (19:1 acrylamide/bisacrylamide) in TBE buffer at 125 V. Isolated orange band was crushed and soaked out of the gel, filtered, then lyophilized.

C.14 Radical Initiators for $Au_{25}(Capt)_{18}$ Synthesis

In each case the procedure above for airfree synthesis was followed, with the radical initiator added as a solution in water contemporaneously with sodium borohydride. In those cases, borohydride was dissolved in 2.5 mL degassed water, and the radical initiator was dissolved in 2.5 mL degassed water to maintain a constant reaction volume.

Table C.1. Radical Initiators in $Au_{25}(Capt)_{18}$ Synthesis

entry	initiator	mmol	amt	equiv
1	4-hydroxy-TEMPO	0.2	34.5 mg	1
2	ABCVA	0.2	56.1 mg	1
3	Ammonium Persulfate	0.2	45.6 mg	1
4	Oxone (1.6% O_2)	0.773 (O_2)	1.54 g	3.87 (O_2)
5	Sodium Percarbonate	0.2	31.4 mg	1
6	Sodium Persulfate	0.2	47.6 mg	1

4-Hydroxy-TEMPO: Gave desired product

Azobiscyanovaleric acid (ABCVA): gave desired product

Ammonium Persulfate: gave featureless optical spectrum

Oxone: returned an orange solid that was largely insoluble

Sodium Percarbonate: gave plasmonic particles

Sodium Persulfate: gave featureless optical spectrum

C.15 Radical Initiators for $Au_{25}(SG)_{18}$ Synthesis

Similar to the radical initiation procedure for the captopril-ligated clusters, the radical initiator was added at the same time as the borohydride. In each case the radical initiator was dissolved in 6.25 mL of degassed water after being placed under argon as described above. Sodium borohydride was dissolved in 6.25 mL degassed water as described above, and the two solutions were added simultaneously to the gold-glutathione polymer by syringe.

Table C.2. Radical Initiators used for $Au_{25}(SG)_{18}$ Synthesis

entry	initiator	mmol	amt	equiv
1	4-Hydroxy-TEMPO	0.2	34.5 mg	1
2	ABCVA	0.2	56.1 mg	1
3	Oxone monopersulfate	0.2	61.5 mg	1
4	Oxone TBA salt		500 mg	

4-Hydroxy-TEMPO: Gave $Au_{25}(SG)_{18}$

ABCVA: Gave $Au_{25}(SG)_{18}$

Oxone monopersulfate: $Au_{25}(SG)_{18}$

Oxone TBA: Did not give desired product

C.16 Etching of 5 nm Aqueous AuNP in O_2 Atmosphere

A suspension of 5 nm colloidal gold in water (1 mL, 0.05 mg Au / mL) was placed in an air free cuvette. This solution was sparged for 10 s with pure oxygen, and the cuvette was sealed. Separately a solution of thioglycolic acid (17.4 μL, 0.253 mmol, 1000 equiv to Au) in 1 mL of nanopure water was made and sparged for 10 s with oxygen, the cuvette was opened under a constant stream of oxygen, and the thioglycolic acid solution was added in one portion and the cuvette was sealed. The cuvette sidearm was fitted with an oxygen balloon and the valve was opened slightly to maintain 1 atm oxygen pressure in the head space. The cuvette was placed in the spectrophotometer and a UV/Vis spectrum was collected every 5 min for a period of 1.5 hr. Spectra were exported to Excel and evaluated therein.

C.17 Etching of 5 nm Aqueous AuNP in Ar Atmosphere

A suspension of 5 nm colloidal gold in water (1 mL, 0.05 mg Au / mL) was placed in a 2-dram vial and deoxygenated by sparging with argon for 5 minutes. Separately, a solution of thioglycolic acid (17.4 μL, 0.253 mmol, 1000 equiv to Au) in 1 mL of nanopure water was freeze/pump/thawed (3 x) then backfilled to Ar. An airfree cuvette was purged with Ar for 10 minutes, and with a constant stream of argon the Au suspension was transferred, followed by addition of the thioglycolic acid solution. The cuvette was placed in the spectrophotometer and a UV/Vis spectrum was collected every 5 min for a period of 1 hr. Spectra were exported to Excel and evaluated therein.

C.18 MALDI Spectra

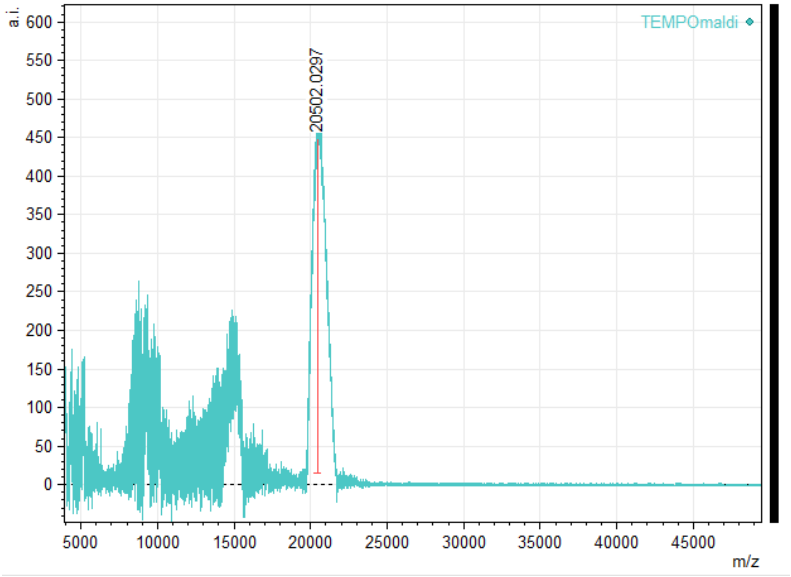

Figure C.1. Au_{102} Synthesis Inert atmosphere with 4-Hydroxy-TEMPO as initiator MALDI Spectrum

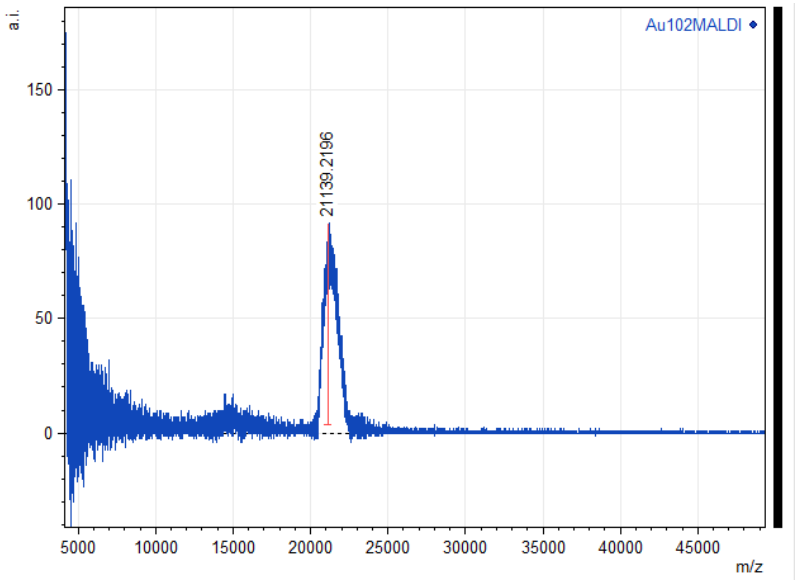

Figure C.2. $Au_{102}(p\text{-}MBA)_{44}$ MALDI Spectrum

C.19 UV/Vis Spectra – Colloidal AuNP

UV/Vis spectra were collected on an HP 8452A Diode Array Spectrophotometer in the case of colloidal nanoparticle etching and on a ThermoFisher NanoDrop spectrophotometer in all other cases. Data were analyzed using Microsoft Excel, with calibration curves constructed using the

built-in linear regression function. Etching of colloidal particles under oxygen atmosphere gave large error across the entire experiment upon first go, and as such was rerun with the data being collected on an Ocean Optics USB4000 Vis/NIR spectrophotometer using an Ocean Optics DT-MINI-2-GS light source. Those spectra were collected using a 40 ms integration time, averaging 30 scans per spectrum, taken automatically every 5 minutes using OceanView software.

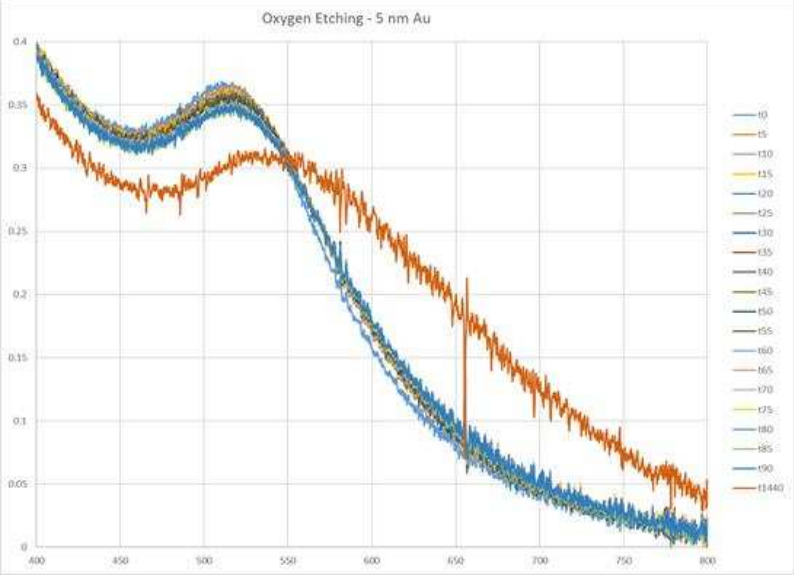

Figure C.3. Etching of Aqueous AuNP under O_2 atmosphere run 1 used in Chapter 4 Figure 4.1

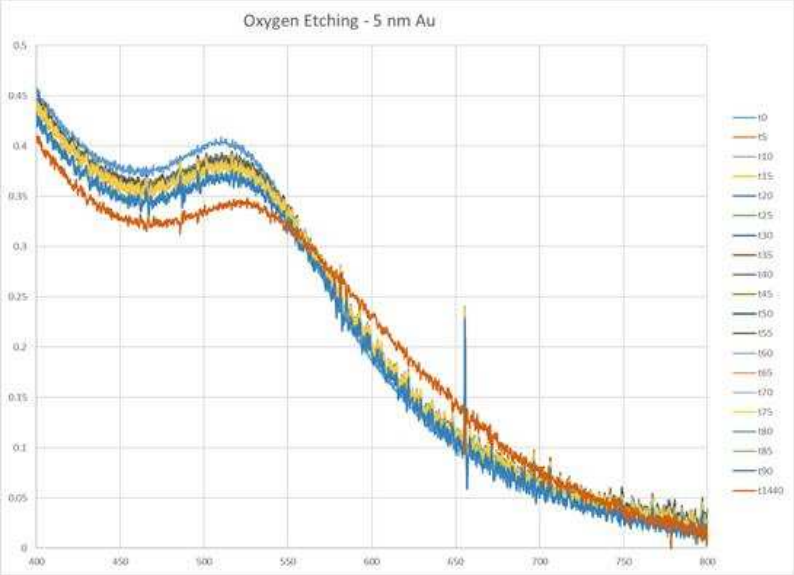

Figure C.4. Etching of Aqueous AuNP under O_2 atmosphere run 2 used in Chapter 4 Figure 4.1

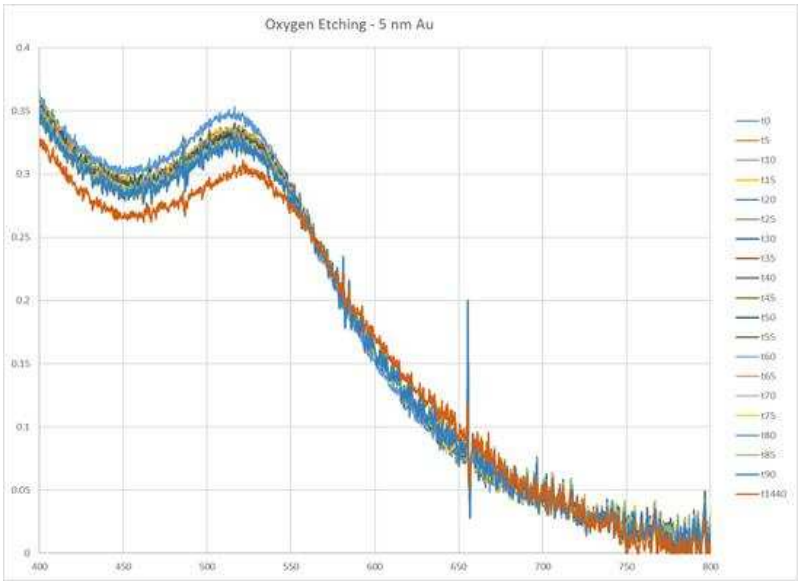

Figure C.5. Etching of Aqueous AuNP under O_2 atmosphere run 3 used in Chapter 3 Figure 4.1

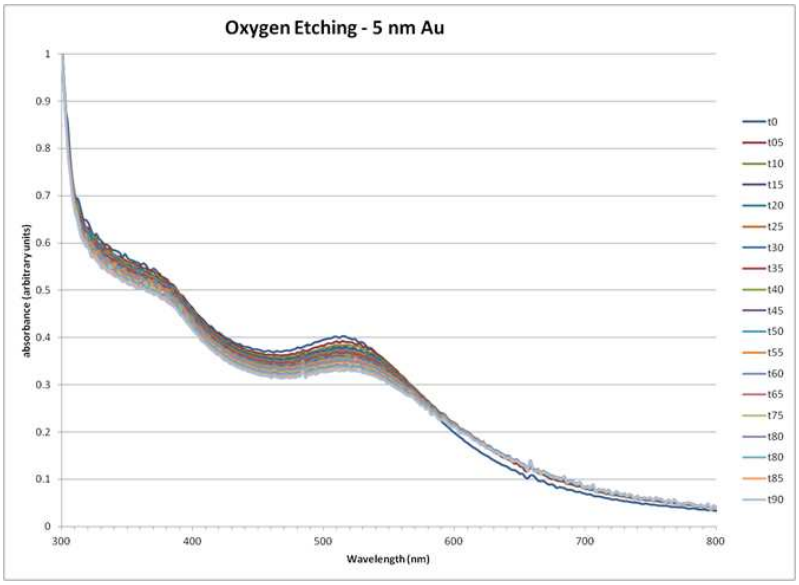

Figure C.6. Etching of Aqueous AuNP under O_2 atmosphere, not used in Chapter 4 Figure 4.1

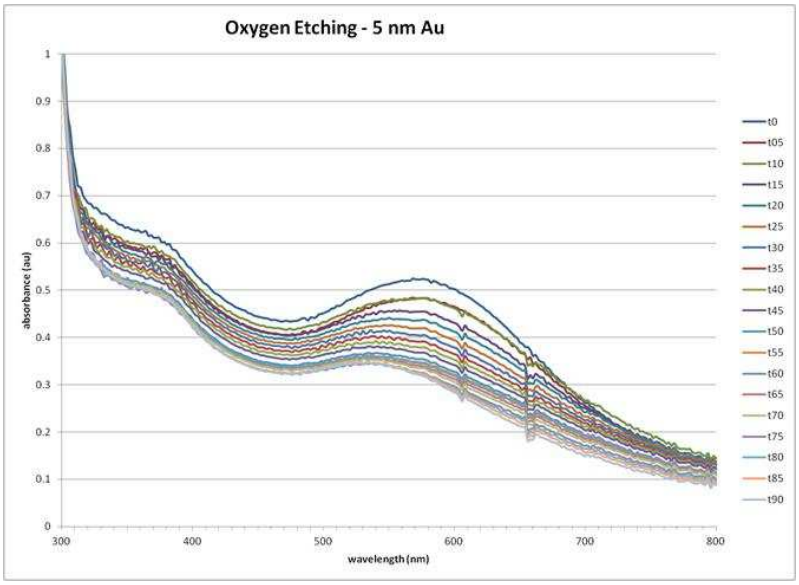

Figure C.7. Etching of Aqueous AuNP under O_2 atmosphere, not used in Chapter 4 Figure 4.1

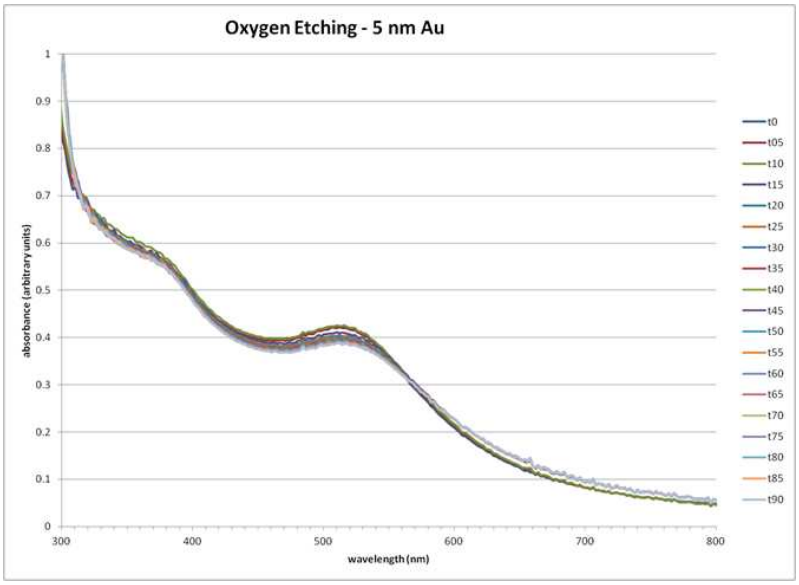

Figure C.8. Etching of Aqueous AuNP under O_2 atmosphere, not used in Chapter 4 Figure 4.1

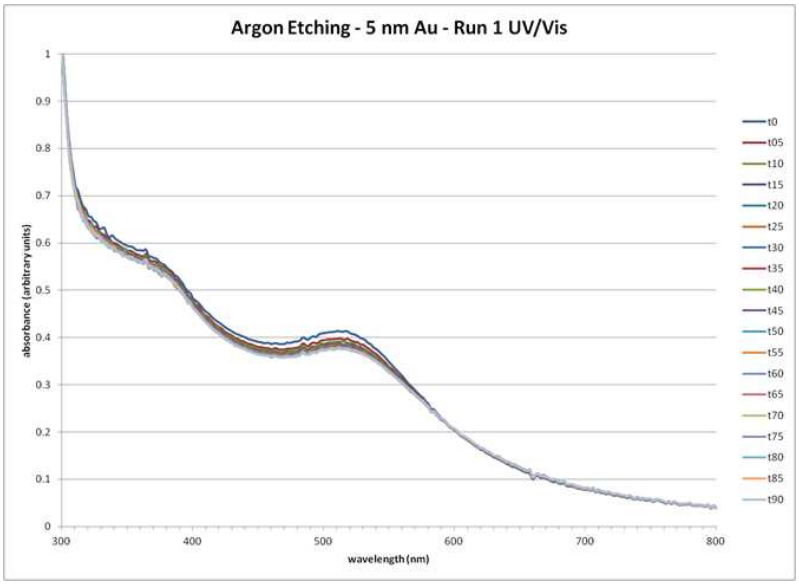

Figure C.9. Etching of Aqueous AuNP under Ar atmosphere, run 1 Chapter 4 Figure 4.1

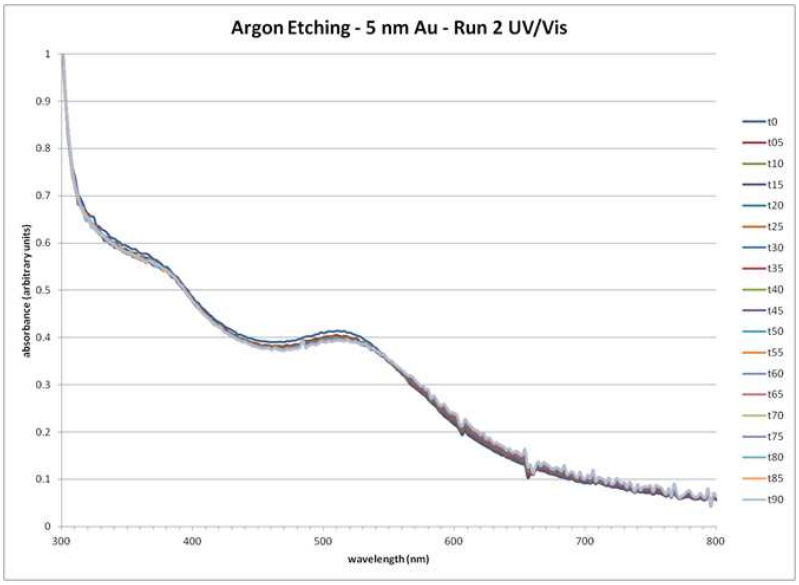

Figure C.10. Etching of Aqueous AuNP under Ar atmosphere, run 2 Chapter 4 Figure 4.1

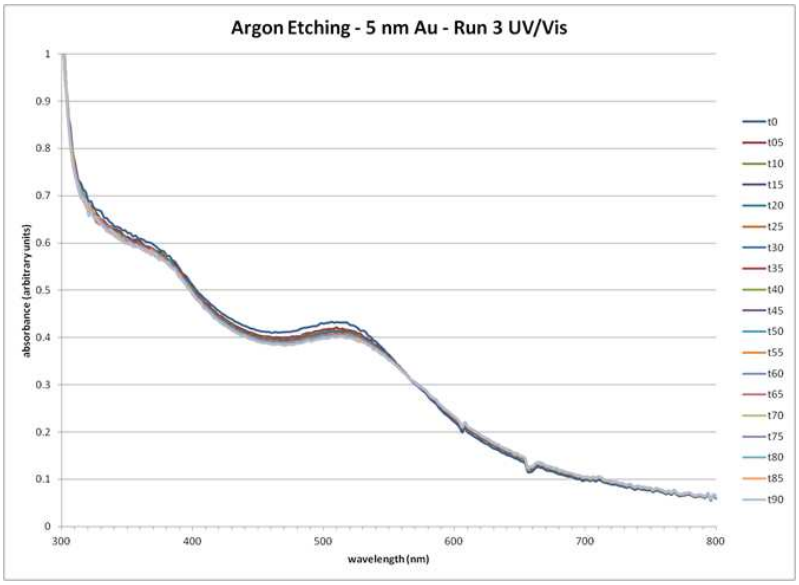

Figure C.11. Etching of Aqueous AuNP under Ar atmosphere, run 3 Chapter 4 Figure 4.1

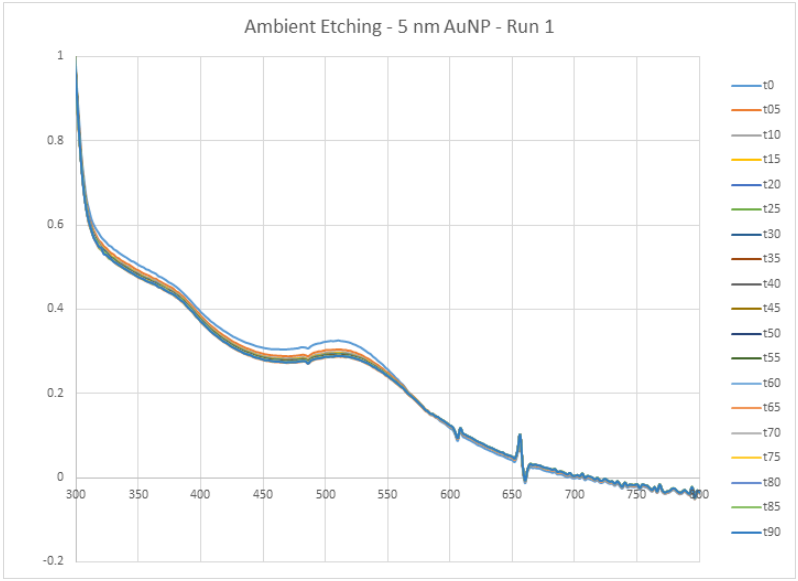

Figure C.12. Etching of Aqueous AuNP under ambient atmosphere, run 1 Chapter 4 Figure 4.1

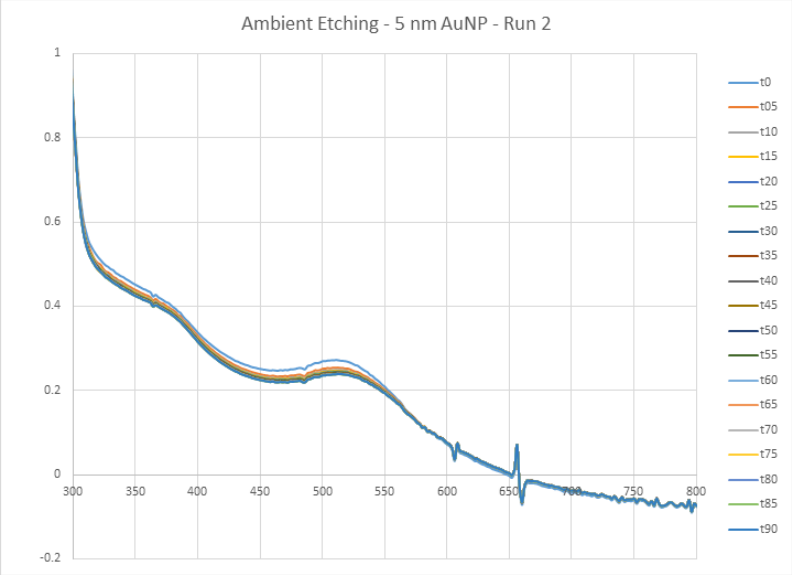

Figure C.13. Etching of Aqueous AuNP under ambient atmosphere, run 2 Chapter 4 Figure 4.1

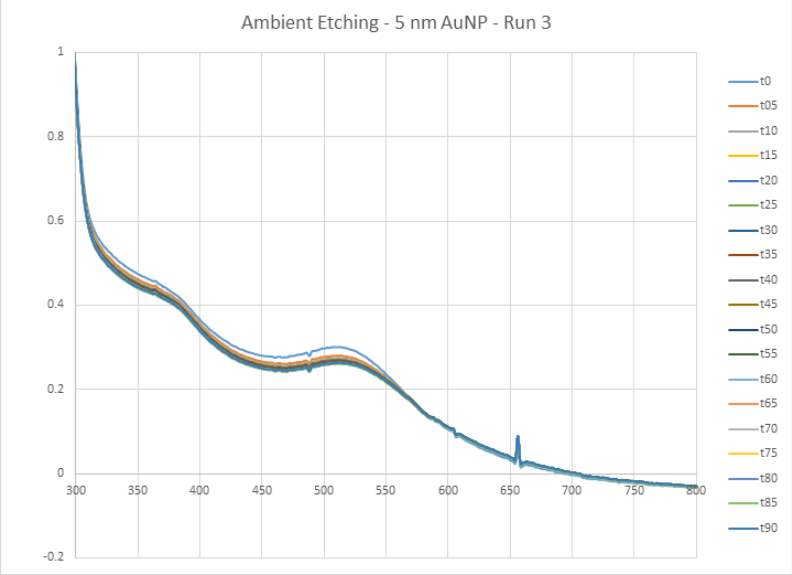

Figure C.14. Etching of Aqueous AuNP under ambient atmosphere, run 3 Chapter 4 Figure 4.1

C.20 Calibration Curves for Aqueous 5 nm AuNP

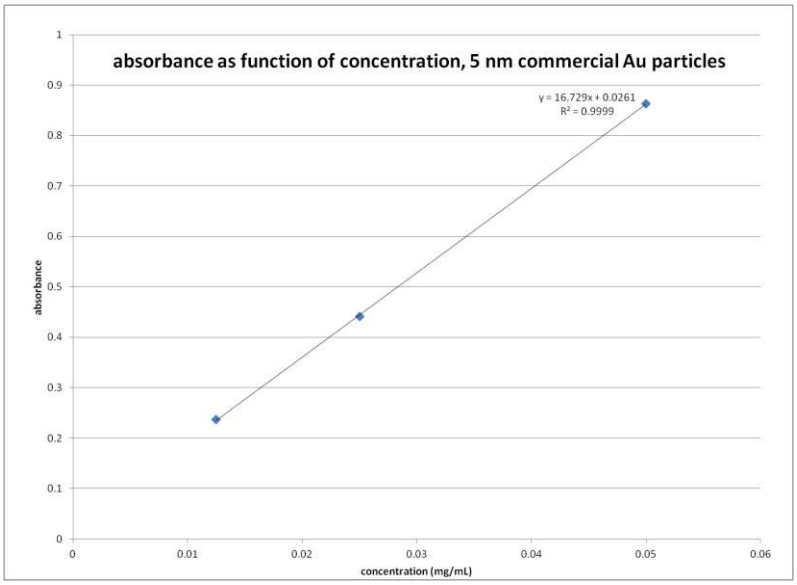

Figure C.15. 5 nm AuNP Calibration, HP 8452A Diode Array Spectrophotometer

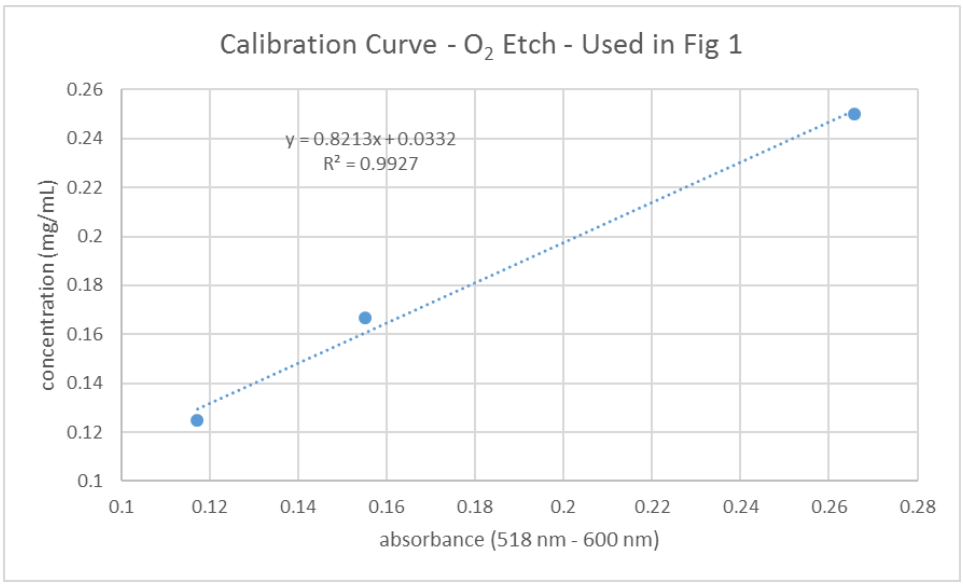

Figure C.16. 5 nm AuNP Calibration, Ocean Optics USB4000

C.21 Tables of Etching Data for 5 nm AuNPs

Table C.3. 518 nm Absorbance (Ambient & Argon atm)

time (min)	Ar - r2	Ar - r3	Amb - r1	Amb - r2	Amb - r3
0	0.4102	0.4316	0.32243	0.26954	0.29817
5	0.4026	0.4165	0.30107	0.2519	0.27775
10	0.4009	0.4149	0.29493	0.2481	0.27288
15	0.4002	0.4131	0.29331	0.24499	0.2703
20	0.3982	0.4111	0.29275	0.24397	0.26892
25	0.3995	0.4087	0.29113	0.24342	0.26692
30	0.3956	0.4068	0.28977	0.24272	0.26637
35	0.3935	0.4073	0.28947	0.24124	0.26548
40	0.3954	0.4044	0.28898	0.24114	0.26452
45	0.3955	0.4066	0.28887	0.24066	0.26393
50	0.3981	0.4054	0.28846	0.23956	0.26324
55	0.3974	0.4056	0.28759	0.23992	0.26316
60	0.396	0.4039	0.28836	0.23944	0.26255
65	0.3964	0.4039	0.28729	0.23912	0.26214
70	0.3953	0.4054	0.28738	0.23881	0.26162
75	0.396	0.4032	0.28738	0.23812	0.26133
80	0.3971	0.4007	0.2873	0.23851	0.26113
85	0.3968	0.3996	0.28776	0.23803	0.26098
90	0.3942	0.3987	0.28727	0.23863	0.26182

Table C.4. 518 nm Absorbance (Initial Oxygen Atm not used in Main Text Fig 1)

time (min)	O2 - r1	O2 - r2	O2 - r3
0	0.4006	0.479	0.4208
5	0.3907	0.4471	0.4196
10	0.3845	0.4534	0.4232
15	0.38	0.4369	0.4086
20	0.3776	0.4251	0.4034
25	0.373	0.415	0.401
30	0.3695	0.4056	0.3992
35	0.3674	0.3958	0.3944
40	0.3647	0.3861	0.3946
45	0.3604	0.3753	0.395
50	0.3608	0.3611	0.3931
55	0.3574	0.3564	0.3921
60	0.3548	0.3563	0.3903
65	0.3501	0.3524	0.3911
70	0.3472	0.3489	0.3878
75	0.3426	0.3435	0.3868
80	0.3384	0.3427	0.3876
85	0.3363	0.3436	0.3872
90	0.3322	0.3453	0.3888

Table C.5. 24 hr Etching Experiments (Ar & O_2)

	O2	Ar
Run 1 - t0	0.3181	0.4262
Run 1 - t24 hr	0.1343	0.376
Run 2 - t0	0.3149	0.4466
Run 2 - t24 hr	0.1815	0.4066
Run 3 - t0	0.3161	0.3817
Run 3 - t24 hr	0.2149	0.3399

C.22 Etching of 5 nm AuNP using Ocean Optics USB4000

As mentioned above, these experiments were re-run owing to the large error in the first set of oxygen etching experiments. However, owing to the HP 8452A having broken beyond repair between the initial experiments and the manuscript submission, we used a recently purchased Ocean Optics USB 4000 spectrophotometer. OceanView software, provided with the instrument, was used to build (via an included wizard) a simple absorbance experiment. Spectra were collected

every 5 minutes for 90 minutes, then again at 24 hrs (1440 min) for each run. The instrument was set at an integration time of 40 ms and 30 scans were averaged per spectrum. Concentrations were again determined using an external calibration curve, shown above. As can be seen from the spectra, some change in the plasmon peak is evident. In order to account for this, we used the difference between the initial maximum at 518 nm and the 600 nm absorbance. This was done for both the calibration and etching experiments. Raw data for these experiments is presented below.

Table C.6. Etching of 5 nm AuNP, USB4000, run 1

time	600.106 nm	518.418 nm	DIFF
0	0.1574	0.3649	0.2075
5	0.1694	0.3604	0.191
10	0.1717	0.3597	0.188
15	0.174	0.3588	0.1848
20	0.1747	0.355	0.1803
25	0.1757	0.3547	0.179
30	0.1753	0.3523	0.177
35	0.1758	0.3558	0.18
40	0.1777	0.3513	0.1736
45	0.177	0.3519	0.1749
50	0.1774	0.3503	0.1729
55	0.1774	0.3507	0.1733
60	0.1771	0.3516	0.1745
65	0.1781	0.3509	0.1728
70	0.1772	0.3493	0.1721
75	0.1802	0.3514	0.1712
80	0.1798	0.3484	0.1686
85	0.1786	0.3472	0.1686
90	0.1794	0.348	0.1686
1440	0.2595	0.3023	0.0428

Table C.7. Etching of 5 nm AuNP, USB4000, run 2

time	518.418 nm	600.106 nm	DIFF
0	0.3965	0.1856	0.2109
5	0.3846	0.1945	0.1901
10	0.3885	0.1974	0.1911
15	0.3849	0.1994	0.1855
20	0.388	0.1998	0.1882
25	0.3833	0.1996	0.1837
30	0.3845	0.2001	0.1844
35	0.3852	0.2008	0.1844
40	0.3821	0.1998	0.1823
45	0.3818	0.2003	0.1815
50	0.3805	0.1999	0.1806
55	0.3785	0.2009	0.1776
60	0.3789	0.2018	0.1771
65	0.3757	0.2019	0.1738
70	0.3788	0.2017	0.1771
75	0.3772	0.2016	0.1756
80	0.3662	0.1918	0.1744
85	0.371	0.192	0.179
90	0.3664	0.1931	0.1733
1440	0.3399	0.229	0.1109

Table C.8. Etching of 5 nm AuNP, USB4000, run 3

time	518.418 nm	600.106 nm	DIFF
0	0.3472	0.1508	0.1964
5	0.3381	0.1584	0.1797
10	0.334	0.1592	0.1748
15	0.3348	0.1596	0.1752
20	0.3336	0.1592	0.1744
25	0.3323	0.1589	0.1734
30	0.3336	0.1615	0.1721
35	0.331	0.1594	0.1716
40	0.3288	0.1594	0.1694
45	0.3317	0.1584	0.1733
50	0.3282	0.1593	0.1689
55	0.3259	0.1586	0.1673
60	0.3246	0.1589	0.1657
65	0.3262	0.159	0.1672
70	0.3255	0.1603	0.1652
75	0.3281	0.159	0.1691
80	0.3278	0.1596	0.1682
85	0.3265	0.1607	0.1658
90	0.3236	0.1582	0.1654
1440	0.3022	0.1709	0.1313

C.23 $Au_{25}(Capt)_{18}$ UV/Vis Spectra

Normalized spectra have been adjusted such that absorbance at 400 nm = 1

On each of Figure C.17 – C.30, the x-axis is wavelength in nanometers and the y-axis is absorbance in absorbance units.

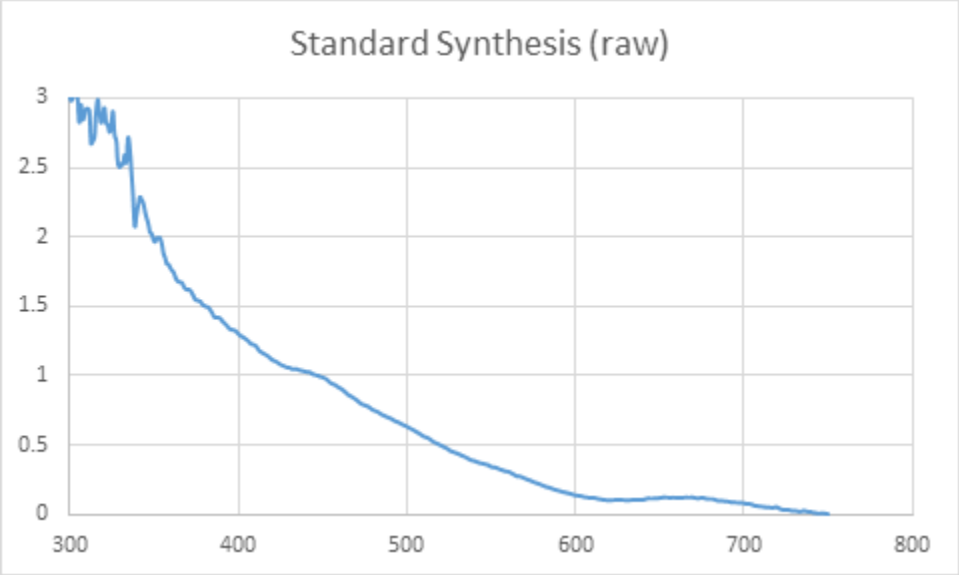

Figure C.17. UV/Vis of $Au_{25}(Capt)_{18}$ synthesized under standard conditions

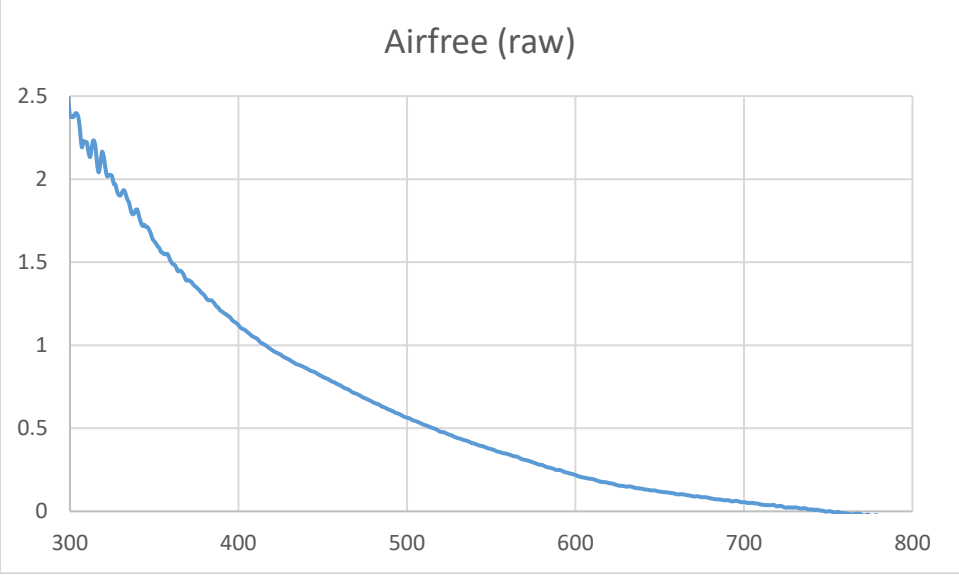

Figure C.18. UV/Vis of $Au_{25}(Capt)_{18}$ synthesis under Ar without radical initiator

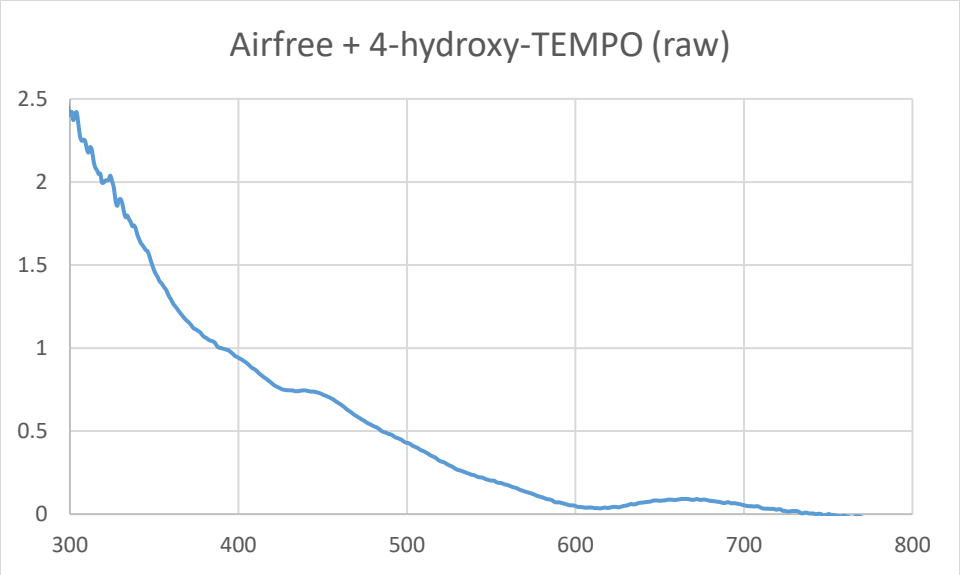

Figure C.19. UV/Vis of $Au_{25}(Capt)_{18}$ synthesis, Ar atm using 4-hydroxy-TEMPO as initiator

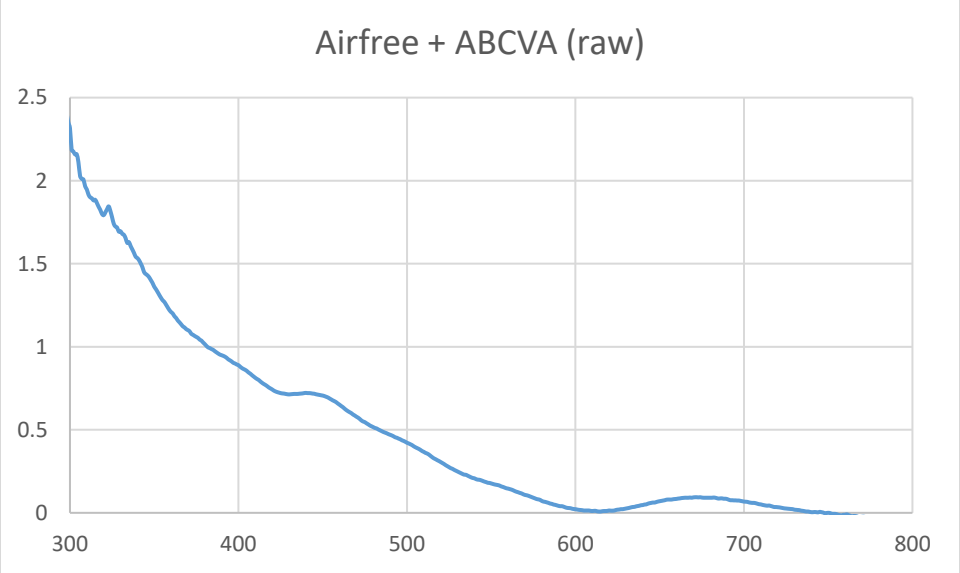

Figure C.20. UV/Vis of $Au_{25}(Capt)_{18}$ synthesis, Ar atm using ABCVA as initiator

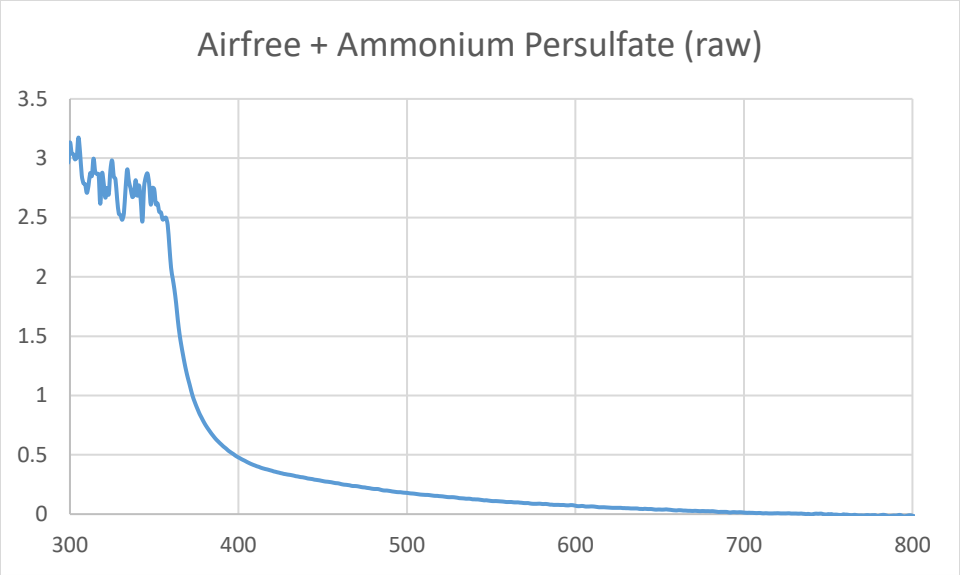

Figure C.21. UV/Vis of $Au_{25}(Capt)_{18}$ synthesis, Ar atm using ammonium persulfate as initiator

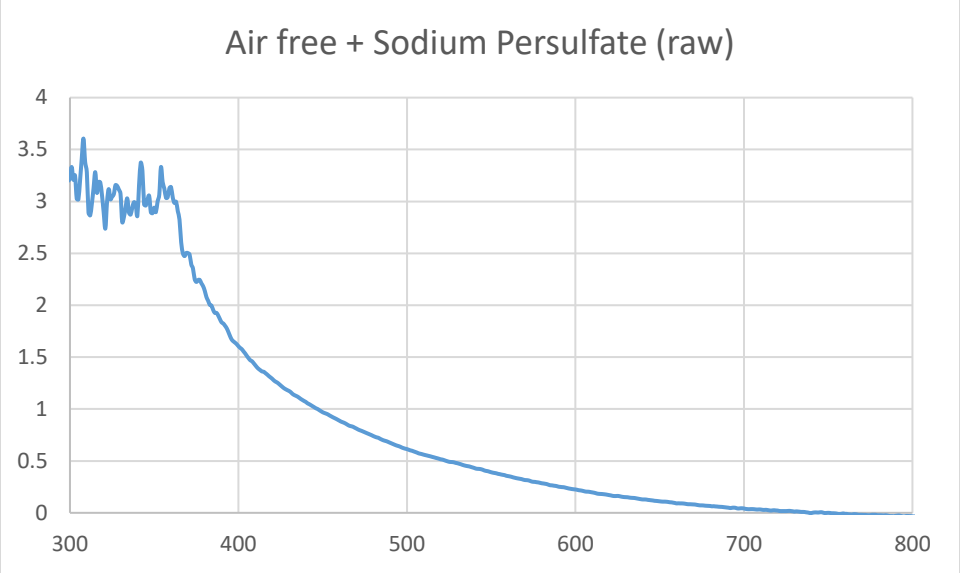

Figure C.22. UV/Vis of $Au_{25}(Capt)_{18}$ synthesis, Ar atm using sodium persulfate as initiator

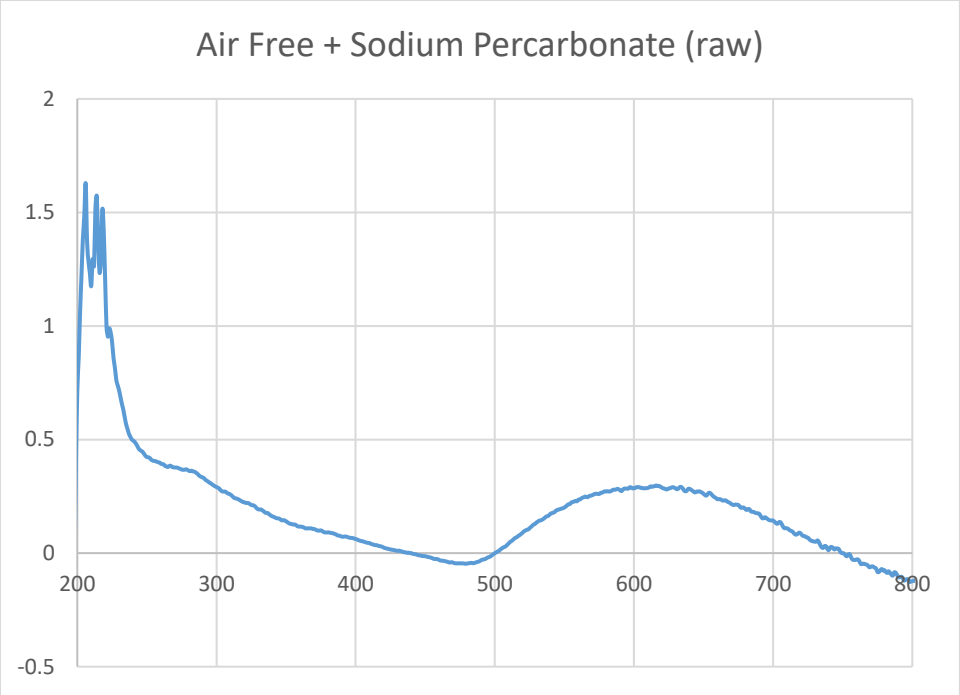

Figure C.23. UV/Vis of $Au_{25}(Capt)_{18}$ synthesis, Ar atm using sodium percarbonate as initiator

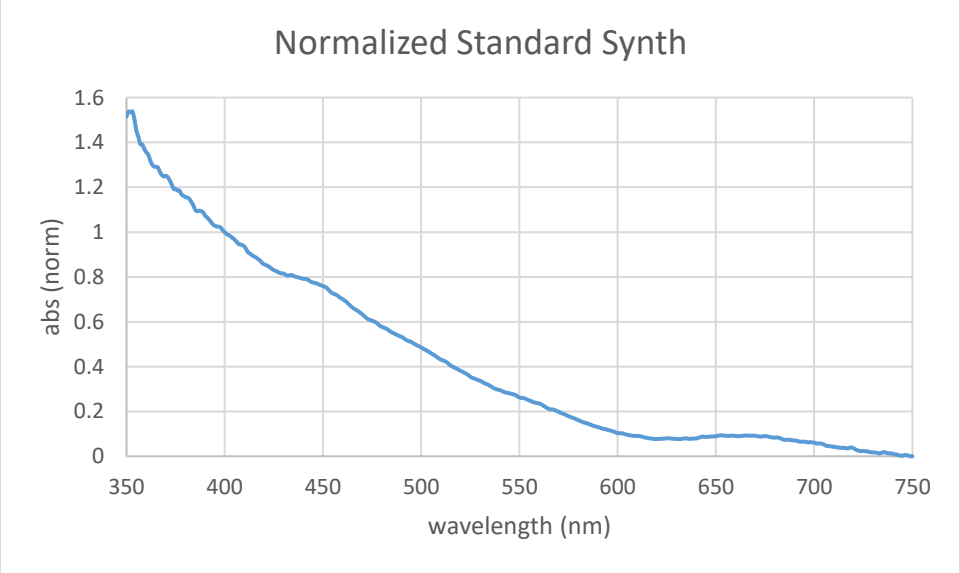

Figure C.24. Normalized UV/Vis of $Au_{25}(Capt)_{18}$ synthesis under standard conditions

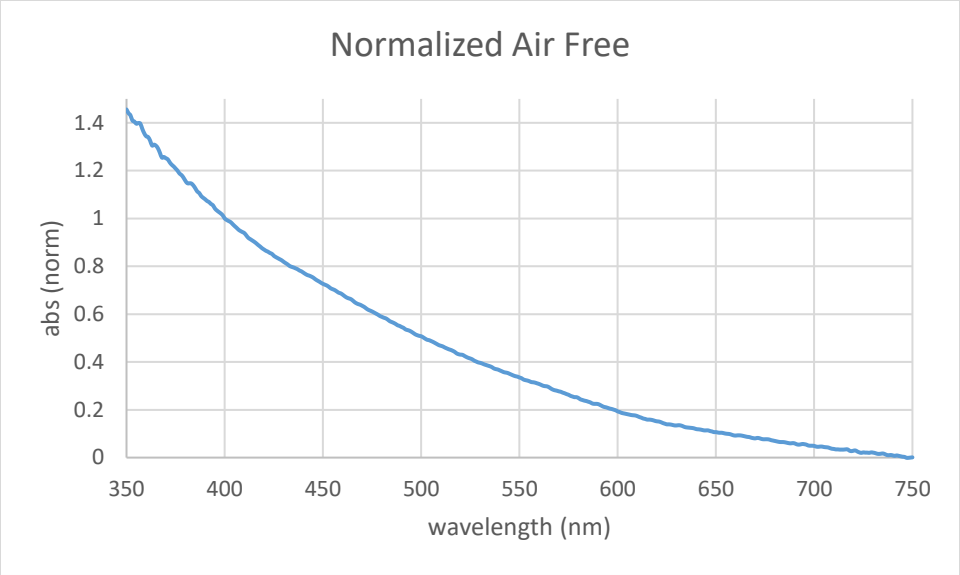

Figure C.25. Normalized UV/Vis of $Au_{25}(Capt)_{18}$ synthesis under Ar atm without radical initiator

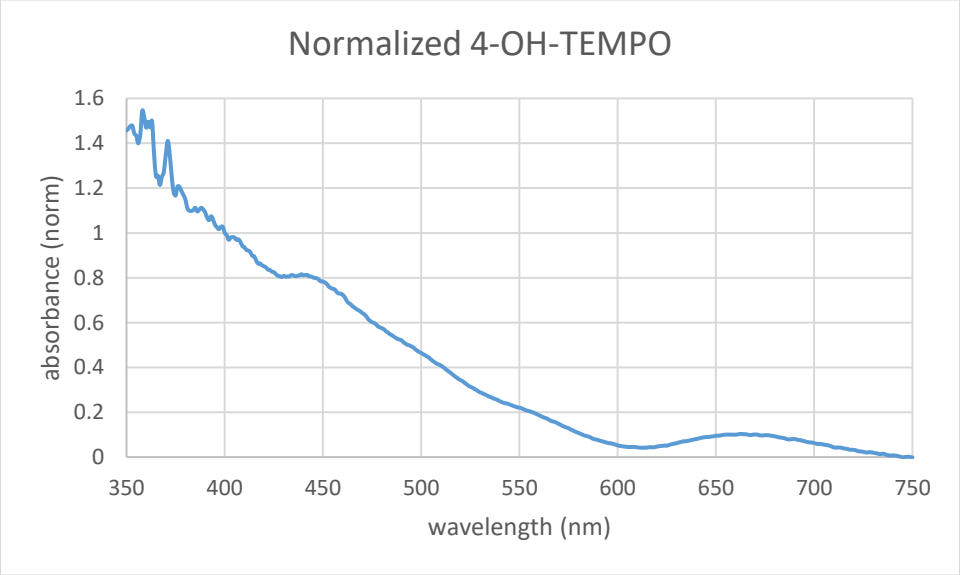

Figure C.26. Normalized UV/Vis of $Au_{25}(Capt)_{18}$ synthesis under Ar atm with 4-hydroxy-TEMPO as initiator

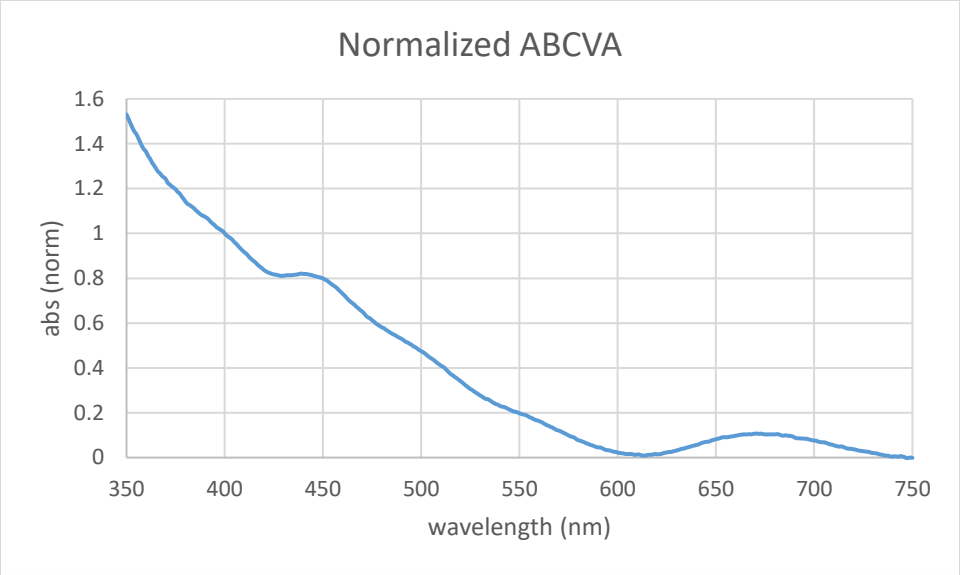

Figure C.27. Normalized UV/Vis of $Au_{25}(Capt)_{18}$ synthesis under Ar atm with ABCVA as initiator

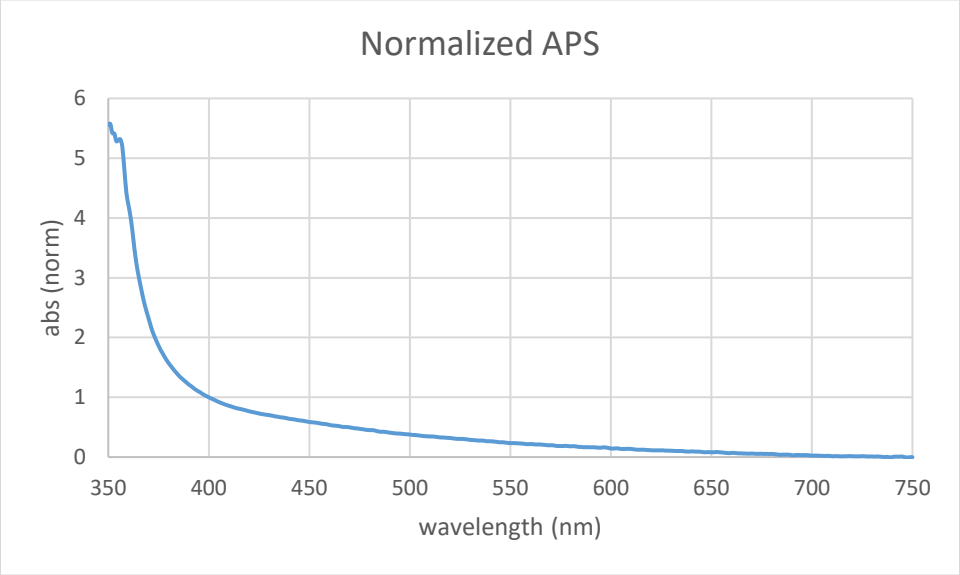

Figure C.28. Normalized UV/Vis of $Au_{25}(Capt)_{18}$ synthesis under Ar atm with ammonium persulfate as initiator

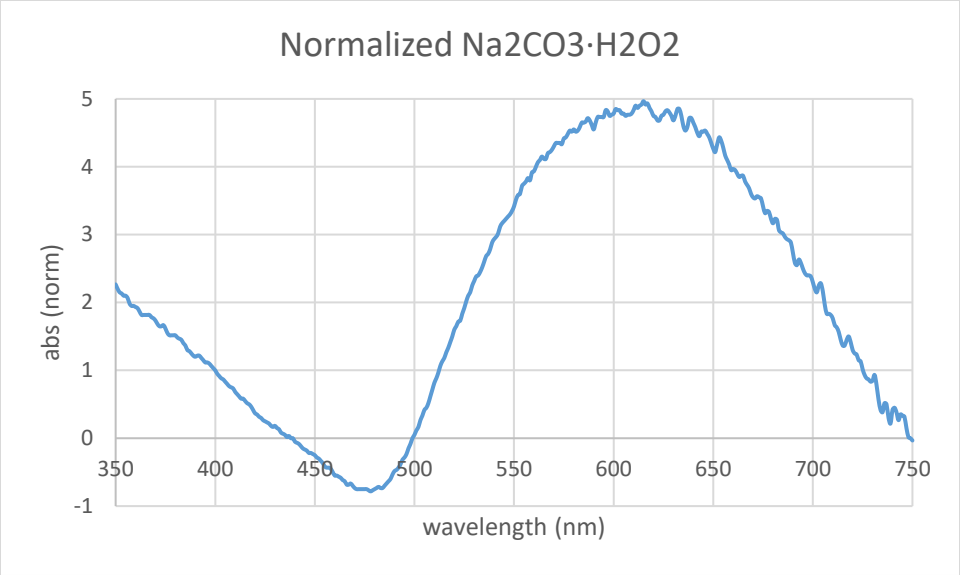

Figure C.29. Normalized UV/Vis of $Au_{25}(Capt)_{18}$ synthesis under Ar atm with sodium percarbonate as initiator

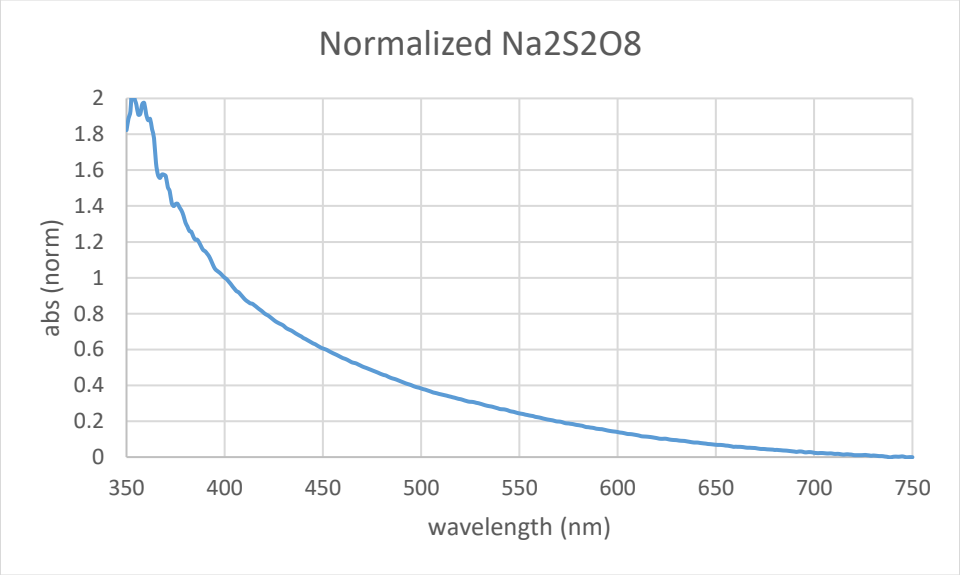

Figure C.30. Normalized UV/Vis of $Au_{25}(Capt)_{18}$ synthesis under Ar atm with sodium persulfate as initiator

C.24 $Au_{25}(SG)_{18}$ UV/Vis Spectra

In the case of normalized spectra, each has been adjusted such that absorbance at 400 nm is equal to 1. On each figure in this section, the x-axis is wavelength in nanometers and the y-axis is absorbance in absorbance units.

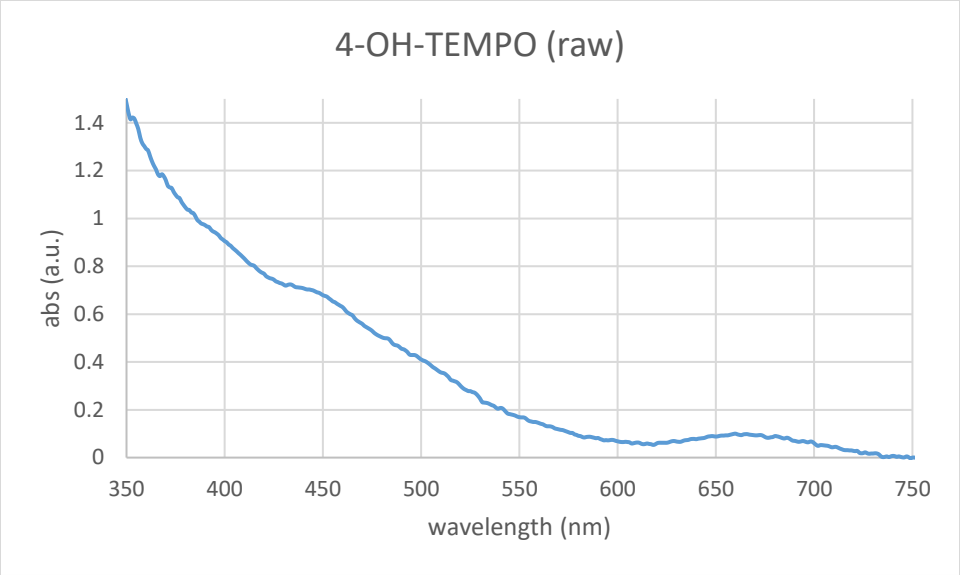

Figure C.31. UV/Vis of $Au_{25}(SG)_{18}$ synthesis under Ar atm with 4-hydroxy-TEMPO as initiator

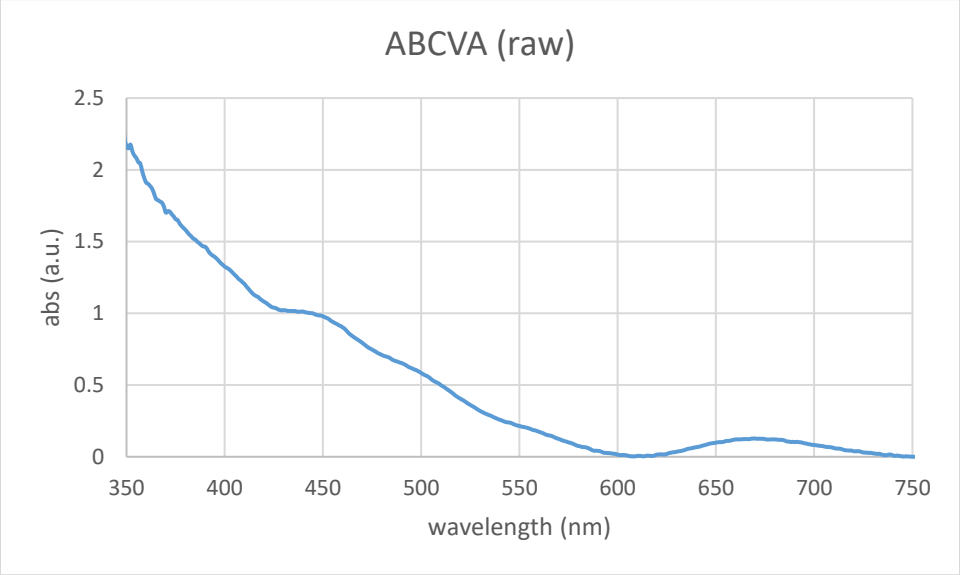

Figure C.32. UV/Vis of $Au_{25}(SG)_{18}$ synthesis under Ar atm with ABCVA as initiator

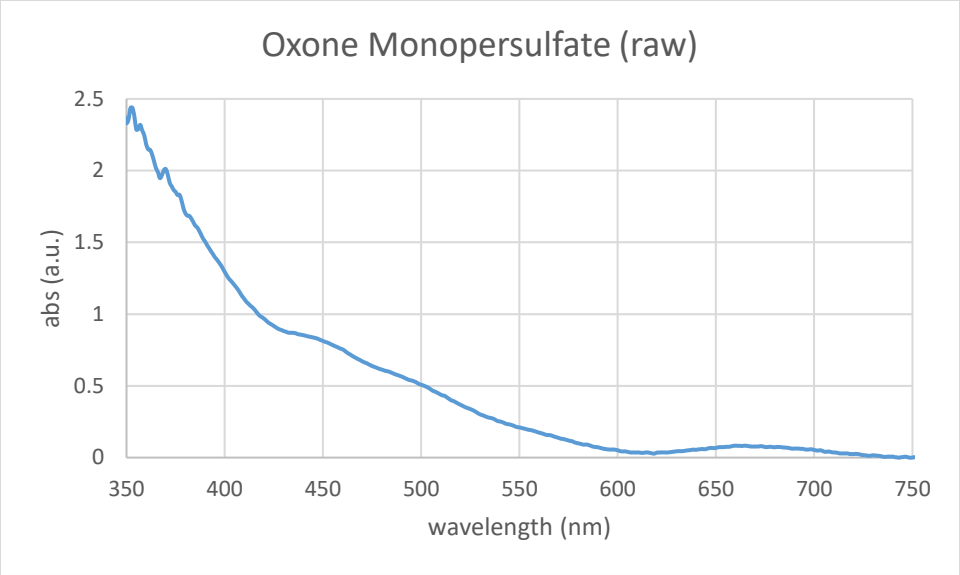

Figure C.33. UV/Vis of $Au_{25}(SG)_{18}$ synthesis under Ar atm with oxone monopersulfate as initiator

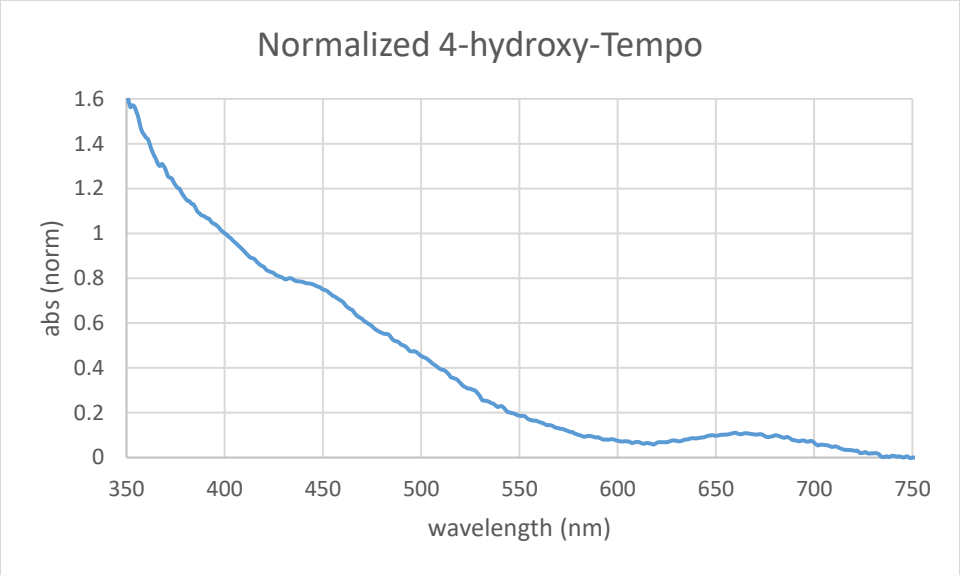

Figure C.34. Normalized UV/Vis of $Au_{25}(SG)_{18}$ synthesis under Ar atm with 4-hydroxy-TEMPO as initiator

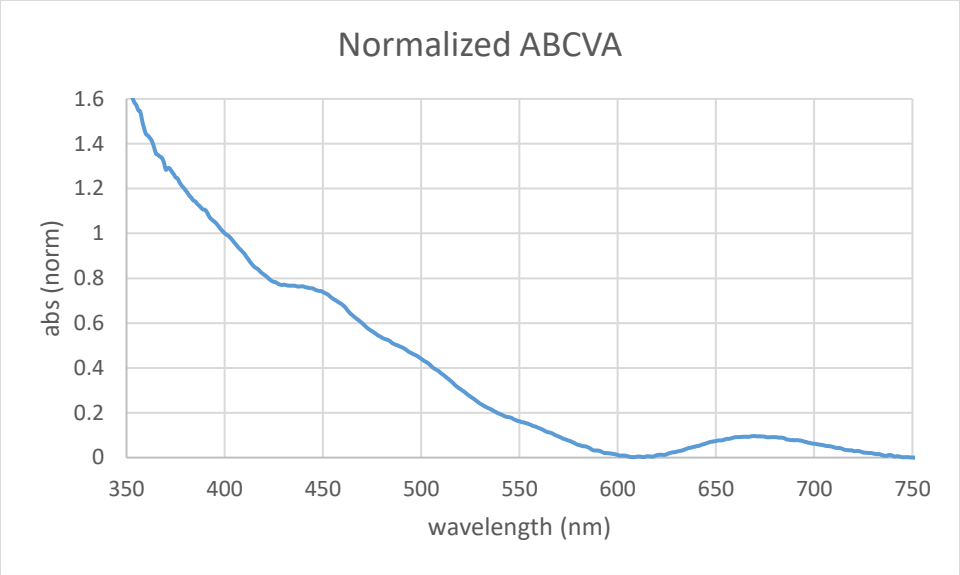

Figure C.35. Normalized UV/Vis of $Au_{25}(SG)_{18}$ synthesis under Ar atm with ABCVA as initiator

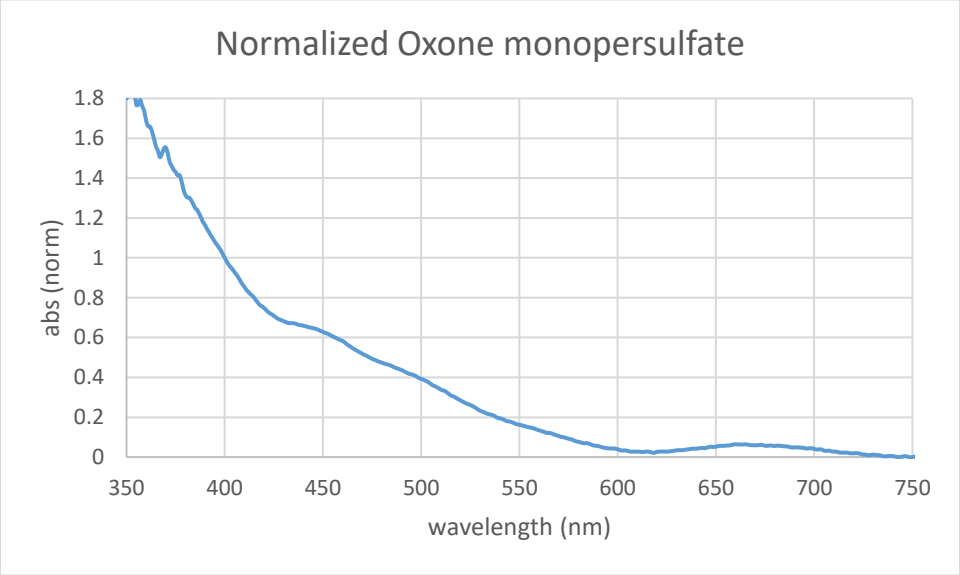

Figure C.36. UV/Vis of $Au_{25}(SG)_{18}$ synthesis under Ar atm with oxone monopersulfate as initiator

C.25 Construction of Chapter 4, Figure 4.3

Each of the gel images below were opened in ImageJ. Using the included ruler, a measurement distance was defined in Image J, and this calibration was used to determine the travel distance of the centroid of the band in each lane which was farthest from the baseline. This distance was then

compared to the travel distance of the Au_{102} standard, which was measured in the same way. These ratios were entered into OriginLab and then used to construct Figure 4.3.

C.26 Gel Images for Chapter 4, Figure 4.3

Each lane is the pellet that was isolated from a particular fractionation step. In the ABCVA, first TEMPO-containing gel, and the Oxone gel each of the lanes is of a reaction mixture after workup but without further purification. In the later sodium persulfate and TEMPO experiments the products were purified by fractional precipitation owing to the difficulty of seeing the results in the crude reaction mixture. Each lane's sample is the pellet from the indicated precipitation step (1, 2, etc) redispersed in 1:1: water/glycerol.

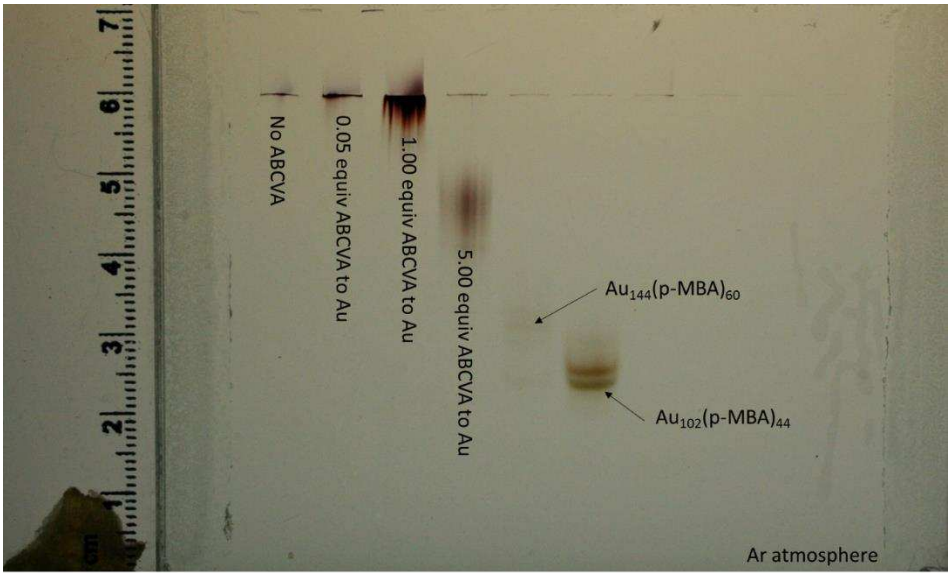

Figure C.37. Initiation of Au_{102} synthesis under Ar atm with ABCVA

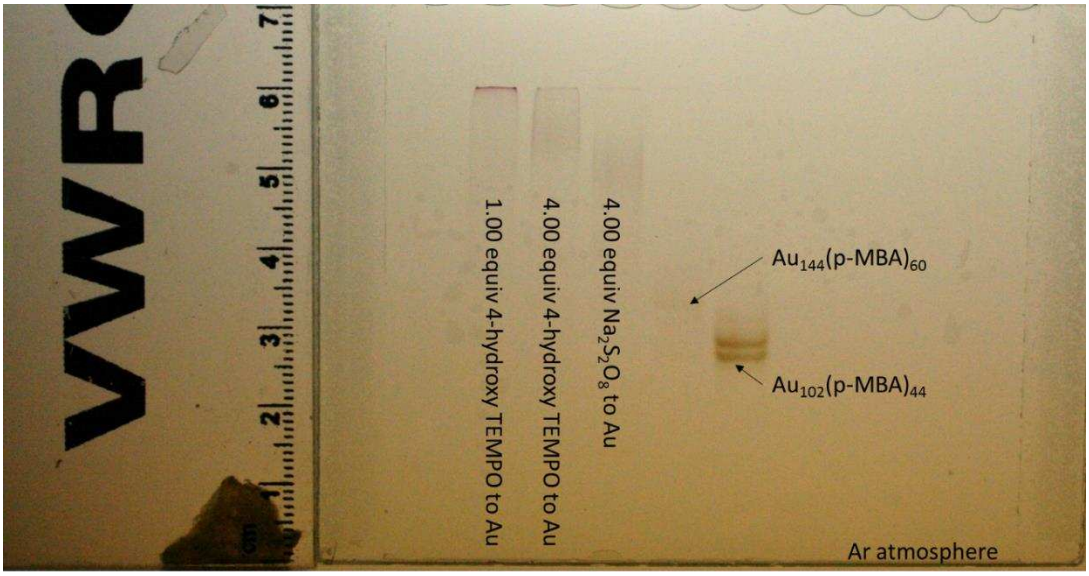

Figure C.38. Initiation of Au_{102} synthesis under Ar atm with 4-hydroxy-TEMPO and sodium persulfate

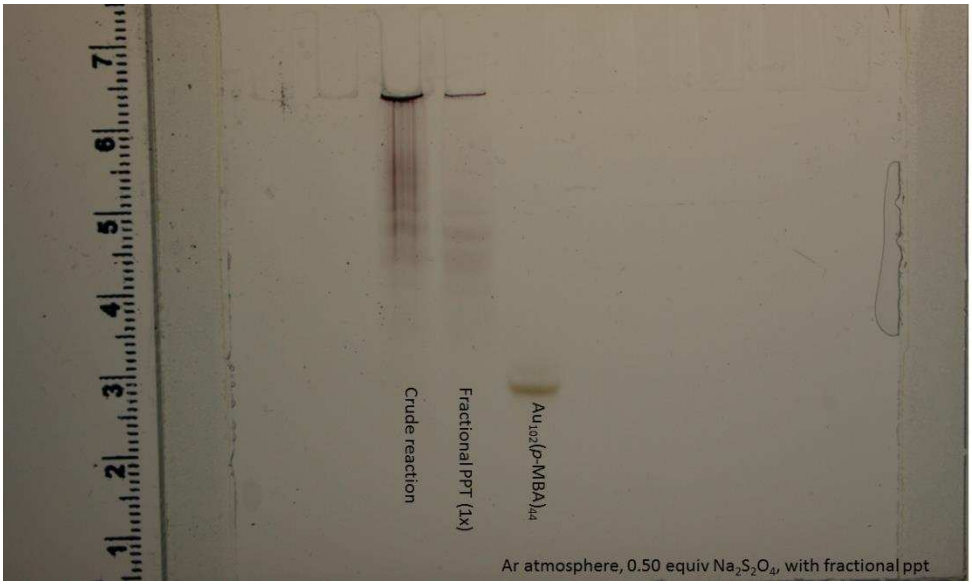

Figure C.39. Initiation of Au_{102} synthesis under Ar atm with 0.50 equiv sodium persulfate

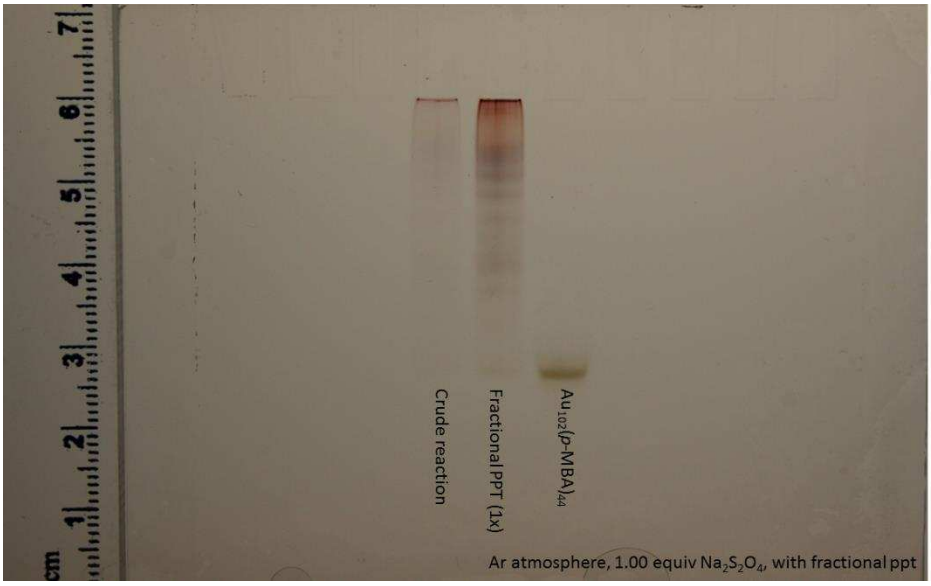

Figure C.40. Initiation of Au_{102} synthesis under Ar atm with 1.00 equiv sodium persulfate

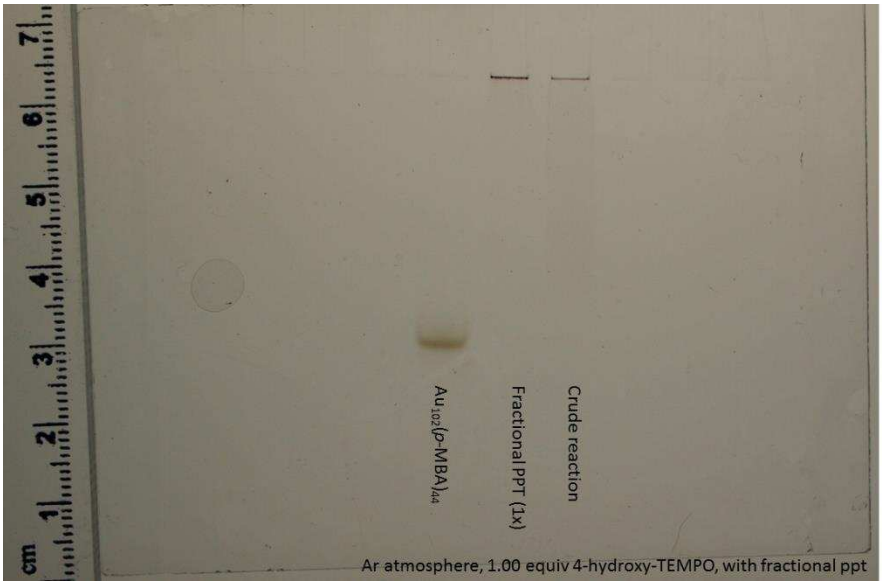

Figure C.41. Initiation of Au_{102} synthesis under Ar atm with 1.00 equiv 4-hydroxy-TEMPO

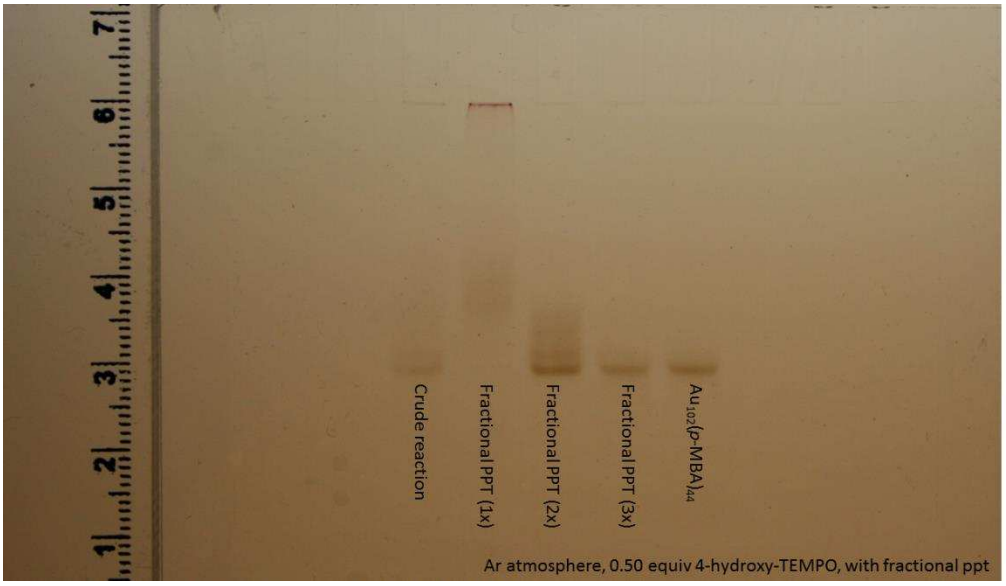

Figure C.42. Initiation of Au_{102} synthesis under Ar atm with 0.50 equiv 4-hydroxy-TEMPO

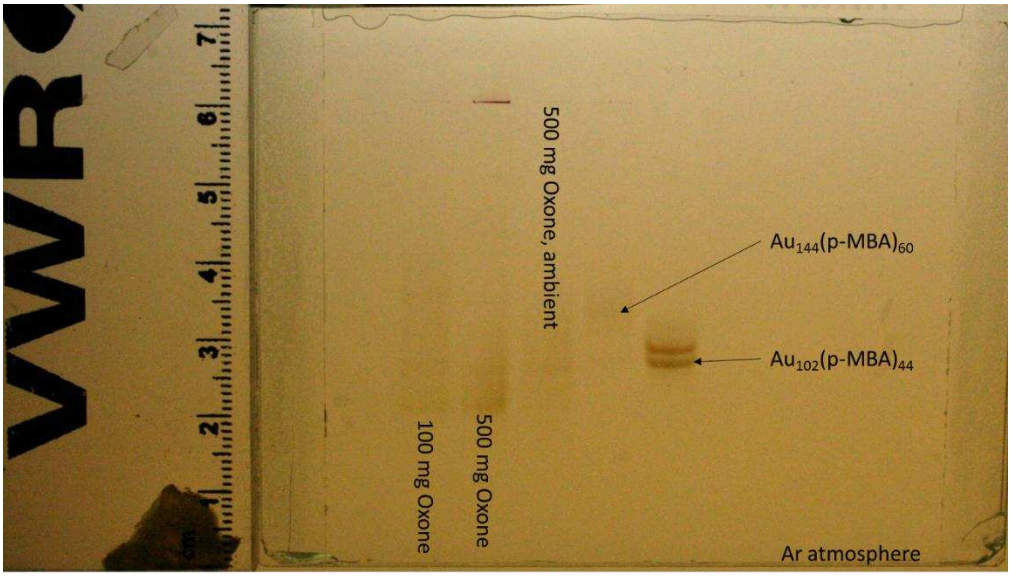

Figure C.43. Initiation of Au_{102} synthesis under Ar atm with Oxone

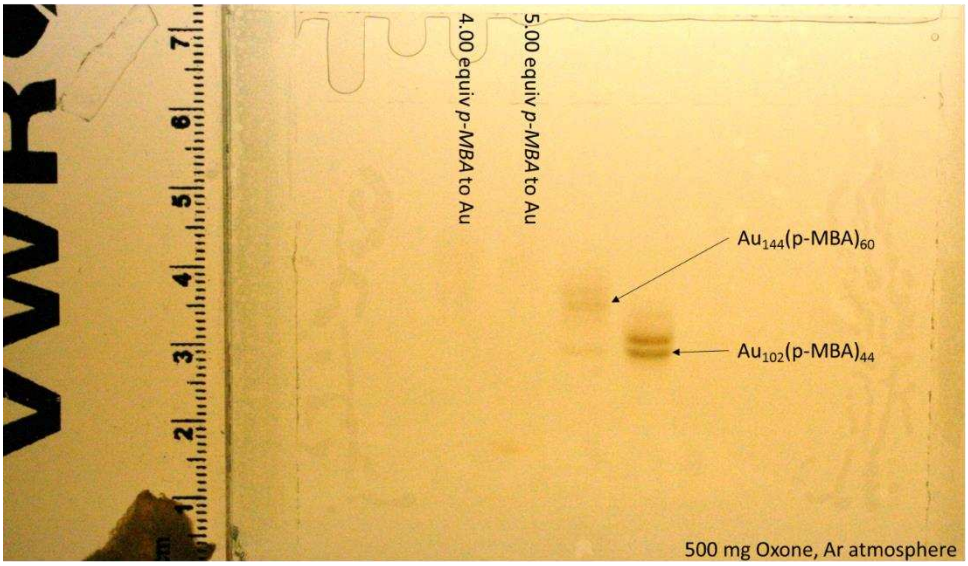

Figure C.44. Initiation of Au_{102} synthesis under Ar atm with Oxone, varying equiv *p*-MBA to Au

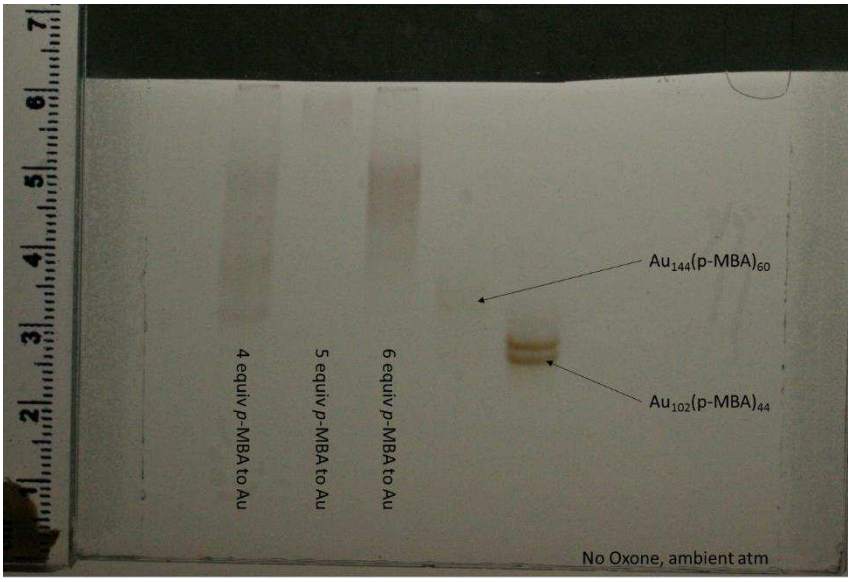

Figure C.45. Variation of *p*-MBA equiv to Au under ambient atmosphere

Figure C.46. Varying $NaBH_4$ equiv to Au under inert atmosphere using Oxone as radical initiator

C.27 Gel Images for Chapter 4, Figure 4.2

Polymer Formation	Ar	O_2	Air	Ar	O_2	Air	Ar	O_2	Air	-
Reduction	Ar	Ar	Ar	O_2	O_2	O_2	Air	Air	Air	-
Lane Number	1	2	3	4	5	6	7	8	9	10

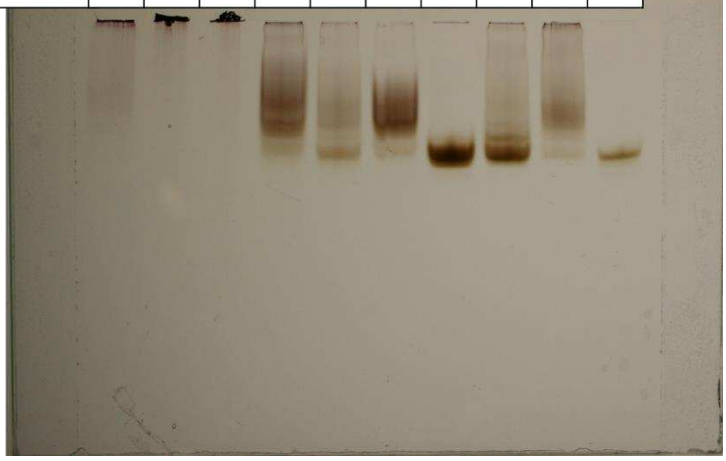

Figure C.47. Uncropped image for Chapter 4, Figure 4.2

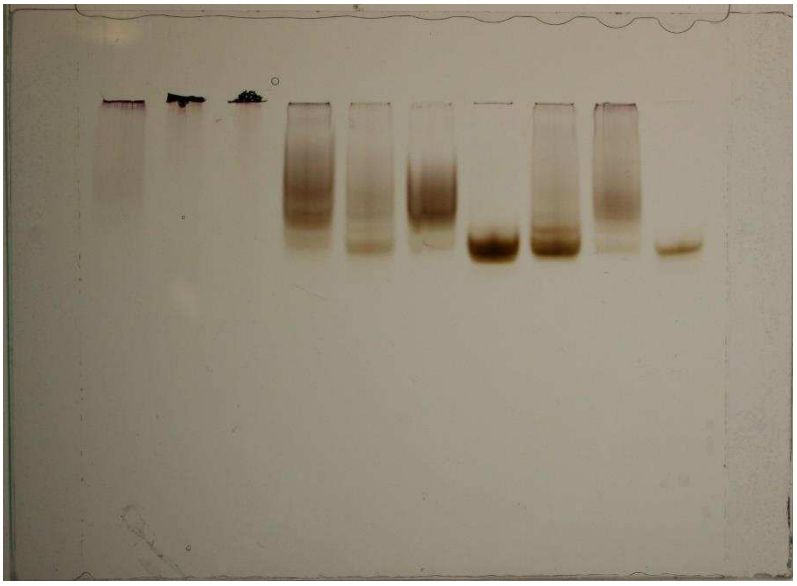

Figure C.48. Uncropped, unadjusted, raw gel image for Chapter 4, Figure 4.2

C.28 Preliminary Crossover Experiment

Procedure for this experiment is the same as above. The gel conditions, however, vary from the standard reported. This gel was run using a 20% acrylamide gel in TBE buffer at a voltage of 110V for 2 hrs.

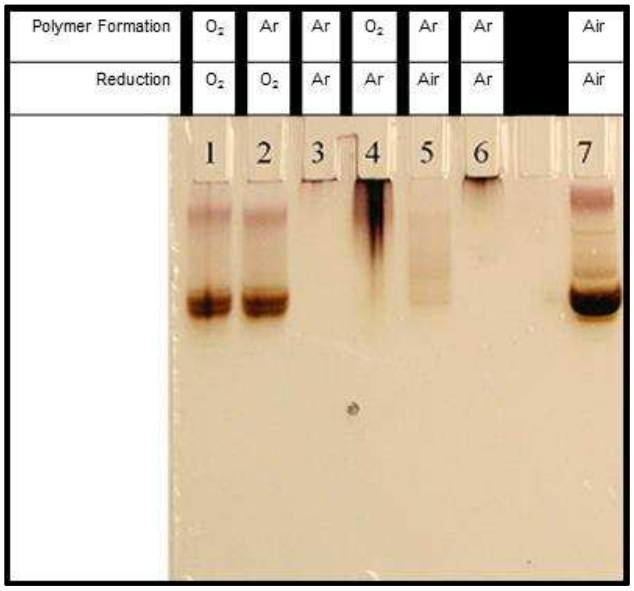

Figure C.49. Initial crossover experiment, not shown in Chapter 4

REFERENCES

1. Heinecke, C. L.; Ni, T. W.; Malola, S.; Makinen, V.; Wong, O. A.; Hakkinen, H.; Ackerson, C. J. Structural and Theoretical Basis for Ligand Exchange on Thiolate Monolayer Protected Gold Nanoclusters. *J. Am. Chem. Soc.* **2012**, *134*, 13316-13322.

2. Wong, O. A.; Compel, W. S.; Ackerson, C. J. Combinatorial discovery of cosolvent systems for production of narrow dispersion thiolate-protected gold nanoparticles. *ACS Comb. Sci.* **2015**, *17*, 11-18.

3. Wong, O. A.; Hansen, R. J.; Ni, T. W.; Heinecke, C. L.; Compel, W. S.; Gustafson, D. L.; Ackerson, C. J. Structure-activity relationships for biodistribution, pharmacokinetics, and excretion of atomically precise nanoclusters in a murine model. *Nanoscale* **2013**, *5*, 10525-10533.

4. Kumar, S.; Jin, R. *Synthesis of water soluble Au25 cluster with high thermal stability*, Presented at the 2012; INOR-581.

5. Kumar, S.; Jin, R. Water-soluble Au25(Capt)18 nanoclusters: synthesis, thermal stability, and optical properties. *Nanoscale* **2012**, *4*, 4222-4227.

6. Levi-Kalisman, Y.; Jadzinsky, P. D.; Kalisman, N.; Tsunoyama, H.; Tsukuda, T.; Bushnell, D. A.; Kornberg, R. D. Synthesis and characterization of Au102(p-MBA)44 nanoparticles. *J. Am. Chem. Soc.* **2011**, *133*, 2976-2982.